PROCESSING AND PROPERTIES OF Y_2O_3 REINFORCED Al-7075 COMPOSITES BY POWDER FORGING

Ph.D. THESIS

by

TILAK CHANDRA JOSHI

DEPARTMENT OF METALLURGICAL AND MATERIALS ENGINEERING
INDIAN INSTITUTE OF TECHNOLOGY ROORKEE
ROORKEE – 247667, INDIA
OCTOBER, 2015

PROCESSING AND PROPERTIES OF Y_2O_3 REINFORCED Al-7075 COMPOSITES BY POWDER FORGING

A THESIS

Submitted in partial fulfilment of the requirements for the award of the degree of

DOCTOR OF PHILOSOPHY

in

METALLURGICAL AND MATERIALS ENGINEERING

by

TILAK CHANDRA JOSHI

DEPARTMENT OF METALLURGICAL AND MATERIALS ENGINEERING
INDIAN INSTITUTE OF TECHNOLOGY ROORKEE
ROORKEE – 247667, INDIA
OCTOBER, 2015

INDIAN INSTITUTE OF TECHNOLOGY ROORKEE
ROORKEE

CANDIDATE'S DECLARATION

I hereby certify that the work which is being presented in the thesis, entitled **"Processing and Properties of Y_2O_3 Reinforced Al-7075 Composites by Powder Forging"** in partial fulfilment of the requirements for the award of the degree of **Doctor of Philosophy** and submitted in the Department of Metallurgical and Materials Engineering, Indian Institute of Technology Roorkee, Roorkee is an authentic record of my own work carried out during the period from July, 2010 to October, 2015 under the supervision of **Dr. Vikram Dabhade**, Assistant Professor, and **Dr. Ujjwal Prakash**, Associate Professor, Department of Metallurgical and Materials Engineering, Indian Institute of Technology Roorkee, Roorkee.

The matter presented in this thesis has not been submitted by me for the award of any other degree of this or any other institute.

(**TILAK CHANDRA JOSHI)**

This is to certify that the above statement made by the candidate is correct to the best of our knowledge.

(V. Dabhade)
Supervisor

(U. Prakash)
Supervisor

Date:

ABSTRACT

Aluminum alloy composites are in recent times finding applications in critical areas of aerospace as well as automobile industries. Aluminum alloy 7075 based composites are suitable for these applications as they offer a high strength to weight ratio coupled with good mechanical as well as tribological properties. The present investigation deals with fabrication and characterization of Al-7075 alloy matrix composites with micrometric as well as nanometric yttria (Y_2O_3) as reinforcement through powder forging route. The powder mixtures (Al-7075 and Y_2O_3 of various volume fractions) were uniaxially cold compacted in a closed rectangular die of cross section 47 x 22 mm using a hydraulic press at 350 MPa. The green compacts were then sintered at 610^oC for 40 minutes under nitrogen atmosphere to obtain the sintered performs. Further, the hot forging of these preforms was carried out leading to forged samples of close to full density.

Based on the above mentioned processing route, Al-7075 forged compacts and Al-7075 forged composites with varying micrometric and nanometric Y_2O_3 were fabricated. Four different studies were carried out. In the first study, microstructural evolution of the sintered preforms of Al-7075 during hot forging at four different temperatures (0.6, 0.7, 0.8 and 0.9 T_m) and under various strains (0.51, 0.92 and 1.14) were studied. The effect of strain at various forging temperatures on the particle morphology, interparticle porosity, prior particle boundary (oxide layer) and hardness were investigated. This was carried out to optimize the forging conditions i.e. forging temperature and strain. In the second study Al-7075 composites reinforced with 1, 3, 5, 10 and 15 vol % Y_2O_3 of micrometric size (~4 μm) and 0.1, 0.5, 1 and 3 vol % Y_2O_3 of nanometric size (~10 nm) were fabricated based on processing parameters optimized in the earlier study. Density, hardness, tensile and compressive properties were determined and correlated with the reinforcement size/content and microstructures. In the third study tribological properties (coefficient of friction, wear rate and wear surface morphology) of these composites were studied at three different loads of 10 N, 20 N and 30 N and sliding speeds of 1 m/s and 2 m/s. The fourth study dealt with machinability studies of these composites using a radial drilling machine with the characterization of drilling forces, cutting torque, surface roughness and chip geometry.

The microstructural studies carried out at different temperatures and strains revealed that a temperature of 0.8 T_m and a true strain of 0.92 are required for the disruption of oxide layer during hot forging of the powder preforms. The hardness values reveal that the strain of 0.92 is sufficient

for optimum deformation and consolidation of the particles even at lower forging temperatures of 0.6 T_m. The densification and mechanical properties of the composites were profoundly affected by the particle size and volume fraction of the Y_2O_3 reinforcement. The hardness with nano Y_2O_3 reinforcement was higher than that of micron Y_2O_3 in the T_6 condition. Both the tensile strength and compressive strength values were higher with the incorporation of nano Y_2O_3 as compared to micron Y_2O_3 in the T_6 condition. The hardness values as well as tensile strength in both the cases peaked at a volume fraction of 0.5% for nano Y_2O_3 and at a volume fraction of 5% for micron Y_2O_3. The basic wear mechanism of pure Al-7075 aluminum alloy and composites consisted of adhesive wear with plastic deformation followed by abrasive wear. Major wear in the samples was due to ploughing, oxidation and delamination. Wear resistance improved with the addition of Y_2O_3 reinforcement in aluminum alloy. Wear rate for all the composites decreased initially with addition of Y_2O_3, optimized at a fixed composition and then again increased with further addition of Y_2O_3. The lowest wear rate was achieved for 5 vol% of micrometric size and for 0.5 vol % for nanometric size Y_2O_3 addition. At a constant volume fraction, the overall wear was found to be lesser for the composites having nanometric Y_2O_3 as compared to micrometric Y_2O_3 for all the test conditions. The machining forces (thrust forces as well as cutting torque) exhibited a similar trend as that of the hardness of the material in both the solutionized as well as in the T_6 condition. Moreover the thrust forces were higher in the T_6 condition as compared to the solutionized condition due to the higher hardness in the peak aged condition. As compared to the Al-7075, the surface roughness was found to be higher for the composites in the solutionized condition. On the other hand the surface roughness was lower for the composites as compared to the pure alloy in the T_6 condition.

ACKNOWLEDGEMENTS

"One swallow doesn't make a summer". This research work could not complete without a continuous support of a team which included the director of the institution to a layman in the department. I would like to express my deepest regard for my supervisors Dr. Vikram Dabhade and Dr. Ujjwal Prakash for their inspiration, constant review and continuous efforts. Their timely help, constructive criticism, positive attitude, painstaking efforts, humanistic and warm personal approaches made me capable to compile the thesis in its present form.

I am grateful to Professor S.K. Nath, Head, MMED, IIT Roorkee and chairman of my research committee for helping morally and financially for the initial setup of research lab. I would like to thank my other committee members Dr. Devendra Singh (internal expert), MMED, IIT Roorkee and Dr. D.K. Dwivedi (external expert), MIED, IIT Roorkee for providing me valuable suggestions. I am thankful to Dr. B.V. Manoj Kumar, MMED, IIT Roorkee for providing the setup for wear testing and helpful discussions during the work. I am also thankful to Dr. P. K. Jain, Head, MIED for allowing to work on the machinability set up and Dr. Rahul S. Mulik, MMED for helping in machinability studies. I am grateful to other faculty members of MMED who continuously supported me time to time during this research work. I am also grateful to The Aluminum Powder Company Limited, North Wales, UK for supplying the AA-7075 powders.

I am very thankful to the lab staff of MMED especially to Mr.Sukhmal Giri, Mr. Dinesh Kumar, Mr. Naresh Kumar Sharma, Mr. Raj Kumar Sharma, Mr. Rajender Singh Sharma, Mr. Shakti Gupta, Mr. Harsh Kumar Ahuja, Mr. Dhan Prakash, Mr. Ashish Kush, Mr. Pradeep Kumar and Mr. Narender Kumar. Special thanks to office staff in particular Mr. Pritam Singh and Mr. Rathore for executing office work.

I wish to duly acknowledge the support provided to my seniors Dr. Sidharth Jain, Dr. Ashish Selokar, Dr. Somnath Bhattacharya and Dr. Mohit Pant for giving me advice and encouragement during my research work. Special thanks to my friends, juniors and colleagues Mr. Sanjay Rathore, Er. Mohit Mahtolia, Dr. Ravikant Chaudhary, Mr. Sandan Sharma, Dr. Devesh Mishra, Mr. R. Sunil Kumar, Dr. Preeti Makkar, Mr. Yashwant Metha, Mr. Nilesh Dorkar, Mr. Anirudh (baba), Mr. Himanshu, Mr. Ramkishore, Mr. Kaushal Kumar, Mr. Ravindra Kumar, Dr. Dharmendra Singh, Mr. Paritosh Dubey, Mr. Vikas Verma and many for walking with me side by side during my stay.

It’s not always the professional people who helped me in completing the job but social relations also kept me pushing towards my duties. I thank people around my social circle especially Dr. Neelam Rawat who advised me time to time, Mr. Ashish Kumar, Mr. Bhoomitra Mehra, Mr. Sanjay Samant and many more for providing moral strength to accomplish the task.

I would like to express my gratitude to my respected parents who provided me continuous motivation and blessing to complete this work. I am grateful to my brother Dheeraj and my wife Ajita for their support, patience and faith in me. I warmly acknowledge Dhruv and Nisha for helping me during my thesis writing. Last but not least, I am thankful to almighty God who gave me strength and patience throughout the way during my Ph D. journey.

I would like to dedicate this thesis humbly to my parents.

Roorkee
Dated:

(TILAK JOSHI)

TABLE OF CONTENTS

LIST OF FIGURES

LIST OF TABLES

LIST OF RESEARCH PUBLICATIONS

RESEARCH PAPERS PUBLISHED/PRESENTED OUT OF THIS INVESTIGATION

Publications:

In International Journals:

1. **Tilak C. Joshi**, Ujjwal Prakash, Vikram V. Dabhade, "Microstructural development during hot forging of Al 7075 powder", Journal of Alloys and Compounds, 639 (2015), 123-130
2. **Tilak C. Joshi**, U. Prakash, Vikram V. Dabhade, "Effect of Nanometric and Micrometric Y_2O_3 Reinforcement on Powder Forged AA-7075 Composites", Communicated and under review.
3. **Tilak C. Joshi**, Vikram V. Dabhade, U. Prakash, "Dry sliding wear behavior of Powder Forged Yttrium Oxide reinforced AA-7075 matrix composites" To be communicated.
4. **Tilak C. Joshi**, U. Prakash, Vikram V. Dabhade, "Effect of reinforcement particle size and metallurgical parameters on Machinability of Aluminum Alloy 7075 composites" To be communicated.

In conferences:

5. **Tilak C. Joshi**, Vikram V. Dabhade, Ujjwal Prakash, "Powder Metallurgical processing of aluminum 7075 alloy with nano yttria dispersion", Transactions of Powder Metallurgy association of India, 39 (2013), 20-26
6. **Tilak C. Joshi**, Vikram V. Dabhade, U. Prakash, "An Overview of Powder Metallurgical Processing of Aluminum and its Alloys", 2nd National Conference on Recent Advances in Mechanical Engineering (NCRAME-2014) Page 312-317.

Conference Presentations:

1. **Tilak C. Joshi**, U. Prakash, V.V.Dabhade, "Microstructural Evalution during Hot Forging of Aluminum Powders" presented at International conference organised by Powder Metallurgy Association of India at The Residence Hotel, Mumbai (India), 2012.
2. **Tilak C. Joshi**, U. Prakash, V.V.Dabhade, "P/M processing of Aluminum 7075 alloy with Nano yttria dispersion" presented at International conference organised by Powder Metallurgy Association of India at Hyatt Regency, Pune (India), 2013.
3. **Tilak C. Joshi**, V.V. Dabhade ,U. Prakash, "P/M Processing of AA 7075 composite and its wear resistance" presented at International conference organised by Powder Metallurgy Association of India at Hotel Le Royal Meridien, Chennai (india), 2014.
4. **Tilak C. Joshi**, Vikram V. Dabhade, U. Prakash, An Overview of Powder Metallurgical Processing of Aluminum and its Alloys", presented at National conference organised by G.B. Pant Engineering College, Pauri (Uttarakhand), 2014.
5. **Tilak C. Joshi**, Sidharth Jain, U. Prakash, V. V. Dabhade, Microstructural development during Forging of Al-Zn-Mg-Cu powder blends, presented in National Seminar at IIT Roorkee (India), 2011.

ABBREVIATIONS

AMC : Aluminium Matrix Composites

COF : Coefficient of Friction

DSC : Differential Scanning Calorimetary

DTA : Differential Thermal Analysis

EDAX : Energy dispersive X-ray spectroscopy

min : Minutes

MMC : Metal Matrix Composites

N : Newton

nm : Nanometer

P/M : Powder Metallurgy

rpm : Rotation per Minute

sec : Seconds

SEM : Scanning Electron Microscopy

TEM : Transmission electron microscopy

UTS : Ultimate Tensile Strength

VHN : Vickers Hardness Number

vol.% : Volume Fraction in %

μm : Micrometer

Chapter 1
INTRODUCTION

Components processing high strength to weight ratio have been in great demand from automotive, aerospace and defense sectors. This need can be easily fulfilled by the use of light metals if they possess good mechanical properties. Light metals like Al, Li, Ti and Mg are the obvious choices as they possess low densities. Aluminum being ductile, having high thermal and electrical conductivity; as well as workability, machinability and availability has been a choice of interest for researchers as well as industries for past few decades. To enhance the strength of aluminum various alloying elements are added to form aluminum alloys. But since these alloys cannot be used in elevated temperature conditions and have high wear rate [Surappa, 2003], composites of these alloys are formed by the incorporation of various types of reinforcements to the aluminum matrix. Reinforcements can be in the form of particulates, whiskers or fibers. These aluminum matrix composites (AMCs) have been a subject of interest (for research and industries) as they exhibit a high strength to weight ratio and primarily for reducing weight and cost which is a major concern in engineering applications. In terms of processing AMCs are superior to other metal matrix composites due to their good formability and machinability. AMCs are processed by various techniques like casting, spray forming, extrusion; powder metallurgy etc.

Powder metallurgical (P/M) processing of AMCs is a high precision technique and cost effective method for producing net near shaped complex products. Various advantages of powder metallurgy process over other conventional processes are attainment of near net shape, variation in chemical composition, ease of dispersion and control of porosities [Sercombe, 2003]. Powder metallurgy route has its unique advantage of reinforcement incorporation with the least segregation and net near shape processing. Particulate aluminum matrix composites (PAMCs) are again a good choice over whisker or fiber composites due to isotropic properties, less cost and availability of standard metal working methods. A large variety of reinforcements are available in particulate form and addition of particulate accelerates aging in PAMCs [Kipouros, 2006]. Powder metallurgy route for fabricating these PAMCs involves blending/mixing of aluminum or alloy powders (either in prealloyed or elemental mix) with reinforcement powders, compaction of these powders, sintering of green compacts to develop metallurgical bonding between powder particles. Sintered composites always attribute some residual porosity restricting the widespread use of these

[Bishop et al., 2000] and for full density they may be further treated by secondary processing techniques like rolling, extrusion or forging.

Amongst the forming processes, due to the involvement of very high strain rates, forging has two major benefits when applied to aluminum powders. Firstly, the high strain rates are responsible for disruption of the oxide film encapsulating the individual powder particles leading to metallurgical contact between the aluminum powder surfaces. Secondly, the pores become flattened/ elongated in the direction of the lateral flow. The stress state around the pore is a combination of normal stress and shear stress which leads to the pore becoming elongated and finally collapsing. The lateral flow is also responsible for powder particles and grains within them getting elongated and resulting in anisotropy in the mechanical properties. However, the anisotropy is lower in powder forged products as compared to wrought products. Processing of powders by forging can be subdivided as load dependent and temperature dependent deformation. It is better to combine and optimize both in terms of temperature and strain to achieve good density as well as superior mechanical properties.

7xxx series based matrix has the highest strength to weight ratios among all AMCs which consist of zinc, copper and magnesium as the alloying elements. In PAMCs, ceramics are basically used as reinforcement due to their high melting point and non reactivity with the matrix. Reinforcements such as aluminum oxide (Al_2O_3), silicon carbide (SiC), silicon nitride (Si_3N_4), boron carbide (B_4C) etc have been attempted by various researchers for the development of P/M AMCs. A few studies have been carried out using Y_2O_3 as reinforcement for the development of P/M AMC's. Y_2O_3 is highly stable at high temperatures due to its high melting point and has negligible reactivity with aluminum (in the solid as well as liquid state) and thus is a suitable reinforcement for aluminum.

Mechanical properties of the powder metallurgically processed aluminum alloys and their composites are governed by powder characteristics, reinforcement properties, density levels, sintering conditions, and secondary processing techniques, etc. Presence of pores in the components fabricated by classical P/M route degrades its mechanical properties and performance and makes them unsuitable for heavy duty applications. For production of parts subjected to high mechanical loads and under heavy stress and dynamic conditions, achieving high density (low porosity level) has become one of the primary objectives. Wear behavior of aluminum alloys and composites is governed by various common factors like load, sliding speed, temperature, and humidity levels but more concern is about an easy oxidation of the surface layers due to above

mentioned factors. Although the oxide layer acts as a lamination on the surface to protect further oxidation, it causes more wear once delaminated. The wear of powder metallurgical (P/M) aluminum products is severe due to the weak particle boundaries and porosities present inside the material. Addition of secondary particles in the form of reinforcement helps in increasing the hardness as well as wear resistance of the material especially in case of aluminum and its alloys. Production of these PAMCs for industrial applications gets in final shape after machining operation. PAMCs offer highest level of machinability amongst all light weight metal based composites. Assessment of machinability operation can be done by several parameters including cutting force, surface finish, chip formation mode, tool life and cutting energy.

The present investigation deals with fabrication and characterization of powder metallurgically processed Al-7075 alloy composites reinforced with Y_2O_3. Al-7075 powders were selected as a matrix and Y_2O_3 was reinforced in different sizes and various volume fractions. Powder forging was selected as a secondary consolidation technique for removing porosity after sintering and breaking of oxide layer at particle boundary. Elimination of prior particle boundry alongwith achieving full density and homogeneous microstructure is accomplished by optimizing the temperature and strain conditions during forging. Mechanical, tribological and machining characteristics of the fabricated composites were carried out and correlated with microstructural evolution. The whole research work has been presented in six chapters in the proposed thesis. **Chapter 1** deals the introduction to aluminum powder metallurgy and a general idea of processing methods including compaction, sintering and forging. Aluminum 7075 alloy and its composites are covered with their various aspects e.g. composition, physical properties, density, mechanical and tribological properties and machinability. **Chapter 2** gives a comprehensive review of literature on different aspects of aluminum matrix composites directly relevant to the study being undertaken. The chapter reviews the powder processing routes of aluminum and its alloys and discusses the various processing parameters. Apart from the processing parameters, the selected alloy composition was discussed in details explaining the role of various alloying elements. Powder forging as a secondary consolidation process in aluminum alloys and its composites is reviewed separately. Mechanical/ tribological properties and machining behavior of powder metallurgically processed AMCs are also reviewed in detail.

Chapter 3 deals with formulation of problem, objectives of present work based on literature review. **Chapter 4** consists of the experimental procedures employed for present work and describes the details of the processing route employed to fabricate these composites by

compaction, sintering and hot forging. Further, various equipments/ instruments used to investigate density, hardness, mechanical properties, wear behavior and machinability of the composites are discussed. Also, various heat treatments given to these composites are described in details in this chapter. **Chapter 5** gives a detailed discussion of the results obtained in the present research work and has been divided in four sub sections from 5.1 to 5.4 for clarity. **Chapter 5.1** deals with optimization of powder processing parameters and microstructural evolution during hot forging. The working factors e.g. temperature and total strain during forging were optimized for prealloyed 7075 aluminum alloy. In **chapter 5.2** mechanical properties obtained from different composites and correlation of hardness and tensile strength with yttrium oxide reinforcement size and content and also microstructural changes are described in detail. **Chapter 5.3** describes the wear behavior of different composites at different wear loads and sliding speeds. Effect of different amount of yttrium oxide addition on wear behavior has been investigated and correlated with their microstructures and hardness. **Chapter 5.4** discusses machinability studies of different fabricated composites with respect to Y_2O_3 reinforcement size and content in the solutionized as well as T_6 conditions. **Chapter 6** mentions the important conclusions arrived from these studies and the future directions in which these studies can be extended.

Chapter 2
LITERATURE REVIEW

2.1 Introduction

The literature review of the thesis work provides a comprehensive review of literature on different aspects of aluminum matrix composites directly relevant to the study being undertaken. The chapter reviews powder processing routes of aluminum and its alloy, and explains the various processing parameters. Aluminum powders, their compaction techniques, sintering process including the effect of atmosphere, particle morphology and liquid phases; and high density processing methods are introduced with respect to previous studies carried out by researchers. Powder forging as a secondary consolidation process in aluminum alloys and its composites is reviewed separately. Aluminum matrix composites and effect of different reinforcements on aluminum alloy based composites is reported. Mechanical/ tribological properties and machining behavior of powder processed AMC's are also reviewed at the end.

2.2 Powder metallurgical processing of Aluminum and its alloys

Powder metallurgy of aluminum has developed as a processing method to address certain limitations found in other traditional fabrication processes mainly casting. Aluminum powder metallurgy has equivalent physical and mechanical properties as compared to wrought aluminum products. A low density, large variations in compositions, corrosion resistance, near-net shape processing and porous product for special purposes are some of the benefits achieved by aluminum powder metallurgy. Some additional benefits includes high material utilization and low energy inputs. Aluminum P/M has emerged as a successful processing technique where it is not possible to fabricate some critical compositions by melting routes as these lead to segregation [Bora et al., 2004; Balasundar et al., 2009; Karanjai et al., 2008; Prakash et al., 2000; Sawant et al., 2014]. Aluminum P/M has been described as a versatile processing technique on account of its ability to modify alloy chemistry to suit specific purposes. The important operating parameters of Aluminum P/M include distribution of particle size, techniques applied to blending of powders, pressing, and sintering methods [Kipouros et al., 2006].

2.2.1 Aluminum Powders

Aluminum powders are the raw material for aluminum P/M processing. A large variety of grades of powder alloys which are generally prepared by inert gas atomization, either partially pre-alloyed or completely pre-alloyed with elemental pre-mixes are available nowadays[Pickens, 1981]. Particle size and its distribution, shape, apparent density and particle microstructure affects the performance of the powder mass during processing as well as properties of the finished product. Hence, it is very important to consider the above aspects before P/M processing. Particle size and its distribution are important in packing of the powders and influence its behavior during compaction and sintering. In general finer powders are preferred over coarser ones as high surface area and larger particle to particle contacts result in better properties after sintering but in case of aluminum powders which are surrounded by very thin oxide layer, particle shape sharply influences the properties of compact [Rehimian et al., 2009]. Generally an apparent density of 66% is achieved with the use of spherical powders and higher densities can be achieved with irregular shaped powders. The difference of two particle morphology types is the ability for oxide skin to fracture in irregular shaped powders during compaction. The sintering of irregular particles takes place quite extensively as compared to those of spherical particles resulting in higher sintered density for the particles of irregular shape (approx. 88 to 91%) compared to spherical shape (approx. 66 to 73%) [Liu et al., 2007].

2.2.2 Compaction

Compaction is a process of combining the loose powders into one cohesive body or powder compact by the application of load. This leads to the formation of compacts / performs of desired shape and density. Compaction also leads to particle to particle contact which is a prerequisite for sintering to take place. The compaction of powders requires a closed surrounding which can hold the loose powders together which is provided by a die [Upadhyaya, 1997]. Due to the high ductility of aluminum powder, high green densities can be obtained at relatively moderate pressure [German, 1984].

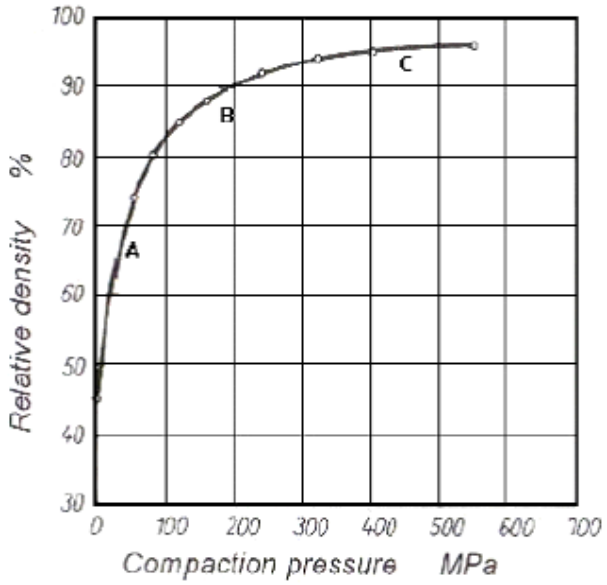

Fig. 2.1 Variation of relative green density with compaction pressure [Jones, 1960]

The variation of relative green density with compaction pressure for aluminum powder is shown in Fig. 2.1. There are three main zones through powder compaction which relate with compaction pressure. In the first zone (A) there is transitional repacking in which the particles rearrange themselves and slide past each other until they cannot move further. Rearrangement of the particles is not uniform. Particles situated in ideal locations are rearranged to cavities without restrain. In the second zone (B), rearrangement of the powder particles is maximized, which leads to an increase in pressure but with little increase in density through plastic deformation. The plastic deformation occurring in this stage has a localized effect only. In the third zone (C), the increase of pressure leads to bulk plastic deformation of the particles. Oxide films on particles are broken and particles start to consolidate by cold welding. Further increase of pressure extends the areas of contacts and increases green strength and density. In the first and second zone, particle rearrangement is dominant while in the third zone, plastic deformation of particles is dominant [Jones, 1960].

If the compaction pressure is applied in uniaxial direction from the top by an upper punch, the density of the compact decreases from the top to the bottom [Thummler and Oberacker, 1993]. This is enhanced by increasing length to cross-section ratio, thus it is more difficult to densify the lower end of the compact. Pressure transmission is reduced further from the top punch due to die wall friction. To improve this, biaxial compaction should be performed by application of upper and lower punches simultaneously.

The green strength of compacts formed by cold isostatic compaction is generally higher than those by die compaction as pressure is applied from all directions. The flexible mould moves with the powder as it densifies, therefore friction effects are minimized. Thus, applied pressure has an almost unrestricted effect on the compact from all sides. The uniform application of pressure results in the uniform density of compacts and less pressure is required to reach the same compact density as compared to die compaction [Schatt and Wieters, 1997]. In addition, it is possible to compact metals powder which are not possible by die compaction, i.e. mostly very coarse and very fine powders and also hard metals. However, dimensional control is not as tight as with die pressing due to flexible tooling [Sands and Shakespeare, 1966]. The working pressure for the compaction of aluminum powders in CIP is between 200 and 400 MPa. The compaction pressure needs to be maintained just for a few seconds. However, if compaction of metals with low compressibility is performed, the decompression must be carried out over a period of several minutes to eliminate crack formation caused by elastic springback [Schatt and Wieters, 1997].

2.2.3 Sintering

Sintering is a process in which the powder particles bond together metallurgically when heated to a sufficiently high temperature (sintering temperature) due to reduction of surface energy [ASM Handbook Vol 7, 1998]. Sintering process depends upon the material selected but generally there are following six stages of sintering (1) initial particle bonding (2) neck growth (3) pore channel closure (4) pore rounding (5) densification or pore shrinkage and (6) pore coarsening. The pore closure and sintering stages successively are shown in Fig. 2.2 (a) to (d). Sintering is dependent on several factors including sintering temperature, sintering time, sintering atmosphere, rate of heating and cooling, powder type and particle shape/size. Apart from these general factors, sintering of aluminum alloys is greatly affected by the other factors, which are discussed with the help of previous research studies performed by various authors in the following sections.

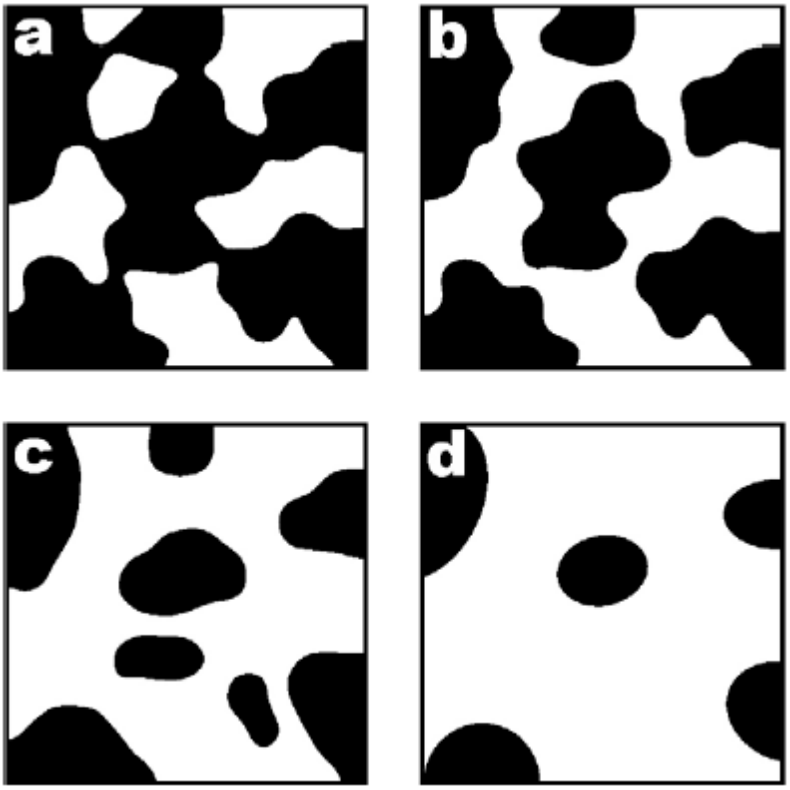

Fig. 2.2 Schematic view of pore closure mechanism. The black regions are pores and white area is aluminum [Peng and Schaffer, 2009]

2.2.3.1 Effect of sintering atmosphere

In the sintering of aluminum powder based systems, the atmospheric effect can only be studied in relation to existence of elements that aid in disruption of the oxide layer of Al_2O_3 which surrounds each powder particle. Pieczonka et al., 2008 studied the sintering of 99.5% pure Al powder in the presence of different sintering atmospheres. They studied dilatometric shrinkage of the powders under N_2, Ar, N_2-Ar, flowing dry N_2-H_2 (H_2 Maximum 5 vol.%) and vacuum. After sintering at 600^oC for 150 minutes, the authors found a notable shrinkage under nitrogen atmosphere only. A small amount of addition of H_2 or Ar in N_2 reduces the shrinkage of sintered sample. The role of N_2 in reducing the oxide layer of powder particles and nitriding during sintering was not clearly explained by the authors. Padmavathi and Upadhyaya, 2011 explained the role of N_2 in reducing the oxide film during sintering. Mg present in trace addition reacts with Al_2O_3 present at the particle surface and forms spinal (Al_2MgO_4). Further the fresh Al in contact with N_2 forms aluminum nitride as per the following reactions:

$3Mg + 4Al_2O_3 \rightarrow 3Al_2MgO_4 + 2Al$

$2Al + N_2 \rightarrow 2AlN$

The above process is a self replicating reaction and generally reffered as a self- gettering mechanism in which oxide present at boundary reduces and the fresh Al particle surfaces come in contact to make a metallurgical bond. A small amount of hydrogen present in atmosphere during sintering reduces the formation of AlN which is a precursor to shrinkage. The above process is graphically presented Fig. 2.3.

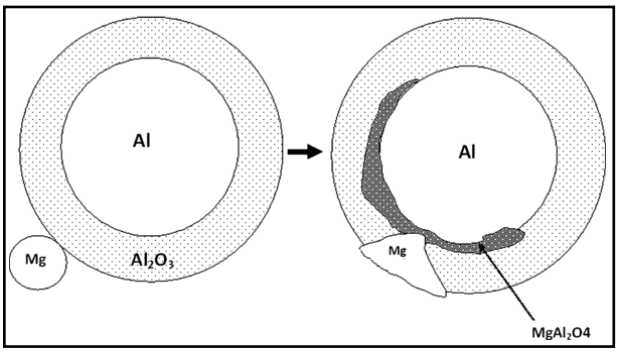

Fig. 2.3 Graphical representation of spinel ($MgAl_2O_4$) formation over an aluminum particle [Padmavathi and Upadhyaya, 2011]

The effect of N_2 on the sintering behavior is discussed in details by Schaffer and Hall, 2002. The authors explained that the self-gettering mechanism is limited to the interconnected pores inside the sample. It is therefore beneficial to have the lowest density of the green compact before sintering for achieving higher shrinkage. Outer region of the sample which is directly in contact with furnace surface is less affected by N_2 compared to the inner interconnected channels, where pores exist. Martin and Castro, 2003 reported a high densification of 2xxx prealloyed powders after sintering using vacuum during sintering compared to flowing N_2 at all sintering temperatures and different holding times. But the samples sintered under vacuum had a low age hardening response due to low cooling rate after sintering compared to N_2. This was attributed to the amount of liquid phase present under liquid phase sintering and also the resulting morphology (shape and size) of precipitates after slow cooling.

Densification of porous compact after sintering is achieved by pore filling or reduction of pores. Schaffer et al., 2005 extensively studied the effect of different gas atmospheres as well as vacuum on the sintering response of different powder blends. They used N_2, Ar, N_2-5 vol.% H_2, Ar–5 vol.% H_2 gases and elemental powder blends of Al-Mg-Si-Cu, Al-Cu-Mg and Al-Mg-Si for the study. Initial sintering kinetics was found similar for N_2, Ar and vacuum and a faster rate of sintering kinetics was found in N_2 at later stages of sintering. The reason behind this acceleration

was formation of AlN but there are other factors associated. Al_2O_3 has a larger contact angle which is almost double in magnitude with molten aluminum, which suggests that Ar and vacuum should exhibit similar or better wettability for liquid aluminum. Release of liquid aluminum is only facilitated by spinel formation as discussed above and not by AlN. It is the formation of AlN that aids pore filling by constituting a negative pressure at the pore site due to consumption of the N_2 gas at the pore site in comparison to Ar. Argon gas is non-reactive with aluminum, hence constitutes a back pressure and hinders pore closure. Densification in vacuum is somewhat midway between N_2 and Ar. H_2 in combination with both N_2 and Ar is disadvantageous to densification due to formation of erratic hydrides like AlH_3 and Al_2H_6 that decompose at low temperatures. In spite of high solubility in molten aluminum, H_2 is diffused-out and further constitutes a back pressure at the pore sites and constrains pore filling. This phenomenon has not been convincingly explained but was in agreement with pore morphology. Liquid fraction pools were found with large grain sizes at brimmed up pore sites. Sintering effectiveness of atmosphere for the selected powder blends finally resulted as N_2 > vacuum > Ar > N_2 - H_2 = Ar - H_2.

2.2.3.2 Effect of particle morphology

The particle size and shape of the aluminum and alloying element particles have a direct relationship with sintering kinetics. The effect of particle shape and size on sintering densification of Al-4Sn was studied by Liu et al., 2007. Authors employed different particle sizes and various shapes having 3, 5 and 15 µm in spherical shape and 6, 7 and 15 µm in irregular shape. Sintering was done at 620^{o}C in Ar atmosphere and it was found that the system underwent a liquid phase sintering and it was more effective at the inner core having interconnected pores however the outer surface remained unsintered. The thickness of outer unsintered layer was found less in irregular shaped powder compared to the spherical powders. The spherical powders have larger pores and interconnected channels while irregular shaped powders show evenly distributed pores. Oxide removal from the surface was not possible in this case due to absence of N_2 and Mg. Hence the disruption of oxide layer from the particle boundary was explained with the help of Hook's law for stress arising due to differential thermal expansion of aluminum and alumina layer. A sintering temperature of 600^{o}C generates a 4000 MPa force due to thermal expansion mismatch of Al and Al_2O_3. This force is enough for breaking of oxide layer on the surface by Hook's law and will generate further stress for breaking of oxide from adjacent powder particles. This thermal stress is more on irregular shaped particles then spherical ones. However the new surface will further

oxidize if any oxygen is present in atmosphere during sintering. This dynamic breaking of oxide layer continues and more effectively removes the oxide layer from the surface of individual powder particles and thus promotes sintering.

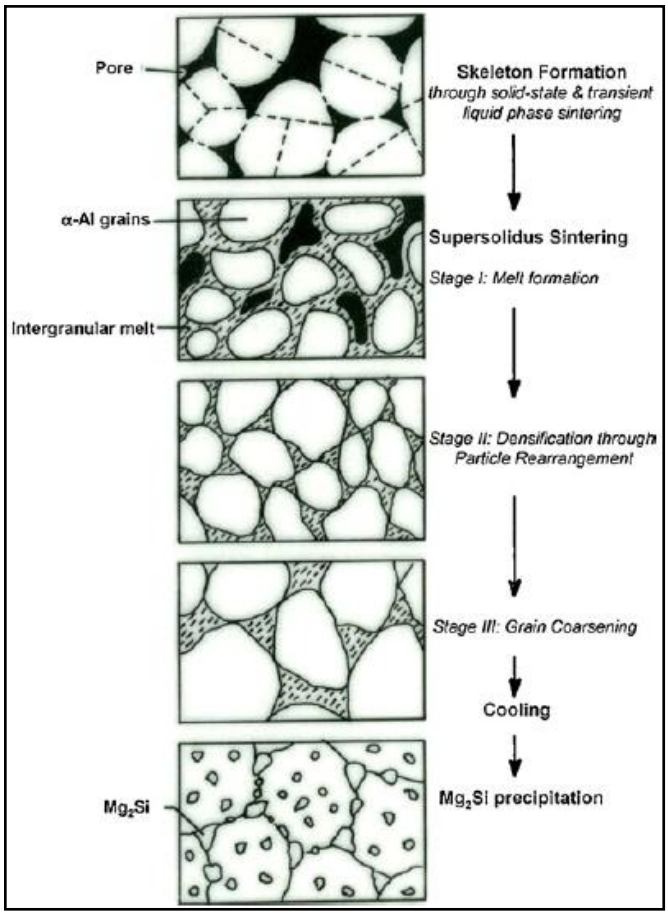

Fig. 2.4 Liquid phase sintering of pre-alloyed 6061in graphical form [Padmavathi, Upadhyaya and Agrawal, 2011]

Effect of coarse and fine powders on sintering response of powder blends was studied by Lumley and Schaffer, 1996. Authors selected coarse powder of 120- 150 μm sizes and fine powders (<45 μm) of Zn, Sn and Cu for the sintering of Al-5Sn, Al-10Zn, and Al-5.5Cu powder blends. Particle size for Al was selected as 60μm (D_{50}) for all the powder blends. The amount of liquid phase was similar for coarse and fine Sn. For fine Zn powder, a completely homogenized solid solution of α-aluminum with Zn was obtained after the sintering by holding the samples at 620^{o}C. Absence of liquid phase was found on the particles boundaries and unsintered microstructures were observed with limited particle connectivity. For coarse zinc powder, α – aluminum reacted with it and starts forming a liquid phase for the initiation of liquid phase sintering. Holding the samples at the sintering temperature further homogenize it. Metallographic

examination revealed that the liquid phase remains three times longer and formed in double amount in case of using coarse zinc powders. Copper powder with aluminum system started forming eutectic above 548^{o}C for liquid phase sintering. Coarse Cu powders helped in forming large liquid pools compared to fine Cu powders. Fine Cu powders thoroughly reacted with aluminum matrix at 600^{o}C and start forming liquid phase throughout over next 5 minutes. While coarse Cu powder penetrates the particle and grain boundaries, initiating a rearrangement in melt pools at 600^{o}C.This process continues for the next remaining duration of sintering. Extensive sintering densification was found for a total sintering time of 40 minutes. A 3% increase in density up to 92% of theoretical density was found for fine powders and for coarse powders a total of 7% increase up to 94% of theoretical density was found. Coarse powder addition resulted in large porosities inside the sintered sample with a well bounded structure. Whereas addition of fine powders resulted in small porosities throughout the sintered region however the structure was found unsintered and loosely bounded.

The authors again investigated the effect of coarse and fine copper in Al-4 Cu elemental system [Lumley and Schaffer, 1998]. It was found that high densification was found in all size of copper addition with high heating rates. Authors selected three particle sizes of Cu as fine < 45μm, intermediate as 75 - 106 μm and coarse 125 - 150 μm and observed sintered densification as well as mechanical strength. The yield strength was tested and found independent of particle size.

2.2.3.3 Effect of liquid phases

Sintering of powders is strongly affected by variation in particle size and its dependency of sintering atmosphere thoroughly discussed in the above section. These two factors also have an interconnection with the liquid phase generated during sintering. The need for transient liquid phase exists to fill the pores completely apart from metallurgical bonding. Schaffer et al., 2001 studied the effect of liquid phase generated by Mg or Sn on aluminum matrix and found that a maximum content of Mg with 0.15wt% was sufficient to cause an optimum shear stress for breaking of the powder particle boundaries. The role of Mg was more clearly explained in the presence of Sn. Sn forms a liquid phase due to its low melting point (232^{o}C) and it only wets aluminum in the presence of Mg otherwise it seeps out. Sn has a maximum solid solubility <0.15% in aluminum while aluminum is completely soluble in liquid Sn. Self diffusivity of Sn is five times less than the diffusivity of Al in liquid Sn [Schaffer, 2004].

Sercombe and Schaffer, 1999 reported a 20% increase in properties with addition of 0.1wt% Sn in a traditional 2xxx series alloy (Al–4.4Cu–0.8Si–0.5Mg). Schaffer et al., 2001 summarized the key factors for designing an ideal liquid phase sintering system. The additive should have a lower melting point than base; a low melting point eutectic is less beneficial as liquid fraction does not form spontaneously. The solubility of the additive in base should be low, ensuring segregation on particle confines, which increases the liquid volume fraction. Solid solubility of the base with the additive is not an essential, but liquid solubility of the base with the liquid additive is a necessary condition. High diffusivity of the base in the additive liquid ensures high rates of mass transport and rapid sintering. Al-Mg system is greatly affected by liquid phase of Sn and its effect on sintering response was studied by MacAskill et al., 2010 with respect to microstructure and mechanical properties. Authors observed that trace addition of Sn in the Al-Ni-Mg alloys promotes sintering and excels the tensile properties compared to 6061 and 2014 alloys.

Martin and Castro, 2003, explored the effect of processing parameters on liquid phase sintering (LPS) of some common pre-alloyed aluminum powder mixes corresponding to age hardenable 2xxx, 6xxx and 7xxx wrought counterparts. Of the 2xxx pre-alloyed powder, two compositions were explored. Both exhibited introductory swelling due to presence of a liquid phase which helped in further densification during later stages of sintering. Higher sintering temperatures for the 6xxx alloy resulted in better final density due to larger liquid fraction which aided progressive densification. However, the age hardening response under T_4 (natural ageing) did not significantly differ for two sintering temperatures, indicating grain coarsening but higher density did not render into higher hardness; hardening phases namely Al_2Cu, Mg_2Si and $MgZn_2$ were detected for the three alloys respectively, in the as sintered state.

In the sintering response of a traditional 7xxx series Al–8Zn–2·5Mg–1Cu alloy mixed with trace additions (upto 0.16 wt.%) of Pb, Sn, Bi, Sb and Se; it was observed that the base composition along with Sb and Bi resulted in a net expansion, Se had no effect while Sn and specifically Pb were beneficial [Schaffer and Huo, 1999]. Maximum improvement in tensile strength was observed with the addition of a pre-alloyed Zn-Pb master alloy; however elemental Pb alongwith the master alloy had no effect in the improvements. The mechanism abaft this observation was not explained and left to further investigation. Zn is the most important element in the 7xxx series high strength alloys, primarily on account of being capable to form a low temperature eutectic (380°C) with aluminum and its ability to form a persistent liquid phase for augmenting sintering densification and further improving the ageing response; but the solid

solubility of Zn in aluminum makes it a non-ideal candidate as a sintering aid, even with traces of Pb. The addition of Cu, however, created a net shrinkage at the sintering temperature. The other benefits of Cu include improved wetting and formation of $CuAl_2$ intermetallic at the particle boundaries when added up to a critical liquid volume fraction due to the formation of a supersolidus liquid phase sintering system (SLPS). German, 1997, has stated that a SLPS occurs when a pre-alloyed powder is heated to a temperature between the solidus and liquids and the liquid phase nucleates within each particle. Densification occurs by viscous flow, which starts when the fractional liquid coverage of the grain boundaries reaches 73%. This liquid phase evolving out of the pre-alloyed particles is very sensitive to heating rates (40^oC/min with a 20 min sintering time), wherein, slower rates cause homogenization activated by solid-solid solutionizing at the sintering time. Particle growth during liquid phase sintering [Yu et al., 1997] was found absent during short sintering times. Hence the sintering parameters eg. sintering temperature, sintering time, heating and cooling rates also have an important significance ensuring the liquid phase sintering.

2.2.4 High Density Processing in P/M route

It has been identified that powder consolidation methods themselves depend on the powder characteristics such as their reactivity, limited ductility at room temperature, high melting points, etc. Over the years, several high density processing routes have been developed which may be categorized as: pressure based densification, temperature (sintering) based densification, and hybrid densification where both pressure and temperature are simultaneously applied. The important high processing techniques are described briefly in the following paragraphs.

2.2.4.1 Hot Pressing

In hot pressing, powder or a green compact is placed at high temperatures in a graphite die for heating and then compacted uniaxially at low strain rate. It is one of the oldest methods of consolidation of powders through P/M route. Heating is carried out in protective atmosphere of argon, nitrogen or sometimes in vacuum depending on the material to be consolidated. Hot pressing of aluminum alloy composites gives significant improvement in relative density, hardness and wear resistance compared to traditional press and sinter route [Hosseini et al. 2010]. Although hot pressing produces quality products but its use is restricted due to some disadvantages like

protective atmosphere, hot die loading, welding of powders to the die walls, tool wear and low production rates.

2.2.4.2 Hot Isostatic Pressing (HIP)

It is a powder consolidation technique in which a hydrostatic pressure is applied to the powders at a higher temperature. The process started in 1976 and is still applicable in aerospace industry [Atkinson and Davies, 2000; Billard et al., 2006]. Many researchers have applied this process for consolidating their powders. HIP was found satisfactory in term of densification however due to high cost associated; the process is applied for special purposes [Vogt et al., 2009]. HIP is applied for a wide temperature range, 480^{o}C for the light metals like aluminum and 1700^{o}C for pressing of heavy metal powders like tungsten. Current applications of HIP include fabrication of nickel based super alloys for aircraft applications and compaction of titanium preforms for hot forging.

2.2.4.3 Equal channel angular pressing (ECAP)

It is a consolidation technique which is based on severe plastic deformation using a channel. The channel is composed of two identical channels which are placed at some angle next to each other (generally right angle). Sample in the form of either green compact or sintered preform is inserted from one end and pressed with a ram so that is can be received from another end. It is advantageous for nanoconsolidation of powders where it is difficult to disperse the nanoparticles into the matrix. Many researchers applied the technique for the consolidation of aluminum, its alloys and its composite powders [Figueiredo et al., 2007; Stolyarova et al., 2003]. The process is successful for producing fine grain structure in pure metals and alloys. It is also a satisfactory method for the dispersion of less amount of reinforcement in a matrix phase however it is not successful for composites having higher amount of reinforcements [Derakhshandeh and Jahromi, 2011]. Recrystallization was found during equal channel angular extrusion of Al-Li based alloys, performed at room temperatures [Giribaskar et al., 2012].

2.2.4.4 Powder Rolling

Powder rolling is the commonly applicable forming process for consolidation of sintered preforms as well as direct powders [ASM Handbook Vol.7]. Rolling is accomplished by squeezing action on the material by placing it between two rollers. Sintered preforms are directly placed

between the rollers whereas powders are filled in a metallic can and rolled. Composites having aluminum alloy matrix (Al-7075) have been developed by powder rolling technique commonly by rolling of blended powders or lamination of sintered Al-7075 powders with other metals [Jimenez et al., 2009]. Apart from improving density and other static mechanical properties, rolling is a method of increasing dynamic properties like fatigue resistance of aluminum alloys [Majzoobi et al., 2009].

2.2.4.5 Powder Extrusion

Extrusion is a high stress, high strain rate process to produce long shapes with constant cross section at high temperatures usually performed on encapsulated powder or powder compacts. Oxide dispersion strengthened alloys, copper, aluminum, stainless steel, tool steels and nickel base super alloys are few examples which are used for high temperature applications and are processed by extrusion. Extrusion of aluminum powder results in a ligament like morphology of the deformed powder particles, which are surrounded by several bands of aluminum oxide [Woods et al., 1998]. UTS of 745 MPa of the 7xxx series extruded alloy at peak aged condition can be achieved by extrusion [Mondal et al., 2007].

2.2.4.6 Powder Forging

Since powder forging is principally applied as consolidation technique for the powders in the present study, it is dealt separately in the coming section.

2.2.5 Aluminum Alloy 7075

Amongst all the aluminum alloys, 7xxx series alloys have highest strength to weight ratio and therefore have found wide applications in automobile and aerospace industries. However these alloys lose their strength when exposed to high temperatures. This rapid decline in strength is directly related to coarsening of precipitates which are then not as effective in obstructing the dislocations. In general mechanical properties of 7075 in T_6 condition (artificially aged condition) proved out to be the best in all 7xxx alloys of aluminum through powder metallurgy as well as other routes. A generalized chemical composition of 7075 alloy in wrought form is presented in Table 2.1.

Table 2.1 Chemical composition of Al-7075 [Bruke and Weiss, 2012]

Element	**Zn**	**Mg**	**Cu**	**Cr**	**Fe**	**Si**	**Mn**	**Ti**	**Al**
Wt %	5.295	2.475	1.590	0.197	0.086	0.044	0.020	0.009	Balance

Different alloying elements have a different role in Al-7075 alloy and the functions of these elements are dependent upon the processing method. Major alloying elements in Al-7075 are magnesium, zinc and copper. In powder metallurgically processed Al-7075 alloy, role of magnesium is to form spinal which helps in breaking of powder particle boundary. Zinc facilitates the liquid phase formation due to its low melting point and in excess form it forms strengthening precipitates with magnesium. Copper enables a super solidus liquid phase sintering system at sintering temperature and helps in filling the pores. These three major alloying elements and their role in alloy system are discussed in details in upcoming sections.

2.5.5.1 Physical and mechanical properties of Pure Al-7075 alloy

Al-7075 is an aluminum alloy which has the highest strength to weight ratio amongst all alloys of aluminum. The physical properties of pure Al-7075 cast alloy, provided by the Aluminum Association, Inc. are listed in the following table.

Table 2.2 Physical and mechanical properties of Pure Al-7075 alloy [ASM Specialty Handbook: Aluminum and Aluminum Alloys, 1993]

Physical Properties	**Metric**	**English**
Density	2.81 g/cc	0.102 lb/in³
Mechanical Properties		
Hardness, Vickers	175	175
Ultimate Tensile Strength	572 MPa	83000 psi
Tensile Yield Strength	503 MPa	73000 psi
Elongation at Break	11 %	11 %
Modulus of Elasticity	71.7 GPa	10400 ksi
Poisson's Ratio	0.33	0.33
Fatigue Strength	159 MPa	23000 psi
Fracture Toughness	29 MPa-m½	26.4 ksi-in½

Machinability	70 %	70 %
Shear Modulus	26.9 GPa	3900 ksi
Shear Strength	331 MPa	48000 psi
Electrical Properties		
Electrical Resistivity	5.15e-006 ohm-cm	5.15e-006 ohm-cm
Thermal Properties		
CTE, linear 68°F	23.6 µm/m-°C	13.1 µin/in-°F
CTE, linear 250°C	25.2 µm/m-°C	14 µin/in-°F
Specific Heat Capacity	0.96 J/g-°C	0.229 BTU/lb-°F
Thermal Conductivity	130 W/m-K	900 BTU-in/hr-ft²-°F
Melting Point	477 - 635 °C	890 - 1175 °F
Solidus	477 °C	890 °F
Liquidus	635 °C	1175 °F
Processing Properties		
Solution Temperature	466 - 482 °C	870 - 900 °F
Aging Temperature	121 °C	250 °F

Al-7075 is an alloy which exhibits age hardening response; hence the properties of wrought Al 7075 in different heat treatment conditions differ which are shown in Table 2.3.

Table 2.3 Properties of wrought Al 7075 in various heat treatment conditions [Bruke and Weiss, 2012]

Properties	**UTS (MPa)**	**Yield Strength (MPa)**	**Hardness (Brinell no. 500kg/10mm)**	**% elongation in 50 mm**	**Shear ultimate strength (MPa)**
7075-O (annealed)	230	105	60	17	150
7075-T_6 (artificially peak aged)	570	505	150	11	330
7075 T_4(naturally aged)	525	455	135	--	230

2.2.5.2 Role of Magnesium

Magnesium (Mg) is an alloying element without which it is not possible to sinter aluminum by any other means. It is either added to aluminum alloys as a major alloying element or present in trace additions. Phase diagram of aluminum with magnesium is presented in Fig.2.5. Mg has a melting point of 650 ˚C which is close to the melting point of aluminum. It has a solubility of 17.4 % at 177 ˚C and it can easily diffuse pure aluminum. Apart from a good solubility in aluminum, it can be easily soluble in other alloying elements of aluminum alloys and form different phases.

One of the major problems associated with aluminum alloys is the presence of oxide layer on the surface of the particles of the aluminum powder. Oxide layer is detrimental for the purpose of sintering as it does not allow the physical contact between the aluminum particles. Further it reduces the wettability which is one of the primary concerns in the P/M of Aluminum alloys. Dew point of <-140˚C or O_2 at partial pressure of $<10^{-50}$atm is required to reduce Al_2O_3, which is not achievable in the actual experimental conditions.

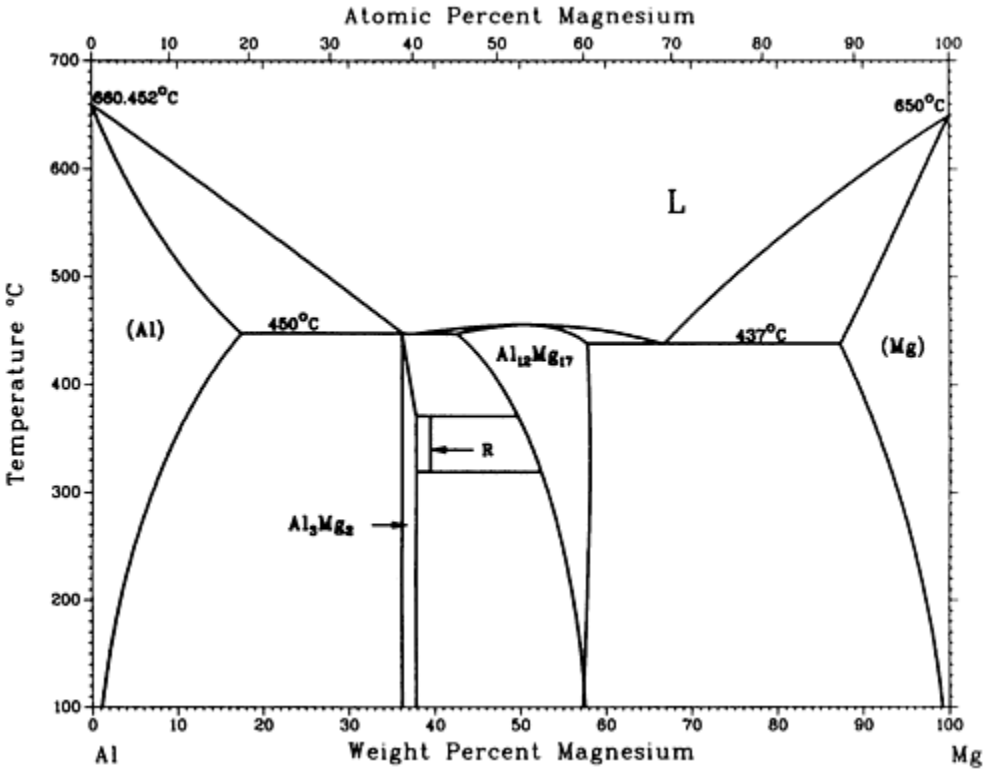

Fig. 2.5 Aluminum- Magnesium phase diagram [J.L. Murray, 1988]

Table 2.4 Solubility of some elements in aluminum at given temperatures [Martin et al., 2003]

Element	Temperature (˚C)	Solubility (%)
Zinc	170	70.0
Magnesium	177	17.4
Copper	275	5.65
Iron	382	0.05
Lithium	327	4.2
Mangenese	385	1.82
Silicon	304	1.65

Other ways by which this oxide layer can be partially removed is by heating or by plasma irradiation or by the mechanical action which can break the layer and introduce the fresh aluminum layer to the wetting liquid. This attribute can be achieved either during compaction or during secondary consolidation [Kondoh, 2001]. It is reported that Mg is highly benificial for the sintering of aluminum and its alloy powders. Mg reacts with oxide present at the powder surface rapidly due to its high affinity for O_2 then Al according to Ellingham diagram. Moreover, it reduces the oxide by the formation of spinel allowing metal - metal contact at particle interfaces and facilitating diffusion. Mg also acts as sintering aid in the presence of nitrogen atmosphere. Another effect of Mg is to enhance the passage of Zn in the matrix which allows some shrinkage at the sintering temperature. Enhancement in mechanical properties has also been reported due to the addition of magnesium as it contributes to the precipitation hardening phenomenon. The reason for this improvement was the high solubility of elements in aluminum in liquid phase as shown in the Table 2.4 due to which it can form not only binary as well as ternary phases with the solvent but as well as with other alloying elements [Martin et al., 2003]. Apart from reducing oxide from the powder surface, magnesium acts as an excellent wetting agent with and without the presence of other alloying elements. MacAskill et al., 2010, studied a ternary Al–1.5Mg–1.5Sn alloy, with Mg having both a master-alloyed and an elemental presence. It was observed that Sn alone, in spite of being the liquid phase, was not able to wet the aluminum, it was only with the presence of Mg that the wetting was activated. Higher densification was achieved in alloys with elemental Mg (upto 99.5% theoretical density). Sn was instrumental in lowering the mass gain observed in sintered

samples, thereby, resulting in increased sintered density, but this effect was pronounced in the presence of elemental Mg. This phenomenon can be attributed to higher wettability induced by Mg, wherein Sn was better able to coat the exposed aluminum particles and hinder AlN formation. Considering only the elemental addition of Mg, the ductility, under tension, increased upto 1.5 wt. % Sn and decreased thereafter.

Kondoh et al., 2001, investigated the effect of Mg on the sintering behavior and mechanical properties of Al-12Si pre-alloyed powder with elemental Sn additions under N_2 atmosphere. Presence of Sn, resulted in negligible nitridation of both the pressed compacts and raw powders, owing to a persistent liquid phase that covered the particles. However, the presence of Mg aided nitriding, even with presence of liquid Sn at the sintering temperature. Consequently, an increased intensity of metallic α-aluminum has been detected aided by Mg, through 0 to1.0 wt% addition. Even under the influence of Sn (upto 1.0 wt%); Mg results in disruption of large surfaces of Al_2O_3, incompletely wetted by liquid Sn; leading to formation of AlN. The presence of Mg, results in higher sintered densification by a factor of 2, smaller pores and a better metallurgical bond between the particles. It also adds an advantage of higher elongation to failure and a dimpled fracture surface as opposed to premature brittle fracture along prior particle boundaries (PPB's) in chemistries with only Sn additions.

2.2.5.3 Role of Zinc

Zinc has a melting point (420˚C) and forms eutectic with aluminum at 380˚C which can lead to the enhancement of the sintering process by generation of liquid phase. Zn has the highest solubility (70 %) in aluminum at elevated temperature providing it a maximum benefit. The Al-Zn binary phase diagram including different phases is shown in Fig.2.6 It has also been reported to impart excellent densification during sintering and high tensile strength [Schaffer, 1999]. It therefore has the potential to enhance sintering by the generation of liquid phases which might persist for long periods but eventually dissolve in the matrix and can contribute significantly to precipitation hardening.

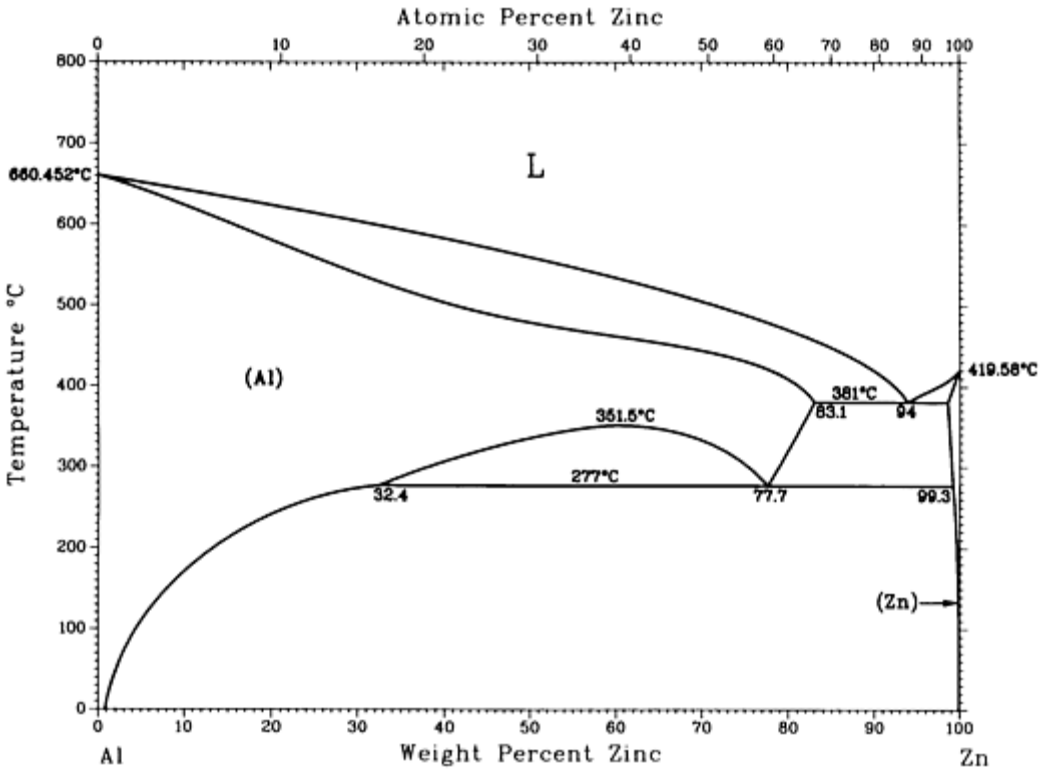

Fig. 2.6 Aluminum- Zinc phase diagram [J.L. Murray, 1983]

Role of Zn was further studied by Mohammadi et al., 2010; and Shahmohammadi et al., 2007. They investigated the phase evolution in elementally prepared Al–5.6Zn, Al–5.6Zn–2.5Mg and Al–5.6Zn–2.5Mg–1.6Cu (wt-%) powder mixes. In the Al-Zn powder mix, an expansion was recorded at 420°C, corresponding to bulk melting of Zn. This liquid phase due to bulk melting was transient in nature owing to excessive dissolution of Zn in aluminum at this temperature. However, this liquid phase aided in a net densification at the sintering temperature (600°C). Addition of Mg to the Al-Zn powder mix improved net densification after an initial dilatation due to melting of Zn by formation of an intermetallic eutectic between $Mg_{17}Al_{12}$ and Mg; further heating to the sintering temperature resulted in ternary intermetallics of Al-Zn-Mg. Densification was aided by presence of these intermetallics and pore filling effects due to capillarity and particle rearrangement. These intermetallics improve the densification and other properties itself and there is no need for excess control for phase selection like in other intermetallic alloys [Tsakiropoulos and G. Shao, 2004; Dey et al., 1994].

The disadvantage of having high solubility of zinc in aluminum as discussed by Schaffer, 1999, stated that expansion occurs during sintering rather than a positive shrinkage in the sintered

compact. This expansion is taken care by the presence of magnesium. Magnesium has a positive effect on shrinkage as already discussed in the previous sections. Presence of Zn has been reported to enhance the rate of precipitation hardening and can also act as sintering aid to the powder metallurgy process. For the Al-Zn-Mg-Cu compacts, initial swelling due to zinc was even more pronounced, but densification was aided at the sintering temperature by formation of Al-Cu eutectic in liquid phase [Schaffer et al., 2001]. The effect of reduced porosity, aided by liquid phase system, has a direct bearing on the mechanical properties of the alloy system investigated. The addition of Mg and Cu to the Al-Zn alloy has a strengthening effect by precipitation hardening; this effect is even more amplified by reduced porosity levels. Increasing the Zn and incorporation of Al-Mg master alloy powder particles is reported to give better strength and overall ageing response.

2.2.5.4 Role of Copper

Copper has a comparatively high melting point (1084˚C) than aluminum and it is added to aluminum alloys for liquid phase sintering as well as for providing high strength. It has a solubility of 5.65 % at 275˚C. The aluminum- copper phase diagram with different phases is shown in Fig.2.7

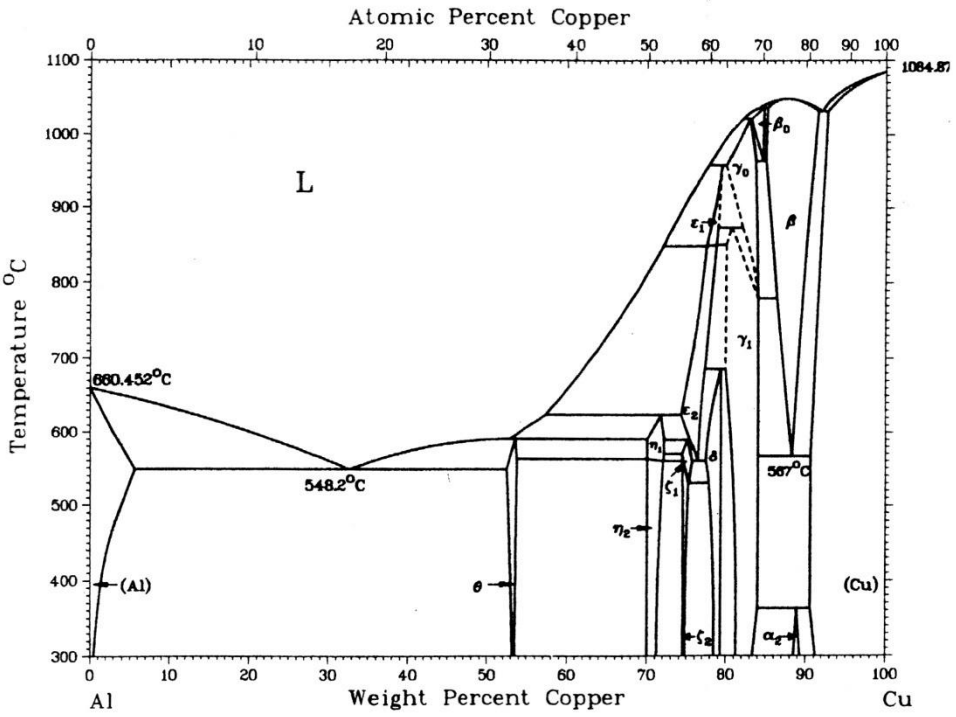

Fig. 2.7 Aluminum- Copper phase diagram [J.L. Murray, 1985]

Addition of Cu is reported to effectively improve the sintering response and to produce high theoretical density as well as high strength. Presence of Cu between 1-2 wt% offer great precipitate hardening effect due to its contribution to the zone forming. Low porosity was also observed with Cu as it forms a eutectic with Al hence improving the densification. Delgado et al., 2005, investigated the addition of Al-12Si (eutectic) pre-alloyed powder to pre-alloyed as well as elemental AA2014 as a sintering aid with a low Cu content. The mechanism described here was reduction in the contact angle of the liquid phase with the aluminum particle, thereby, increasing the time for Al_2Cu (θ) to stay in the liquid phase, which forms at 548°C. This aluminum-copper eutectic is transient in nature and in low Cu levels may be completely absorbed into α-aluminum. The Al-Si eutectic forms at a higher temperature of 578°C. Increased densification alongwith improved mechanical properties was observed at sintering temperatures in the 580-620°C range, with the addition of Al-12Si. Hence, increased wetting of the low temperature Al-Cu eutectic can be aided by introduction of another liquid phase, with reduced contact angle; will ensure delayed absorption into α-aluminum, increasing the duration of transient aspect and hence improved densification.

Moreover Cu also contributes significantly to the corrosion resistance of the 7xxx alloy. It has also been reported that Cu acts as a pore filling agent in the presence of reinforcements resulting in little more densification and better sintered strength. Due to limited solubility of Cu in Al at room temperature, the quantity of Cu added to 7xxx alloys has been restricted to less than 2.5 %.

2.2.5.5 Precipitation and dispersion hardening

Precipitation hardening involves the hardening of the material over a sustained time, is also called age hardening, or ageing. It is a heat treatment process through which, the hardness or strength of some heat-treatable aluminum alloys can be increased by the formation of nano sized second-phase precipitates within the matrix. The fine precipitates in the alloy impede dislocation movement by forcing the dislocations to either cut through the precipitated particles or go around them. By impeding dislocation movement at the time of deformation, the alloy is strengthened [Tibor, 2011].

Major aluminum alloy system with precipitation hardening includes Al-Cu system with strengthening from $CuAl_2$, Al-Cu-Mg system (Mg intensifies precipitation), Al-Mg-Si system with strengthening from Mg_2Si and Al-Zn-Mg with strengthening from MgZn2 & Al-Zn-Mg-Cu

systems [ASM Handbook Vol. 4, 1991]. The precipitation-hardening process mostly involves following three basic steps:

(a) Solution heat treatment, or homogenization, is the first step where the alloy is heated between the solvus and solidus temperatures and soaked until all of the soluble phases are dissolved and a homogeneous solid-solution structure is produced.

(b) Quenching is the second step where the solid solution is rapidly cooled to a lower temperature, usually room temperature. This forms the formulation of a supersaturated solid solution since the solubility of one or more alloying elements in aluminum decreases with decreasing temperature.

(c) Aging is the final step of the process that allows controlled decomposition of the supersaturated solid solution and the formation of strengthening precipitates. It is the process where the supersaturated solution is heated below the solvus temperature to produce a finely dispersed precipitates. When ageing occurs at room temperature, it is called natural ageing. Ageing above room temperature is called artificial ageing.

The general array of precipitate aging after a solutionising and quench treatment in 7075 alloy matrix can be expressed as [Evangelista et al., 1988]: Supersaturated solid solution → Guinier-Preston zones (GPZ) → η' (MgZn2) → η (MgZn2). There are two types of GP zones GP (I) and GP (II). GP (I) are formed over a wide temperature range from room temperature to 140-150^{o}C independent of quenching temperature. GP (II) are formed due to quenching from temperature above 450^{o}C by aging temperature above 70^{o}C. The GP (II) zones consists of a zinc rich layer. At higher temperature GP zones transforms into transition precipitate known as η' (MgZn2). At peak aging GP zones diameter is 2 to 3.5 nm along with some amount of η'. Nature of these zones is still uncertain (have high concentration of Zn atoms and Mg atoms as well). To gain hardness, the specimen should be heat treated to yield a fine dispersion of small particles (coherent). Unfortunately there is a tendency when thermodynamic equilibrium is reached for small precipitates to shrink and large precipitates to grow. This will lower the surface to volume ratio of the precipitates, the surface energy and therefore the energy of the system. As a result at some point in the aging of AA-7075, the precipitate begins to coarser and on average the spacing between them gradually increases. As the temperature of heat treatment is increased, the spacing of the precipitates also increases. At this point the hardness and yield point will begin to decrease with time of aging. Coarsening is dependent on movement of atoms (diffusion). Movement of atoms is dependent on the temperature. At higher temperatures the atoms move faster so peak

aging time reaches sooner as well as coarsening of precipitates also occur earlier. Precipitation kinetic of Al-Cu-Mg and Al-Cu-Mg-Sn alloys was presented in details by Banerjee et al., 2010.

Shercliff & Ashby, 1994, explained three physical elementary mechanisms involved during the precipitation process namely nucleation, growth and coarsening. Based on the treatment of these three processes, modelling of the precipitation kinetics in aluminum alloys can be divided into two main approaches. One of the approaches is based on the Shercliff-Ashby process model in which only one average particle size is assumed and the three processes are considered in isolation with the assumption that one process is essentially complete before the next one begins. This process model draws knowledge of the kinetics of microstructure evolution with dislocation behavior, in order to determine the mechanical properties. Adachi et. al., 2001, developed the super-high strength Al-Zn-Mg-Cu alloys (Mesoalite) by the combination of precipitation hardening with other distinct strengthening mechanisms. Authors fabricated these alloys with different chemical compositions of the alloying elements. They found UTS values ranges 573 to 910 MPa and compressive strength upto 1 GPa in the critically developed alloy compositions. Such high strength achievement of these alloys is explained especially by nano-scale coherent precipitates [Shao and Tsakiropoulos, 2000]. Marlaud et al., 2010, observed evolution of precipitates with a different heat treatment process on a Al–Zn–Mg–Cu alloy. They applied retrogression and re-ageing (RRA) treatment which is a three-step heat treatment, in place of traditional two step heat treatment; applying a small plastic strain to the sample thereafter holding it at different temperatures for three different sets of time intervals. During the treatment nucleation of new precipitates was observed with a high Cu concentration leaving the matrix Zn rich. Du et al., 2006, studied evolution of precipitates in 7xxx series alloy with respect to precipitate size and volume fraction. Authors have modeled precipitate size and volume fraction by applying Shercliff and Ashby equations and modeled particle coarsening effect by explaining the evolution of the average size of the precipitates, using LSW (Lifshitz–Slyozov–Wagner) model. They investigated nature of precipitates with the help of TEM after aging at 120 °C for 24 h and found these precipitates as metastable η′ and equilibrium η.

The evolution of precipitates requires temperature to nucleate and time to grow, not necessarily processed by conventional aging process. A similar process; generally termed as creep aging, was seen during creep testing of 7075 aluminum alloy by lin et al., 2013. Intermediate precipitates ($Al_{18}Mg_3Cr_2$ and Al_3Zr) and coarse insoluble precipitates (Al_7Cu_2Fe and Mg_2Si) were found during the study. They found the main aging precipitates in η′ and η phases, and observed

an increament in the amount of aging precipitates with increase in creep temperature and applied stress. Precipitation free zone (PFZ) was found at the grain boundary and the width of this zone was observed smaller in the creep aged sample than that in the traditionally aged sample due to a high dislocation density at the grain boundary resulting in higher nucleation of precipitates at grain boundary region. The precipitation free zone at the grain boundary was further studied by Cai et al., 2007, with its relation to different types of grain boundaries (GBs). The authors obtained 502 GBs in total with a misorientation axis/angle and PFZ width by TEM measurements. Different width of PFZ was observed with different sets of GBs and suggested that the formation and growth of PFZs at GBs should be closely associated with the core structure in addition to the geometric structure of GBs.

2.3 Powder Forging

Forging in powder metallurgy denotes the cold or warm consolidation of either loose powders or sintered preforms at higher strain rates. Griffiths et al., 1976 reported three principal modes of compact consolidation of loose powder or powder compacts by forging, namely (1) free axis-symmetric compression, in absence of lateral constraints (2) upsetting, regarded as plane-strain compression with restrained flow along one principal direction (3) re-pressing under total constraint in a closed die configuration. Pore closure characteristics were presented as: (1) pore closure in pressing direction with pore alignment along lateral direction-minimum densification under a tri-axial stress state (2) pore closure in pressing direction followed by enhanced densification due to lateral restriction imposed under a bi-axial stress state (3) pore closure in pressing direction to near full density by fully constrained deformation of the powder compact respectively for the three deformation modes discussed above. The lateral spread of pores results in a particle to particle shearing effect, which is responsible for elongation and final closure of pre-existing, predominantly spherical pores with increasing deformation strain and/or restrictions posed by a rigid die for upsetting or re-pressing modes. Closed die upsetting will eventually approach re-pressing mode in the last stages of deformation, when the flowing material contacts the die walls. During upsetting there is a limit of imposed lateral strain above which pore flattening causes a tensile strain and initiates crack [Upadhyay, 1997].

Forging process is determined by several factors which include preform porosity, projected area of load, oxygen content, alloy composition, particle size and shape of preform. In addition to processing variables, other factors encompass like compact and die temperature, lubricant,

imposed strain and strain rate. Hydraulic presses in manual or automated operating mode generate 10^{-1} s^{-1} in comparison to a Weingarten friction screw-type press which is capable of upto 10 s^{-1}; followed by a mechanical percussion press offering an average strain rate of upto 32 s^{-1} [Venugopal et al., 1990]. Hendrickson et al., 2000 have outlined the following conditions for realization of porosity free sinter-forged steel components (1) the applied forging stress should be at least 5 times greater than the bulk flow stress of the material being forged; (2) excessive lateral plastic flow by upset forging is not a sufficient pre-condition for attaining pore closure and enhanced ductility of the component, in fact, large deformation strains may impact tooling life and cause surface cracking on the preform; (3) the tool-workpiece contact time should be limited to a few milliseconds- only achievable by presses capable of high ram speeds (4) for components undergoing high tensile and/or fatigue service, the residual porosity should be below 0.5% alongwith very low oxygen content; (5) forging tools and equipments coupled with an integrity having real time monitoring of forging strokes and ram speed are concerned factors. Other ideal parameters include the control of overall cycle time of preform loading, forging and ejection under protected atmosphere.

2.3.1 Powder Forging of Aluminum Alloys

Powder forging of Al- alloys generally has equipments and setup similar as traditional forging. Sintered performs are generally forged in a closed die whereas loose powders are either forged directly in a closed die or forged in a semi- closed open die by filling in metallic can. High strength sinter forged aluminum alloys of SUMI-ALTOUGH^{TM} series were developed by Odani, 1994 having alloying element beyond solubility limits. The aluminum alloy series of non-equilibrium dispersion strengthended alloys were formed by rapid solidification process (RSP). Aluminum alloys like Al-Si, Al-Si-X, Al-X and Al-C (X- Fe, Ni, Mn, Cr) fabricated with powder forging route were found with higher mechanical and thermal properties than conventional ingot metallurgy [Das, 1990]. He reported specific expansion in high-temperature strength, wear resistance and elastic modulus. Specific applications of these powder forged alloys were reported in compressor vane, piston, cylinder liner and connecting rod for high temperature strength, wear resistance and elastic modulus.

Powder forging of Al faces a problem of oxide layer on individual powder particle. To avoid this Iwata et al., 1989, described a method for fabricating pistons by powder forging of rapidly solidified Al-20Si-4.8Fe-2.2Cu-1.2Mg-1.1Mn, pre-alloyed powder. The major steps

included cold compaction, canning and degassing at 400-500ºC under high vacuum, followed by extrusion at 350-500ºC, de-canning the extruded sample and forging it under shaped dies at 400-500ºC to yield a rough piston, which was further solutionized and artificially aged. The maximum strain was limited to 43% with a strain rate of 0.24. The authors overcame surface cracking by limiting the oxygen content to below 600 ppm by vacuum degassing of starting powder with an oxygen content of upto 2000 ppm. The role of major alloying additions has been justified as: Fe- high modulus, Si- abrasion resistance, Cu- interparticle bonding under high Fe/Si content and age hardenability, Mn- dispersoid strengthening at elevated temperature.

The forging of powder samples can be also performed after pre-consolidation of powders. Siegert and Ringhand, 1994, have outlined the benefits of pre-consolidated (by extrusion) forging stock which can be worked on conventional forging system shown in Fig.2.8. It is used to fabricate powder forged connecting rods by closed die flashless forging for improved surface finish, better feedstock utilization and higher fatigue resistance. DISPALTM series of RSP powders reported in the study comprise of spray deposited DISPAL-STM (Al-17Si-5Fe-3.5Cu-1.1Mg-0.6Zr) for elevated temperature and high stress applications. Optimum workability condition was determined by hot torsion tests which rely on strain, strain rate and temperature.

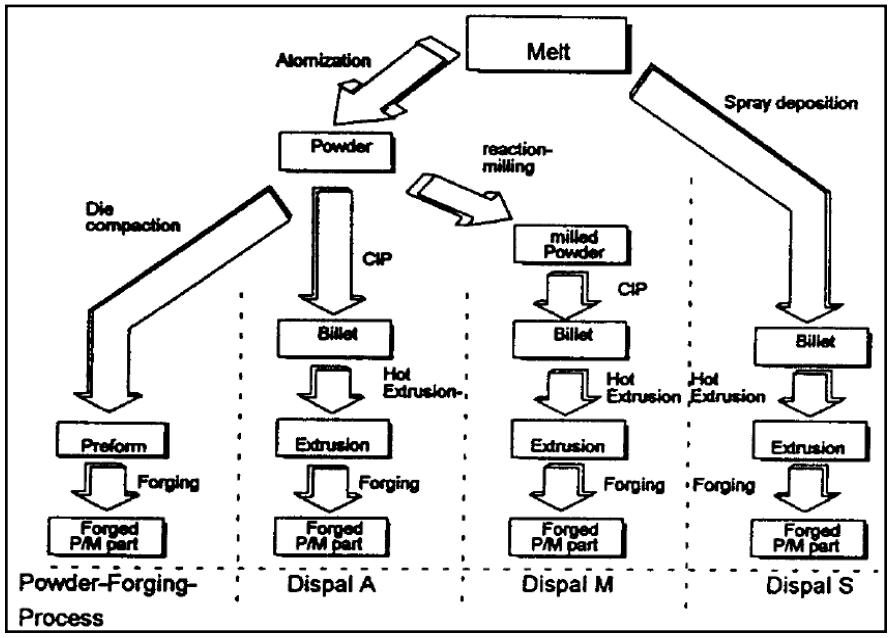

Fig. 2.8 Processing routes for powder forged connecting rods (Siegert and Ringhand, 1994)

Effect of deformation strains have a direct relation with microstructure and properties of material, either the deformation is provided by forging, extrusion or by complicated forming

processes with laser heating [Mosecker et al., 2013]. Dashwood and Schaffer, 2002, have investigated the effect of deformation strain on pore closure during hot upset forging of high density (~96%) sintered Al–3.8Cu–1Mg–0.8Si–0.1Sn P/M alloy preforms over 350-500ºC, employing strain rates of 1, 10^{-1}, 10^{-2} and 10^{-3}. An increase in porosity was observed while moving away from the center of the preform, due to a circumferential hoop stress that develops over the freely expanding outer layers during upsetting. Higher densification was achieved for higher temperatures by pore closure under a net compressive stress, in spite of lower strain distribution in comparison to lower temperatures. This effect was attributed to softening and dissolution of $CuAl_2$ (θ) phase with increasing temperature, resulting in homogeneous deformation and increased strain rate sensitivity at higher temperatures.

A major application of aluminum powder forging was found for the fabrication of powder forged Al-alloy pistons. Park et al, 2001, fabricated powder forged aluminum alloy pistons by optimizing the alloy chemistry with additions of Cu, Si, Mn, Mg and Ni to pre-alloyed Al-4.5Cu-0.5Mg-0.7Si (Si was varied from 0.5-1.5 wt.%). The authors also optimized sintering conditions by varying the sintering temperatures from 560-600ºC and sintering time from 20-30 min. Optimum parameters were established as: Si-1.5 wt%, 25 min and 580ºC. The aspect ratio (*d/h*) of sintered preforms was maintained at 1.0, 1.2 and 1.5 for determination of hot workability. Preforms were incrementally formed to the final shape of the piston, by visual inspection and FEM analysis. The authors optimized the starting shape of the sintered preform for final forging such that the forged piston was free of any density gradients and surface cracks, with complete die-filling. Forging temperature was optimized at 420ºC; with die maintained at 250ºC. Tensile strength (T_6- condition) of the optimized powder forged piston was upto 500 MPa, almost twice of that recorded for conventionally gravity cast piston and about 60% more than wrought forged counterpart of equivalent hardness.

Disruption and dissolution of oxide layer over powder particles is known to strengthen secondary processed aluminum P/M alloys. The oxide particles strengthen the metal by pinning grain boundaries during recovery, thereby retarding recrystallization [Hansen and Bay, 1972], alongwith enhancing wear resistance. Park et al., 2001 reported higher strength in comparison to conventional pistons when sintering atmosphere was changed from argon to nitrogen.

Optimization of mechanical properties of Al-7075 powder metallurgical alloy was carried out by hot forging. Ichikawa and Morita, 2010, experimented with the hot forging process parameters for achievement of optimum mechanical properties (T6- UTS > 500 MPa; elongation >

2%) for monolithic AA7075 powder metallurgical alloy. The authors have proposed constrained die upset forging for deformation based densification of the sintered compacts. Such forging is characteristic of pore closure obtained by combination of compressive and lateral strains. The degree of deformation (defined as the ratio of projected area of the sintered preform to the forged specimen) is limited to 40% for cold forging and 70% for hot forging. A 3% upsetting (re-pressing) ratio is sufficient to achieve pore closure in near fully dense sintered compacts. External cracks are generated at upsetting ratios greater than 70%. Lateral deformation enhances mechanical properties by dynamic recrystallization and fracture of precipitates.

Though the Al-Zn-Mg-Cu alloys produces approximately 99 % of theoretical density by sintering but remaining 1 % porosity need to be removed for better mechanical properties [Bishop et al., 2009]. The authors further investigated isothermal hot deformation behavior of sintered AA2024 and AA7075 pre-alloyed compacts within 360-520ºC, employing true strain rates of 10^{-3}, 10^{-2}, 10^{-1} and 10^{0} s^{-1}. The authors have proposed hot working of the sintered compacts to disrupt and disperse the oxide layer over powder particles and eliminate post-sinter residual porosity. The study resulted in very low elongation to failure for the sintered specimens, although with reasonably higher tensile strengths in both as-sintered (T_1) and artificially aged (T_6) states. An almost linearly increasing dependence was reported for flow stress with increasing strain rates, at a given temperature. Similarly, a decrease in flow stress with increasing temperature, was observed at a given strain rate. Hot-deformed densities were in the range of 99.5% of theoretical density for both the alloys. A linear variation of flow stress was found with temperature and strain which shows a good forgeability of sintered performs. Tensile strength of Al- 7075 and Al-2024 was improved as 28% and 22% respectively by powder forging, as well as ductility also got 5 times improved. Bishop et al. 2011 composed the hot forged P/M alloys with similar wrought alloys and found superior tensile strength and ductility of P/M alloys in T_6 condition.

The effect of hot forging on sintered pre- alloyed compositions was studied by Mosher et al. 2011. The authors studied isothermal hot forging characteristics of sintered hypoeutectic Al-6Si-4.5Cu-0.5Mg (Al-6Si) and hypereutectic Al-15Si-2.6Cu-0.5Mg (ALUMIX-231^{TM}, Ecka Granules, Germany) aluminum based pre-alloyed compositions at 360-480ºC. The authors employed true strain rates of 10^{-3}, 10^{-2}, 10^{-1} and 10^{0} s^{-1} for a total upsetting strain of 0.75. Flow stress increased in ALUMIX-231^{TM} with starting higher green densities and strain rates, showing higher values than Al-6Si. Reduction in peak flow stress was observed with increasing temperature. The flow curves were characteristic of peak stress followed by softening, most likely

promoted by dynamic recrystallization (DRX). Higher densification (increase in compact density over sintered density) was generally achieved by hot upsetting temperatures below 480ºC at slower strain rates for both the alloys. Strain rate and upsetting temperature had little effect on final forged density. The final forged density was more sensitive to starting sintered density and consequently compaction pressure in both the cases. Highest forged density of 98.3% was reported for ALUMIX-231^{TM} and 99.6% for Al-6Si, both compacted at 600 MPa. Al-6Si was more easily hot deformable, as pore closure and uniform distribution of hard Si particles was achieved. ALUMIX-231^{TM} generated voids by agglomeration and inter-particle cracking during forging due to little post-sinter porosity and higher volume fraction of hard Si particles.

Strain has an inherent role on metallurgical properties of powder samples and it was explained by Topping et al. 2013. The authors reported high strain rate forging (HSRF) of hot isostatically pressed (HIP) cryomilled P/M 5083 alloy for development of bulk nano-structured material. Canned and degassed batches of cryomilled P/M 5083 were consolidated by HIP'ing at different temperatures ranging from 125-500ºC, followed by HSRF at 400ºC, employing an initial ram speed of 6000 mms^{-1}. HIP'd compacts with different levels of porosity were consolidated to full density by HSRF. The increase in strength reported in the work was due to several factors. These factors included Hall-Petch effect attained by control over grain size; dislocation pile-ups by HSRF; solid solution strengthening by dispersoids and orowan loops formed around finely dispersed nitrides (AlN) and oxides (Al_2O_3/$MgAl_2O_4$). The secondary phases in the form of dispersoids and disrupted oxides are thermally stable [Tang et al., 2007] and their preferential presence at PPB's retards further grain growth by promoting Zener pinning at particle boundaries. The authors have reported the increase in average grain size with increase in the temperature during HIP'ing.

2.3.2 Powder Forging of Aluminum Matrix Composites

Powder metallurgically processed aluminium matrix composites have been successfully consolidated by powder forging similarly like Al-alloys however the role of reinforcement plays an important role. Sawtell et al., 1996 describes the omission of degassing prior to hot consolidation of cold compacted aluminum alloy based SiC particulate composite. Composites with upto 50 vol% reinforcement were developed by heating the cold compact (minimum 375ºC) in air or an inert environment, followed by hot upsetting, forging, extrusion or rolling. The authors have reported equivalent mechanical properties (UTS, elongation to failure, fracture toughness and

fatigue limit) by simplification of the overall fabrication process. The process explained replaces expensive canning and degassing steps, previously associated with hot consolidation of such aluminum composites. The mechanism of prior oxide film disruption and development of matrix interparticle bonding is aided by the abrasive action of hard ceramic reinforcement. Hunt, 2000a, has discussed the suitability of a large variety of reinforcements in P/M aluminum matrices for powder forging. The primary advantage gained from low cost direct powder forging of aluminum based composites was near-net shape fabrication of automobile components processed using conventional equipment. Hunt, 2000b, has compared the specific properties of different materials for automobile connecting rod. The author reported powder forged P/M 2080/15 vol.% SiC_p as a suitable DRA composite with equivalent specific modulus and specific fatigue strength in comparison to Ti-6Al-4V and ductile cast iron.

Powder forging of aluminum particulate composites by different authors was summarized by Badini et al. 2001. The author concluded some general observations on Al powder forging carried out by previous studies as: 1) microstructural degradation is caused by opening up of voids and cracks 2) fracture of reinforcing phase increases with increasing strain rate or decreasing deformation temperature 3) forgeability follows the same behavior as monolithic alloys showing decrease in flow stress with increasing temperature or decreasing strain rate 4) conditions for obtaining defect free forgings are either at higher temperatures or lower strain rates, which the authors remark as being commercially unviable 5) metal matrix composites with matrices of wrought alloy compositions exhibit better forgeability than matrices with Al-Si based cast compositions. Badini et al., 2001, have reported defect free forging of HIP'd P/M 2124/26 vol.% SiC_p composite using an upsetting ratio of 3.5:1 at 340ºC - 440ºC, employing a strain rate of $0.14s^{-1}$. Particle cracking or development of cavitation voids at the reinforcement-matrix interface was not observed after forging. However reinforcement banding and preferential alignment of SiC particles along a plane perpendicular to the forging direction was visible. The authors attribute the defect free processing to the fine size of the SiC particles (< 3 µm). An increase in tensile ductility was reported for as-forged composites in comparison to as-received material in both as-forged and T_4 (solutionized and quenched) state.

Chawla et al., 2002, evaluated the mechanical properties of sinter forged P/M 2080 alloy reinforced with 20 vol% SiC_p (average size 29 µm) and compared it with extruded composites. The process has been schematically shown in Fig.2.7. Important advantage with direct powder-forged consolidation of DRA composites has been highlighted as the realization of net/near-net

shape objects with elimination of bulk machining. The machining operation in case of ceramic reinforced materials is not only difficult but economically unfeasible for price-sensitive auto components. Forging results in a platelet like structure of SiC reinforcements sometimes looks like forging bands and generally termed as “pancaking”. However these structures are less prominent compared to reinforcement bands during extrusion of discontinuous reinforcement aluminium composites due to a less strain applied in forging. The sinter forged composite had higher strength with low elongation to failure in comparison to extruded counterpart. The reason explained for such behavior is the low strain deformation under forging causes lesser particle fracture. Extrusion induces higher particle damage, thereby lowering their effective load bearing capacity, but higher deformation strain in extrusion ensures better metallurgical bonding between the two aluminum particles, resulting in increased elongation to failure.

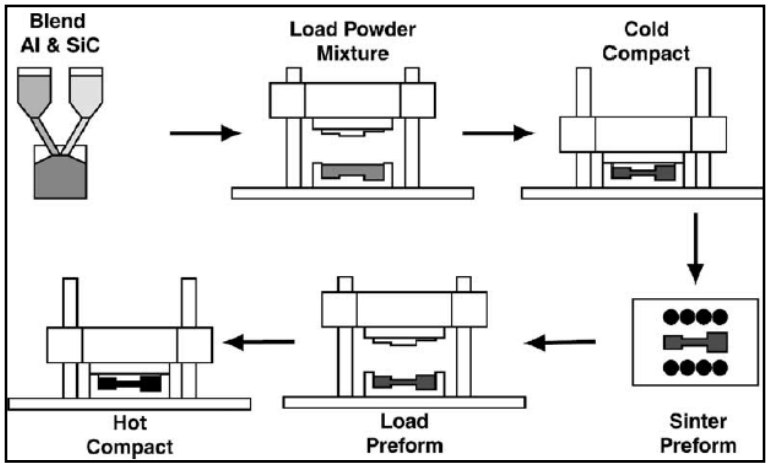

Fig. 2.9 Schematic representation of sinter forging process [Chawla, et al., 2002]

Effect of forging on different AMC’s having various reinforcement particle size has been studied by Chawla et al., 2002. Reducing the SiC particle size from 29 µm to 5 -10 µm creates non-uniform distribution of SiC by particle agglomeration. This result a failure by “pull-out” or matrix-particle interface decohesion. Comparing with sinter-extruded counterparts, the authors revealed that strength increased with reducing reinforcement particle size. The authors attribute fatigue performance of deformation processed composites to the presence of Fe-rich inclusions at the specimen surface which act as crack nucleation sites. Generally particulate composites offer better fatigue life under high-cycle/low-stress tests than unreinforced alloys due to load sharing by the high modulus reinforcement. Fatigue behavior of sinter-forged composites was equivalent to

sinter-extruded composites except in the high-cycle test regime. In high cycle test, poor interparticle bonding resulted in diminished fatigue life.

Baker et al., 1996, have reported the breakdown of particulate-whisker agglomerates by using a combination of closed and open die forging for fabrication of P/M 6061 SiC particulate and SiC whisker reinforced hybrid composites. The heated and degassed cans were hot forged at 530^{o}C. Strain of 35% was given under a closed die followed by open die upsetting to a strain of 40%. Single step closed die forging resulted in composites with reinforcement agglomeration, which was overcome by a secondary step of open die upsetting. This resulted in better mechanical properties (elongation and ultimate strength). The composites displayed an accelerated ageing response in comparison to monolithic alloy due to availability of nucleation sites near dislocations generated by difference in coefficient of thermal expansion of matrix and reinforcement.

2.4 Particulate Aluminum matrix composites

Aluminum matrix composites reinforced with particle reinforcements are reviewed in this section with different matrix materials composed of aluminum and its different alloys as well as various types of reinforcements.

2.4.1 Aluminum and alloy matrix

The best known characteristic of aluminum is its light weight, the density being one-third that of steel or copper alloys. Certain aluminum alloys have better strength to weight ratio than that of high strength steels [Avner S. H., 1997]. The most important characteristics of aluminum is its ductility, workability and machinability due to which it can be subjected to any mechanical processes. Its resistance to corrosion due to formation of oxide layer at the metal surface is beneficial for general purpose but is undesirable for the powder metallurgy technique. Depending upon the addition of other elements aluminum has different grades of alloys as shown in the table 2.5.

Aluminum alloys can be sub divided as heat treatable and non- heat treatable alloys. Basic requirement for the alloy to be heat treatable is increasing solubility of the alloying element in matrix with increasing temperature [ASM Handbook Volume 4, 1991]. The 2xxx, 6xxx and 7xxx series alloys fulfill this requirement and hence are heat treatable. These alloys exhibit nucleation of precipitates with respect to time and temperature due to alloying elements present in the system.

Table 2.5 Designation system for Aluminum Alloys

Major Alloying Element	Designation
Aluminum, 99.0% and greater	1xxx
Copper	2xxx
Manganese	3xxx
Silicon	4xxx
Magnesium	5xxx
Magnesium and silicon	6xxx
Zinc	7xxx
Other elements	8xxx
Unused series	9xxx

The 2xxx series of heat treatable aluminum alloys comprises a range of alloys all containing copper, together with other possible elements such as Mg, Mn and Si. The alloys of this series are used to manufacture high-strength products, and are largely confined to the aerospace industry. In the naturally aged T_4 condition, these alloys have mechanical properties similar to mild steel, with a typical proof stress of 250 N/mm^2, ultimate tensile strength approaching 400 N/mm^2 and good ductility. In the full strength T_6 condition, the proof and ultimate stress can reach 375 and 450 N/mm^2 respectively, but with reduced ductility. 6xxx series of aluminum alloys mainly contain Mg and Si. They combine reasonable strength with good corrosion resistance and excellent extrudability. 7xxx series of alloys mainly contain zinc and magnesium. These alloys can go up to tensile strength of 550N/m^2 [Kutz, handbook, 1994]. The application of such alloys is almost entirely in aircrafts. Alloy 7075(5.5Zn-2.5Mg-1.5Cu), alloy 7079(4.3Zn-3.3Mg-0.6Cu), alloy 7178 (6.8Zn-2.7Mg-2.0Cu) develop highest tensile strength obtainable in aluminum alloys apart from the fact that they have inferior corrosion resistance and poor extrudability. HAZ softening at welds is less severe for these alloys making some of the 7xxx alloys quite good for welding as compared to 6xxx alloys. There can be a possibility of stress-corrosion due to poor corrosion resistance found in these alloys.

Incorporation of micro-scale and nano scale particulates in aluminum alloys can greatly enhance their mechanical characteristics. Some researchers have shown that particulate reinforced aluminum matrix composites can be used above 300 – 400˚C which may make them competitive

with costly Ti alloys at elevated temperatures [Naiqin et al., 2005]. Moreover as compared to 2xxx and 6xxx series matrix, 7xxx series matrix with ceramic particulates reinforcements has produced inconsistent results [Sankar and singh, 1998].

2.4.2 Reinforcement

In a discontinuous reinforced metal matrix composite system, the reinforcement strengthens the metal matrix both extrinsically, by load transfer to the reinforcement, and intrinsically, by increasing dislocation density [Nair et al., 1985]. The interaction between the particulate reinforcement and the metallic matrix is the basis for the enhanced physical and materials properties associated with discontinuous reinforced metal matrix composite systems [ASM Handbook Vol. 21, 2001].

2.4.2.1 Reinforcement size

Reinforcement added to the AMCs are generally of different sizes and these have their own pros and cons. Normally micron-sized particles are used to improve the ultimate tensile and yield strengths of the matrix, but the ductility of the AMCs deteriorates significantly with high particle concentration [Yang et al., 2004; Mazahery et al., 2009]. It is of interest to use nano-sized particles to strengthen the matrix, while maintaining good ductility, high temperature creep resistance and better fatigue resistance [Deng et al., 2010].

Ma et al., 1996, studied aluminum composite reinforced with nanometric Si_3N_4 particles. They added 1 vol.%Si_3N_4 (10 nm) to aluminum matrix and found that it has a tensile strength comparable to that of the 15vol.%SiC_p (3.5 micrometer)/Al composite, but the yield strength and ductility of Si_3N_4/Al composite are higher than those of the SiC/Al composite. Another study by Hai et al., 2012, fabricated aluminum matrix composites reinforced with nano-sized Al_2O_3 particles by casting and studied their microstructure and tensile properties. They added the milled nano-Al_2O_3/Al composite powder to alleviate the problems associated with poor wettability and nanoparticle distribution in the melt. Compared with the alloy matrix, the ultimate tensile strength and yield strength of 1 wt.% nano-Al_2O_3/2024 composite were enhanced by 37% and 81%, respectively. The improvement was due to uniform distribution of reinforcement and grain refinement of aluminum matrix.

Badini et al., 2001, studied the effect of submicron SiC particle reinforcement added to 2124 aluminum alloy with respect to microstructure and strength. Authors fabricated the

composite material by HIP followed by open die forging at sample temperatures ranging from 340^{o}C to 440^{o}C. The forged composite reportedly maintained good mechanical strength and ductility better than that displayed by as HIPed material; as well as good formability which was explained due to small size of the micron reinforcement.

Table 2.6 Characteristics of commonly used particulate reinforcements [ASM Handbook Vol 21, 2001]

Relative size	**Particle diameter (d_{50}), (μm)**	**Advantages**	**Limitations**
Fine	1.7	Greatest strength and stiffness contribution	Tendency to agglomerate
	6.5	Highest fatigue resistance, lowest resultant coefficient of thermal expansion	Blending difficulty (powder/casting), lowered ductility, high cost, segregation during casting
Medium	9.3	Excellent balance between properties (elevated strength and good ductility) and ease of manufacturing	Necessary for high-volume reinforcement systems, good balance between manufacturing ease and resultant ductility
	22.8		Good balance between properties and raw material costs
Coarse	1700	Good wear resistance, High ductility and ease of manufacturing, great for armor applications	Lowest benefit to resultant Properties

2.4.2.2 Reinforcement Content

Strength of any composite directly depends upon the quantity of reinforcement added to the matrix; which generally increases with increase in the reinforcement content upto a certain extent. The limit of addition of reinforcement depends on the area of application of respective composite. Some properties are better at a higher level of reinforcements but other deteriorates. Smaller size of the reinforcement can be added in a large quantity but a low quantity can be useful for improving the properties if nano sized reinforcements are used. Previously many researchers

added different contents of reinforcement for the optimization of matrix to reinforcement ratio to obtain superior properties.

Slipenyuk et al., 2006, investigated the properties of powder processed particle reinforced MMC's specified by reinforcement concentration. The authors proposed a model for observing the effect of volume fraction of the reinforcement (0–20 vol.%) on microstructure and mechanical properties (yield stress, tensile strength, elongation to fracture and Young's modulus) for Al–6Cu–0.4Mn/SiCp composites. The model proposed allows for calculation of the critical concentration of the reinforcement in the composite depending on matrix alloy and reinforcement mean particle size.

2.4.2.3 Reinforcement type

In P/M AMCs, ceramics are basically used as reinforcement due to their high melting point and non reactivity with the matrix. Aluminum oxide (Al_2O_3), silicon carbide (SiC), silicon nitride (Si_3N_4), boron carbide (B4C) etc. have been extensively attempted by various researchers for the development of P/M AMCs. Among these Al_2O_3 and SiC were the most commonly used [Ma et al., 1999; Ahmed et al., 2007; Nam et al., 1998; Su et al., 2012; Kumar et al., 2011; Verma et al., 2001]. During early 90s the composites having aluminum as a matrix and SiC as a reinforcement were on the boost and said to be the "most exciting development in MMC today" [Robi et al., 1990].

Previous studies have demonstrated that the beneficial effect of rare earth elements on corrosive wear is greatly attributed to the improvement in properties of the passive film. Moreover, it has been demonstrated that addition of Ce or Y to Al–Zn–Mg leads to improved resistance to stress-corrosion as evidence by a dramatic 10–20-fold increase in time to failure [Bajza and Boczur, 1980]. The corrosion-inhibiting effect of rare earth compounds in aqueous solution has already been established [Hinton et al., 1984; Seon, 1989; Arnott, 1987; Mansfeld et al., 1987].

2.4.2.4 Y_2O_3 as reinforcement

Y_2O_3 or yttrium oxide is an oxide of yttria which is a rear earth material and is commercially called yttria. It appears white in colour and now days is widely used in ODS steels in nuclear applications. It is manufactured by heat treatment of yttrium hydroxide. Physical properties of Y_2O_3 are given in table 2.7.

Table 2.7 Chemical Composition and Physical properties of Y_2O_3

Chemical Composition		
Element	**Content (wt%)**	
Yttrium	78.7	
Oxygen	21.1	
Physical properties		
Properties	**Metric**	**English**
Density	5.01 g/cc	0.180 lb/in^3
Molecular Weight	225.81	-
Melting Point	2410°C	4370°F

A few studies have been carried out using Y_2O_3 as reinforcement for the development of P/M AMC's [Yarra et al., 2010; Ahmed et al., 2010]. Y_2O_3 is highly stable at high temperatures due to its high melting point [Hassana et al., 2011; Tun et al., 2007], has negligible reactivity with aluminum (in the solid as well as liquid state) and thus is a suitable reinforcement for aluminum [Zhang et al., 2001; Bouaeshi et al., 2007]. It is known that some rare earth elements, such as yttrium and cerium, have been often used as alloying elements to improve oxidation resistance.

Yarra et al., 2010, studied the densification of Al-Y_2O_3 composite powder by equal channel angular pressing. The effect of ECAP on consolidation behaviour of powder, microstructure, density and hardness was discussed. The powder was encapsulated in an aluminum can. Room temperature back pressure aided ECAP results in a nearly full denser (97% of its theoretical density) compact at room temperature. Nano Indentation technique was used to determine the modulus of the ECAP consolidated compact. It was found by the micro hardness tests and density measurements that high densification, homogeneous microstructure and high mechanical strength (Hardness and Young' modulus) could be achieved effectively as a result of the severe plastic deformation of ECAP and the well bonded powder contact surface during powder ECAP. This high densification as well as good powder bonding represents the promising future of ECAP for powder processing. The main deformation mode in ECAP of solid (non-porous) materials is simple shear involving large plastic shear deformation in a very thin deforming layer of a work piece moving through a die.

2.4.3 Mechanical behavior of aluminum matrix composites

The mechanical behavior of a composite material is a primary concern before it can be used for any application either as a part or as whole. Hardness, tensile strength, ductility, compressive strength, impact strength, fatigue, creep etc, are some mechanical properties which have to be analyzed after fabrication of any composite material. Aluminum based composite materials needs specific characterization of one or more of the mechanical properties listed above but hardness, tensile strength and elongation are the values which can alone be helpful for predicting the other mechanical properties. A large number of researchers have done a huge amount of work related to characterize the mechanical properties of aluminum based composite. In this part of literature the previous work done by researchers in the field of high strength aluminum based composites has been discussed. SiC was quite popular reinforcement for aluminum matrix in late 80s due to its availability and low cost. Nair et al., 1985 reviewed SiC reinforced aluminum composites by blending, cold compaction and hot pressing routes and discussed it. The author compiled the previous work done by other authors and concluded that they only focused on the accumulation of data without any detailed discussion behind the failure of aluminum based composites. The author analyzed the hardness, tensile, fracture, ductility, creep and corrosion behavior of aluminum based composites reinforced with SiC and discussed the possible failure modes.

Ceschini et al., 2009, fabricated AA6061 composite reinforced with 23% Al_2O_3 particles and post processed by open die hot forging and discussed the effect on microstructure and tensile properties. Microstructural characterization and density measurements showed that hot forging did not induce crack on the AA6061 composite reinforced with 23% Al_2O_3 particles and reduced the porosity with respect to the initial material. The concurrent effect of plastic deformation and high temperature during forging, instead, led to a recrystallization of the aluminum alloy matrix, with a consequent grain refinement. These microstructural modifications induced an improvement in the tensile strength and an increase, from 50% at room temperature to 165% at 300^{o}C, of elongation at failure in the forged composite.

Baradeswaran et al., 2013 investigated the effect of B_4C on the mechanical properties of aluminum 7075 matrix composites. The author added different amounts (ranging from 5 to 20 vol%) and different sizes (16 to 20 micrometer) of B_4C on the matrix and found an increase in hardness, UTS and compressive strength with increase in the reinforcement content. The reason of improved mechanical properties with the addition of more reinforcement is explained as more

resistance offered by the larger number of particles but no detailed discussion for different sizes of reinforcement was given.

Mobasherpour et al., 2013, added nano-size Al_2O_3 reinforcement in 7075 aluminum alloy matrix by mechanical alloying and studied the effect of nano reinforcement on the mechanical behavior of the composite. Authors observed the effect of 40-50 nanometric size reinforcement on UTS of different composites with varying reinforcement content (1, 3 and 5 vol %). Densities of nanocomposites were found higher than the base metal and nano reinforcement was found uniformly distributed over the matrix which resulted in increase in hardness value upto 204 HB and about 60 % improvement in UTS.

A useful work done by Ahmed et al., 2007a, critically reviews the effect of ceramic reinforcement on the mechanical properties of 7xxx series matrix based composites. The author summarized the results of Doel et al., 1996, Razaghian et al., 1998, Shang et al., 1989, Pandey et al., 2000 and compared these with his own work [Ahmed et al., 2007b]. He observed that some researchers obtained a sharp increase in the tensile strength after addition of reinforcement in 7xxx series matrix as well as some found decrease in the property compared to pure alloy matrix. The author tried to explain the unexpected behavior of these composites with the help of different strengthening mechanisms like thermal mismatch strengthening, particulate strengthening, grain and sub-grain strengthening and work hardening in relation to the ceramic reinforcement added to matrix alloy. Concluding the study author suggested future work for better explanation of the ambiguous behavior of 7xxx series matrix based composite materials.

After reviewing 7xxx based composites Ahmed et al., 2010 synthesized nanometric SiC particulate-reinforced Al 7075 matrix composites and characterized it by tensile testing and microstructural observations. They reinforced different volume fractions (1 and 5 vol %) of nano SiC in particle form with a mean size 50 nm to 7075 alloy matrix and blended it in a ball mill at 250 rpm in ethanol for preventing oxidation of aluminum. The mixtures were then pressed (CIP at 400 MPa), degassed and sintered in nitrogen atmosphere. Further HIP was performed in argon atmosphere for increasing the density and final consolidation was given by means of extrusion. All the samples were given T_6 heat treatment before tensile testing. Tensile tests revealed that the strength of composites continuously decreases with the addition of reinforcement. The authors discussed some points of failure in details with the help of fractured surface as observed in SEM images. They described segregation of nano reinforcement at the grain boundaries as a major point of failure of these composites. Segregation of Mg was another reason for the premature failure of

the nanocomposites. Equilibrium segregation and nonequilibrium segregation were explained with respect to dislocations, grain boundaries and point defects or vacancies. Various reasoning for the segregation of Mg (including the reaction of SiC reinforcement) were explained in the study. The nanocomposites fabricated by taking care of many factors were not successfully concluded to be superior to the pure alloy matrix in terms of mechanical behavior [Doel et al., 1996].

A comparison of mechanical properties by different authors using Al-7075 as the matrix and particulate reinforcements was carried out and is presented in table 2.8.

Table 2.8 Experimental comparison of mechanical properties by different authors

Material	**Reinforcement**	**Particle size**	**Volume fraction (%)**	**UTS (MPa)**	**Elongation (%)**	**Temp. (^{o}C)**	**Reference**
Al-7075		-	-	619	24	RT	Doel and Bowen, 1996
Al-7075	SiC	5 µm	15	630	10	RT	
Al-7075	SiC	13 µm	15	645	4.8	RT	
Al-7075	SiC	60 µm	15	504	1	RT	
Al-7075		-	-	590	15	RT	Razaghian et al., 1998
Al-7075	SiC	14 µm	15	543	7	RT	
Al-7075		-	-	185	30	250	
Al-7075	SiC	14 µm	15	202	17	250	
Al-7075		-	-	37	104	400	
Al-7075	SiC	14	15	37	46	400	
Al-7075		-	-	603	11.8	RT	Ahmed et al., 2007
Al-7075	SiC	50nm	1	505	9.8	RT	
Al-7075	SiC	50nm	5	514.3	6.1	RT	
Al-7075		-	-	262.2	50.4	215	
Al-7075	SiC	50nm	1	239.5	33.6	215	
Al-7075	SiC	50nm	5	245	19.5	215	
Al-7075		-	-	44.4	86.8	350	

Al-7075	SiC	50nm	1	47	74	350	
Al-7075	SiC	50nm	5	44.3	38	350	
Al-7075		-	-	590	10.2	RT	Shang and Ritchie, 1989
Al-7075	SiC	5	15	530	3.1	RT	
Al-7075	SiC	16	15	535	1.1	RT	
Al-7075	SiC	5	20	470	1.9	RT	
Al-7075	SiC	16	20	560	1.8	RT	
Al-7075		-	-	622	10	RT	Pandey et al., 2000
Al-7075	SiC	10	15	694	1.8	RT	
Al-7075		-	-	592	13	RT	Kang, 2004
Al-7075	SiC	13	10	566	7	RT	
Al-7075	SiC	50nm	1	635	7	RT	
Al-7075	SiC	50nm	5	594	3	RT	
Al-7075	Al_2O_3	50nm	1	602	5	RT	
Al-7075	Al_2O_3	50nm	5	375	4	RT	
Al-7075		-	-	574	9.6	RT	Ren, 2007
Al-7075	SiC	50nm	1	634	8.9	RT	
Al-7075	SiC	50nm	5	547	3.1	RT	

RT= Room Temperature

2.4.4 Tribological behaviour of aluminum matrix composites

Wear has been defined as a systems response to the imposed conditions, rather than a material property and it can be called a tribo-system response [Kato, 2000]. Wear mechanisms are classified based on the different parameters being operative during a particular occurrence of material loss by wear, namely: mechanical wear (adhesive, abrasive and fatigue wear), chemical wear (corrosive wear) and thermal wear (melt and diffusive wear) [Kato, 2002]. Wear is such an intense phenomenon that soft magnesium alloys, WC reinforced cast irons, biocomposites as well as hard materials such as hot working tool steels also get affected by it [Raghu et al., 1994; Kambakas and Tsakiropoulos, 2006; Karanjai et al., 2008; Pant and Bleck, 2005].

The incorporation of ceramic particles in an aluminum alloy increases its load-bearing capacity and hence the load and sliding speed range within which there is a mild dry sliding wear occurs. This has been investigated in detail by many researchers and opens new opportunities for the application of aluminum based metal-matrix-composites (AMC's) where sliding resistance is of concern. Some investigations have also analyzed the wear behavior of AMC's in the case of external heating, in the temperature range up to 200^{o}C or 500^{o}C. It has been found that wear increases as temperature is increased, because of the thermal softening of the composite, and becomes severe at a critical temperature. Friction coefficient was also observed to increase and this was attributed to an increase in the adhesion forces. Most experimental investigations were carried out using hard steel as a counter face.

Theory of dry sliding wear proposed by the Archard's model, is given by the following equation:

$W = k\,(L\,d\,/\,3H)$

were wear volume loss (W) is directly influenced by the normal load (L) and sliding distance (d) but inversely related to the hardness(H) of the material and k denotes the wear coefficient [ASM Handbook vol. 18, 1992]. Originally developed for adhesive wear, the equation was found suitable to predict wear behavior of materials under abrasive contact. However, a direct usage of the equation was not possible for MMCs, due to the complex interplay of constituents [Hutchings, 1994].

Several factors, singular and combinatorial, have been found to be responsible for tribological behavior of discontinuously reinforced AMC's. Some of the major extrinsic factors affecting the tribological behavior are sliding distance, normal load, sliding velocity, reinforcement orientation, external temperature and surface finish. Intrinsic factors include reinforcement type, reinforcement size, reinforcement shape, heat treatment, reinforcement volume fraction and spatial distribution [Sannino and Rack, 1995].

P/M 7091 (Al-1.59-Cu-2.28Mg-6.11Zn-0.40Co-0.07Fe) alloy reinforced with 20 vol.% SiC whiskers (0.5 μm diameter, aspect ratio = 6) were tested for abrasive wear resistance against SiC papers of varying grit size [Wang and Rack, 1991a]. Composite hardness was related to whisker alignment, reported to be maximum for whiskers aligned normally to the test surface. Wear resistance decreased with increasing grit size upto 60 μm, steadily increasing wear was observed thereafter with increasing grit size of the counterface paper. Whisker reinforced composite displayed consistently better wear loss than particulate composite having similar

volume fraction of reinforcement. Minor improvement in wear loss was reported for normally aligned whiskers. Material loss by grooving and whisker pull-out was observed. The anisotropy created by preferential alignment of reinforcement in extruded P/M composite has a direct bearing on the wear performance for both particulate and short fiber composites [Sahin and Murphy, 1998; Sahin, 1998], a direct difference created by an effective area fraction of the hard ceramic reinforcement at the contact plane [Hutchings, 1994].

Wang and Rack, 1991b, investigated the dry sliding wear behavior of P/M 2124 alloy with upto 20 vol.% SiC whisker reinforced composite against a 17-4 PH steel disk. Wear rate decreased with increasing reinforcement content for the composite pins, consequently an increase in wear loss was reported for the steel disk. Coefficient of friction was largely insensitive to reinforcement content. Wear regime consisted of two parts: an initial run-in period followed by a steady state sliding. The wear mechanism for the composite pins changed from abrasive in the initial part of test to adhesive in the steady state part, as evident by debris morphology, which changed to plate like from initially fine particulate type. Surface finish is reported to play an important role during the initial run-in duration [Alahelisten et al., 1993], where hard SiC whiskers are able to abrade the steel disk, absent in case of mirror polished composite pins against a smoother disk. Sub-surface examination of worn composite pins revealed a severely deformed zone for upto 100 μm from the contact plane, with plastic flow of the matrix along the sliding direction.

Formation of a third-body tribolayer composed of hard ceramic wear debris generated as a result of asperity fracture is an important aspect of MMC wear behavior, following which, after an initial high wear volume loss, there is a steady improvement in pin wear resistance, aided by the abrasive action of these embedded particles in the softer aluminum alloy matrix.

Transition from mild to severe wear rates for different AMC's has been investigated by Alpas and Zhang, 1994, for AA6061, AA2024 and AA2124 matrices reinforced with fine/coarse particulate Al_2O_3 and SiC. Based on the effect of applied normal load three broad wear rate regimes were marked as low load (1-10 N) upto 10^{-5} mm^3 m^{-1}; intermediate (30-150 N) upto 10^{-3} mm^3 m^{-1} and severe (230-300 N) with a wear rate of upto 10^{-1} mm^3m^{-1}; similar transition of wear regimes was reported for all combinations of matrices and reinforcement size/volume fraction. For AA6061 based composites the wear rate was found to increase by a factor of 10 for sliding against a ceramic counterface in comparison to hardened steel. Composites with coarse particles exhibit lower wear rate at low loads; but this advantage does not appear in intermediate and higher load regimes. Increasing the volume fraction of reinforcement, shifts the transition loads to higher

values for respective matrices, maximum benefits are attained in the intermediate regime, which extends into the severe wear rate zone load range. Tribo-layer formation was observed in the low load regime from the XRD analysis of wear debris, it was found to be composed of Fe-oxides, abraded by the action of ceramic reinforcements. The in-situ oxidized debris are known to lower the coefficient of friction by providing a lubricating effect. Increasing the reinforcement particle size, resulted in higher abrasion of the steel counterface, whilst, limiting damage to the composite pin. Nearly equivalent wear rates were reported for monolithic and reinforced pins in the intermediate regime, the authors have attributed this feature to negligible increment in the load carrying capacity of the matrices under severe plastic deformation induced surface failure of the test pins. Ceramic particles further provide paths for cracks and decohesion, thereby releasing excess material at the tribo-contact plane. The severely deformed zone is reported to grow about 10 times in the highest load test regime, sub contact plane temperatures rise to about 0.4 T_m (melting point of the matrix alloy on the absolute scale), defined as the critical temperature for onset of severe wear by plastic delamination.

Formation of a complex tribo-layer has also been reported by Iwai et al., 1995 for P/M 2024/upto 16 vol.% SiC whisker reinforced composites under dry sliding tests. Transition from initial severe wear to mild wear is relatively fast with increasing reinforcement content due to reduced adhesion by presence of small ceramic debris between the composite and counterface [Akbulut et al., 1998]. Wear rates are found to be dependent on the size of wear debris [Miyajima and Iwai, 2003] for both particulate and short fiber reinforced composites undergoing dry sliding wear against a hardened steel counterface. Increasing the volume fraction of reinforcement content resulted in smaller sized particles at the tribo-interface, thereby reducing wear rate [Yu et al., 1996]. The dependence of reinforcement volume fraction with a normalized wear rate (wear rate of MMC divided by wear rate of monolithic alloy) was examined by the workers and the highest increase in wear resistance was achieved in case of short fibers followed by whiskers and particulates, in that order, for increase in respective volume fractions.

Elevated temperature wear of AA6061/20 vol.% Al2O3 particulate reinforced composites has been investigated by Singh and Alpas, 1995. The composite exhibited mild wear till 200ºC, beyond which severe wear was reported. Increase in load further enhances the wear rate at higher temperature. The transition temperature for onset of severe wear from the present work is reported as 200ºC for the composite and 150ºC for the unreinforced alloy, beyond which seizure was observed. Wear by excessive plastic deformation generating large flaky debris, as a result of

delamination failure [Suh, 1977] of the composite and monolithic alloy were recorded above the respective transition temperatures. The composite had a slightly higher flow stress till 200ºC in comparison to the alloy, but the delayed onset of severe wear at higher temperature was ascribed to localized work hardening of sub-surface layers of the composite against bulk flow softening [Singh and Alpas, 1996]. This work hardening was due to severe shear strains at the contact plane, of the order of 10^3, and dispersion of alumina particles in the matrix.

2.4.5 Machinability of aluminum matrix composites

Aluminum based composite materials are now a day's finding their applications in cylinder block liners, vehicle drive shafts, pistons in automobiles, and bicycle frames. Production of these components for industrial applications gets in final shape after machining operation. AMCs offer highest level of machinability amongst all light weight metal based composites. Assessment of machinability operation can be done by several parameters including cutting force, surface finish, chip formation mode, tool life and cutting energy. Smith et al., 1998, reviewed machinability aspects of materials processed by powder metallurgy. The author raised serious issues on machinability of sintered P/M parts due to low tool life during their operation. Low tool life can be explained with the help of porous structure of the sintered samples due to which thermal conductivity of the sample decreases resulting in a temperature rise of tool tip. Another reason for tool wear is an impact or shock to the tool tip at microscopic level during machining. In P/M parts density variations due to compaction further results in loss of machining efficiency.

Some aluminum alloys are sensitive to age hardening and this behavior changes their hardness with respect to treatment condition, finally affecting machinability of the material. Demir et al., 2009, performed experiments to study this effect on 6061 aluminum alloy. He tested samples for machinability with respect to turning operation at different heat treatment conditions namely as received material, solutionized condition and age hardened at different time durations. The author explained that the variations of cutting forces are less prominent at higher cutting speeds at different heat treated conditions. At slow cutting speeds variation of cutting forces is large, cutting forces are higher due to more contact between tool and chip compared to higher speeds where cutting forces are low due to softening of the material as the temperature rises during machining operation.

There are several types of machining operations but drilling, turning and boring are the most performed operations for industrial applications. Kouam et al., 2010, compared the cutting

forces during drilling of 6061-T_6, 7075-T_6, A356-T_0 and A319-T_0 and the recorded average thrust force for the drilling operation. The author concluded that only 7075 aluminum alloy is sensitive to cutting forces with varying cutting speeds and found decrease in the thrust force with increasing speeds.

Feed rate is another governing factor of machinability forces in connection with the cutting speeds. Feed rate determines the chip thickness and directly affects the cutting forces. Balout et al., 2002 and Shaw, 2005 studied the relation of feed rate and machinability forces and found that thrust forces increases as the feed rate increases for metallic samples. Deformation of the material during machinability operation can be studied with the help of geometry and microstructure of the chips formed. Xie et al., 1996 experimented machinability with different aluminum alloys at different cutting speeds. The author studied the chips collected from different sets of experiments with the help of SEM and analysed chip segmentation by developing a factor called "Flow localization parameter". A set of SEM images were developed in an earlier study in order to explain the chip geometry at different cutting speeds as shown in Fig. 2.10. The figure explains formation of large chips at low cutting speeds and small chips at higher cutting speeds. The chip length also depends on the material either it is brittle or ductile in nature. Comparatively ductile material like 6061 and 7075 has a considerable chip length at moderate cutting speeds. Chip length and size not only depends upon the cutting speeds but also influenced by different feed rates. Based on the study feed rates and cutting speeds can be optimized with desirable continuous or discontinuous chip formation for different materials.

Mohan et al., 2008, optimized the machinability of aluminum matrix composites reinforced with 20vol% SiC. The author performed machining operations at different temperatures (ranges from 50 to 350^{o}C) and different cutting speeds (25 to 300 m/min) and correlated these with flow, fracture, workability and hot deformation. Dynamic material model (DMM) was applied to optimize the machinability operation at a narrow region of 150^{o}C and 150 m/min.

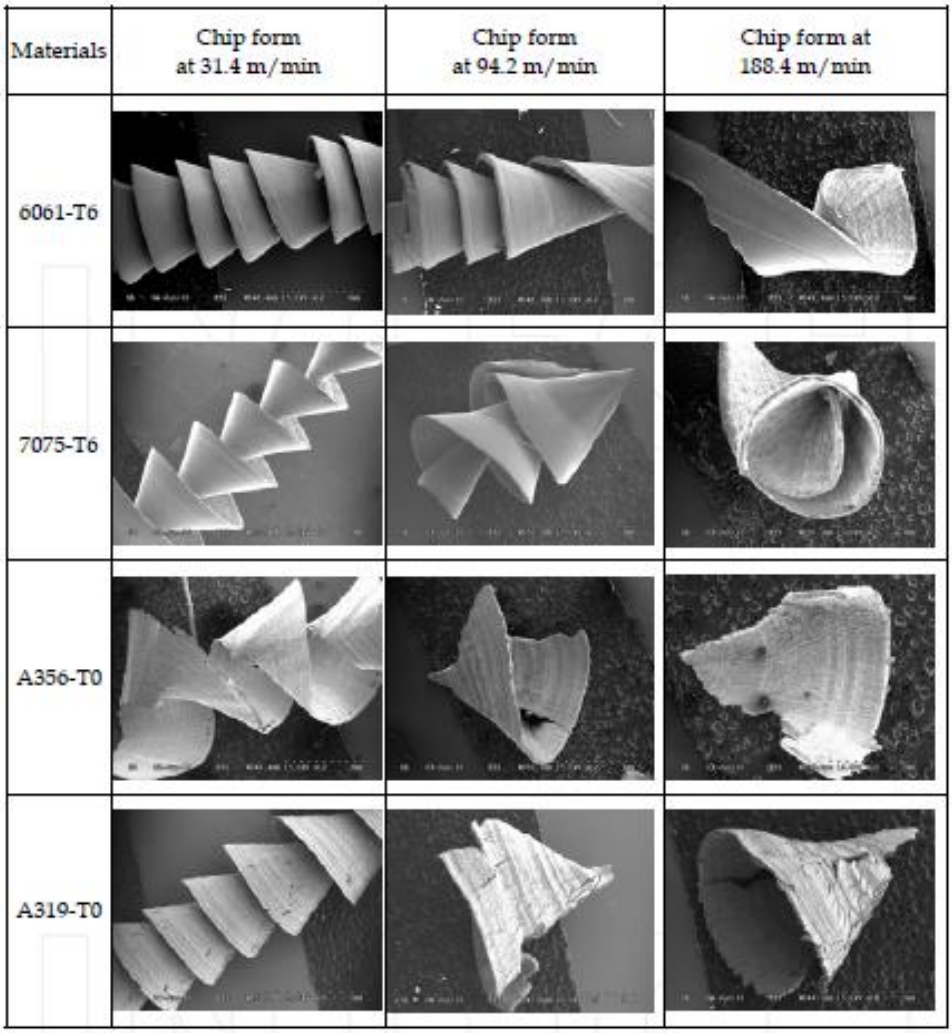

Fig. 2.10 SEM images of chips collected at 0.15 mm/rev feed rate and at different cutting speeds during the drilling of aluminum alloys [Songmene et al., 2011]

Based upon the earlier studies it can be summarized that machining of aluminum and its alloys is relatively easy due to less hardness, less cutting forces and high tool life apart from the fact that sometimes chip length can create problems which can be solved by selecting suitable cutting speeds and feed rates.

Chapter 3
FORMULATION OF PROBLEM

3.1 Formulation

An extensive review of available literature was carried out and following points were observed. Based on these points, the plan of the present research work was formulated.

- Composites with Al-7075 matrix have been mainly studied with SiC, Al_2O_3, Si_3N_4, and B_4C as reinforcements. Y_2O_3 as a reinforcement in Al-7075 has not been reported.
- A few studies reported a comparison of micrometric and nanometric size reinforcement mainly with respect to the mechanical properties of aluminum composites. Studies on wear and machinability in these systems have not been explored thoroughly.
- Some studies have been performed on processing of Al-7075 composites through P/M route however these studies were limited to press and sinter (presence of porosity). Studies pertaining to secondary consolidation by powder forging (close to theoretical density) of the sintered Al- 7075 composites has not been reported.
- Closed die forging of Al-7075 composite has not been reported and no studies discussed the effect of forging temperature and strain on microstructure evolution of the alloy system.
- Most of the studies indicated an increase in composite properties with the addition of reinforcements but degradation of properties and reason behind it has not been explained in details.
- Wear studies were performed in most of the metal matrix composites containing aluminum as a matrix and wear loss was studied with different amount of reinforcement content. However the effect of reinforcement particle size on the wear loss of composites has been scarcely reported.
- Machining of soft aluminum matrix is easier compared other metals thus a less amount of work has been carried out on the machining behavior of AMCs. Research work carried out previously was based upon the optimization of processing parameters and none has correlated the results with metallurgical parameters (microstructure and mechanical properties).

3.2 Objectives of the Research Work

- To develop micrometric and nanometric Y_2O_3 reinforced Al-7075 composites by powder metallurgical (P/M) route employing uniaxial cold compaction followed by sintering and hot forging (to close to theoretical density) for structural and tribological applications.
- To optimize powder forging route as a secondary consolidation technique at various temperatures and strains with respect to microstructural evolution.
- To investigate the effect of Y_2O_3 reinforcement size and volume fraction on the microstructural characteristics and mechanical properties (hardness, tensile and compressive strength) of the developed composites. Further, to understand the aging characteristics of these composites with respect to Y_2O_3 size and content.
- To investigate the wear mechanisms of the developed composites and correlate the wear behavior with the microstructure and mechanical properties.
- To study the machinability of these composites with respect to reinforcement (Y_2O_3) size and content in the solutionized as well as T_6 condition.

Chapter 4

EXPERIMENTAL PROCEDURE

4.1 **Introduction**

This chapter deals with the details of materials and equipment used for fabrication of composites by the powder forging route i.e. aluminum alloy and reinforcement powders, their blending/mixing, compaction, sintering, sintering atmosphere and post processing technique of forging. Further, various equipments/ instruments used to investigate density, hardness, mechanical properties, wear behavior and machinability of the composites are discussed.

4.2 **Materials**

4.2.1 **Pre-alloyed aluminum alloy powders**

Chemical composition (wt.%) of commercially pure prealloyed aluminum alloy 7075 powder (60 μm) which was produced by gas atomization, is shown in Table 4.1. The reported composition was as provided by the suppliers. The alloy powder was procured from The Aluminum Powder Company Limited, North Wales, UK.

Table 4.1 Chemical composition of aluminum alloy powder (wt. %)

Element	**Zn**	**Mg**	**Cu**	**Cr**	**Fe**	**Si**	**Mn**	**Ti**	**Al**
Wt %	5.295	2.475	1.590	0.197	0.086	0.044	0.020	0.009	Balance

4.2.2 **Yttrium oxide (Y_2O_3)**

Yttrium oxide powder, a rear earth element, commercially known as yttria, was used as reinforcement. Pure yttrium oxide (99.8% purity) was procured from Alfa Aesar, India. Yttrium oxide of two particle sizes of micron size (~4 μm) and nano size (~10 nm) were used in the present investigation.

4.2.3 **Lubricant for cold compaction and hot forging of pure powder and composite powder blends**

The lubricant for die wall during cold compaction of pure alloy powders and composite powder blends was stearic acid ($CH_3(CH_2)_{16}CO_2H$) flakes supplied by HIMEDIA^{TM}. The flakes of

stearic acid were completely dissolved in acetone (technical purity; RANKEM^{TM}) by heating the acetone upto 50ºC. This stearic acid dissolved in acetone was used as a thin layer between die wall and punch face. During hot forging, boron nitride aerosol spray supplied by GE Momentive^{TM} (GE, USA), was used as a lubricant as well as release agent between die, punch and preforms. This lubricant is effective upto 850ºC and acts like boron nitride coatings during hot forging.

4.2.4 **Gas atmosphere:**

Pure nitrogen gas (technical grade, purity > 99.999%) was used as a sintering atmosphere for pure alloy and composites. Nitrogen gas was purged 4-5 times after creating vacuum inside the sintering furnace and closed nitrogen atmosphere was created for sintering.

4.3 **Processing**

4.3.1 **Blending of yttrium oxide with AA-7075 matrix powders**

The composite powder mixtures consisting of micrometric Y_2O_3 reinforcement were ball milled in a Planetary Ball mill (RETSCH PM-400^{TM}) at 100 rpm for 30 minutes for homogeneous mixing. Ball to charge ratio was maintained at 10:1 during the ball milling (mixing) operation. The dispersion of Y_2O_3 nanoparticles in the matrix powder was carried out by a modified dispersion method. The nano powders were initially in the form of agglomerates due to their high surface energy. These were first ultrasonicated in acetone solution for 10 minutes. Acetone containing nanoparticles of yttria was heated to 70^{o}C during ultrasonic treatment. At this temperature acetone vaporizes fast and bubbles came out at the surface rapidly. These bubbles split out at surface releasing high energy during the blasting. This energy creates a shock wave to break the agglomerates of nanoparticles. After this treatment prealloyed 7075 powders were mixed in this solution with a stirrer for 15 minutes. The powder mixture was kept for some duration for the complete vaporization of acetone. The dried powder mixture was further mixed in the planetary ball mill at 100 rpm for 30 minutes to avoid an inhomogeneous distribution of reinforcement powders. Ball to charge ratio was maintained at 10:1 during the ball milling (mixing) operation.

Composite powder blends were prepared by the addition of 1 to 15 volume fraction of micrometric Y_2O_3 and 0.1 to 3 volume fraction of nano Y_2O_3. The compositions of composite powder blends and their designations used in the figure captions are presented in Table 4.2.

Table 4.2 Composition of composites and their designation

Composition	Designation
Pure Al-7075	Al-7075
Pure Al -7075 + 1 vol % micron Y_2O_3	1 M
Pure Al -7075 + 3 vol % micron Y_2O_3	3 M
Pure Al -7075 + 5 vol % micron Y_2O_3	5 M
Pure Al -7075 + 10 vol % micron Y_2O_3	10 M
Pure Al -7075 + 15 vol % micron Y_2O_3	15 M
Pure Al -7075 + 0.1 vol % nano Y_2O_3	0.1 N
Pure Al -7075 + 0.5 vol % nano Y_2O_3	0.5 N
Pure Al -7075 + 1 vol % nano Y_2O_3	1 N
Pure Al -7075 + 3 vol % nano Y_2O_3	3 N

4.3.2 **Uniaxial cold compaction of pure alloy and composite powder blends**

Cold compaction of loose alloy powder and composite powder blends were done uniaxially in a hydraulic press (60 Tons capacity). A floating platen type die was used for compaction with a die cavity of size 48 mm x 23 mm x *h* mm (make: Precision Engineering Works, Delhi) made from high chromium hot die steel of mirror finish having hardness ≥ 52 HRC. The height (h) depends upon the amount of powder filled in the die cavity and the pressure applied during cold compaction. In practice the maximum height of green compacts was kept 15 mm to avoid breaking of the green compacts during ejection. Punch for pressing was fitted at the bottom of the die cavity and after filling the loose powder to the die cavity, die was lightly tapped for packing of the powder. Second punch was inserted at the top of the die cavity and this punch beard the load applied from the press. Compaction pressure was selected in press tonnage and converted to corresponding MPa by dividing it with the projected area of the die cavity.

4.3.3 **Optimization of Compaction Pressure**

A set of experiments were carried out to optimize the compaction pressure i.e. to determine the lowest compaction pressure at which a crack/defect free compact would form. Density values of green compacts with different compaction pressures is shown in Table 4.3. A low compact density during compaction i.e. green density was desired in the present investigation due to various

reasons. Firstly the driving force for sintering is maximum when the green density is low as a large amount of free surface area/porosity is available. Secondly due to the good ductility of the Al-7075 particles a high compaction pressure would tend to plasticaly deform the powders leading to a considerable pore filling. Such a structure would not sinter well and this also does not fulfill the purpose to study the densification occuring during hot forging of undeformed powder particles. Initially powders were compacted at a pressure below 350 MPa which lead to fragmentation of the compact after removal from the die. The compacts compacted at 350 MPa had enough green density for handling and did not show any presence of cracks. Thus a pressure of 350 MPa was chosen for green compaction.

Table 4.3: Green density with increasing compaction pressure

Compaction Pressure (MPa)	Green Density (g/cc)	Relative Green Density (%)
250	2.15	77.2(Sample not retained)
350	2.25	80.9
450	2.36	84.8
550	2.5	90.1
650	2.6	93.7
750	2.64	94.9

4.3.4 **Sintering**

4.3.4.1 **Sintering equipments and sintering cycle**

Green compacts of pure alloy and composites were sintered in a tube furnace having end caps (flanges) for maintaining the gas atmosphere. The tube furnace was self-assembled with an alumina tube having a total length of 1 meter and an outer diameter of 75 mm. The end caps machined from stainless steel (AISI 304) had a gas inlet port with a valve control, a vacuum pump fitted at one terminal and a pressure gauge (+760 to -760 mm Hg) for reading the pressure inside the tube fitted at another end. Heating of the alumina tube was facilitated by the coil of KANTHAL-A1^{TM} wire which was wound around the tube, having 2.5 kW rated load. A maximum heating rate of 30^{o}C min^{-1} and maximum operating temperature of 950^{o}C was limited for safe operations. The total hot zone of the furnace was 200 mm and it was extended 100 mm on each side from the center of the tube. The hot zone was calibrated with the help of a standard

thermocouple (Chromel/Alumel-K type). One thermocouple was placed at the centre touching the outer surface of the alumina tube for measuring the heat zone temperature. Heating rate, holding and other temperature programs were controlled by a programmable controller/PID Control (make: WEST6400^{TM}). The controller included 8 programmable segments, 4 programs in memory storage, 1 minute time sensitivity and ± 1^{o}C temperature accuracy. PID, WEST6400^{TM} make (± 1^{o}C accuracy, 1 min sensitivity, 8 segment programmable cycle, 4 memory stored programs). A typical sintering cycle for the present system is shown in Fig. 4.1. The sintering cycle consisted of following segments: (1) heating the samples with a heating rate of 10^{o}C/min to degassing temperature, (2) holding for degassing of the premixed lubricants (if any) and other impurities at 400^{o}C. Degassing was done by creating vacuum inside the tube, backfilling a technical grade pure nitrogen inside and again purging out this nitrogen by vacuum pump (3-4 times), (3) heating up again upto the sintering temperature, (4) holding of the samples at the sintering temperature and (5) shutting down the furnace and allowing the samples for furnace cooling to room temperature.

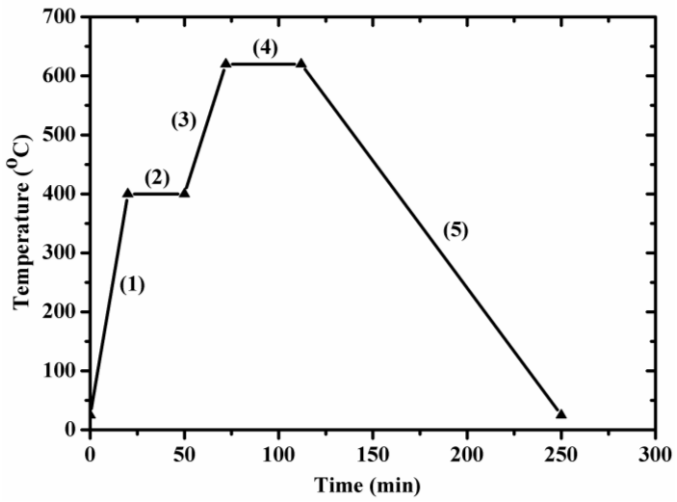

Fig. 4.1 A typical sintering cycle

4.3.4.2 **Sintering temperatures**

The prealloyed powder used for present study is 7075 aluminum alloy which contains Al, Zn, Mg and Cu. The presence of alloying elements in this alloy powder leads to a critical liquid volume fraction of 12% due to partial melting, generating a super solidus liquid phase sintering system (R. M. German: Metall. Mater. Trans. A, 1997, 28, 1553–1567). This 12 % liquid volume fraction is calculated by means of DTA trace (Fig. 4.2). The area calculated between the point where melting starts and the peak point (where the alloy is in complete liquid state). 12 % area of

this total area was calculated from the initial point. Now this line is extended vertically and where it cuts the temperature axis, that temperature is selected as sintering temperature. The estimation of liquid volume fractions was determined by thermodynamic investigations of pre-alloyed powders and equipment used for the study is described in Section 4.4.3.

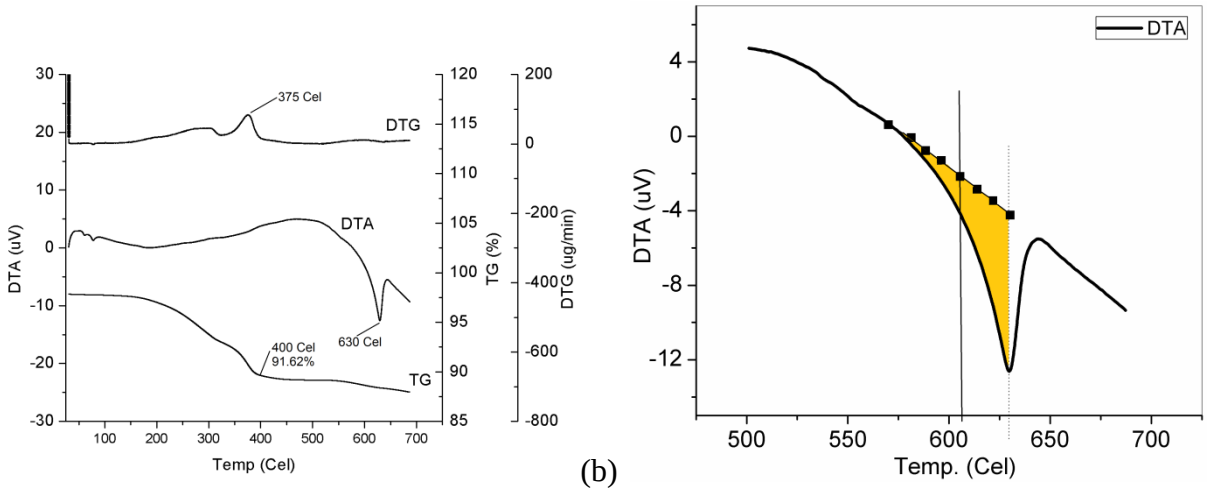

Fig. 4.2 (a) DTA curve for Al-7075 powder and (b) Enlarged section of DTA curve

4.3.4.3 **Gas conditioning**

Sintering of aluminum alloy powder is greatly affected by purity of the gas and dryness of the sintering atmosphere. Nitrogen gas was dried and remaining oxygen in the gas was removed for sintering with the help of a small self fabricated gas purification station. The nitrogen gas was passed through a dry and air tight column of silica gel for removing any moisture present in the gas. Oxygen present in the gas was removed by passing the gas from a stainless steel tube filled with heated pure copper and magnesium chips at 500^{o}C. The copper chips were changed after each operation or recharged by dipping these into diluted H_2SO_4 solution for removal of the oxide layer.

4.3.5 **Forging of sintered preforms**

4.3.5.1 **Forging accessories and operation**

Hot forging of pure alloy and composite preforms were performed on a floating platen type spring loaded die (make: Precision Engineering Works, Delhi) having cavity size of 50 mm in length and 25 mm in width. The hot forging die was similar but with a slightly larger die cavity than the cold compaction die. The die was made of hot die steel (H13) having an average hardness of 53 HRC. The die was polished to mirror finish (less than 1µm) for close tolerance between die

and punch. The forging die itself fitted with a punch rested in a base plate at the bottom and moving die cavity was supported by four springs. Ejection of the hot forged samples was carried out with spacer blocks which were placed upon the floating die. During ejection, the bottom punch also served as the ejector for forged samples. Die-punch clearance was maintained at 0.05 mm. Sintered preforms were spray coated with boron nitride hot working lubricant (Section 4.2.3) which was sprayed over the preforms and die walls. The preforms were held for 30 min at forging temperature inside a muffle furnace. At the time of forging the samples were quickly transferred to the die cavity of a manually operated Weingarten-type friction-screw press (make: BIRSON^{TM}, Ludhiana, India). Hot forging of the pure Al-7075 samples was carried out at four different temperatures 0.6 T_m, 0.7 T_m, 0.8 T_m and 0.9 T_m (269^{o}C, 35^{o}C, 449^{o}C and 540^{o}C respectively) and three different strains (true) of 0.51, 0.92 and 1.14 in a closed rectangular die. The forging operation of composite samples was performed at 0.8 T_m and a strain value of 0.92. The forging press as shown in Fig. 4.3; had a 15 kW prime mover and 100 kN capacity. Ram velocity during forging was kept constant in the range of 250 - 275 mm s^{-1} for all the operations. Major components of forging set-up include: (1) Ram, (2) Top Punch, (3) Die cavity (H13 hot die steel), (4) Moving platen (EN-8 alloy steel), (5) Die base (EN-8 alloy steel), (6) Heating element and (7) Proximity sensors. The ram velocity was measured by proximity sensors placed at the column of the press in between the top and bottom dead centers of the forging hammer. The forging die was heated with two rod type resistance heaters inserted directly into die block. Samples after forging were immediately water quenched for preventing the structural changes due to age hardening. The samples were roughly polished for removing the lubricant and oxide present at the surface. Die cavity was cleaned with a wire brush and with a rough cloth for removing any flush or lubricant remaining before each forging operation. Samples for further characterization were kept in a freezer which was maintained at -18^{o}C.

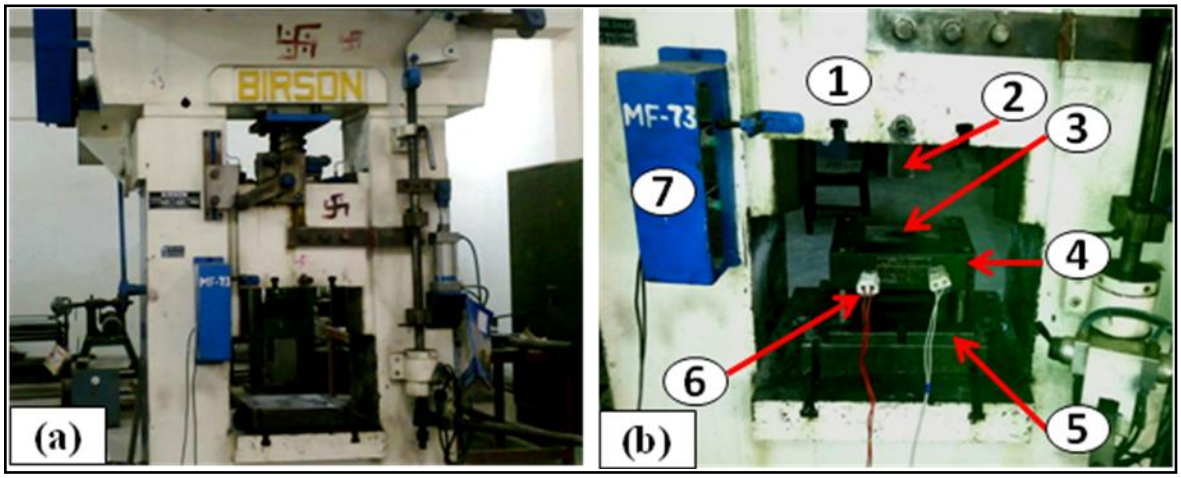

Fig. 4.3 (a) Friction screw forging press and (b) Major components of forging set-up

Fig. 4.4 Samples after hot forging

4.3.5.2 **Calculations for true strain during forging**

The sintered preforms were cut to appropriate initial sizes for powder forging. Hot forging of the preforms was carried out at three different strains (true) of 0.51, 0.92 and 1.14 in a closed rectangular die. The selected strain values correspond to the restriction of final shape of the die cavity. These true strain values were calculated by measuring the initial and final cross sectional area (with respect to forging load) of the sample before and after forging. Final cross sectional area of the sample was 50 mm x 25 mm (length x width). The initial length of the sample was same as of final length but the initial width of the sample was selected as 15 mm, 10 mm and 8 mm for

obtaining true strain values of 0.51, 0.92 and 1.14 respectively. The calculations for three individual true strain conditions are presented below.

Final length of the sample after forging = 50 mm

Final width of the sample after forging = 25 mm

Final cross sectional area of the sample after forging (Af) = 1250 mm^2

Condition 1:

Initial length of the sample before forging = 50 mm

Initial width of the sample before forging = 15 mm

Initial cross sectional area of the sample before forging (A1)= 625 mm^2

True strain = ln(A1/Af) = ln(750/1250) = -0.51

Condition 2:

Initial length of the sample before forging = 50 mm

Initial width of the sample before forging = 10 mm

Initial cross sectional area of the sample before forging (A1)= 500 mm^2

True strain = ln(A1/Af) = ln(500/1250) = -0.92

Condition 3:

Initial length of the sample before forging = 50 mm

Initial width of the sample before forging = 8 mm

Initial cross sectional area of the sample before forging (A1) = 625 mm^2

True strain = ln(A1/Af) = ln(400/1250) = -1.14

4.3.6 **Solutionizing and ageing**

Hot forged samples of Al-7075 and composites were solutionized at 482ºC for 2 h in a furnace. Solutionized samples were water quenched to room temperature and quickly transferred for artificially age hardening (T_6) to an oil bath (make: EIE Instruments Ltd., Ahmedabad, India). Artificial aging was carried out in heated silicone oil at 121ºC for different durations. The oil bath was equipped with Platinum/Rhodium thermocouple (±1ºC sensitivity), an oil stirrer and a programmable timer based PID controller (±1 min, upto 99 h cycle). Samples obtained after different aging durations were quenched into ice cold water to prevent further aging.

4.4 **Characterization**

4.4.1 **Determination of powder morphology**

Powder morphology of micrometric size powders was determined by scanning electron microscopy using ZEISS SUPRA 55VP^{TM} SEM operated in secondary electron imaging mode with 20 kV accelerating voltage. Thin layer of powder was spread on a conductive aluminum stubs containing carbon tapes at the surface. Nano size reinforcement powder particles were examined by transmission electron microscope using a FEI TECNAI 20^{TM} TEM operated at a voltage of 200 kV, equipped with a LaB_6 filament and a CCD camera. This instrument has a resolution of 0.36 nm (point to point). Ultrasonically dispersed nano particles were viewed in TEM at higher magnifications for particle shape and surface morphology. Alloy powders were mixed with cold setting phenolic resin, mounted and polished as per standard metallographic practice. The polished mounts were etched with Keller's reagent for imaging. OLYMPUS-D50^{TM} metallurgical microscope was used for the imaging of polished mounts at different magnifications.

4.4.2 **X-ray diffraction (XRD)**

The starting powders were subjected to X-ray diffraction using D8-Advance Bruker-axe, diffractometer fitted with goniometer with Cu-K_α radiation (λ_{Cu}= 0.154 nm) used to identify the different phases. The vertical θ-θ goniometer had a range of 0°-360° (2θ). The detector moves around the sample and measures the intensity and position of peaks which satisfy Bragg's law. An Expert High Score Plus^{TM} software which has inbuilt inorganic JCPDS (Joint Committee on Powder Diffraction Standards) was used to index the peaks of various phases present in the pattern.

4.4.3 **Thermal analysis of powders**

Differential thermal analysis (DTA) was used for analyzing the Al-7075 alloy powder and to determine the melting point and sintering temperature of the alloy powder. The thermal studies were conducted on EXSTAR 6300^{TM} in which approximately 10 mg of powder was tested which was referenced against 10 mg alumina standard. The alloy powder melted under flowing nitrogen (100 ml min^{-1}) and energy input or output in the form of heat flow was recorded in µV. The heating rate was kept at 10ºC min^{-1} upto 700ºC. Heat flow trace during heating of the powder was analyzed at the points where the curve's shape changed. The curve regions where the alloy starts

melting as well as the L+S region were used to determine the appropriate sintering temperature (Section 4.3.3.2).

4.4.4 **Determination of oxygen content in powders**

Oxygen content in the samples was determined using TC236^{TM} (Leco, USA) oxygen/nitrogen analyzer equipped with EF-100^{TM} (Leco, USA) electrode furnace for complete combustion of samples loaded in a graphite crucible. Powders were cold pressed into pellets of 10 mm diameter and of about 2 g weights. Pellets were cut into 4 roughly equal parts for determination of oxygen content. Oxygen content was determined using infra-red detection of CO_2 gas liberated from sample combustion which was referenced against CO_2 gas liberated on combustion of empty crucible. Electrode current was maintained at 1050 Amp for electric arc melting under a protective atmosphere of pure argon gas. The flow rate of argon gas was maintained at 625 $cm^3\ min^{-1}$. Powder samples of approximately 0.5 gm weight were analyzed and quantity of the oxygen present was recorded in ppm (parts per million).

4.4.5 **Density measurement**

Theoritical density of the Al-7075 alloy as well as the density of the fabricated samples was determined after compaction, sintering and hot forging. Density after compaction and sintering was determined by dimensional measurement method in which density was calculated by dividing the mass of the sample by its volume and were further confirmed by Archimedes principle/water displacement technique. The density obtained after hot forging were determined by image analysis.

4.4.5.1 **Calculation of theoretical density of Al-7075 alloy**

Theoretical density (ρ_m) of Al-7075 alloy was calculated with the help of the inverse rule of mixtures. The chemical composition of Al-7075 alloy was converted into volume (%) fractions from (mass) weight (%) fraction and the respective volume fractions of the constituents were added for obtaining the total volume fraction of the alloy powder. Now the density was calculated using the formula:

$$\rho_m = \frac{100}{(\frac{M_1}{\rho_1}) + (\frac{M_2}{\rho_2}) + (\frac{M_3}{\rho_3}) + ...+ (\frac{M_x}{\rho_x})} \quad \text{..... (Eq. 4.1)}$$

where (M_1, M_2, M_3….M_x) and (ρ_1, ρ_2, ρ_3… ρ_x) represent (mass) weight fractions and elemental densities of the constituents respectively.

4.4.5.2 **Calculation of theoretical composite density**

The inverse rule of mixtures was extended to compute the theoretical composite density (ρ_c) from the respective weight fractions (%) and theoretical densities of the matrix and reinforcement particles, using the formula:

$$\rho_c = \frac{100}{(\frac{M_m}{\rho_m}) + (\frac{M_f}{\rho_f})} \quad \text{..... (Eq. 4.2)}$$

where (M_m, ρ_m) and (M_f, ρ_f) represent weight fractions (%) and density of matrix and reinforcement particles respectively.

4.4.5.3 **Green density of powder compacts and sintered density of preforms**

Green compacts obtained after cold compaction and preforms obtained after sintering were examined for density by weight and volume method. Weight of green compacts and preforms was recorded by an electronic weighing balance of 120 gm weighing capacity with an accuracy of 0.1 mg using AUW120^{TM} (Shimadzu, Japan). Dimensions of the samples were carefully measured using a digital vernier caliper to an accuracy of 0.01 mm (make: MITUTOYO^{TM}, 150 mm measuring range). Measurements were repeated on at least 2 identically processed compacts, and average weight and volume values were used to report green densities of the powder compacts.

The green and sintered densities were further confirmed by Archimedes principle/water displacement technique with oil-impregnation using the ASTM standard B962-08. According to the standard, the density calculations were done by using the formula:

$$\text{Density D} = \frac{A\rho}{B-(C-E)} \quad \text{..... (Eq. 4.3)}$$

All densities were reported in gcm^{-3}.

A = the mass of the green part or test piece in air, g,

B = the mass of the oil-impregnated green part or test piece, g,

C = the mass of the oil-impregnated part/test specimen and specimen support immersed in water, g,

E = the mass of the oil-impregnated part/test specimen support immersed in water, g,

and

ρ = the density of the water, g/cm3.

4.4.5.4 **Density measurement of forged samples**

Density of the forged samples was determined on metallographically polished unetched samples by image analysis (Radical Meta Check 5.0^{TM} software). The samples were mirror polished by final cloth polishing and optical unetched micrographs were analyzed for porosity measurement. The porosity was detected with the help of software which determines the dark area exhibited by the porosity. The deduction of porosity fraction gives the relative density in the forged samples.

4.4.5.5 **Densification parameter**

Densification parameter (ψ) was calculated using the following formula:

$$\psi = \left(\frac{\rho_s - \rho_g}{\rho_t - \rho_g}\right) \quad \text{..... (Eq. 4.4)}$$

where ρ_s and ρ_g are sintered and green densities respectively; theoretical density ρ_t corresponds to ρ_m and ρ_c for monolithic alloys and composite formulations respectively.

It is a dimensionless parameter, expressed as a percentage number which is useful in capturing the effect of net density progression activated by sintering. Positive values are indicative of density enhancement by sintering (shrinkage) and negative values indicate a final expansion of sample after sintering.

4.4.6 **Microstructure**

4.4.6.1 **Sample preparation**

Sintered and hot forged compositions were sectioned along required surfaces by precision cutting saw, ISOMET 4000^{TM} (Buehler, USA). Samples were mounted in 20 mm diameter cold setting phenolic resin based quick hardening compound. Mounted samples were manually polished on 240, 600, 800, 1200, 1500 and 2000 standard grit SiC papers (3M^{TM}, India). Polishing direction was turned over by 90º after each paper. Care was taken to frequently dip the polished surface in

kerosene oil to ensure the release of SiC particles from the soft aluminum matrix. Paper polished samples were ultrasonically cleaned in distilled water before cloth polishing. The cloth polishing was manually performed using an aqueous suspension of fine magnesium oxide (heavy) (99% purity, Loba Chemie, Mumbai, India) on open-nap (rough) billiards cloth. The cloth was mounted on 8" diameter aluminum discs which were rotating at 150-200 rpm. The rough cloth polishing was followed by another polishing cycle on closed-nap (fine) billiards cloth. Samples were finally cleaned ultrasonically in distilled water after cloth polishing.

4.4.6.2 **Optical micrography**

Sample surfaces were eached after cloth polishing with Keller's reagent (95 ml H_2O, 2.5 ml HNO_3, 1.5 ml HCl, 1.0 ml HF). Keller's reagent applied by a cotton swab was most effective in revealing particle boundaries and sub-particle grains for pure 7075 alloy and its composites. Optical microscopy was performed on DMI5000M^{TM} (Leica, Switzerland) and D50^{TM} (Olympus, Japan) metallurgical microscopes, having 1000X and 2000X maximum compound magnifications respectively with facility for image capturing and editing.

4.4.7 **Mechanical behavior**

4.4.7.1 **Hardness**

The hardness (Vickers) values for pure alloy and composite samples were measured using VM50^{TM} (FIE Instruments, India) hardness testing machine at 1 Kg load for 15 s dwell time. Average of 5 measurements was reported for each composition in VHN. Standard hardness test block (RTA^{TM}, India) was used to calibrate the instruments prior to testing of samples. Test surfaces were parallel and polished to 2000 grit finish by using SiC polishing papers. Distance between successive indents was maintained at more than 5 times the indent diagonal at the sample surface.

4.4.7.2 **Tensile Test**

Tensile tests of all the samples were carried out using computerized universal testing machine H25K-S^{TM} (Housnfield) 25kN, at a constant crosshead velocity of 1 mm min^{-1}. All tests were conducted at room temperature by secure placement of test pieces in suitable grips to avoid any slippage. The test specimens of dumbbell shape, as shown in Fig. 4.5, were machined from hot forged samples conforming to different compositions and heat treated conditions. Nominal gauge

dimensions were fixed at 25 mm length x 6 mm diameter. Samples were polished to remove any tool markings due to machining.

Fig. 4.5 Tensile test pieces machined from hot forged samples

Load (N) and displacement (mm) logged by the interfaced computer was converted to engineering stress-strain. At least two samples were tested for a given composition and processing condition and one representative test result was reported. Analysis of fracture surfaces was conducted using ZEISS SUPRA 55VP^{TM} scanning electron microscope for surface morphology and reinforcement interactions with the matrix.

4.4.7.3 **Compression Test**

Compression tests of base alloy and composite samples were carried out in order to determine the damage evolution and failure mechanism as a function of reinforcement content at room and elevated temperatures. Cylinders of size 6 mm diameter x 9 mm height (h/d=1.5) were machined out of forged samples using wire EDM. Compression tests at room temperature were performed on H25K-S^{TM} (Housnfield) 25kN universal testing machine at a cross head velocity of 1mm min^{-1}. Test samples were coated with graphite paste, to ensure a uniform coefficient of friction between the sample and compression platens. Load (P) in N and ram displacement (Δh) in mm, recorded for compression tests was converted to true stress (σ) MPa and true strain (ε) using the following relations:

$$\sigma = \frac{P(h_O - \Delta h)}{A_O . h_O} \quad \text{..... (Eq. 4.5)}$$

$$\epsilon = \ln\left(\frac{h_O}{h_O - \Delta h}\right) \quad \text{..... (Eq. 4.6)}$$

where A_O and h_O denote the initial cross-sectional area and the height of the sample, in mm^2 and mm respectively.

4.4.8 **Wear Test**

Dry sliding wear behavior of Al-7075 and its composites was observed using TR-201E-M2^{TM} (Ducom, Bangalore, India), pin/ball-on-disc tribometer, as shown in Fig. 4.6. Specifications of the tribometer are detailed in Table 4.4. The tribometer was interfaced with a continuous data logging software, WINDUCOM-2000^{TM}, (Ducom, Bangalore, India) which recorded frictional force and pin height loss at 1 s^{-1} frequency. Test pins (Fig. 4.7) of 6 mm diameter x 25 mm height, with hemispherical ends (3 mm diameter) were machined out of the hot forged samples and tested against hardened steel counterface disc (58 HRC).

(a)  (b) 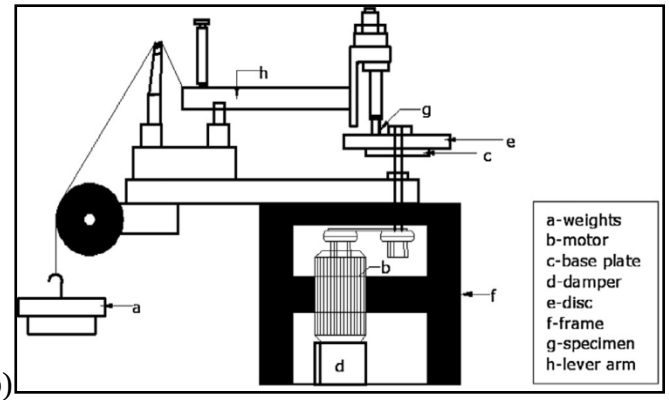

Fig. 4.6 Ducom TR-201E-M2^{TM} tribometer (a) Photograph and (b) Schematic diagram

Fig. 4.7 Wear sample pins

Table 4.4 Specifications of Ducom TR-201E-M2^{TM} tribometer

Attribute	Value
Diameter of wear disc	100 mm
Pin diameter	3-10 mm
Pin holder length	20-30 mm
Wear track diameter	0-80 mm
Disc rotation speed	200-2000 rpm (± 1%)
Normal load	10-100 N (in steps of 5N)
Friction force limit	0-100 N (resolution 0.1N, ± 1%)
Timer	99/59/59 (h/min/s)
Wear range	2000 μm (resolution 1 μm, ± 1%)

Wear tests were conducted at three different loads of 10 N, 20 N and 30 N and at a sliding speed of 1m/s. To determine the effect of sliding speed on wear behavior, wear tests were performed at a two different sliding speeds of 1m/s and 2 m/s at 20 N load. All the tests were performed for a fixed sliding distance of 1500 m, at room temperature and at a relative humidity level of 40 ± 5%. Counter disc was freshly prepared after each test by polishing it and total three tests for each condition was performed to obtain the average value of wear loss. The wear volume loss was determined with the help of weight loss and the calculation of pin volume loss is given as below:

Pin Volume loss = Weight loss/Density of pin material …… (Eq. 4.7)

Weight loss of all the samples was determined to an accuracy of 0.1 mg. The wear rate was evaluated by dividing the volume loss of the pin by the load and the sliding distance and reported in ($mm^3N^{-1}m^{-1}$). For analysis of wear mechanism, wear scar diameter, wear tracks as well as wear debris were analyzed by scanning electron microscopy (ZEISS SUPRA 55VPTM) equipped with OXFORD EDAXTM energy dispersive x-ray spectroscopy (EDS) detector.

4.4.9 **Machinability Studies**

Machining experiments in the form of drilling were conducted on a radial drilling machine. Specifications of the machine are given in Table 4.5.

Table 4.5 Specifications of Radial Drilling Machine

Make	Batliboi Pvt. Ltd. Surat India
Spindle Speed range	90-4500 rpm
Feed Rate range	0.03-0.3 mm/revolution
Main motor power/speed	1.5 kW/1420 rpm
Elevating motor power/speed	0.75 kW/1420 rpm

Experimental set-up of machining consists of (1) drilling machine, (2) fixture for holding the sample, (3) piezoelectric drill dynamometer (Kistler® make), (4) charge amplifier and (5) connecting cables, an analog to digital converter and a computer for data acquisition. Thrust force signals ware recorded by a four component drill dynamometer (Kistler 9272 make). A charge amplifier (Kistler 5070 make) was used to amplify these signals. The amplified signals were passed through signal conditioning equipment to a computer system using a data acquisition card. These signals were recorded by dedicated data acquisition and finally analyzed by evaluation software (Dyno-Ware®). Samples were held in a rigid fixture attached to dynamometer mounted on machine table. Square headed bolts were used to mount the dynamometer rigidly on machine table which were fitted into T-slots. The experimental set-up for machinability studies is shown in Fig. 4.8.

(a)

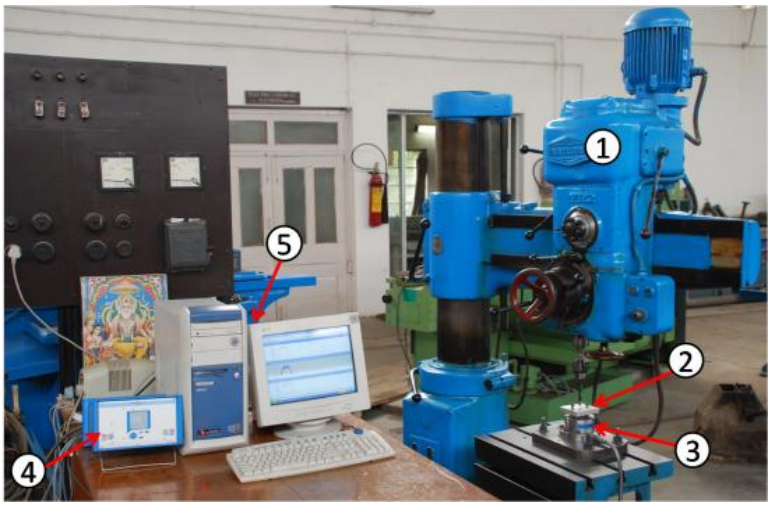

(b)

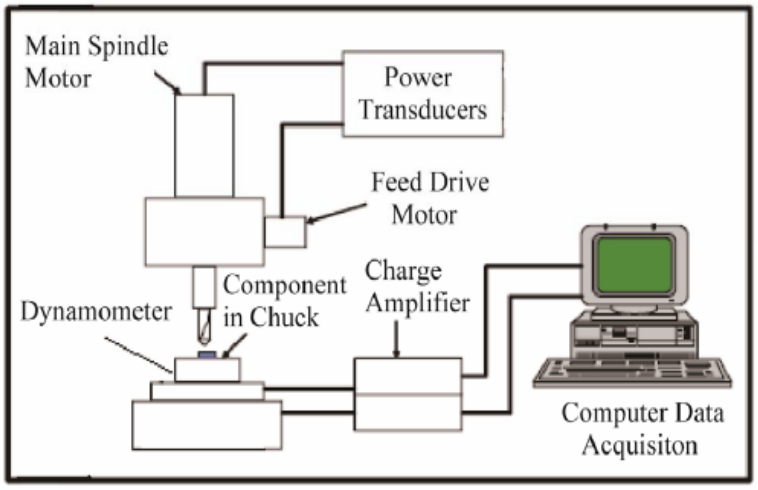

Fig. 4.8 Test set up for machinability (a) Photograph showing major parts and (b) schematic diagram

(a) 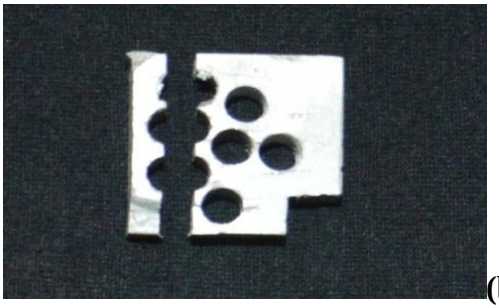 **(b)** 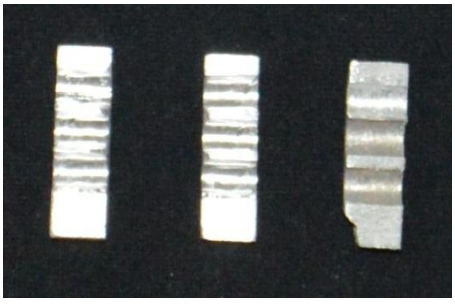

Fig. 4.9 (a) Machined sample and (b) Machined surface for roughness and SEM analysis

Samples for machinability tests were prepared by leveling the surface by belt polishing followed by paper polishing. The process parameters used during machining experiments are

shown in Table 4.6. Measurement of surface finish of machined surface was carried out after drilling operation by measuring surface roughness. Surface roughness was measured using a surface profilometer (Mytutoyo SJ-400, Japan). Sample after machining and machined surface for roughness are shown in Fig. 4.9. The roughness was measured by reporting the average of three readings at individual surface of the drill hole.

Table 4.6 Process parameters for machinability test

Process parameters	Value
Cutting speed, V (rpm)	140
Feed, f (mm/rev)	0.12
Drill Diameter (mm)	5
Depth of cut, (mm)	7
Cutting environment	dry

4.4.10 **Flow Chart for Research Process**

The detailed flow charts, including major processing steps as well as characterization tools employed at various stages of the research work are shown in Fig. 4.10.

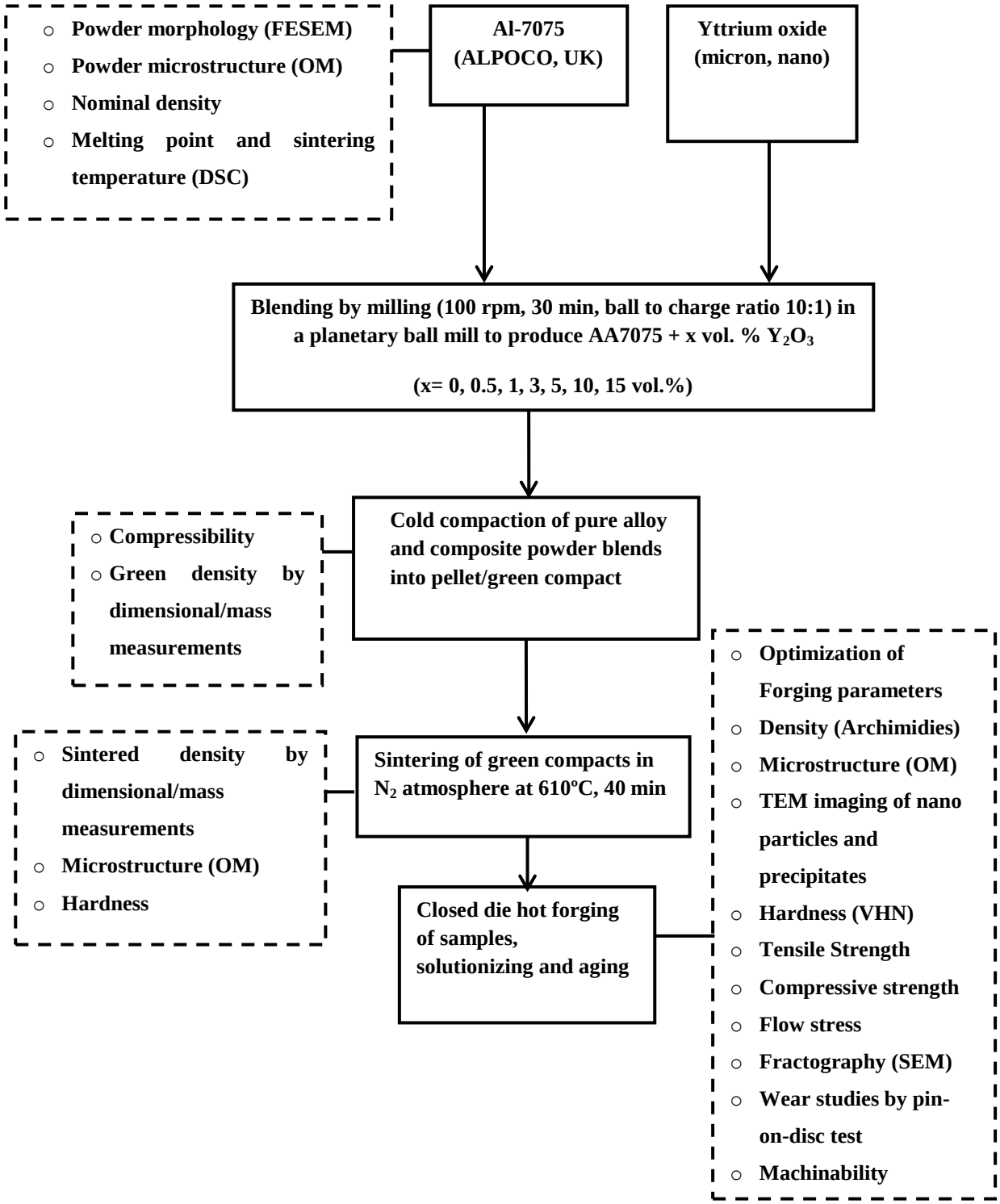

Fig. 4.10 Flow chart for fabrication and characterization of Al-7075 composites

Chapter 5

RESULTS AND DISCUSSION

This chapter provides a detailed discussion on the results obtained in the present research work and has been divided in four sub-sections from 5.1 to 5.4 for clarity. Sub-section 5.1 commences with the characterization of the Al-7075 and Y_2O_3 powders employed in the present study. The working factors e.g. temperature and total strain during forging were optimized for prealloyed 7075 aluminum alloy and correlated with microstructural evolution and hardness during hot forging. Mechanical properties obtained from different composites and correlation of hardness and tensile strength with Y_2O_3 reinforcement size and content as well as microstructural changes are described in sub-section 5.2. Sub-section 5.3 describes the wear behavior of different composites at different wear loads and sliding speeds. Effect of different amount of Y_2O_3 addition on wear behavior has been investigated and justified with their microstructures and hardness. Machinability studies of different fabricated composites with respect to Y_2O_3 reinforcement size and content in the solutionized as well as T_6 conditions were discussed in sub-section 5.4.

5.1 Microstructural evolution during hot forging of Al-7075 powder

This sub-section presents the microstructural evolution attained during hot forging of Al-7075 prealloyed powders at various temperatures and strains. Preforms were fabricated by uniaxial compaction at 350 MPa followed by sintering at 610^{o}C for 40 min in nitrogen atmosphere. Sintered preforms were subsequently hot forged at various temperatures (0.6, 0.7, 0.8 and 0.9 T_m) and under various strains (0.51, 0.92 and 1.14). The effect of strain at various forging temperatures on the particle morphology, interparticle porosity, prior particle boundary (oxide layer) and hardness has been investigated. This sub-section commences with the characterization of the Al-7075 and both micrometric and nanometric Y_2O_3 powders.

5.1.1 Characterization of Pure Al-7075 alloy Powders

The chemical composition of the Al-7075 powders as provided by the supplier is shown in Table 5.1. Major alloying elements were Zn, Mg and Cu while Cr, Fe, Si and Mn were in minor amounts as impurities.

Table 5.1: Chemical composition of prealloyed Al-7075 powder

Element	**Al**	**Zn**	**Mg**	**Cu**	**Cr**	**Fe**	**Si**	**Mn**
Wt %	90.293	5.295	2.475	1.590	0.197	0.086	0.044	0.020

5.1.1.1 Morphology, size and structure

The microstructure of the polished cross section of the Al-7075 powders is shown in Fig. 5.1(a) while that of the loose powder is shown in Fig. 5.1(b). The particle size distribution of the particles was of bimodal mode comprising of large particles of around 216 µm and finer particles of around 12 µm with an average particle size of 60 µm. The finer particles were generally rounded while the larger ones were mainly elongated. The powders exhibited a dendritic structure along with some porosity. This microstructure is typical of a gas atomized powder in which powder particles cool rapidly and do not get sufficient time to develop a sub grain structure from the dendrites [Rokni et al., 2014].

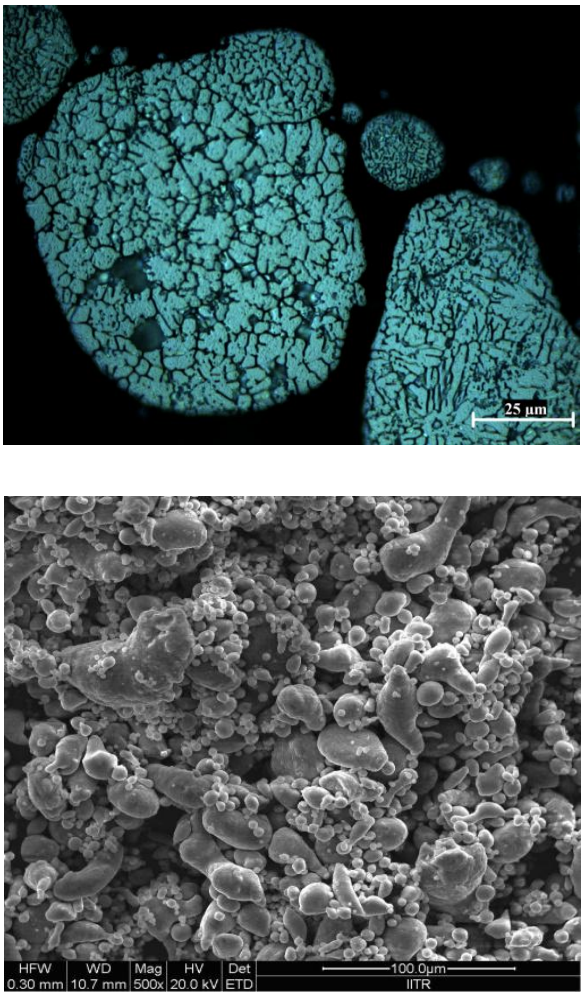

Fig 5.1: Pure Al- 7075 prealloyed powders (a) Optical microstructure of cross section and (b) SEM image

5.1.1.2 X-ray diffraction (XRD) of Al-7075 powder

The X-ray diffraction (XRD) pattern of Al-7075 powder is shown in Fig. 5.2. All peaks corresponding to Al (FCC) were observed in the diffraction pattern of Al-7075. Since the Al-7075 powder was gas atomized, the oxide content was minimal. These powders form a thin oxide film when exposed to atmosphere but this oxide content was below the detectable limit of XRD. The oxide content in Al-7075 powder was determined separately and discussed in upcoming section. Peaks of other alloying elements (Zn, Mg, Cu) were also absent due to their low amounts and these were not detectable in the XRD as a volume fraction of more than 5-7% is required for detectability.

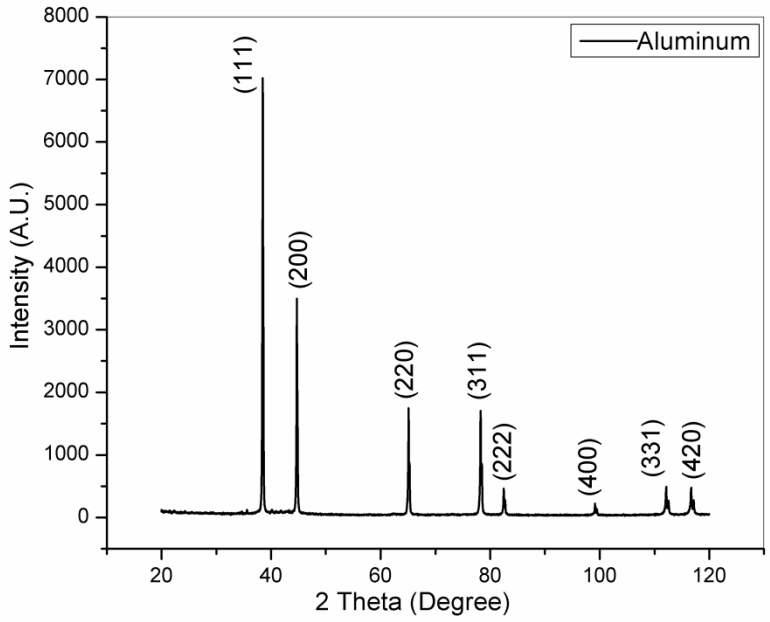

Fig 5.2: X-ray diffraction (XRD) of Al-7075 powder

5.1.1.3 Thermal analysis of powder

The thermal analysis data shows differential thermal analysis (DTA), differential thermogravimetry (DTG) as well as thermogravimetry (TG) output. DTA/DTG/TG curves of the Al-7075 powders are shown in Fig. 5.3. The DTA curve shows a sharp endothermic peak at 630^{o}C which corresponds to the melting point of the alloy system. This DTA peak started growing around 580^{o}C and the system started changing to a liquid state from solid phase due to eutectic formation of Al-Cu [Mohammadi et al., 2010]. The TG curve exhibited a continuous drop with the temperature as the weight of the sample decreased till 400^{o}C. This loss in weight represents delubrication process in which acrawax (lubricant) escapes from the system. Acrawax was premixed in the pure Al-7075 powder for ready to press use by the powder supplier. The delubrication is further confirmed by DTG curve in which the rate of the reaction was disturbed between 325^{o}C to 400^{o}C with a peak appearing at 375^{o}C. After 400^{o}C no disturbance was seen during the heating process. We can thus conclude that the premixed lubricant has been removed completely till a temperature of 400^{o}C.

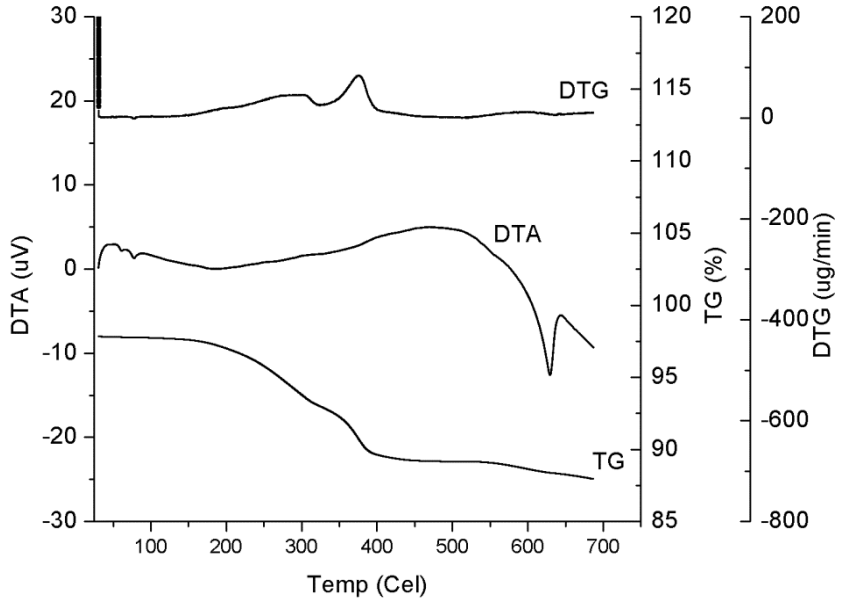

Fig 5.3: DTA curve for pure Al 7075 powder

5.1.1.4 Oxygen content

The oxygen content of the Al-7075 powders as determined by oxygen analyzer was 1647± 57 ppm which is equivalent to approximately 0.16 wt%. This was comparable to the amount noted by Unal et al., 1998, which was 0.2 wt% with an oxide layer of 4 nm for gas atomized powders. Though the oxide layer of the Al-7075 powders was not determined in the present study, it is likely to be of the same order i.e. 4 nm. Atomized Al powders generally exhibit an oxide layer of 4-15 nm which depends upon the atmosphere in which they were atomized and stored.

5.1.2 Characterization of Y_2O_3 reinforcement Powder

5.1.2.1 Morphology, size and structure

Yttrium oxide (Y_2O_3) powder of micrometric (~ 4 μm) and nanometric (~ 10 nm) size supplied by Sigma Aldrich, India was used as reinforcement material. SEM image of micrometric Y_2O_3 reinforcement powder is shown in Fig. 5.4(a) while agglomerates of nano Y_2O_3 reinforcements are seen in the TEM image in Fig. 5.4(b). Micrometric Y_2O_3 particles of larger size were spongy in shape however smaller particles were angular. Nano particles of Y_2O_3 were in the form of agglomerates and individual particle exhibited rounded morphology.

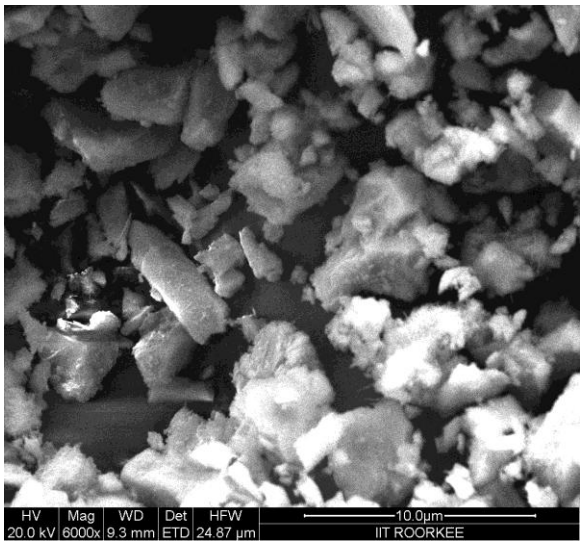

(a)

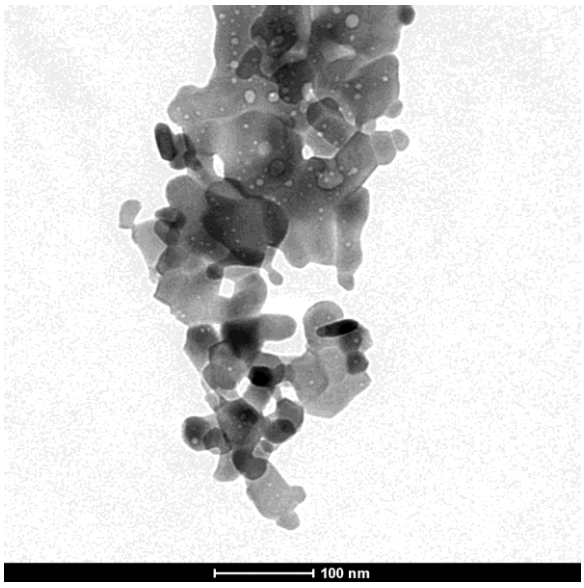

(b)

Fig 5.4: SEM images of (a) Yttrium oxide particles (micron) and (b) Yttrium oxide particles (nano)

5.1.2.2 X-ray diffraction (XRD) of Y_2O_3 powder

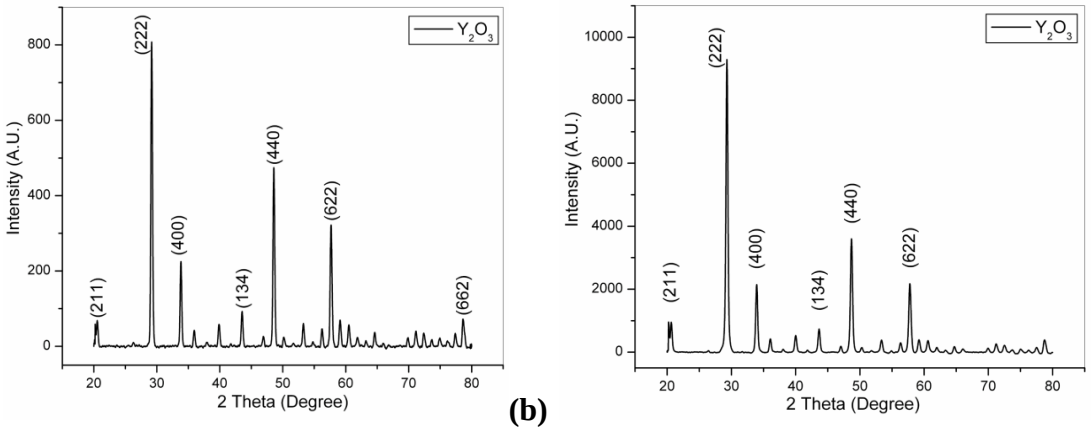

Fig 5.5 (a) pattern of micrometric Y_2O_3 powder and (b) nanometric Y_2O_3 powder

The X-ray diffraction (XRD) pattern of micrometric Y_2O_3 powder and nanometric Y_2O_3 powder is shown in Fig.5.5 (a) and (b). All peaks corresponding to Y_2O_3 phase were observed in both the diffraction pattern of Y_2O_3. The XRD pattern did not show any separate peak of any other oxide or any other impurities. All the major peaks of Y_2O_3 powder in both sizes lies at the similar 2Θ angle but the intensities of these peaks were found higher for nanometric Y_2O_3.

5.1.3 Density of Pure Al-7075 alloy

The average relative green density of the compacts pressed at 350MPa was approximately 81% and upon sintering average relative sintered density of approximately 89% was obtained. Forging of the sintered compacts at various tempeartures (0.6, 0.7, 0.8 and 0.9 T_m) and strain conditions (0.51, 0.92 and 1.14) lead to density levels in excess of 98% relative forged densities and in some cases reached almost 100% of theoretical density. It was difficult to determine a trend of the forged densities with respect to the forging temperatures and strains as the density values were very close to each other and within error margin. The average of the relative forged density was approximately 99.6 %.

5.1.4 Microstructure evolution during sintering

The microstructure after sintering is shown in Fig. 5.6. Porosity is visible at the triple points, particle junctions and within the particle (formed during atomization of the powders) in the form of dark black spots. This porosity has to be eliminated to obtain full density and for the

improvement of mechanical properties. The presence of prior particle boundaries (PPBs) indicates very less neck formation (diffusion between the particles). The oxide at the PPBs layer seem to be hindering the formation of necks and thus sintering between the particles.

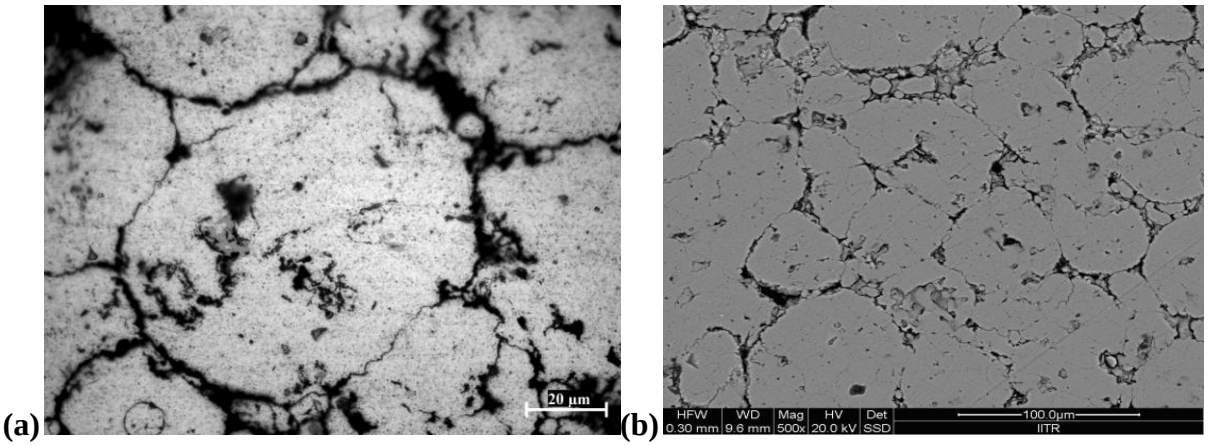

Fig 5.6: Sintered Al- 7075 prealloyed powders (a) Optical microstructure and (b) SEM image

5.1.5 Effect of forging temperature and strain on microstructure

5.1.5.1 Microstructure evolution in longitudinal section

The optical microstructure of longitudinal section of hot forged samples is shown in Fig. 5.7. Oxide layer around the particles is clearly visible in the optical microstructures. Although the oxide layer of an individual aluminum powder particle is 4-15 nm thick, its presence as well as its breakup can be observed by optical microscopy. The grain boundaries in powder metallurgical aluminum are prior particle boundaries at which two particles are in contact, so effectively the oxide layer is twice. Further on heating during sintering due to trace amounts of oxygen in the sintering atmosphere (which in this case was nitrogen) further growth of the oxide layer is likely to take place due to the high affinity of aluminum with oxygen. Again, due to etching the grain boundary (along with the oxide layer) scatters the light in the optical microscope which causes the oxide layer to appear significantly larger.

At 0.6 T_m when the sintered perform was hot forged with a total strain of 0.51, the particle shape did not change but sample porosity got eliminated to a certain extent and the oxide layer at the particle boundary remained intact/adherent. When strain is increased (0.92) at the same temperature, the particle shape changes and becomes elongated in the direction normal to the forging load. This shape change only deforms the particles but does not lead to the disruption of

the oxide layer at the particle boundary. Also the porosity gets almost eliminated at this strain. When the strain is increased to 1.14 further elongation of the particle is observed but no disruption of the particle boundary. At the strain value 1.14 stretched deformation bands can be observed which are elongated normal to the direction of forging load. Increasing the temperature to 0.7 T_m has no significant effect on the particle boundaries at a strain of 0.51 only that there is further elimination of porosity as compared to the same strain at 0.6 T_m. Increasing strains at this temperature has the similar effect as that was observed at 0.6 T_m i.e. the particles were further deformed and flattened. Now increasing temperature to 0.8 T_m, at lower strain of 0.51, there is further reduction of the porosity at this temperature as compared to that at 0.7 T_m. Providing a higher strain (0.92) at this temperature was sufficient to initiate the breaking of powder particle boundaries by shear and dispersing the aluminum oxide into the metal matrix which was initially in the form of particle boundary. At this strain the particle boundaries were seen opened to a certain extent and the aluminum alloy powder particles formed a continuous network throughout the matrix. On providing a further strain (1.14) at this temperature the structure was similar to that of a structure of 0.92 only that further shearing and disruption of oxide layer was observed.

At a temperature of 0.9 T_m slight deformation/flattening of the particles was observed even at a lower strain of 0.51 which was not observed at this strain at lower temperatures. This is due to the softening of the particles at this high temperature in spite of the lower strain. Interparticle porosity is negligible at this stage due to the deformation of the particle which leads to elimination of the pores. At a further strain of 0.92 the structure was similar to that of 0.8 T_m of strain 1.14. Here there was disruption of oxide boundary as discussed earlier. At higher strain of 1.14 at this temperature there was also complete disruption of oxide layer which got disrupted in the matrix as Al_2O_3 particles. This led to the vanishing of the prior particle boundaries. The oxide particles are seen disrupted in the longitudinal direction which is the direction of the deformation.

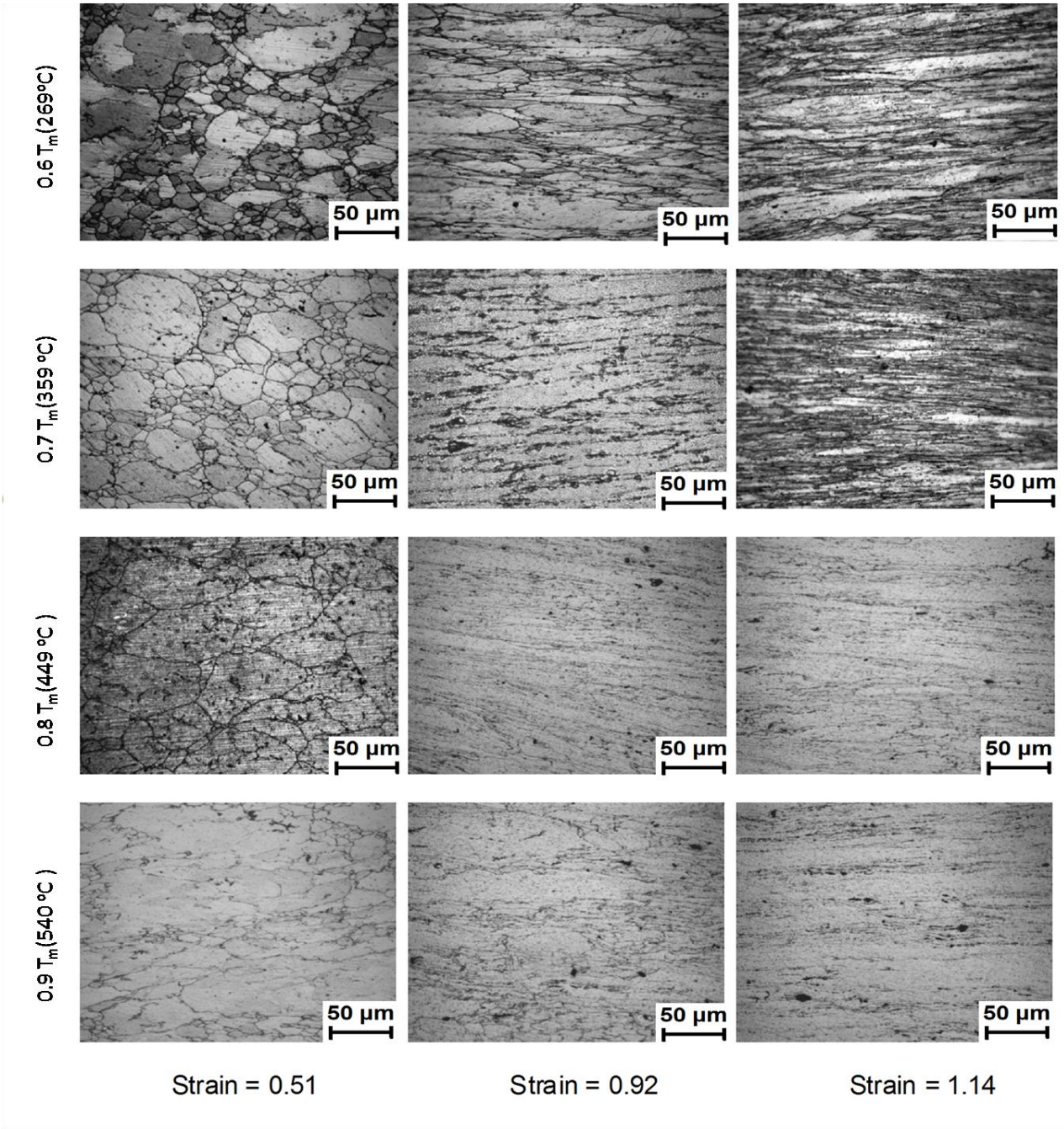

Fig 5.7: Longitudinal section of Al-7075 hot forged at different conditions

5.1.5.2 Microstructure evolution in transverse section

The effect of hot forging temperature and strain on the microstructure of the specimens in the transverse direction is shown in Fig. 5.8. The microstructures are of two types: one at a lower temperature and lower strain values and the other at higher temperature and higher strain values. The former exhibit a structure of less deformed particles (with presence of some interparticle porosity) and presence of particle boundaries while the latter exhibits some coalesced particles

formed due to the shearing of the particle boundaries. At lower strains (0.51) at all temperatures the structure was similar to the corresponding structure in the longitudinal section as seen in Fig. 5.7. This was due to the very low level of deformation experienced by the particles due to which the structure appeared similar in the longitudinal as well as transverse direction. On increase in strain especially at high temperatures the particles coalesced leading to metallurgical contact between the particles due to the shearing of the grain boundaries. Thus the coalesced particles appeared as one entity in the transverse section. Due to this, a bimodal type of structure was observed in which the larger areas comprised of coalesced particles while the smaller ones were those in which complete shearing off of the boundaries did not occur.

At low temperatures and low strain values the powder particles have a tendency to fill the die space without much deformation during forging. During this deformation only powder particle shape changes but particle boundary remains undisturbed. As the strain value increases, the powder particle boundaries get disturbed due to friction and shear. At higher temperatures this disturbance increases under strain due to softening of the powder particles. At low temperatures, particle boundary which is in the form of aluminum oxide does not get ruptured but at higher temperatures the powder particle boundary ruptured due to the combined effect of softening of particles and high disturbance in the matrix caused by strain consequently transforming the system into an in situ composite of aluminum-aluminum oxide. At 0.9 T_m, incipient melting [Greasley and Shi, 1993] occurs causing inhomogeneity in the material. Incipient melting is caused by high temperature and surface stress conditions, when the powder processing extends hot working ranges. Increase in forging temperature may help in softening the material and it causes easy breaking of the oxide layer but uniformity in the microstructure loses due to thermal instability and hot shortness as reported in another study [Greasley and Shi, 1993].

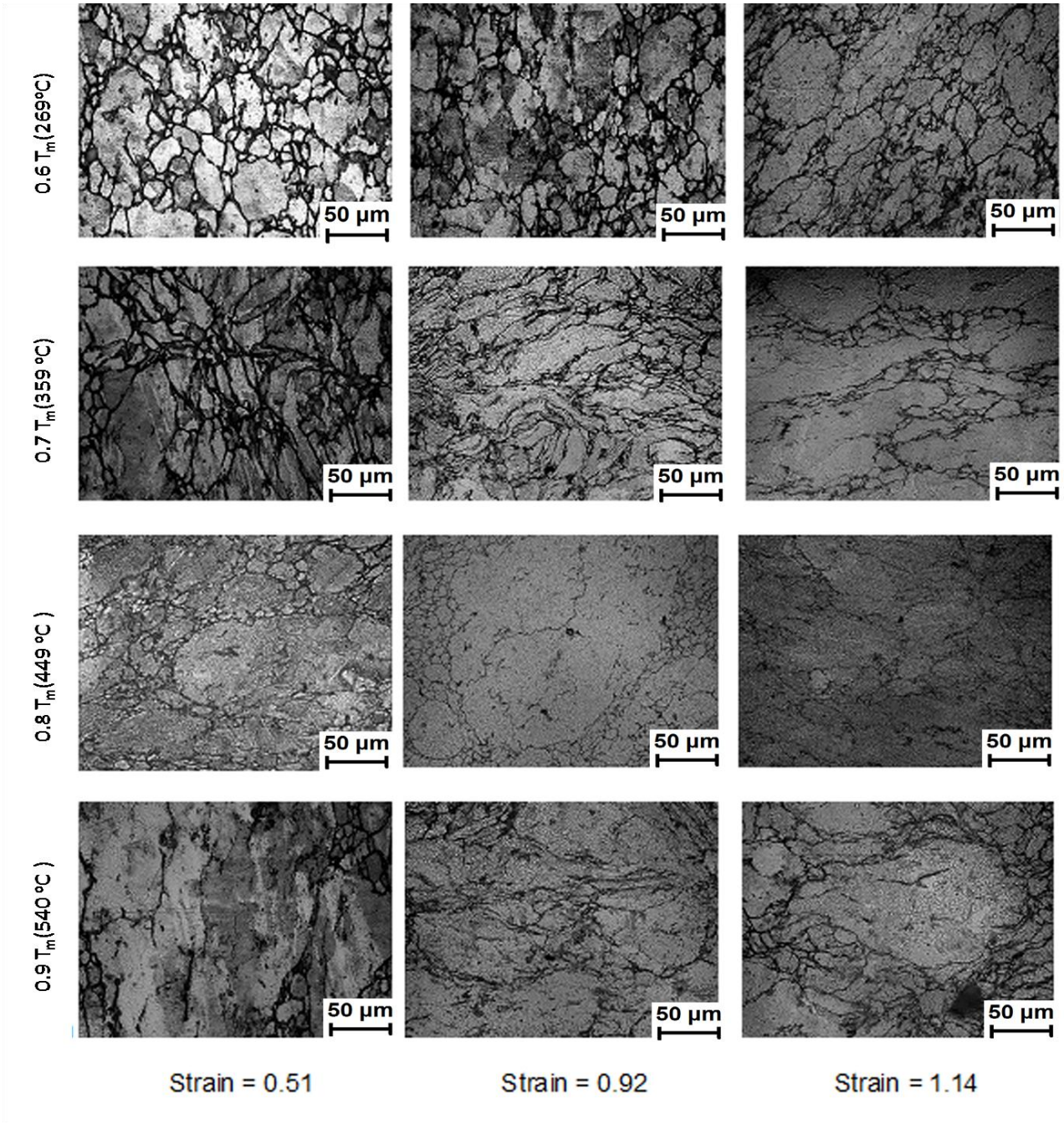

Fig 5.8: Transverse section of Al-7075 hot forged at different conditions

The oxide layer on the selected samples with minimum temperature/minimum total strain, intermediate condition and with maximum temperature/ maximum total strain was studied in detail by SEM (Fig. 5.9). At 0.6 T_m and lowest strain (0.51), the oxide layer is seen around the particle boundary as a continuous network. At an intermediate strain (0.92) and 0.8 T_m the oxide layer is seen disrupted with some round oxide particles dispersed into the system. These oxide particles help in improving the properties as an in-situ reinforcement. At higher strain (1.14) and 0.9 T_m the

oxide layer can be seen disrupted unevenly. In some places (Fig. 5.9.c) the oxide particles from the PPBs flowed to another location leading to clusters of Al_2O_3 causing inhomogeneity. At some locations dimples were observed which are most likely due to the removal of small particles of aluminum oxide during polishing (Fig 5.9.c).

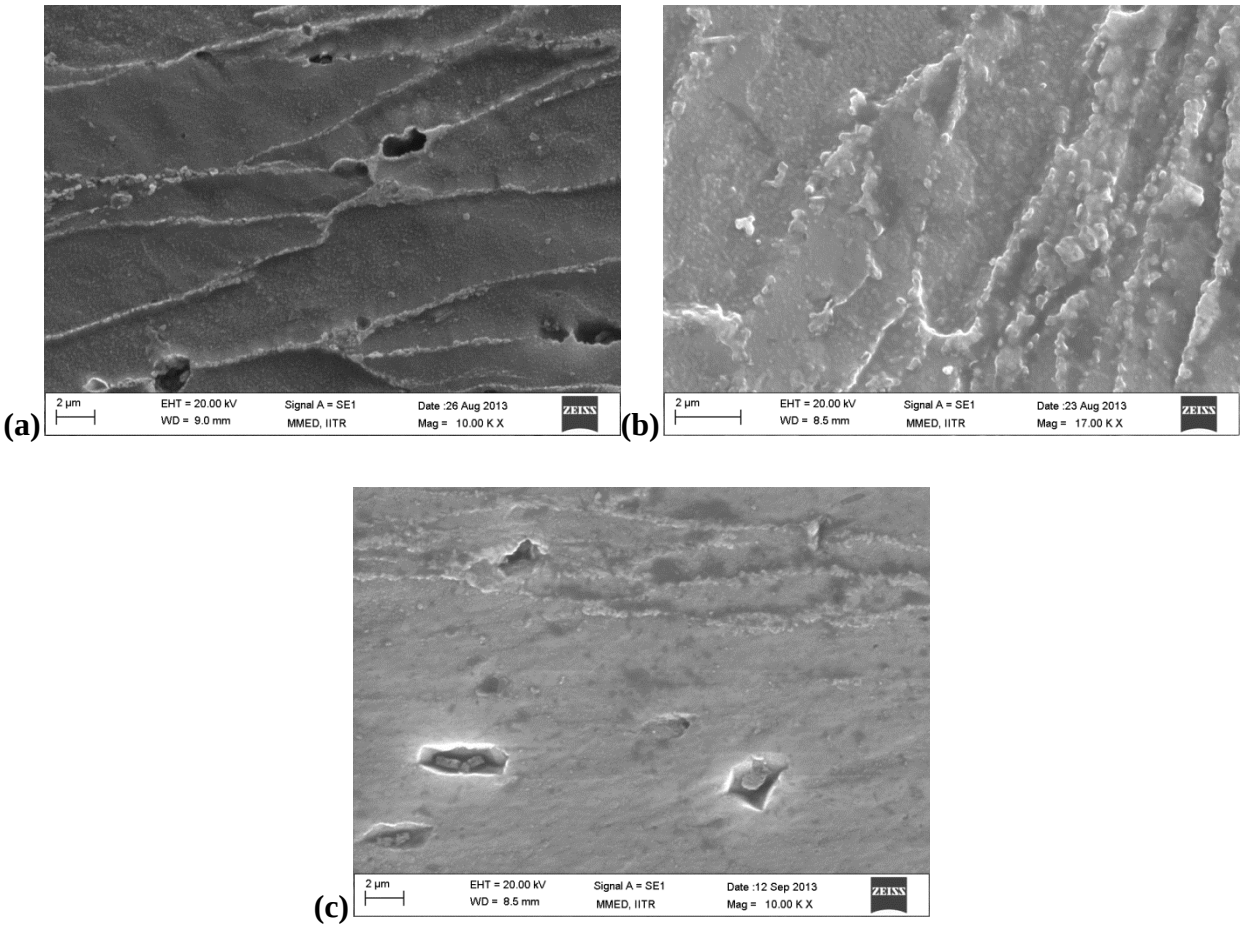

Fig 5.9: SEM images of (a) 0.6 T_m and 0.51; (b) 0.8 T_m and 0.92 and (c) 0.9 T_m and 1.14

Microstructural investigations at higher magnifications (Fig. 5.10) revealed the occurrence of dynamic recrystallization (DRX) at the highest strain (1.14) in preforms hot forged at 0.8 T_m and 0.9 T_m. This indicates that temperatures of 0.8 T_m and beyond and strains of 1.14 and beyond are required for DRX to occur in the 7075 powders. The prior grain boundary was partially diminished during DRX and new grain boundaries were formed. In the process of recrystallization, existing grain boundaries diminish due to cryatallization of new grains at the grain boundary. These grains grow with time and replace the existing grains. In the present condition the new grains did not get sufficient time to grow to replace the existing grains due to immediate

quenching after the hot forging operation. At this intermediate condition, the existing grain boundaries are visible throughout the structure while the recrystallized grains are visible at some locations.

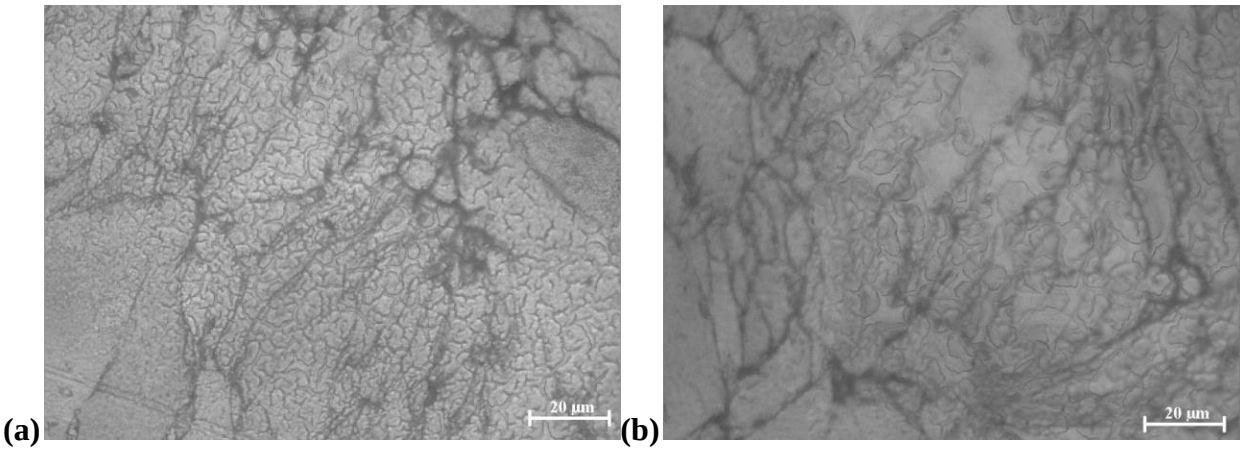

Fig 5.10: Dynamic recrystallization from the transverse section of Al-7075 hot forged for a temperature 0.9 T_m and strain value (a) 0.92 and (b) 1.14

5.1.6 Hardness

5.1.6.1 Hardness in longitudinal section

The hardness values (Fig. 5.11) were moderately higher in the longitudinal sections which ranged from 48.9 to 59.2 VHN as compared to that of the transverse sections which varied from 47.3 to 55.5 VHN. This can be attributed to the larger degree of deformation taking place in longitudinal direction as compared to the transverse section as observed and discussed in section 5.1.6.1. The moderate difference in the hardness levels between the longitudinal and transverse directions indicates a lower level of anisotropy in these powders (processed by powder hot forging) as compared to those in conventional forged materials which exhibit a considerable higher order of anisotropy [P/M Forging, ASM handbook, Vol. 7, 1984]. The plastic deformation leads to combined effects of filling of pores, strain hardening and shearing of particles which leads to disruption of oxide layer at the particle boundaries. All these factors lead to an increase in the hardness. The hardness values were increasing with increase in strain as well as temperature except for the temperature of 0.9 T_m where there was a slight drop in hardness.

In the longitudinal section the hardness values at lower strain (0.51) were found to increase linearly with temperature. This can be attributed to the softening and slight deformation of the particles which lead to pore removal as evident in the microstructure shown in Fig. 5.11. The hardness values at 0.92 and 1.14 strain were almost similar but were considerably higher than that

obtained at 0.51 strain. Further at these strains there was only a slight increase in hardness with increase in temperature till a temperature of $0.8T_m$ after which there was a slight drop at $0.9T_m$. The increase in the hardness can be attributed to the combined effects of deformation of the particles (which leads to pore removal and strain hardening) as well as shearing off of the oxide layer at the particle boundary whereas the slight drop in hardness is likely to be due to the dynamic recrystallization (DRX) which nullifies the effect of strain hardening. Dynamic recrystallization occurs during hot forging due to the combined effect of temperature and strain. Since all the samples were water quenched immediately after hot forging, the DRX state of those samples is frozen and this state does not get disturbed further at room temperature. The absence of the drop of hardness in the 0.51 strain samples indicates that the strain was not sufficient for DRX to take place at this strain in spite of the high temperature. In both the cases at 0.92 and 1.14 strains the hardness values slightly dropped at the 0.9 T_m. The drop of hardness at higher temperature (0.9 T_m) is again due to DRX. At higher temperatures when 7075 alloy is deformed with a large value of strains DRX occurs above 0.8 Tm which is a reported fact [Rafi et al., 2010; Vedani et al., 2006; Ganesan et al., 2004].

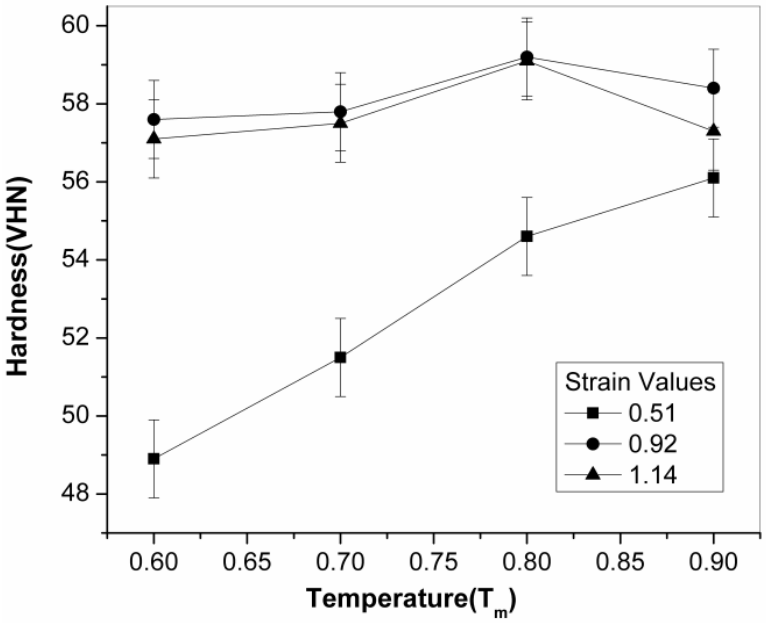

Fig 5.11: Hardness values for longitudinal section of hot forged Al-7075 at different conditions

5.1.6.2 Hardness in transverse section

In the transverse section the hardness values were again (as in the longitudinal section) found to increase with increase in temperature till 0.8 T_m after which they decreased slightly at 0.9 T_m (Fig 5.12).The hardness values were lowest for 0.5 strain while those for 0.92 and 1.14 strain were almost similar at 0.8 T_m and 0.9 T_m. At 0.7 T_m the 0.92 strain samples exhibited a higher value while at 0.6 T_m the 1.14 strain samples exhibited a higher hardness value. The higher hardness for the 0.92 and 1.14 strain samples as compared to the 0.51 strain samples can again be attributed to the higher degree of plastic deformation. The drop in hardness values at 0.9 T_m i.e. beyond 0.8 T_m can again be due to dynamic recrystallization as observed in the longitudinal section as discussed above.

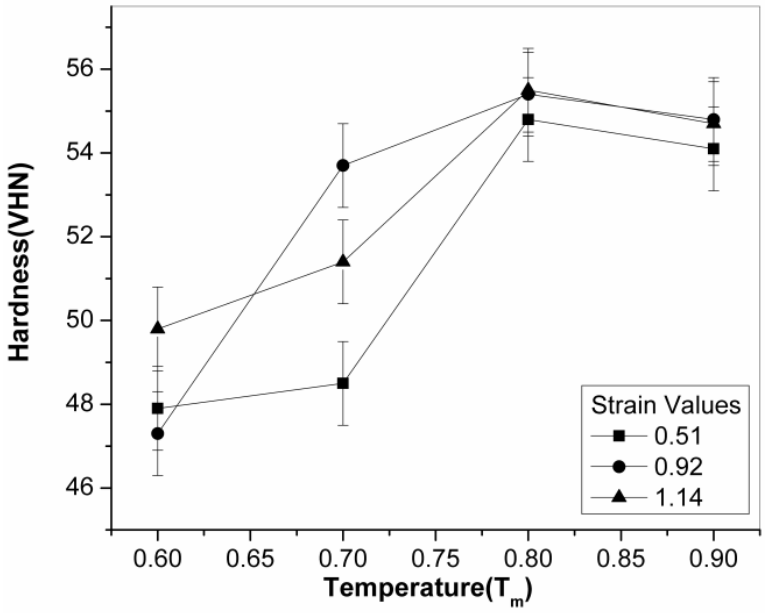

Fig 5.12: Hardness values for transverse sections of hot forged Al-7075 at different conditions

In general in both the longitudinal as well as transverse sections hardness values were lower for low strain values as compared to that of higher strains and when compared at different temperatures, these were found to increase with increase in temperature. At lower temperatures and low strain values, the powder particle boundaries were not completely broken (only deformation of the particles took place) thus hardness value is lower than the samples at higher strain values. At higher temperatures the powder particle boundary (which is in the form of aluminum oxide) disruption takes place and due to strain this ruptured particle boundary dispersed

into the matrix. In this way system became an in-situ composite of aluminum- aluminum oxide in which aluminum oxide is dispersed throughout the matrix.

5.1.7 Summary

- Forging of the sintered preforms lead to a relative density in excess of 99.6% whereas the average density of the sintered preforms was of the order of 89% while the average green density was of the order of 81%.
- The deformation of the particles after forging was larger in the longitudinal direction as compared to the transverse direction. Further, the deformation of the particles was found to increase with increase in both temperature and strain in both the directions.
- In the longitudinal direction at low temperatures and strain there was a tendency for particles to initially fill the pore space followed by the flattening of the particles whereas at high temperature and strain apart from the above mentioned there was a disruption of the oxide layer at the particle boundary. At a temperature of 0.8 T_m and strain of 0.92 the initiation of disruption of oxide layer was observed.
- In the transverse direction at a lower temperatures and strain values the structure was that of less deformed particles and presence of particle boundaries (with some interparticle porosity) while at high temperatures and strains presence of coalesced particles due to shearing of particle boundaries was observed.
- The hardness values were marginally higher in the longitudinal section (48.9 to 59.2 VHN) as compared to the transverse section (47.3 to 55.5 VHN) which indicates a lower level of anisotropy in these powders processed by sinter-forging.
- In general the hardness values were lower for low strain values as compared to that at higher strain and were found to increase with increase in temperature. There was a drop in hardness at 0.9 T_m due to dynamic recrystallization.

5.2 Mechanical Properties of Powder Forged Micrometric and Nanometric Y_2O_3 Reinforced Al-7075 Composites

Present sub-section deals with densification studies as well as the mechanical properties of powder forged Al-7075 composites reinforced with nanometric Y_2O_3 particles (0.1 to 3 vol %) and micron Y_2O_3 particles (1 to 15 vol %). The role of nanometric and micrometric Y_2O_3 reinforcement on the green, sintered densities as well as the densification parameter has been discussed. Microstructural studies have been carried out on the sintered as well as forged samples of these composites. In depth studies have been carried out on the hardness of these composites in the as-forged, solutionized as well as peak aged (T_6) conditions. Tensile as well as compressive strength of these composites in the peak aged conditions has been reported with respect to reinforcement size and content as well as the microstructure. Further, fractographs of the fractured surface of the tensile samples have been studied to determine the nature and mode of the fractures.

5.2.1 Microstructure of composites

5.2.1.1 Sintered Structure

Figure 5.13(a) shows the sintered microstructure of pure Al-7075, Fig.5.13(b-c) of Al-7075 with 0.5 vol% nanometric Y_2O_3 and 3 vol% nanometric Y_2O_3 while Fig.5.12.(d-e) show that of Al-7075 with 3 vol% micrometric Y_2O_3 and 15 vol% micrometric Y_2O_3 respectively. The microstructure of pure Al-7075 indicates presence of porosity between the particles as well as at the triple points which appear as dark regions in the micrographs. There are few areas between the particles where neck formation seems to have occurred but overall the structure does not seem to have sintered well. It is well known that the presence of oxide layers on the particle surface hinders diffusion and subsequent neck formation in aluminum and its alloys. The microstructure of Al-7075 with 0.5 vol% nanometric Y_2O_3 shows the presence of nanometric Y_2O_3 particles (in the form of clusters) mainly at the triple points of the particles. Nanometric Y_2O_3 particles are also present between two adjacent Al-7075 particles.

The microstructure of Al-7075 with 3 vol% nanometric Y_2O_3 is similar to that of Al-7075 with 0.5 vol% nanometric Y_2O_3 only difference being that the porosities have almost being completely filled up by the Y_2O_3 particles both between the two adjacent particles and at the triple points. The Y_2O_3 particles seem to have prevented the particle to particle contact between the Al-7075 particles and separated/pushed them apart. The structure of Al-7075 with 0.5 vol% nanometric Y_2O_3 appears to be more densified as compared to that of 3 vol% nano Y_2O_3; this is

also evident from the sintered density values shown in Fig. 5.13(b). As compared to pure Al-7075 the 0.5 vol% nanometric Y_2O_3 and 3 vol% nanometric Y_2O_3 structures also show larger areas of neck formation which is likely due to the shearing off of the Al-7075 oxide layer by the harder Y_2O_3 particles during the compaction process.

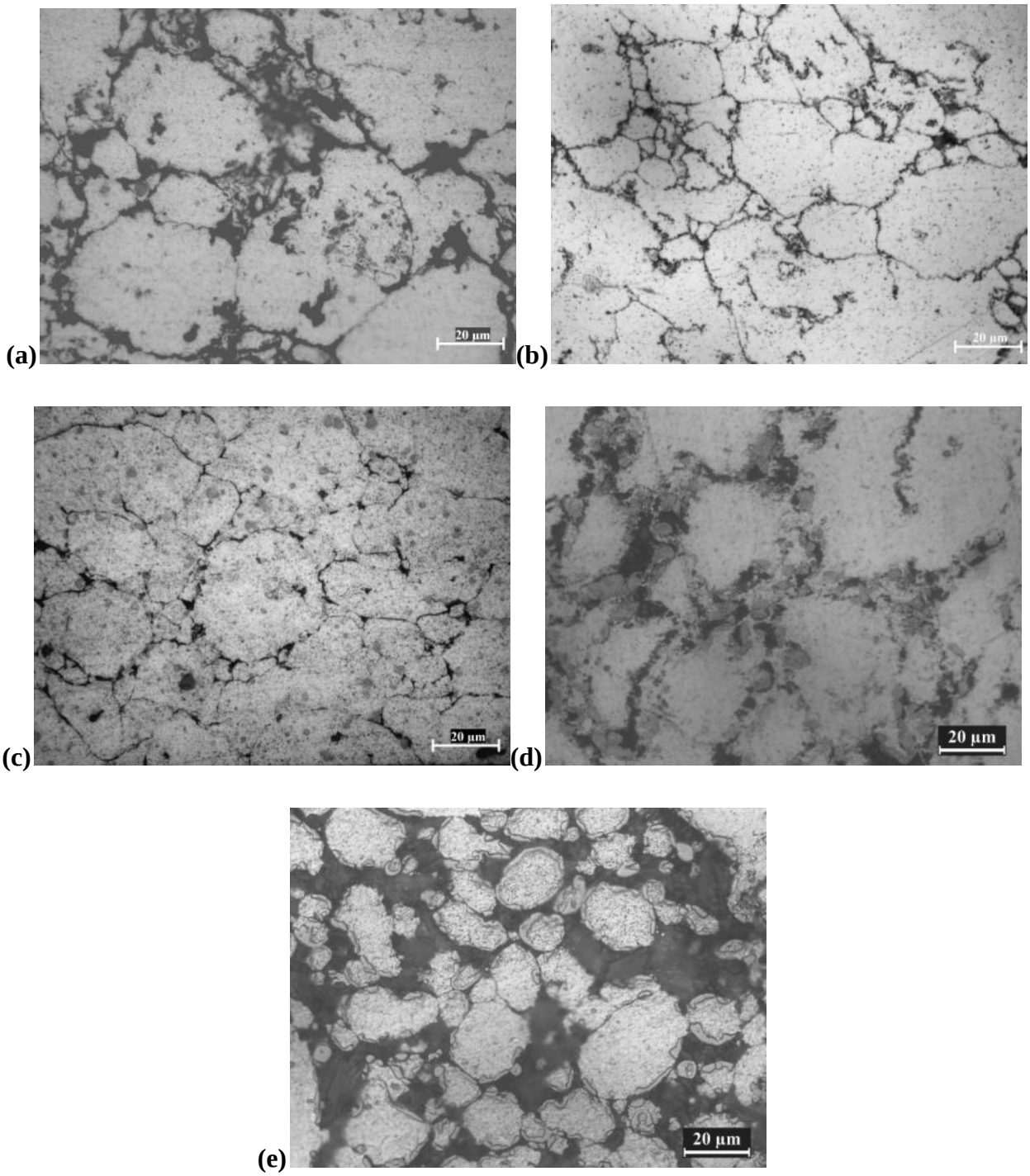

Fig.5.13: Sintered optical microstructures of (a) Pure 7075; (b) 0.5N; (c) 3N; (d) 3M and (e) 15M

The microstructure of Al-7075 with 3 vol% micrometric Y_2O_3 (Fig.5.14 (d)) indicates the presence of micrometric sized Y_2O_3 particles between the Al-7075 particles leading to considerably less contacts between the Al-7075 particles. Porosity is also visible as dark regions while the Y_2O_3 particles appear as grey regions. Overall the presence of Y_2O_3 in this structure seems to be hindering the sintering process between the Al-7075 particles leading to a less densified structure. For the same volume fraction of Y_2O_3 the 3 vol% nanometric Y_2O_3 structure (Fig.5.14 c) appears to be better densified as compared to the 3 vol% micrometric Y_2O_3 structure, this is due to the finer particle size of the nanometric Y_2O_3 as compared to the micrometric Y_2O_3. The nanometric Y_2O_3 particles occupy the interparticle porosity space between the Al-7075 particles leading to good packing of the overall structure whereas in the case of micrometric Y_2O_3 as the Y_2O_3 particles try to occupy the interparticle space between the Al-7075 particles, these tend to separate / push the particles apart due to their larger particle size. The structure of Al-7075 with 15 vol% micrometric Y_2O_3 indicates larger regions of Y_2O_3 (which appear as grey) between the Al-7075 particles. The volume fraction of Y_2O_3 is such that there is hardly any contact between the Al-7075 particles and further any neck formation between the particles.

5.2.1.2 Forged Optical Microstructures

Figure 5.14(a) shows the longitudinal section of the forged microstructure of pure Al-7075, of Al-7075 with 0.5 vol% nanometric Y_2O_3 and 3 vol% nanometric Y_2O_3 (Fig.5.14(b-c)) while Fig.5.13(d-e) shows that of Al-7075 with 3 vol% micrometric Y_2O_3 and 15 vol% micrometric Y_2O_3 respectively. As mentioned earlier, the forging temperature and strain conditions were found to be sufficient to initiate the breaking of powder particle boundaries (oxide layers) by shear and dispersing the aluminum oxide into the metal matrix which was priorly in the form of particle boundary. The structure of forged Al-7075 (Fig. 5.14(a)) shows stretched deformation bands which are normal to the forging load. Each deformation band culminated from an individual particle present in the sintered structure. Some porosity is visible as small dark spots at the triple points between the bands (deformed particles).

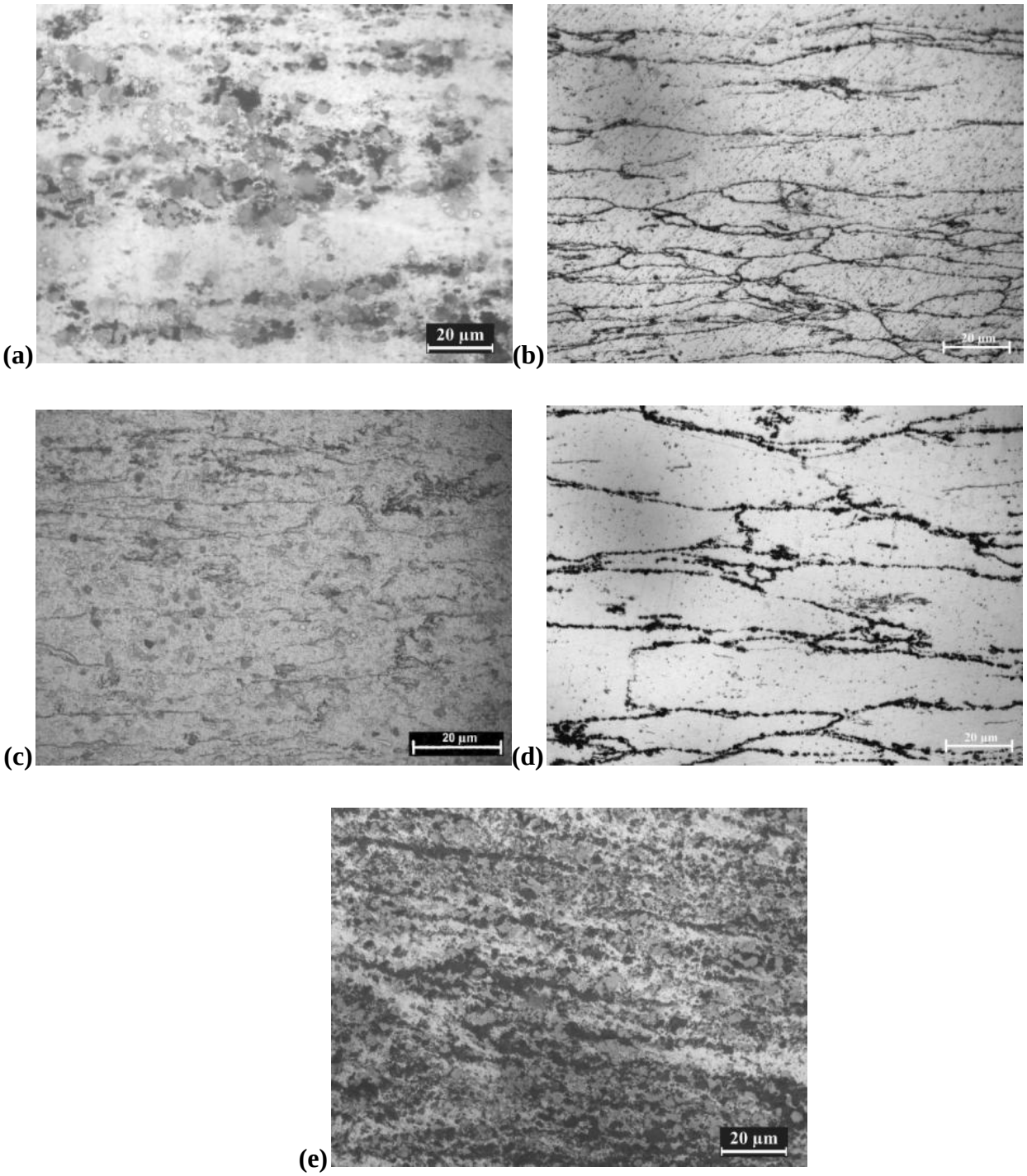

Fig. 5.14: Forged optical microstructures of (a) Pure 7075; (b) 0.5N; (c) 3N; (d) 3M and (e) 15M

The micrographs of Al-7075 with 0.5 vol% nanometric Y_2O_3 and 3 vol% nanometric Y_2O_3 respectively shows the presence of nanometric Y_2O_3 at the triple points and between the deformed particles. The nanometric Y_2O_3 seems to have completely filled up the porosity leading to a well densified structure. The presence of nanometric Y_2O_3 is also likely to play a role in the removal of

the oxide layer on the Al-7075 particles as the particles get sheared and deformed during forging. Nanometric Y_2O_3 due to their fine size and high hardness are likely to enhance the oxide layer removal which has been reported in high strain processing techniques like forging. The oxide layer removal will lead to metallurgical contact between the exposed surfaces of the deformed particles. The micrographs of Al-7075 with 3 vol% micrometric Y_2O_3 and 15 vol% micrometric Y_2O_3 respectively shows the presence of bands (layers) of Y_2O_3 particles between the deformed Al-7075 particles. The 3 vol% micrometric Y_2O_3 micrograph shows the presence of Y_2O_3 mainly in a layer form as well as in isolated form. Porosity is also seen which is mainly isolated. The micrograph of 15 vol% micrometric Y_2O_3 is similar to that of 3 vol% micrometric Y_2O_3 but the level of porosity is considerable and mainly in the form of layers. Some isolated porosity is also visible.

5.2.2 Relative Densities of Composites

5.2.2.1 Realtive green densities

Figures 5.15 shows the variation in relative green density with the addition of nanometric as well as micrometric Y_2O_3 in Al-7075 powders. The addition of nanometric Y_2O_3 particles lead to an increase in the relative green density while the addition of micrometric Y_2O_3 particles led to a decrease in the realtive green densities of Al-7075 powders. The increase in the relative green density with addition of nanometric Y_2O_3 can be attributed to the filling of voids (triple points) between the Al-7075 particles by the nanometric Y_2O_3 particles as they are finer than the void space. This leads to improved packing of the compacted powders leading to an increase in the relative green density. The increase is initially steep (till a nano Y_2O_3 content of 1 vol %) after which it is less steep till a nanometric Y_2O_3 content of 3 vol%. The initial steep increase can be due to the filling of the triple junction void space between the Al-7075 particles by the gradual increase in the nanometric Y_2O_3 particles upto a 1 vol% while the less steepness beyond 1 vol% i.e. till 3 vol% Y_2O_3 can be due to the complete filling of the void space between the Al-7075 particles and due to the nanometric Y_2O_3 particles filling the space between two adjacent Al-7075 particles leading to expansion in the green compact. The harder Y_2O_3 particles as compared to the Al-7075 particles are also likely to cause friction during the compaction process. Further interparticle friction can occur between the Y_2O_3 particles, between the Al-7075 particles and Y_2O_3 particles as well as between both these particles and the die walls. An increase in nanometric Y_2O_3 particles also leads to an increaes in the frictional forces between the particles as well between them and the die walls during compaction. This can be another reason for the two slopes

apart from the reason discussed above. In contrary to the behavior of relative green density with the addition of nanometric Y_2O_3, the addition of micrometric Y_2O_3 in Al-7075 powders lead to a decrease in the relative green density. The micrometric Y_2O_3 particles (just as the nano Y_2O_3 partcles) occupy the void space (triple points) between the Al-7075 powders as well as the space between two Al-7075 particles. As the micrometric Y_2O_3 particles are not as fine as the nanometric Y_2O_3 particles, they are still fine enough to occupy the void space (triple point) between the Al-7075 particles without pushing them apart. This should increase the relative sintered density but at the same time they also occupy the space between two Al-7075 particles leading to a drop in the relative green densities. The role of the later being more dominant as the present study carried out was for 1 vol% micrometric Y_2O_3 and beyond. Further, as discussed in the case of nanometric Y_2O_3 the hard micrometric Y_2O_3 particles are also likely to cause interparticle friction between themselves and between them and the die walls. There will also be a lesser tendency (as compared to nanometric Y_2O_3 particles) for the micrometric Y_2O_3 particles to get embedded in the softer Y_2O_3 particles.

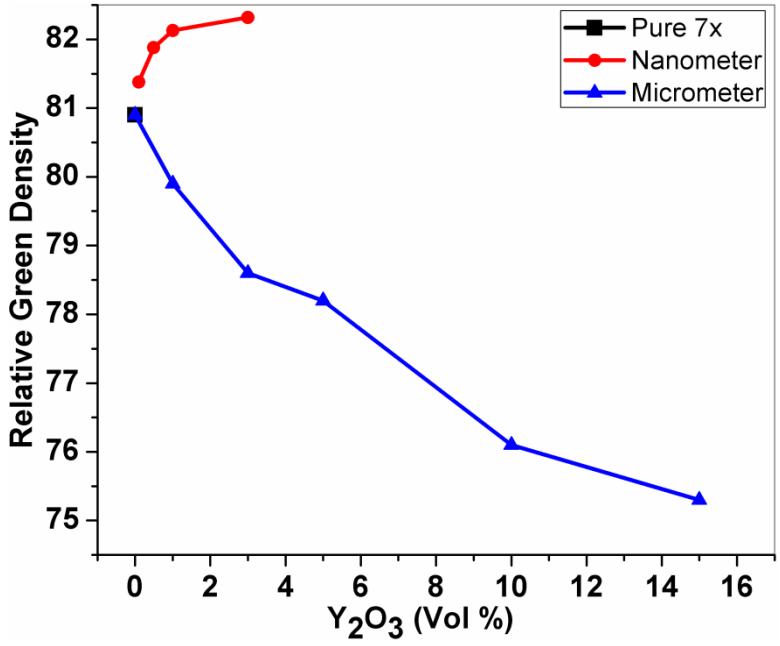

Fig 5.15: Relative densities for different compositions after compaction

5.2.2.2 Realtive sintered densities

Figure 5.16 shows the variation of relative sintered density with the addition of nanometric and micrometric Y_2O_3 particles. In both the cases the relative sintered density was found to

decrease with increase in Y_2O_3 content. In case of nanometric Y_2O_3 as explained earlier during compaction the nanometric Y_2O_3 particles are present at the void space (triple points) and also between two adjacent Al-7075 particles. As the sintering temperature of Al-7075 particles (610^oC) employed in the present investigation is not high enough for the Y_2O_3 particles to sinter these only cause a hinderance to the sintering of the Al-7075 particles. The nanometric Y_2O_3 particles between the Al-7075 particles hinder the formation of necks between the Al-7075 particles i.e. do not allow the diffusion to occur. Further, the nanometric Y_2O_3 particles at the void space (triple points) between the Al-7075 particles do not allow pore closure to take place during the later stages of sintering. Further, the gases present in the closed porosity in the green compact has no place to escape during heating (sintering) and causes the compact to expand. The combined effect is the drop in sintered density with the addition of nanometric Y_2O_3. A previous study on the densification of nanocomposite showed the similar behavior after sintering [Cho et al., 2013]. The same is the case of micrometric Y_2O_3 which shows a similar trend as that of its relative green density. Further, for a similar vol% of nanometric and micrometric Y_2O_3 (i.e. 1 and 3 vol%) the nano Y_2O_3 compacts show a lower relative sintered density as compared to the micrometric Y_2O_3 compacts. The likely reason being the presence of larger number of Y_2O_3 particles for a given vol% for nanometric Y_2O_3 as compared to micrometric Y_2O_3. The larger number of particles envelope the Al-7075 particles prevening their contact and neck growth (sintering).

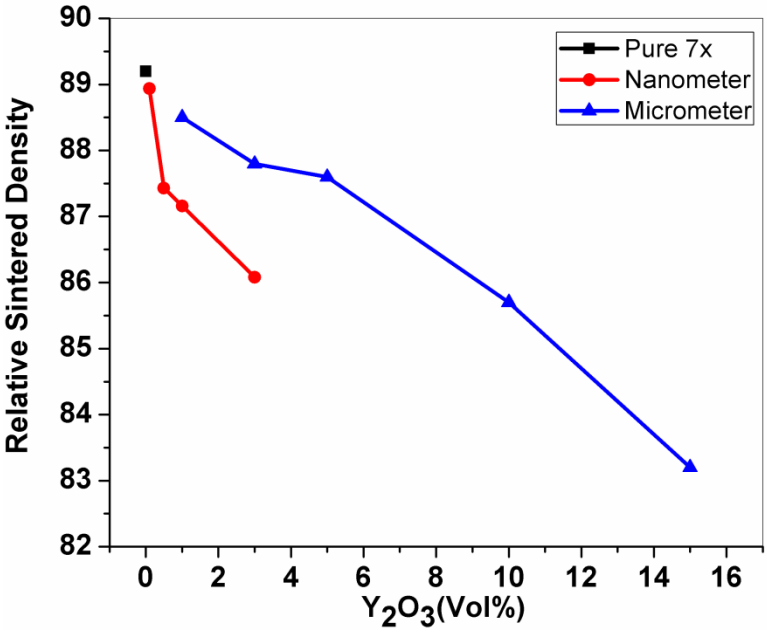

Fig 5.16: Relative densities for different compositions after sintering

5.2.2.3 Densification parameter

The variation of densification parameter with nano and micrometric Y_2O_3 content is shown in Fig. 5.17. Densification parameter was found to be positive for Al-7075 particles as well as with the addition of nanometric and micrometric Y_2O_3 in Al-7075 as the sintered densities were greater then the green densities for all compositions. There was a considerable drop in the densification parameter with the addition of nanometric Y_2O_3 which was not the case with the addition of micrometric Y_2O_3 (wherein there was a gradual drop). This considerable drop in the densification parameter with nanometric Y_2O_3 addition (inspite of the increase in the green density) implies that sintering was greatly affected by the nanometric Y_2O_3 addition. As explained earlier the Y_2O_3 particles in both the cases will occupy the void space (triple points) between the Al-7075 particles as well as between two Al-7075 particles. For a given vol% of Y_2O_3 the number of particles involved will be considerably larger in the case of nanometric Y_2O_3 as compared to micrometric Y_2O_3. In the case of nanometric Y_2O_3 the particles will envelope the Al-7075 particles causing very little contact between two Al-7075 particles. This will hinder the sintering process (neck formation). In the case of micrometric Y_2O_3 this effect of Y_2O_3 particles enveloping the Al-7075 particles will be considerably lower leading to sintering (neck formation) to take place. This is the likely reason for the densification parameter to be considerably lower in the case of nanometric Y_2O_3 as compared to micrometric Y_2O_3.

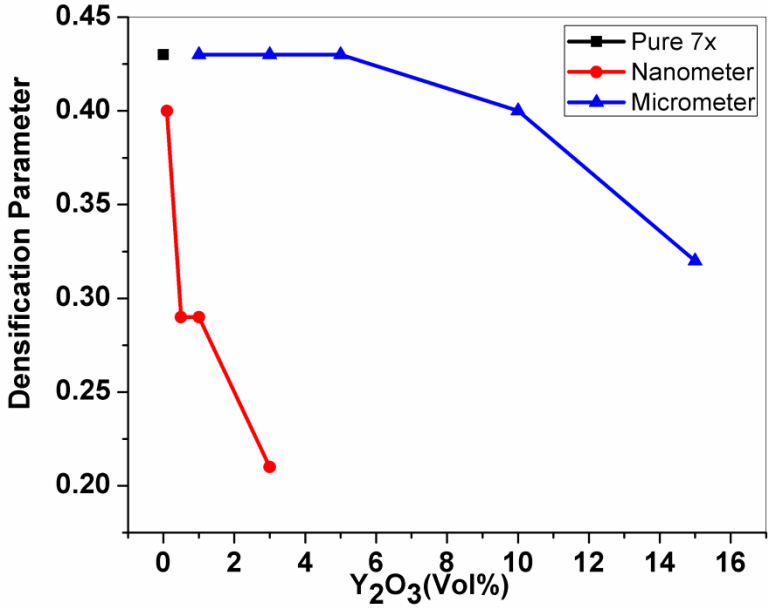

Fig 5.17: Densification parameter for different compositions

5.2.2.4 Realtive Forged densities

Figure 5.18 shows the variation of relative forged density with nanometric and micrometric Y_2O_3 content. Forging at a tempearture of $0.8T_m$ (450^oC) lead to densities in excess of 99.4% of theoretical density for Al-7075 powders as well as with the addition of nanometric and micrometric Y_2O_3. The forged densities were overall higher in the micrometric Y_2O_3 composites as compared to the nanometric Y_2O_3 composites. With the addition of nanometric Y_2O_3 the forged densities were found to increase at 0.1 and 0.5 vol% after which they were found to decrease at an amount of 1 and 3 vol%, while with the addition of micrometric Y_2O_3 the densitites were found to increase at 1 vol% after which there was a decrease with further addition. The increase in the forged densties initially (as compared to that of Al-7075 powders) in the case of both nanometric and micrometric Y_2O_3 can be attributed to the shearing of the oxide layer present on the surface of the Al-7075 particles during the forging operation which improves the density. In the previous sub section 5.1, it was established that a forging tempeature of $0.8T_m$ and strain of 0.9 was sufficient for pore filling by plastic deformation as well as the removal of the oxide file present on the Al-7075 particles due to shear during the forging operation [Joshi et al., 2015]. The role of Y_2O_3 during hot forging would be to further aid the shearing of the oxide layer present on the Al-7075 particles (when present in smaller volume) and also to hinder plastic deformation (by obstruction of dislocations) at higher volume as observed in the present study.

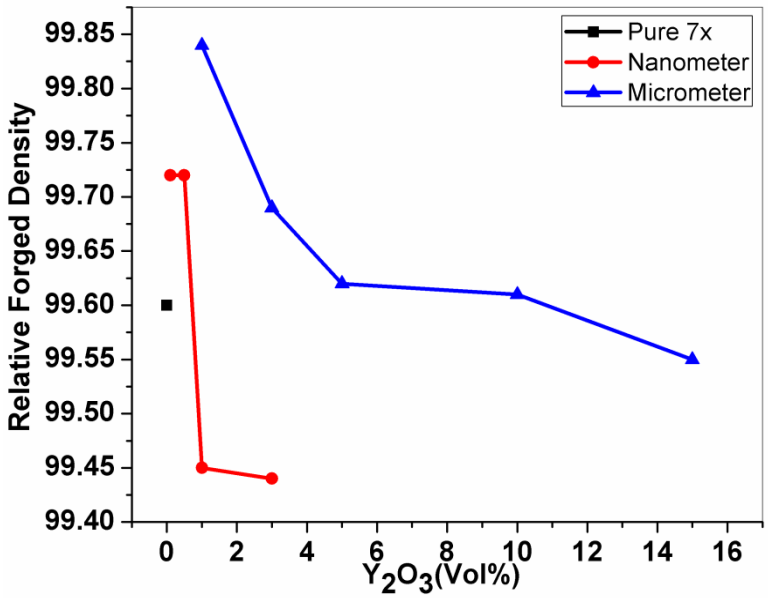

Fig 5.18: Relative forged density for different compositions

5.2.3 Hardness of composites

5.2.3.1 As-Forged hardness

The hardness values of the nanometric and micrometric Y_2O_3 reinforced composites in the as-forged condition are shown in Fig.5.19. The hardness values for the nanometric Y_2O_3 composites exhibited a sharp increase till a Y_2O_3 volume fraction of 1% after which the hardness value were steady till a volume fraction of 3% while in the case of micrometric Y_2O_3 there was sharp increase till a volume fraction of 5% after which the hardness slightly increased. For similar volume fractions (1% and 3%) the hardness value for both nano and micrometric Y_2O_3 was almost similar. In the as-forged condition the hardness values can be attributed to various hardening mechanisms such as grain boundary hardening, solid solution hardening, dispersion hardening (Orowan boming) and strain hardening. Further, during the forging process the Al_2O_3 (present on the particle surface) gets removed due to friction and shearing which leads to the dispersion of Al_2O_3 in the Al-7075 matrix leading to further increase in hardness.

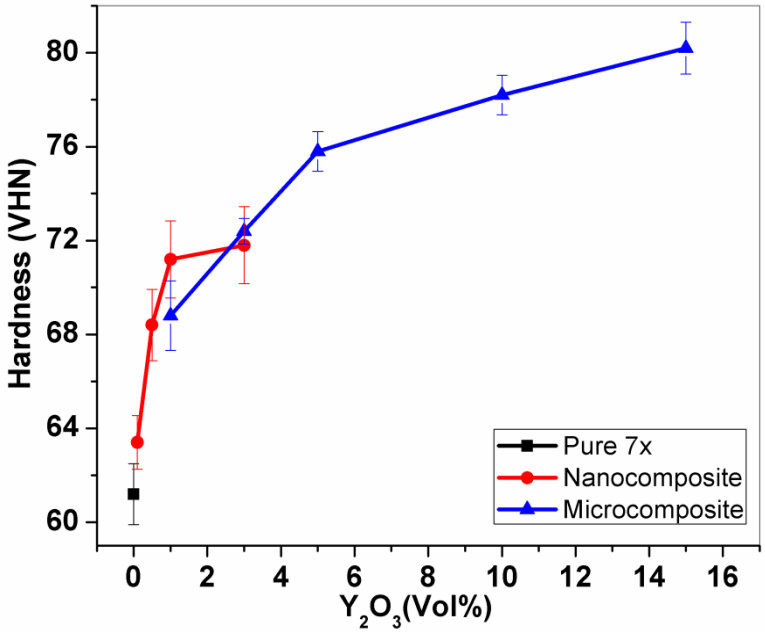

Fig 5.19: Hardness of different composites in as-forged condition

Strengthening through grain boundary is natural for powder metallurgical products due to the presence of small grains inside an individual powder particle. Researchers have tried to improve the properties by different grain refinement methods [Lesch et al., 2007] but in powder metallurgical processing grains are already finer as compared to cast structure. Although Zn, Mg

and Cu are added in the 7075 alloy for the purpose of precipitation hardening, in the as-forged condition (in the absence of artificial ageing) they contribute to increase in hardness by solid solution hardening. The presence of nano and micrometric Y_2O_3 contributes to hardness by Orowan boming (dispersion hardening). The hardening due to dispersion of second phase mainly depends upon size, shape, volume and distribution of the second phase (which in this case is nanometric and micrometric Y_2O_3), the strength, ductility and strain-hardening behavior of the matrix and second phase, the crystallographic fit between the phases and the interfacial energy and interfacial bonding between the phases [Dieter, 1961]. In the present study the difference between the two reinforcements i.e. nanometric and micrometric Y_2O_3 is only in the size, shape and volume while the other factors are similar. Further, the distribution of both the Y_2O_3 particles in the matrix of 7075 is dissimilar due to their particle size (tendency to form agglomerates). As discussed earlier, the nanometric Y_2O_3 particles fill the porosities (both between the particles and at the triple points) whereas the micrometric Y_2O_3 particles seem to have prevented the particle to particle contact between the Al-7075 particles and separated/pushed them apart. This difference in the structure is also likely to influence the hardness values (due to second phase) in both the cases. The former structure comprising of nanometric Y_2O_3 particles is likely to exhibit a higher hardness as these particles seems to be more uniformly distributed around the 7075 particles as compared to the micrometric Y_2O_3 particles. But at the same time the nanometric Y_2O_3 particles have a stronger tendency to agglomerate as compared to micrometric Y_2O_3 particles due to which the hardness levels are likely to lower. The role of Orowan mechanism in which dislocation get pinned up between two reinforcement particles is likely to be more prominent in the presence of nano Y_2O_3 as compared to micrometric Y_2O_3 due to the presence of more number of Y_2O_3 particles for a given volume of Y_2O_3 as well as the finer particle size of Y_2O_3. But as evident from Fig. 5.19, the hardness values for similar volume fractions of micrometric and nanometric Y_2O_3 (1 and 3 vol %) are almost similar. The nanometric Y_2O_3 particles due to their fine particle size form agglomerates and clusters which occupy the pore space between the Al-7075 particles as discussed earlier in section 5.2.1.2. These agglomerates and clusters behave as one individual particle and hence do not provide the desired hardness by the Orowan mechanism. On the other hand the micrometric Y_2O_3 particles have a less tendency to agglomerate and provide the hardness by Orowan mechanism though the effect of finer and larger number of particles is not likely to be evident.

The hardness values are also influenced by strain hardening as the samples were immediately quenched in water after the hot forging operation i.e. not enough time was allowed for dynamic recovery to occur. In a previous study by the authors [Joshi et al., 2015] and also explained in the sub-section 5.1, it was observed that dynamic recrystallization (DRX) initiated and occurred at strain values of 1.14 and beyond at a temperature of 0.8 T_m. Thus, the present forging condition did not lead to the occurrence of DRX which was further confirmed by SEM analysis at higher magnifications. The absence of DRX suggests that the strain hardening effect was retained in the samples inspite of the high forging temperature involved. The presence of fine grains, deformed particles, Al_2O_3 layer and Al_2O_3 particles as well as the Y_2O_3 reinforcement is likely to affect the strain hardening coefficient. The effect of nanometric and micrometric Y_2O_3 reinforcements on strain hardening is likely to be similar to that of Orowan pinning as discussed earlier. This effect has not been explored and discussed in the present study as it is beyond the scope of the study.

5.2.3.2 Solutionized hardness

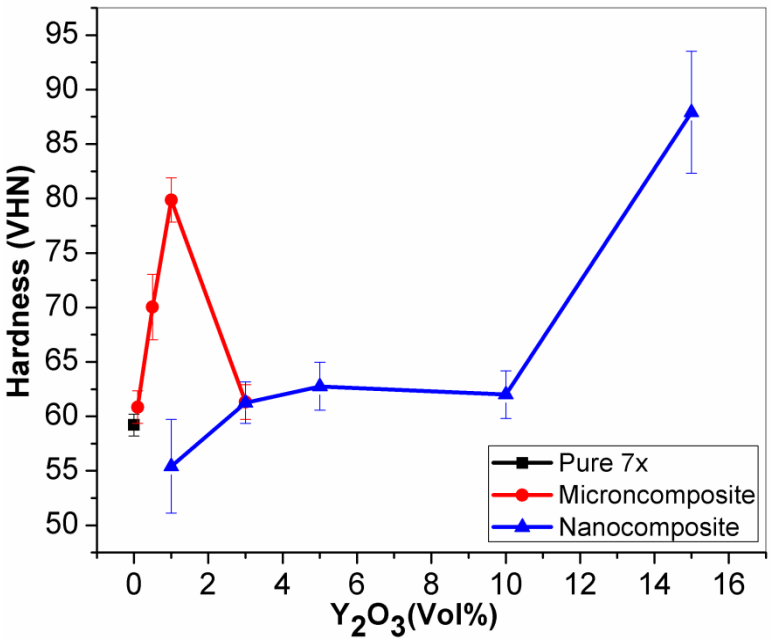

Fig. 5.20: Hardness of different composites in solutionized condition

Hardness of Al-7075 and composites in the solutionized condition is shown in Fig. 5.20. The hardness of nanocomposites increases with the addition of nanometric Y_2O_3 in Al-7075 till the volume fraction of 1 vol%. Further addition of nanometric Y_2O_3 (3 vol%) decreases its hardness

due to formation of nano-clusters. The composite having micrometric Y_2O_3 has solutionized hardness in the same range of Al- 7075 except for 15 vol% Y_2O_3 addition. An addition of 1 vol% micrometric Y_2O_3 led to a decrease in the hardness value. Increasing the Y_2O_3 volume fraction with 3, 5 and 10 vol% resulted in a small increment of hardness whereas adding 15 vol% Y_2O_3 increased the hardness considerably. In the process of solutionizing when the material is subjected to solutionizing temperature for a long duration, all the precipitates present in the system goes to the solution and a single phase forms. When the samples are rapidly cooled to room temperature by quenching, the solid solution remains in single phase having a super saturated condition which is unstable. This unstable condition is due to dissolved precipitates in the solid solution and these try to come out. The dominant hardening mechanism is likely to be due to the Y_2O_3 reinforcement i.e. dispersion hardening (orowan boming). Though one would expect lower hardness in the solution condition as compared to the as-forged one due to relieving of the residual stresses, this was not observed in the present study. This is likely due to occurrence of some natural aging in both the conditions which overcomes the stress relieving factor.

5.2.3.3 Aging and Peak aged hardness

The aging curves for the micron and nanometric Y_2O_3 composites are shown in Fig. 5.21. Hardness was found to peak at 24 hrs due to uniformly distributed precipitates after the artificial aging treatment at 121^{o}C. Some reports indicate accelerated aging kinetics after addition of reinforcement [Sharma et al., 2006] while some reports have indicated a slower kinetics of aging after addition of reinforcement [Pal et al., 2008]. But in the present study (during the aging treatment) no change in the peak aging time was observed with the addition of reinforcement. A similar study performed on Al-7075 based composites found no change in the peak aging time with the addition of reinforcement [Ahmed et al., 2010]. Further the presence of different fractions of Y_2O_3 led to considerable deviation in the hardness values as compared to that of pure Al-7075 in the under aged, peak aged and over aged conditions (Fig.5.21(a)). This deviation was significant in the nanometric Y_2O_3 composites as compared to the micrometric Y_2O_3 composites (Fig.5.21 (b)).

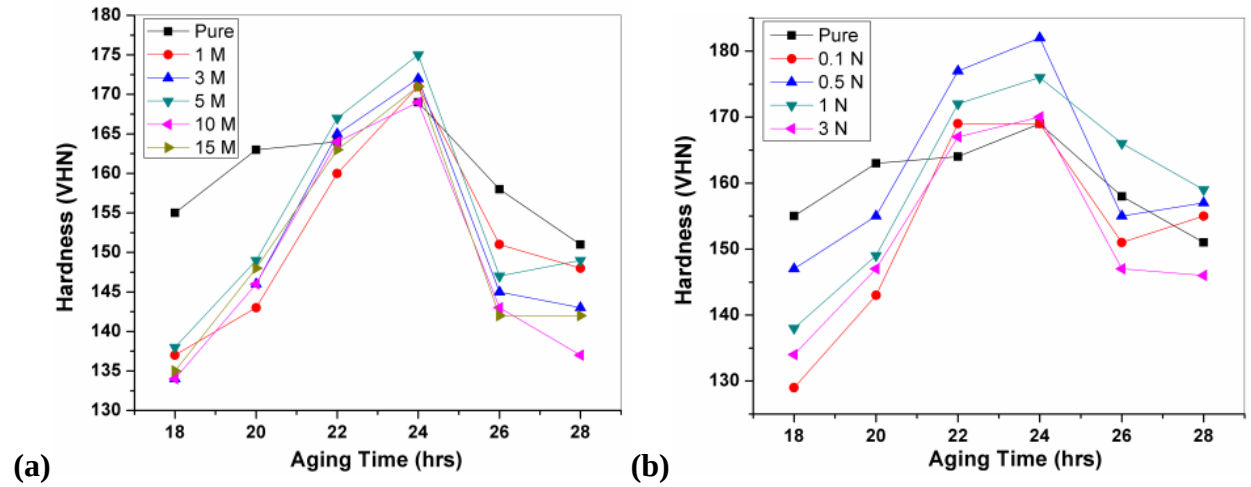

Fig 5.21: Comparison of aging curves of (a) Al- 7075 and nanocomposites and (b) micron-composites

In general the hardness values were lower in the presence of Y_2O_3 reinforcements compared to Al-7075 in the underaged and overaged conditions while in the peak aged condition these were higher. This deviation in hardness for different volume fractions can be attributed to various factors. Firstly, the thermal stress generated from the thermal mismatch between the Al-7075 martix and Y_2O_3 reinforcement generates a large dislocation density which accelerates the precipitation kinetics. Secondly the presence of Y_2O_3 particles retards the formation of GP zones as the interface between Y_2O_3 and Al-7075 acts as a vacancy sink. A lower vacancy density lowers the density of GP zones thus lowering the precipitation kinetics. Lastly, segregation of alloying elements at the Y_2O_3 – Al-7075 interface and presence of undissolved coarse precipitates causes depletion of solute inside the matrix. A lower level of super-saturation reduces the driving force for precipitation [Sharma et al., 2006; Pal et al., 2008]. These factors as well as the size of the precipitates in the underaged, peakaged and overaged conditions all contribute to the hardness values. An assessment of all these factors with respect to the present findings has not been carried out as it was beyond the scope of the present work.

Deviation of hardness values with different ageing time, different reinforcement size and content could also be explained in relation with number of dislocation pile ups and their distribution across the matrix. Addition of nano reinforcement causes more homogeneous dislocation density regions which are present in more numbers than micrometric size reinforced composite. For a given volume of reinforcements nanoparticles are larger in number as compared

to micrometric particles but they have a tendency to form clusters. Nanoparticle clustering is visible in TEM images (Fig.5.22 (a)). The cluster acts as an individual particle of larger size and hinders a number of dislocations around it. Hence the effective age hardening by nanoparticles was lost due to agglomerate cluster formation.

(a) 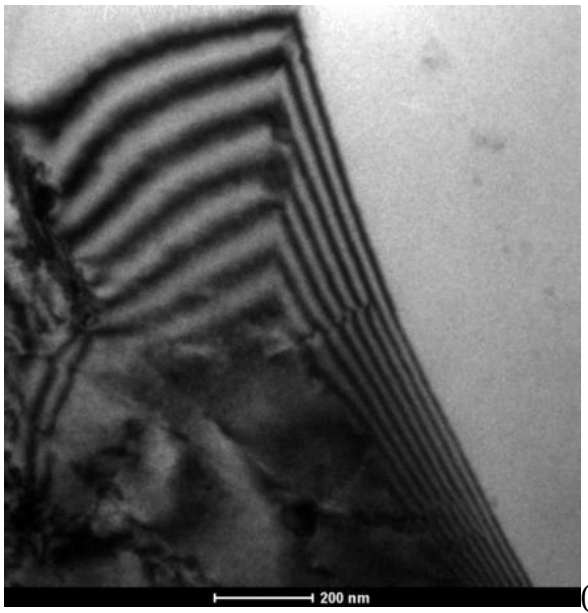

(b) 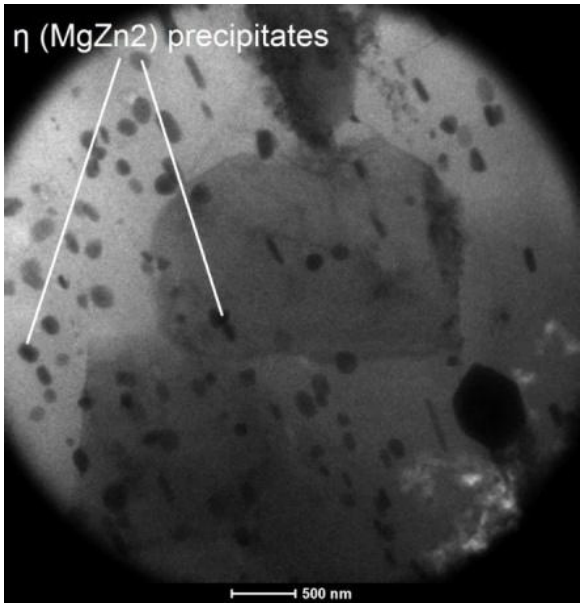

Fig 5.22: TEM images showing (a) Dislocation pile up and (b) Precipitates in T_6 condition

The hardness values of the nanometric and micrometric Y_2O_3 reinforced composites in the T_6 condition at the peak ageing time (24 hrs) are shown in Fig.5.23. Though the main contribution to the obtained hardness can be attributed to precipitation (as the composites were treated to the T_6 condition) other hardening mechanisms as discussed above also play a role. A comparison of the hardness values in the T_6 condition with those in the solutionized condition indicates a considerable increase in hardness after the T_6 treatment. Further, for both the micrometric and nanometric composites the hardness value was higher as compared to that of pure Al-7075 alloy. In the nano Y_2O_3 reinforced composites the hardness values were found to increase considerably till a nano Y_2O_3 content of 0.5 vol% after which the hardness values dropped while in the case of micrometric composites there was a slight increase till Y_2O_3 content of 5 vol% after which there was a decrease. This indicates that the nanometric Y_2O_3 reinforcement of 0.5 vol% and micrometric Y_2O_3 reinforcement of 5 vol% influences the precipitation in such a manner that leads to a maximum hardness.

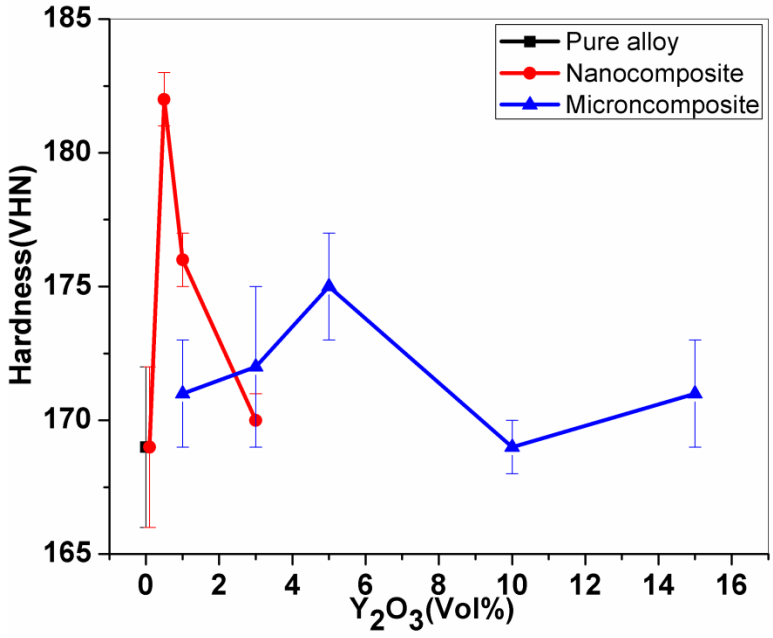

Fig 5.23: Hardness of different composites in T_6 condition

In case of pure Al-7075, aging process initiates with supersaturated solid solution of alloying elements. The precipitates nucleate from the solute atoms in this super saturated solution and grow with time. Increase in temperature accelerates the growth of these precipitates upto a certain time interval. Beyond this time (also known as peak aging time) precipitate coarsening occurs. Uniformly distributed $MgZn_2$ precipitates may be seen over the surface in Fig. 5.22(b). The $MgZn_2$ precipitates in 7075 matrix and Al-Zn-Mg-Cu system have been confirmed by earlier reports [Campos et al., 2010; Ning et al., 2007]. With the introduction of micrometric and nanometric Y_2O_3 to the pure Al-7075 alloy, dislocations are created due to thermal mismatch of soft aluminum matrix and hard reinforcement during cooling as explained earlier. During aging process nucleation of precipitates occurs. The dislocations produced due to thermal mismatch are hindered by these precipitates resulting in an increase in dislocation density at those points [Giribaskar et al., 2008]. This increased dislocation density further acts as a nucleation site for precipitates resulting in the formation of additional precipitates in the composite. In the present case in case of nanometric Y_2O_3 a volume fraction of 0.5% while a volume fraction of 5% was optimum for the production of optimum level of dislocation density as well as dislocations which create sites for the precipitation in the peak aged condition. At lower volume fractions of both micrometric and nanometric Y_2O_3 the reinforcement content is not sufficient for enough

dislocation to be generated while at higher fractions due to agglomeration of the Y_2O_3 particles enough dislocations are not generates as an agglomerated cluster acts as an individual particle. This has been observed and discussed in the microstructural studies of these composites in section 5.2.1.2. Further the higher hardness values obtained for 0.5 vol% Y_2O_3 as compared to 5 vol% Y_2O_3 in the peak aged condition can be attributed to the smaller size of the Y_2O_3 which produces a larger number of regions wherein the dislocations are generated which increases the dislocation density as well as acts as a site for the nucleation of precipitates. The combined effect of reinforcement particles, additional precipitates and dislocation density cause an increase in hardness of the composite samples compared to the pure alloy.

5.2.4 Tensile Strength of Composites

Comparison of ultimate tensile strength of both micron and nanometric Y_2O_3 composites as well as pure Al-7075 is shown in Fig. 5.24. The strength values are those obtained in the peak aged condition (24hrs ageing time) and correspond to the hardness values shown in Fig.5.24. The tensile strength values obtained are mainly due to the formation of precipitates as discussed above in section 5.2.3.3 but other strengthening mechanisms such as solid solution strengthening, dispersion strengthening (Orowan boming), grain boundary strengthening, strain hardening and the presence of Al_2O_3 also play a role. These mechanisms also lead to an increase in hardness and have been discussed in detail earlier in section 5.2.3.3.

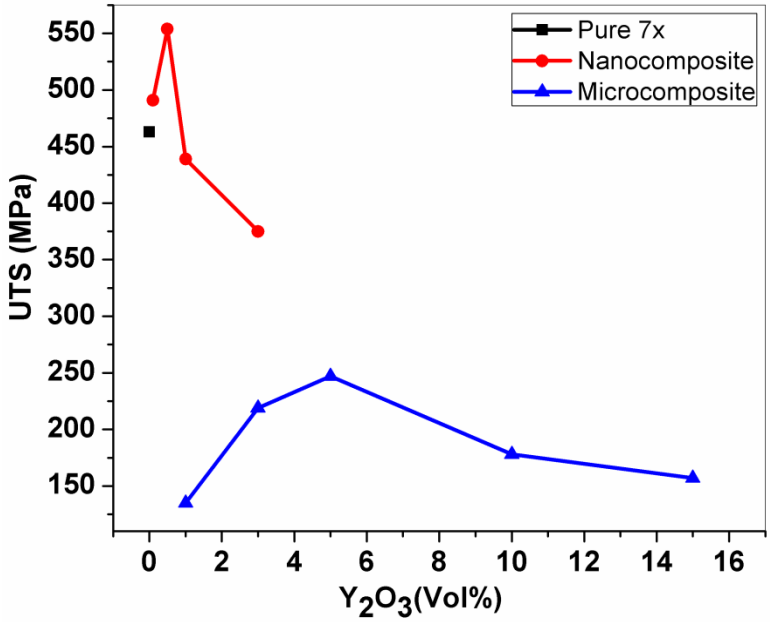

Fig. 5.24: Tensile strength of pure Al-7075 and its composites

In the peak aged condition the tensile strength of pure Al-7075 was observed to be 463 MPa. The incorporation of micrometric Y_2O_3 in pure Al-7075 led to a considerable drop in the tensile strength values while with the incorporation of nanometric Y_2O_3, an increase was observed at volume fraction of 0.5 and 1, however beyond that there was a drop. Amongst the micrometric composites the addition of 3-5 vol% Y_2O_3, lead to an increase in strength while for higher volume fractions of Y_2O_3 particles (10-15%) led to a drop in the strength values. Whereas the incorporation of nanometric Y_2O_3 particles (at volume fraction of 0.1 % and 0.5 %) lead to an increase in strength while for higher volume fractions of Y_2O_3 particles (1 % and 3 %) led to a drop in the strength values. For the micrometric Y_2O_3 reinforced composites the strength values varied between 135 MPa to 247 MPa and peaked at 5 vol% of Y_2O_3 at which the strength value was 247 MPa. For the nano Y_2O_3 reinforced composites the strength values varied between 375 MPa to 554 MPa and peaked at 0.5 vol% of Y_2O_3 at which the strength value was 554 MPa. A similar trend was observed for the hardness values in the peak aged condition as discussed in section 5.2.3.3. This trend in the strength values can be explained on the same lines as the hardness values i.e. the effect of dislocation formation due to difference in the CTE values between the alloy and reinforcement (Y_2O_3) and the tendency for Y_2O_3 to form agglomerates at higher volume fractions.

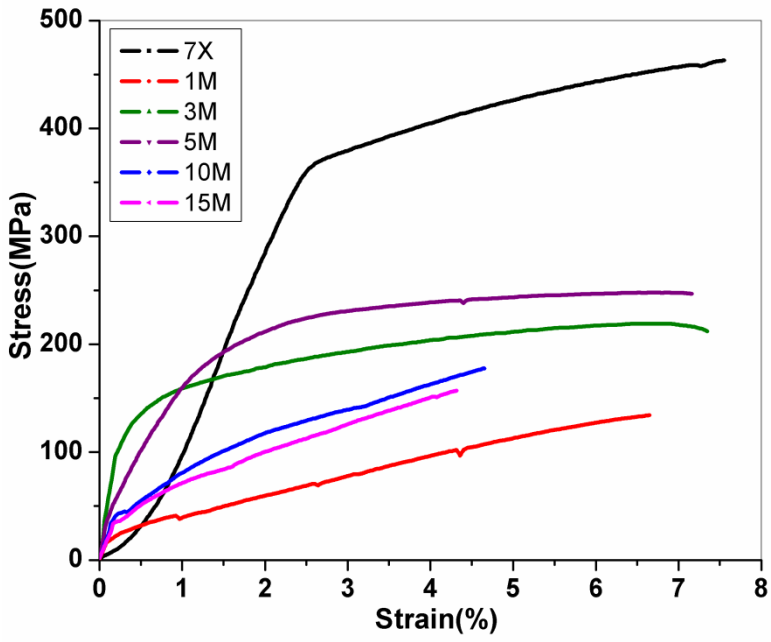

Fig. 5.25: Tensile curves for micrometric composites

Stress-strain curves for pure Al-7075 alloy and micrometric composites in T_6 condition under tensile loading are shown in Fig. 5.25. The UTS as well as ductility in case of pure Al-7075 was higher than the micrometric composites. The tensile strength as discussed earlier was highest in 5 vol% micrometric Y_2O_3 amongst all micrometric composites. Ductility decreased with the addition of hard reinforcement due to poor bonding of matrix and reinforcement. The ductility of Al-7075 was measured as 7.5% at fracture. The ductility of micrometric composites were slightly lower then that of pure Al-7075 except for composites having higher amount of Y_2O_3 (10 vol% and 15 vol%) wherein the ductility values dropped to around 4.5%.

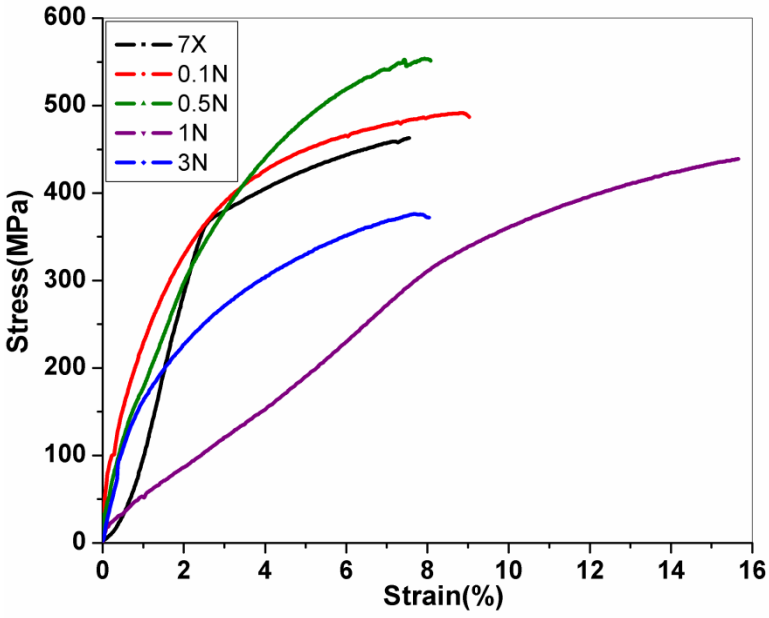

Fig. 5.26: Tensile curves for nanometric composites

Stress-strain curves for pure Al-7075 alloy and nanometric composites under tensile loading are shown in Fig. 5.26. The tensile strength of these composites with respect to pure Al-7075 is already discussed above and 0.5 vol% nanometric Y_2O_3 exhibited the highest strength. Ductility values of nanocomposites were not much affected with the addition of Y_2O_3 reinforcement. The ductility of Al-7075 as well as nano composite samples were around 8% except for 1 N which exhibited more than 15 % ductility.

The overall tensile strength for powder forged micrometric composites were lower as compared to the pure alloy while that of the nanometric composites were higher. This is in line with reported studies as discussed in section 2.4.3 (Table 2.8). Further, the strength values in

general for the micrometric composites were lower than those reported while for the nanometric composites they were at par with those reported. It should be noted that most of the reported studies employed extrusion for processing of composites which produces large anisotropy and the reported strengths are in those direction in which maximum strength was achieved.

The present study employed powder forging which results in considerably less anisotropy as compared to extrusion due to creation of triaxial strain. Further, though high temperature properties were not studied in the present investigation, powder forging is more helpful for high temperature performance of the fabricated composites than extrusion as the latter exhibits extrusion bands which leads to degradation of high temperature properties.

5.2.5 Fractography of tensile samples

To obtain an insight into the behavior of both the reinforcement during tensile loading the fractured surfaces of the failed tensile specimens were studied by SEM (Fig.5.27). The micrometric Y_2O_3 composites exhibited inhomogeneous microstructures (fractographs) where coarse dimples and inhomogeneous fracture surfaces were clearly seen. In addition to this shearing is visible in the fractograph (Fig. 5.27 (a)) and at some places many micro cracks (Fig. 5.27 (b)) which explains the reason for failure of 5 vol% micrometric Y_2O_3 composites. Strength decreases in the composites having reinforcement content more than 5 vol% due to clustering of reinforcement along the particle boundary and creation of micro pores. These clustering of particles are seen in Fig. 5.27(c) as well as in Fig. 5.28 and were confirmed as Y_2O_3 by EDS scan. This is the reason for the overall low values of strength in these composites. On the other hand the fracture surfaces of nanometric Y_2O_3 composites seem to be more homogeneous (Fig. 5.29). A majority of elongated dimples helped in the improved elongation in these composites as compared to micron composites. Further, no microcracks were observed in these composites as those seen in the micrometric Y_2O_3 composites.

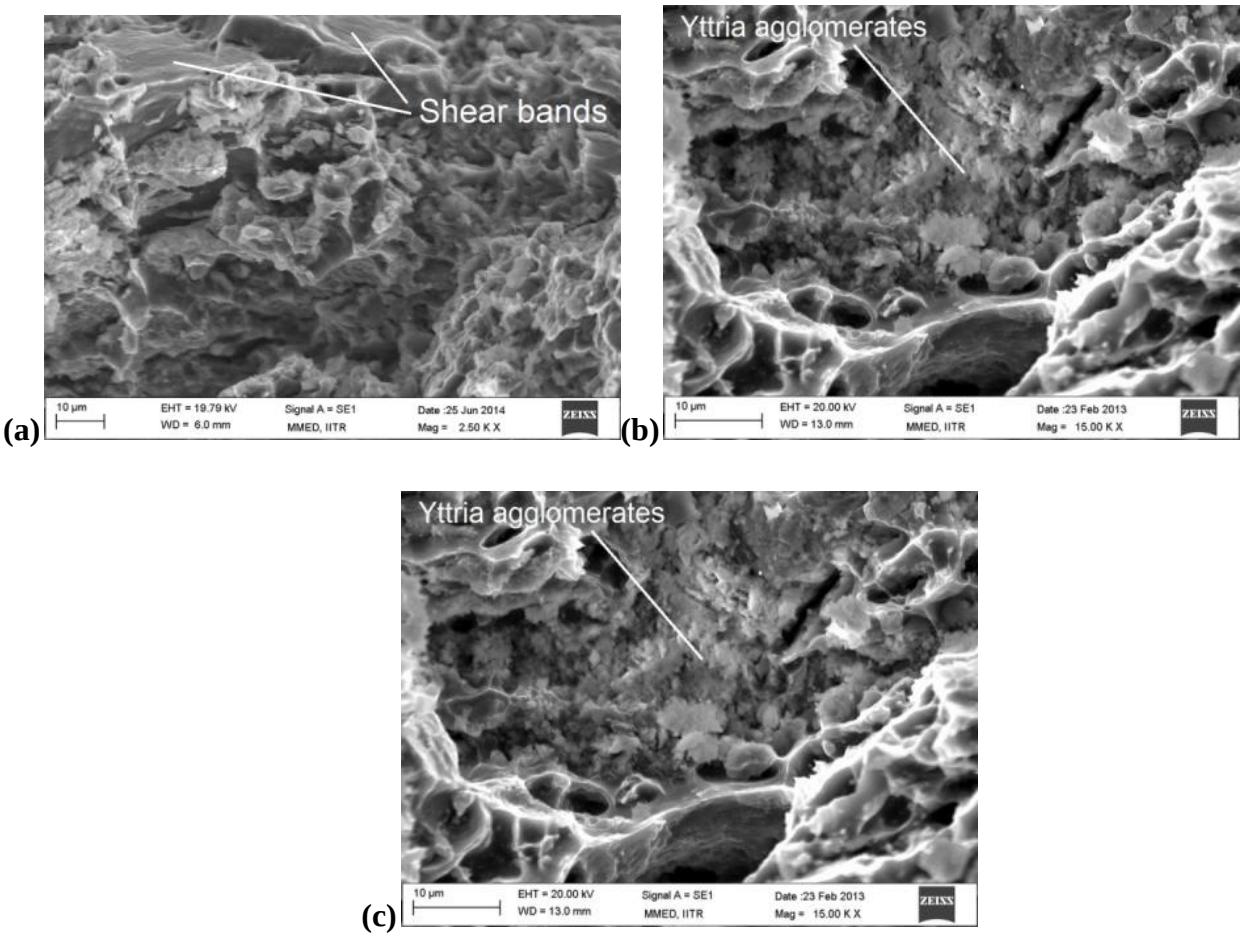

Fig 5.27: Tensile fractographs for (a) 3 M; (b) 5 M and (c) Y_2O_3 agglomerates in 15 M

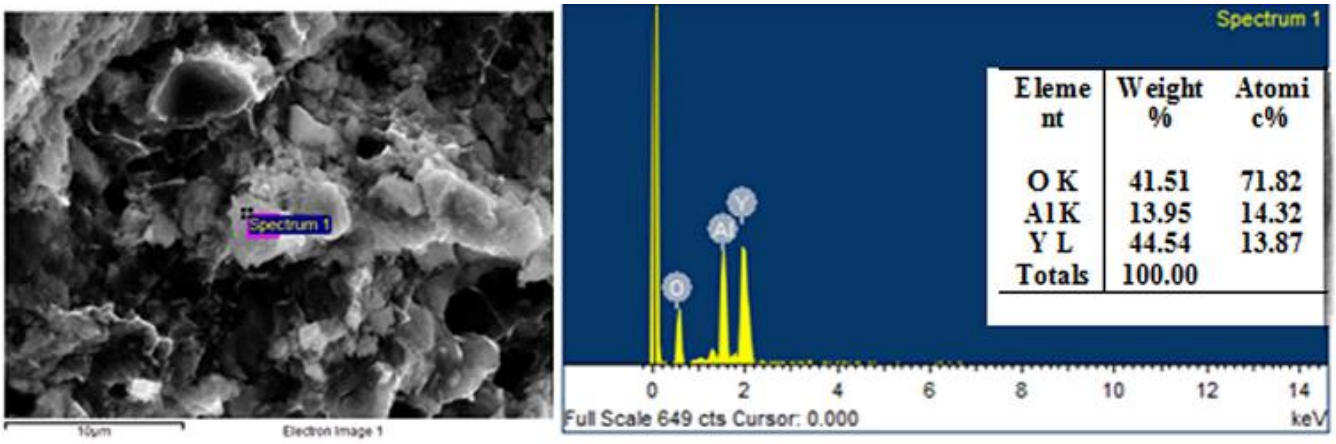

Fig 5.28: EDS scan for the fractograph of 15M

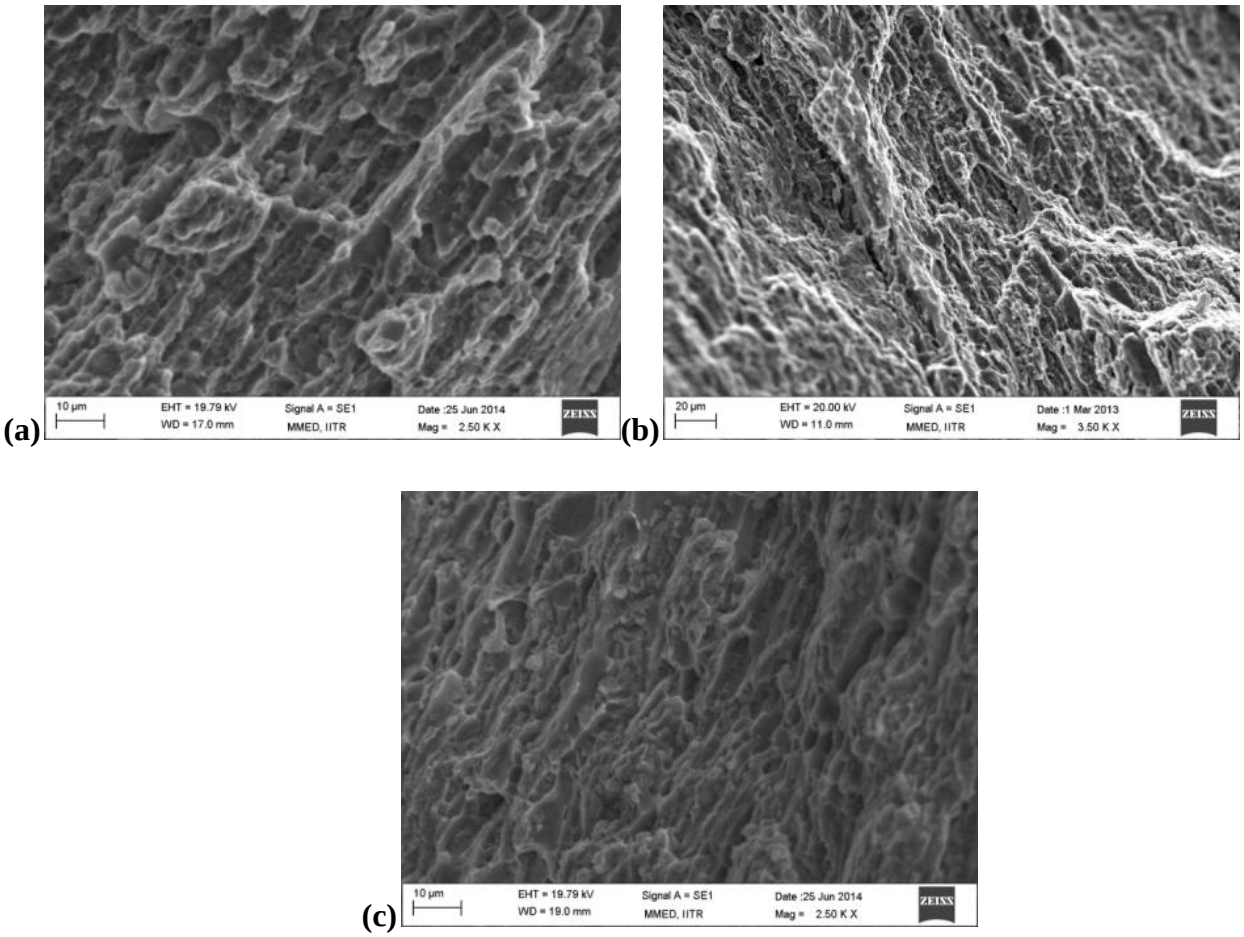

Fig 5.29: Tensile fractographs for (a) Al-7075 (b) 0.5 N and (c) 3 N

5.2.6 Compressive Strength of Composites

Compressive strength was measured as a function of flow stress i.e. stress at which the material starts flowing on the application of compressive load (Fig 5.30). Compressive strength for pure Al-7075 was found to be 463 MPa, for nanometric Y_2O_3 composite compressive strength ranged from 431 MPa to 726 MPa and that for micrometric Y_2O_3 composites ranged from 265 MPa to 440 MPa. Highest value of compressive strength for nanometric Y_2O_3 composites was found to be 726 MPa for 0.5 vol% and that for micrometric composites was 440 MPa for 5 vol% reinforcement. The amount of reinforcement content affected compressive strength in the same way as it affected the tensile strength.

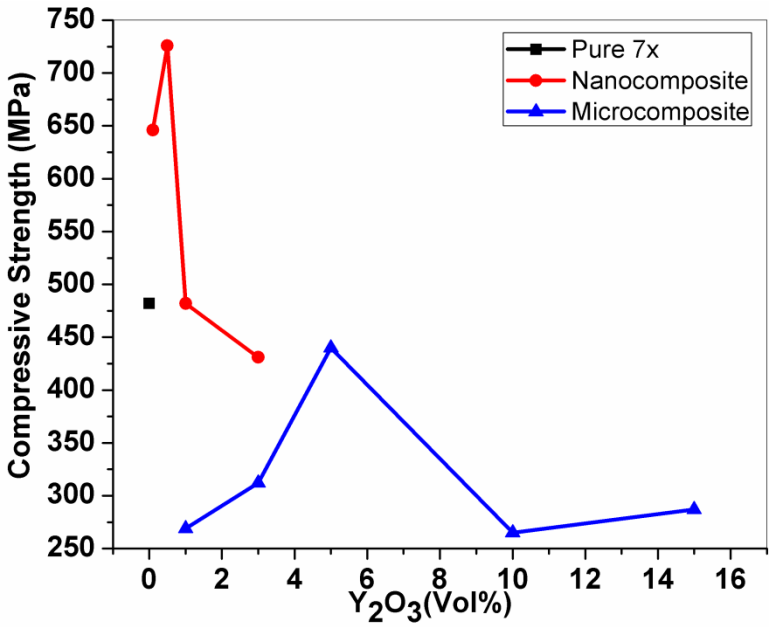

Fig 5.30: Compressive strength for pure Al-7075 and its composites

Stress-strain curves for pure Al-7075 alloy and micrometric composites under compressive loading are shown in Fig. 5.31. Addition of micrometric reinforcement did not led to any improvement in the compressive strength. A sudden drop was observed in Al-7075, 10 M and 15 M samples due to cracking of the sample during compression.

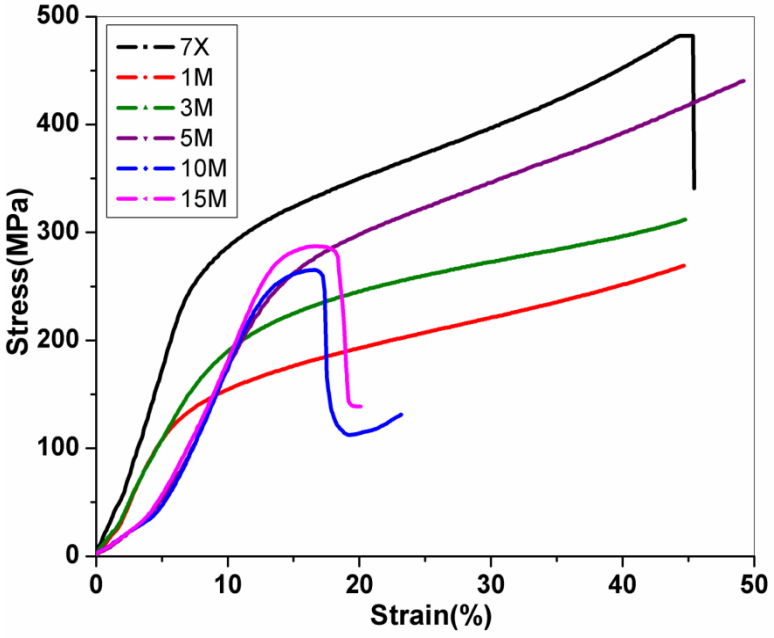

Fig. 5.31: Compression curves for micrometric composites

Stress-strain curves for pure Al-7075 alloy and and nanometric composites under compressive loading are shown in Fig. 5.32. The compressive strength and load bearing capacity increases upto an extent then decreases with the addition of nanometric reinforcement in pure Al-7075 alloy. Almost all the samples except 3 vol% nanometric composite cracked after reaching a maximum compressive strength and a sudden drop was observed at the end of compression.

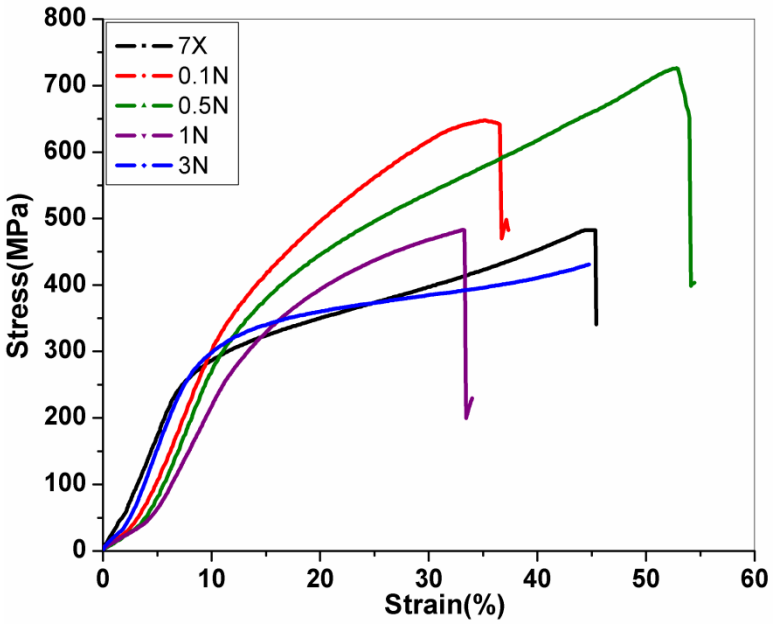

Fig. 5.32: Compression curves for nanometric composites

5.2.7 Summary

- Aluminum 7075 alloy composites with varying contents of micrometric and nanometric Y_2O_3 reinforcements were successfully processed using the powder forging route. The process included room temperature uniaxial compaction of powders, sintering and hot forging of these sintered performs at a temperature of 0.8 T_m and strain of 0.9 to obtain densities in excess of 99.4%.
- The incorporation of nanometric Y_2O_3 in the Al-7075 powders lead to an increase in the green density while the same led to a decrease in the sintered density. In case of micrometric Y_2O_3 this led a decrease in both the green as well as sintered density. This has been explained on the basis of Y_2O_3 particles filling the pore space between the triple points (which increases the density) and between two adjacent particles (which decreases the density) as this prevents neck formation between particles. Densification parameter was

found to be positive for both the composites as the sintered density was higher than the green density. Further, with addition of Y_2O_3 the densification parameter was found to decrease; the decrease being higher with nanometric Y_2O_3 as compared to micrometric Y_2O_3.

- The variation between the relative forged densities with micrometric and nanometric Y_2O_3 reinforcements was marginal and in excess of 99.4% relative density. The relative forged density was slightly higher in case of micrometric Y_2O_3 reinforcement as compared to nano Y_2O_3 reinforcement. With the incorporation of Y_2O_3 the forged densities were higher at low volume % as they played a role in the oxide removal from the particle surface while at higher volume % they led to a decrease in the forged densities as the role of friction seems to have played a more dominant role.
- The incorporation of nano and micrometric Y_2O_3 did not cause any change in the peak aging time though the different fractions of nano Y_2O_3 in particular led to considerable deviation in the hardness values as compared to that of pure Al-7075 in the underaged, peak aged and over aged conditions. In the as-forged condition the hardness levels at same volume fractions of nano and micrometric Y_2O_3 were similar. In the T_6 condition the hardness values were considerably higher than those in the solutionized and as-forged condition. Further, the hardness values with nanometric Y_2O_3 reinforcement were higher than that of micrometric Y_2O_3 in the T_6 condition.
- Both the tensile strength and compressive strength values were higher with the incorporation of nanometric Y_2O_3 as compared to micrometric Y_2O_3 in the T_6 condition. The tensile strength values in general for the micrometric composites were lower than those reported in literature while for the nanometric composites they were at par with those reported. The hardness values in both the cases peaked at a volume fraction of 0.5% for nanometric Y_2O_3 and at a volume fraction of 5% for micrometric Y_2O_3.
- The nanometric composites exhibited a well densified structure as compared to the micrometric composites for similar volume fractions of Y_2O_3. This is due to the ability of the finer nano Y_2O_3 particles to occupy the void space between the Al-7075 particles and the inability of the larger micrometric Y_2O_3 particles to do so.

5.3 Dry Sliding Wear Behavior Powder Forged Micrometric and Nanometric Y_2O_3 Reinforced Al-7075 Composites

This sub-section presents the tribological behavior of Al-7075 and its composites at peak aged condition. Wear studies using pin-on-disc tests were carried out at various loads and sliding speeds. The variation in coefficient of friction and wear rate was determined with respect to different volume fractions of micrometric and nanometric yttrium oxide additions to 7075 alloy matrix. Wear surface and wear debris were also analyzed for the explanation of wear mechanism of the fabricated composites.

5.3.1 Frictional Behavior

5.3.1.1 Coefficient of Friction for micrometric composites

Figure 5.33 shows typical coefficient of friction (COF) plots of pure alloy and micrometric composites with respect to sliding distance for different loads and at different sliding speeds. COF against sliding distance for pure alloy (Al-7075) showed more fluctuations at slower sliding speeds as compared to that at higher speeds (Fig. 5.33a). Addition of small amount of Y_2O_3 reinforcement to Al-7075 results in more fluctuations in the COF value at each combination of load and sliding speed. Further addition of Y_2O_3 reinforcement helps in stabilizing the COF along the sliding distance at lower loads of 10 and 20 N. But at a higher load of 30 N the COF value is more deviating from its average value. However at higher sliding speed of 2 m/s, COF value is more fluctuating with sliding distance. Larger fluctuations in COF were found in Al-7075 and composite containing 15 vol% micrometric Y_2O_3 reinforcement. The larger fluctuations in the composite containing 15 vol% micrometric Y_2O_3 are due to agglomerated reinforcement particles.

The coefficient of friction depends upon deformation of the surface asperities, adhesion of flat regions of the sliding surfaces and ploughing of the surface by wear particles and hard asperities. During the wear progress of Al-7075, the surface asperities deform easily due to acting load at the time of sliding. At a moderate load of 20 N and slightly higher sliding speeds, these asperities wear out faster and the exposed surface is oxidized. The oxidized surface acts as a tribolayer and it stables the COF with sliding distance. Upon addition of reinforcement, asperities became little harder and are not easily worn out resulting in less fluctuation in COF value as sliding continues. When a higher amount of reinforcement is added to the matrix, it leads to agglomeration of the reinforcement which plough out in the form of wear debris. These wear debris act as an obstacle during a smooth run between disc and the sample pin which results in

fluctuating COF values. Increase in load causes formation of more wear debris and the surface becomes rough resulting in further variation in COF value with respect to sliding distance.

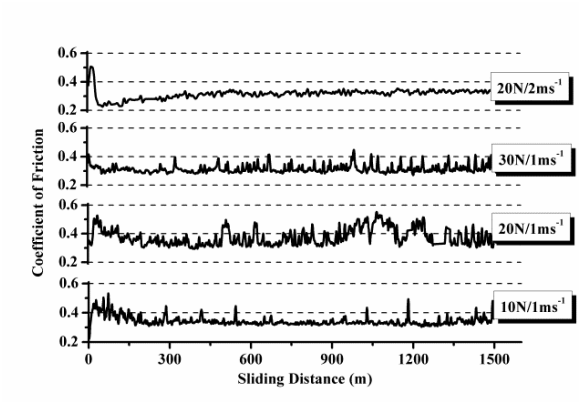

(a)

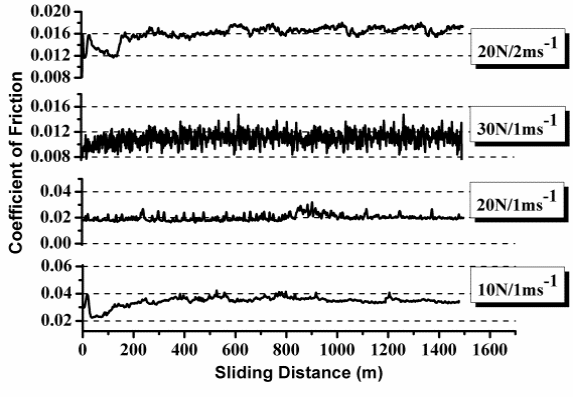

(b)

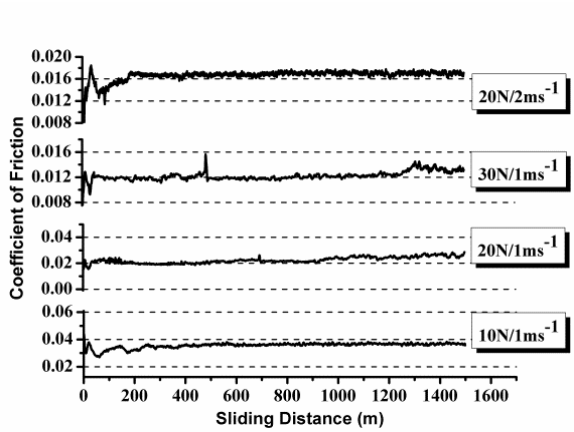

(c)

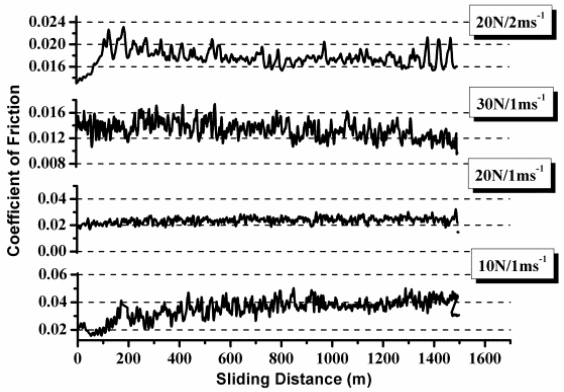

(d)

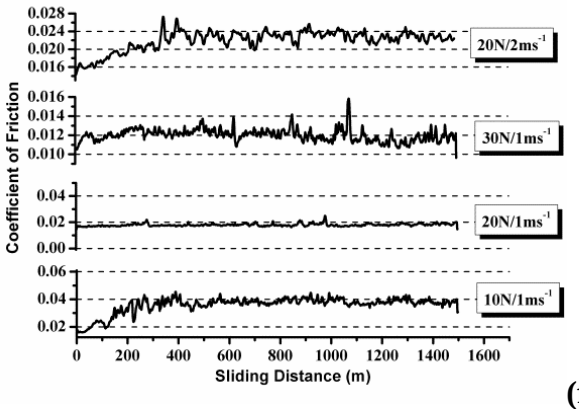

(e)

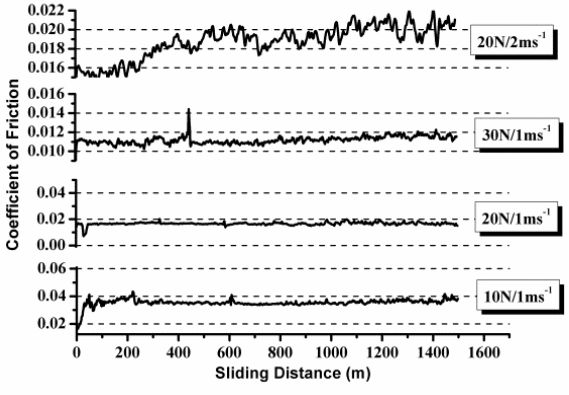

(f)

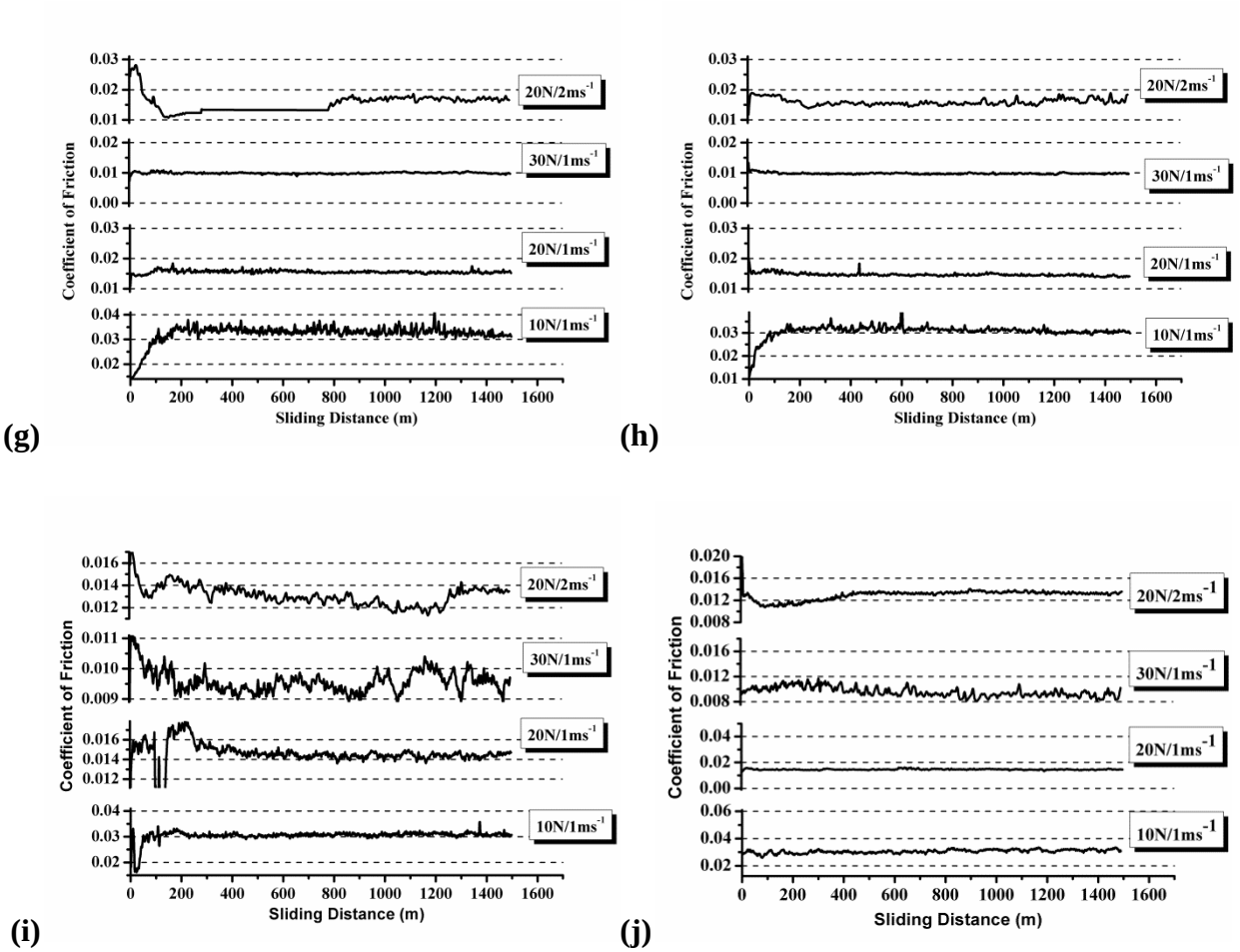

Fig 5.33: COF plots against sliding distance for (a) Al-7075; (b) 1M; (c) 3M; (d) 5M; (e) 10M; (f) 15M; (g) 0.1N; (h) 0.5N; (i) 1N and (j) 3N

5.3.1.2 Average COF for Micrometric Composites

The average value of coefficient of friction (COF) at different loads (10, 20 and 30 N) for varying contents of micrometric Y_2O_3 is shown in Fig. 5.34(a). At a constant speed of 1 m/s and 10 N load there was no significant change in the average COF of micrometric Y_2O_3 reinforced composites with increasing reinforcement content. At 20 N and 30 N loads the average COF increased upto 5 vol% and decreased thereafter. The variation between average COF and micrometric Y_2O_3 reinforcement content at different sliding speeds (1 and 2 m/s) and constant load of 20 N is shown in Fig. 5.34(b). It can be observed that average COF for micrometric composites is less for 2 m/s than 1 m/s upto 5 vol% of Y_2O_3 reinforcement addition however a reverse trend was found beyond this value. At low sliding speeds, cyclic plastic deformation of the surface layers takes place due to tangential and normal load. Reinforcement particles nucleate the crack or void at the deformed surface layers. Addition of the reinforcement in excess of 5 vol % lowers the

plastic deformation of soft aluminum 7075 matrix. At higher sliding speeds the asperities of test sample and disc are less in contact with the disc causing less friction between the disc and sample pin while at slow speeds it encounters more asperities so more friction is generated. When the sliding speed is increased to 2 m/s, the COF value increases similarly as in 1m/s but a drop in COF is seen at 10 vol% addition rather than 5 vol% addition of reinforcement.

Average COF value shows a continuous trend with different loads for all composites. The COF value is low at 10 N load, increases with 20 N load then decreases at 30 N load. Increasing the load upto 20 N supports the pullout of material from the sample which acts as a third body. At higher speed, when plowing of the reinforcement particles occurs, abrasive wear become a dominant wear mechanism. The reinforcement particles were in the form of agglomerates when added in a larger quantity and plow out together causes a rough surface as well as higher COF. At high speed, both the wear surfaces find less time to contact as well as less area of contact was made. The less area of contact provides fewer disturbances in the movement of sample pin over counterdisc during the wear test run resulting in a lower value of COF. This low COF is retained till a sufficient amount of wear debris spread out at the surface which can be only possible when a larger reinforcement amount (15 vol%) is present in the matrix material.

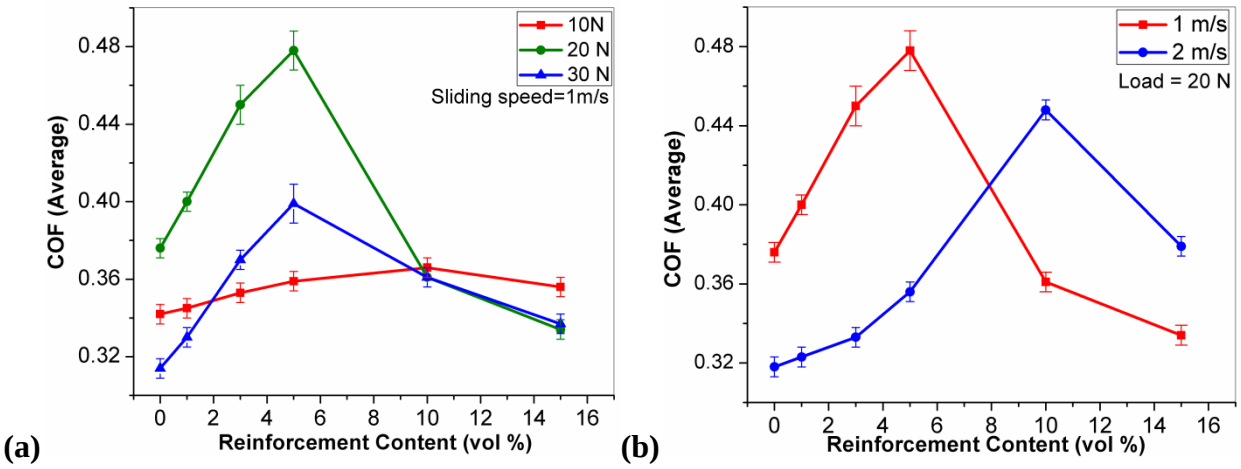

Fig 5.34: Average Coefficient of friction (COF) at (a) Micrometric composites at constant speed (1 m/s) and (b) Micrometric composites at constant load (20 N)

5.3.1.3 Coefficient of Friction for Nanometric composites

Typical coefficient of friction plots for Al-7075 and nanometric composites with respect to sliding distance (at different loads and different sliding speeds) are shown in Fig. 5.35. The COF

values plotted with time show that the COF curves are smoother at all loads and sliding speeds for composite having 0.5 vol% nano Y_2O_3 reinforcement. For other nanometric composites, the COF is fluctuating against sliding distance. The reason behind these fluctuations is similar as explained for micrometric composites in previous section.

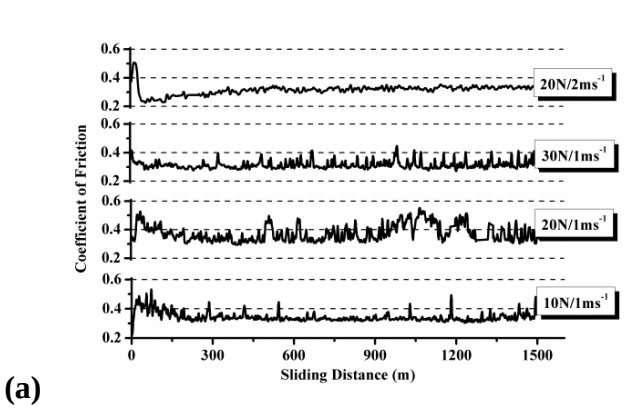

(a)

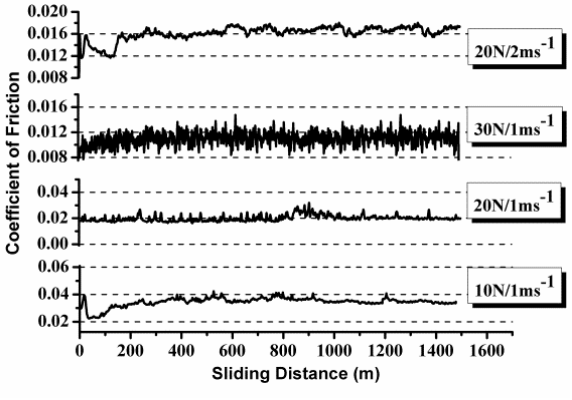

(b)

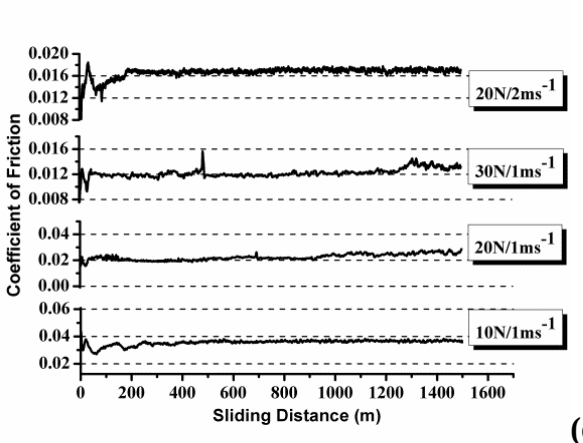

(c)

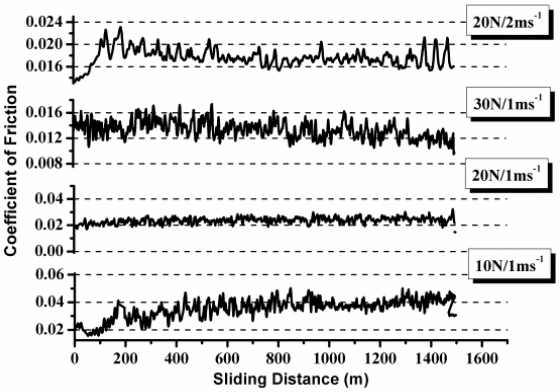

(d)

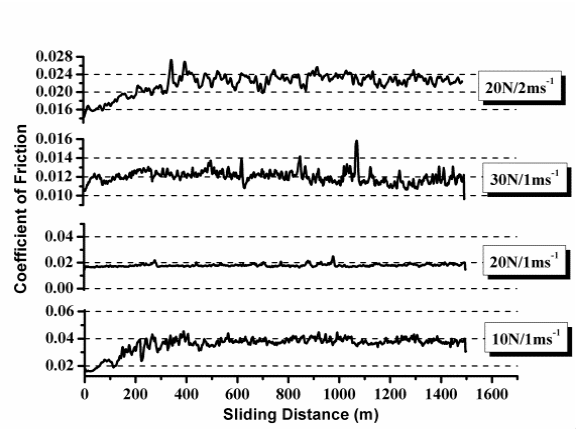

(e)

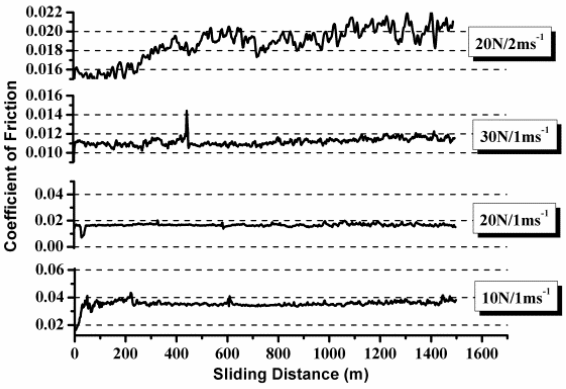

(f)

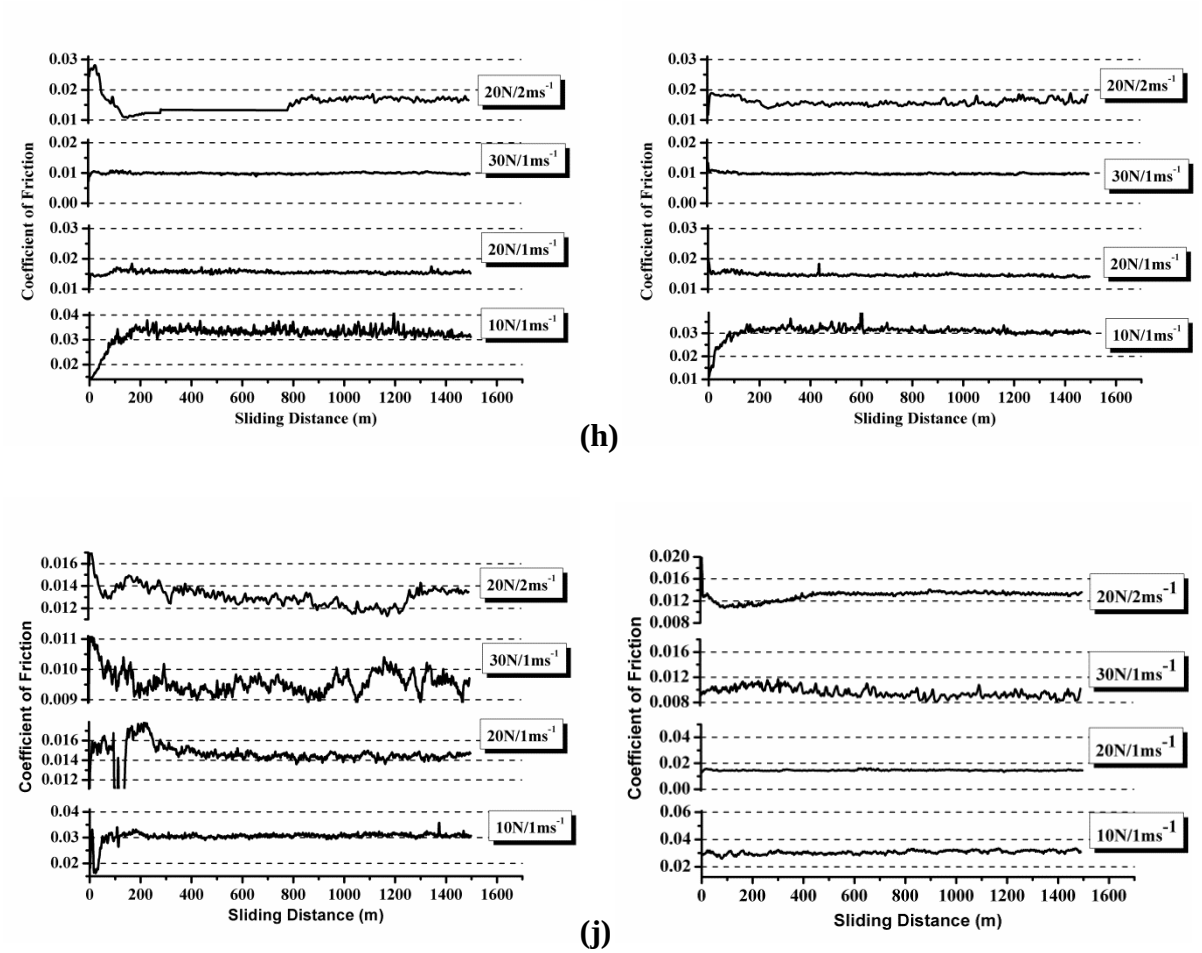

Fig 5.35: COF against sliding distance for (a) Al-7075; (b) 1M; (c) 3M; (d) 5M; (e) 10M; (f) 15M; (g) 0.1N; (h) 0.5N; (i) 1N and (j) 3N

5.3.1.4 Average COF for Nanometric Composites

The average value of coefficient of friction (COF) at different loads (10, 20 and 30 N) and a constant sliding speed of 1m/s for varying contents of nanometric Y_2O_3 is shown in Fig. 5.36(a). At a constant speed of 1 m/s, there is a continuous drop in the average COF with increasing reinforcement content at all loads. Increase in reinforcement content provides more loose particles in between the sample and counterdisc during wear operation. The nanometric Y_2O_3 particles were almost spherical as seen in the TEM image (Fig. 5.36(a)). The spherical particles spread on the surface act as a rolling media between two mating surfaces and reduce COF continuously with their increasing content. Comparing the average COF value for individual composition it can be noted that average COF value decreases with increasing load except for the Al-7075. Increasing load fractures the hard debris as well as nanoparticle agglomerates and increases the number of tiny rollers on the surface resulting in a low COF. In case of Al-7075, the nanoparticles are absent

and increasing load makes the surface rough causing higher COF value. Increasing load further upto 30 N suppresses the wear debris and creates a tribolayer which is smooth and having less friction. The variation in average COF of nanometric composites at different sliding speeds (1 and 2 m/s) and constant load of 20 N is shown in Fig. 5.36(b).

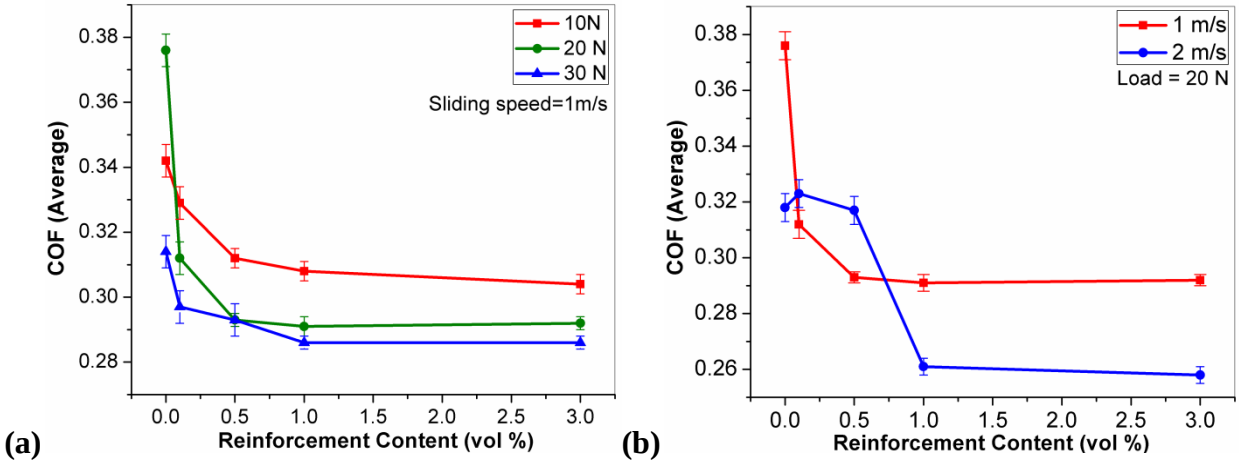

Fig 5.36: Average Coefficient of friction (COF) at (c) Nanometric composites at constant speed (1 m/s) and (d) Nanometric composites at constant load (20 N)

At 1 m/s average COF value was found to decrease and at higher sliding speed of 2 m/s it first increased and then decreased. Addition of nanometric Y_2O_3 reinforcement of 0.1 and 0.5 vol% is not sufficient to create optimum quantity of rolling media in between the mating surfaces and COF was thus found more for a speed of 2 m/s. Adding more reinforcement with 1 vol% and 3 vol% increases the number of secondary particles and thus sufficient nano particles escaped from the surface during wear progress which acts as a rolling media eventually decreasing the average COF.

5.3.2 Wear Behavior of Composites

5.3.2.1 Wear Rate of Micrometric Composites

The variation of wear rate at different loads (10, 20 and 30 N) and a constant sliding speed of 1m/s for varying contents of micrometric Y_2O_3 is shown in Fig. 5.37 (a). The wear rate decreased with increasing load from 10 N to 20 N and it was almost same for 20 N and 30 N for the pure alloy. With the addition of micrometric Y_2O_3 reinforcement, the wear rate first decreased till 5 vol% and then increased upto 15 vol% reinforcement for a sliding speed of 1 m/s. This drop in the wear rate can be attributed to the high hardness of the material, uniform distribution of reinforcements and better interfacial bonding between the alloy particles and the reinforcement.

Adding more than 5 vol% of micrometric Y_2O_3 reinforcement, the agglomeration of reinforcement particles takes place. Similar agglomeration of particles was observed by Chawla et al., 1998. They explained that reducing the reinforcement particle size from 23 μm to 5 μm creates non-uniform distribution of reinforcement by particle agglomeration, leading to higher matrix-reinforcement interfacial area, which is of lower strength, resulting in failure by "pull-out" or matrix-particle interface decohesion. During sliding wear these agglomerates plough out in a bunch resulting in a drastic increase in the wear rate. Moreover nano-pores which remained in between the agglomerates are difficult to remove resulting in a decrease in hardness value. Earlier study of Al–Al_2O_3 composites [Yilmaz and Buytoz, 2001] have shown that the hardness decreases with the increasing amount of porosity. This decreased hardness finally increases the wear rate of the composites having more amount of reinforcement. The agglomerates of Y_2O_3 reinforcement are difficult to bind together with alloy matrix. These agglomerates hold some amount of porosity in between due to non wettability of individual particle. Regarding this porosity, one can conclude that porosity has a noticeable effect on hardness of the composites as well as wear behavior. In fact, as the amount of porosity decreases the surface hardness and wear resistance increases. Moreover, the influence of hardness on the wear rate is defined by Archard's equation [Archard, 1953]:

$$Q = kW/H$$

where Q is wear volume per unit sliding distance; k is the wear coefficient; W is the load applied and H is the hardness of the sample surface.

At higher loads the difference in increase in wear rate with reinforcement content is not prominent due to suppression of the wear debris which had formed a tribolayer on the surface of the material and prevented further wear of the material. At varying sliding speeds wear rate decreased upto 5 vol% reinforcement for 1 m/s due to higher hardness of the material, while in 2 m/s it decreased upto 10 vol% thereafter increasing with further addition of reinforcement (Fig. 5.37. b). The wear rate was high for higher reinforcement content at 1 m/s due to more wear debris generated in the form of more agglomerated reinforcement particles. At 2 m/s sliding speed, a drop in wear rate was sustained by the material for a large amount of reinforcement addition. At higher sliding speeds there is a temperature rise and oxidation rate is higher at the surface. This oxidation forms a tribolayer of aluminum oxide at the surface and prevents further wear. Adding more reinforcement provides a sufficient contact of these reinforcement clusters to counter disc which

results in more wear. Though the COF value is low for 15 vol% due to rolling action of the debris as discussed in above section, once the debris are removed from the material, they increased the wear as well as wear rate.

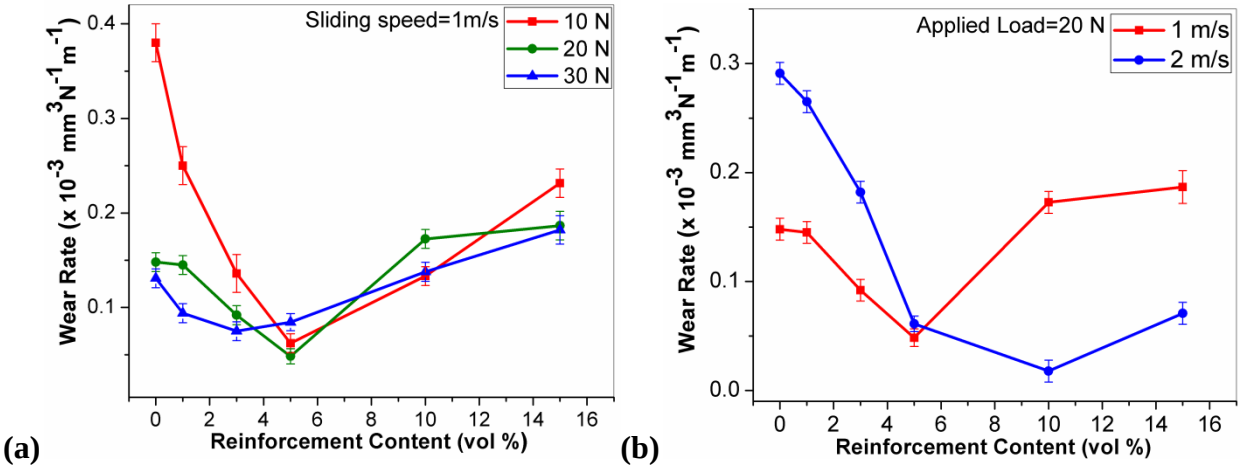

Fig. 5.37.Wear Rate for (a) Micrometric composites at constant speed (1 m/s) and (b) Micrometric composites at constant load (20 N)

5.3.2.2 Wear Rate of Nanometric Composites

The variation of wear rate at different loads (10, 20 and 30 N) and a constant sliding speed of 1m/s for varying contents of nanometric Y_2O_3 is shown in Fig. 5.38 (a). The overall wear rate decreased with the addition of Y_2O_3 reinforcement to pure 7075 alloy matrix at a constant speed. Adding 0.1 vol % nano Y_2O_3 to the alloy resulted in a sharp decrease in the wear rate. Addition of 0.5 vol% Y_2O_3 led to a slight wear rate drop thereafter the wear rate increased when 1 and 3 vol% nano Y_2O_3 was added. The largest drop (0.37 to 0.07) in the wear rate was found for 10 N load and at a slow sliding speed of 1 m/s. At a load of 20 N and 30 N the wear rate was almost same for pure alloy. At 0.1 vol% nano Y_2O_3 reinforcement wear rate decreased with increasing load. At 0.5 vol% nano reinforcement, the wear rate was almost similar at different loads. Wear rate first increased then decreased for increasing load with 1 and 3 vol% nano reinforcement. Comparison of wear rate for nanometric Y_2O_3 at different sliding speed at a constant load of 20 N is shown in Fig. 5.38 (b). Decrease in the wear rate is observed with the addition of reinforcement upto 0.5 vol% at a sliding speed of 1 m/s and upto 1 vol% at 2 m/s. The nano particles are generally spherical in shape and acts as a rolling media reducing COF as well as wear rate. The reinforcement content of more than 1 vol% reduces the COF as discussed in above section but once they got removed from the surface, they create a path for fresh surface removal. One more

reason for increasing wear rate at higher reinforcement content was their agglomeration inside the matrix due to which they pull out in a bunches and increases wear.

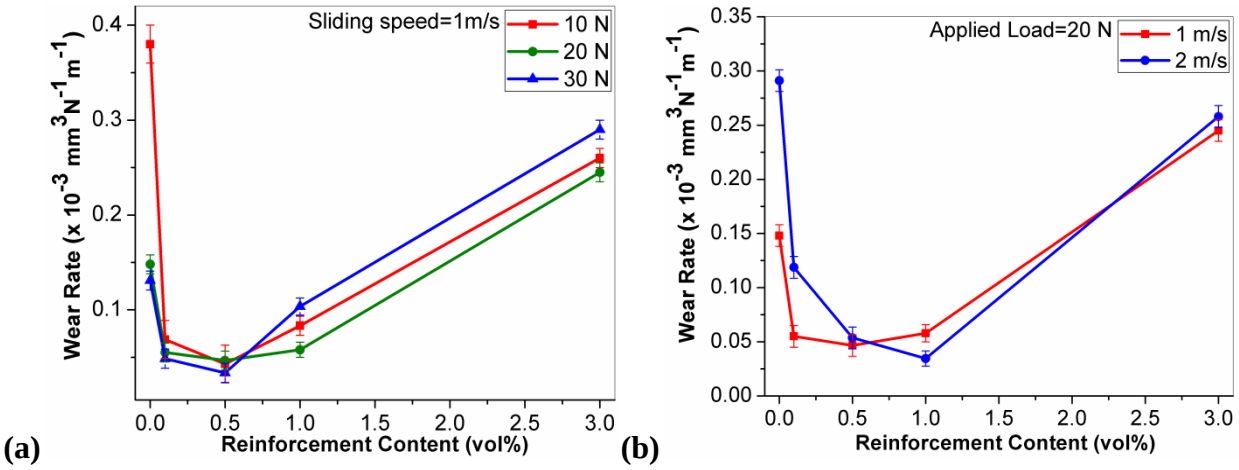

Fig 5.38: Wear Rate for (a) Nanometric composites at constant speed (1 m/s) and (b) Nanometric composites at constant load (20 N)

Nanometric Y_2O_3 composite with reinforcement content 1 vol% shows a higher wear rate at a low sliding speed of 1 m/s. At higher sliding speed of 2 m/s, the time of contact between the asperities reduces as well as early oxidation of surface due to temperature rise forms a tribolayer on the surface which prevented further wear. Addition of further reinforcement fraction of 3 vol% again flips the wear rates due to clustering of nanoparticles and non homogeneous distribution of hard reinforcement in the matrix. The clusters are pulled out from the matrix easily at 2 m/s and increase the wear rate.

Observation of wear curves explains that adding nano Y_2O_3 reinforcement helps in decreasing the wear rate (Fig.5.38 a). Nano Y_2O_3 particles distribute the load during wear and acts as a load bearing phase. But above a certain limit delamination wear [Suh, 1973] at the surface is a dominant mechanism due to which the wear rate increases at 1 vol% reinforcement content. At higher sliding speed (Fig.5.38 b), a tribolayer forms on the surface of the sample due to oxidation. This layer prevents further wear of the surface upto some extent and reduces wear rate. Secondly the nano reinforcement powders split out from the sample surface acts as rolling media and reduce the COF as well as wear in the same manner as 0.5 vol % nano reinforcement was acting for a sliding speed of 1 m/s.

5.3.3 Wear surface analysis

5.3.3.1 Wear surface of pure Al-7075

Fig. 5.39 shows the SEM images of wear tracks of pure alloy at different loads and different speeds. With increasing load the delaminated wear tracks develop more spacing while with increasing speed the surface is more worn out. More wear grooves can be seen in the form of parallel scratches in Fig. 5.39 (a) which indicates more wear of the surface at a load of 10 N and at a sliding speed of 1 m/s. In Fig. 5.39(b) and Fig. 5.39(c) the depth of these wear scratches decreases and at a load of 30 N, delamination of surface starts appearing at 1 m/s. At higher speed plastic flow can be seen at the wear surface of pure 7075 alloy increasing the wear of corresponding surface (Fig. 5.39 d). At higher load and higher sliding speeds, fragments from soft aluminum matrix attach to the steel wear disc which is harder. As sliding continues, the attached fragments came off the surface and are transferred back to the original surface of sample pins. Some fragments remains as loose wear particles which further acts as wear debris.

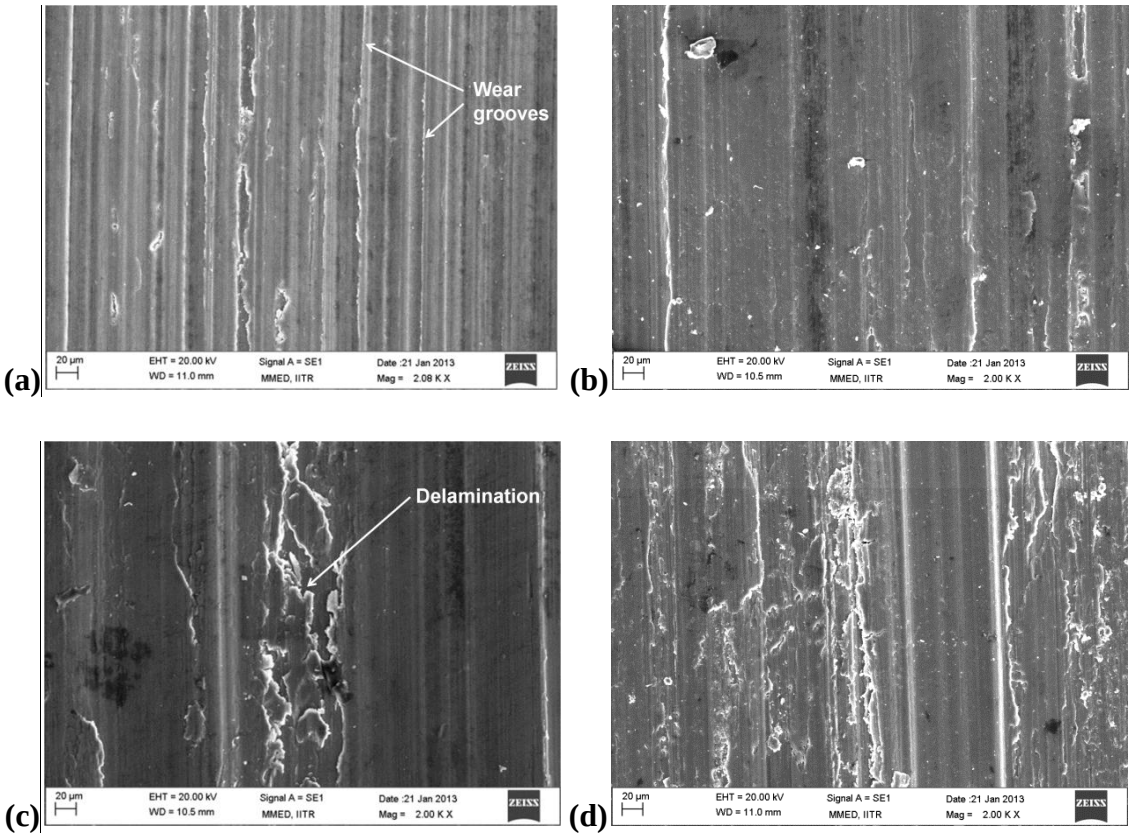

Fig 5.39: Wear tracks of Al-7075 (a) 10N/1ms^{-1}; (b) 20N/1ms^{-1}; (c) 30N/1ms^{-1} and (d) 20N/2ms^{-1}

5.3.3.2 Wear surface of Micrometric Composites

Wear surface of micrometric Y_2O_3 composites is shown in Fig 5.40. The surface cracks and wear debris are almost same upto 5 vol% composite at all the loads for a constant sliding speed. Wear surface was ploughing out at double sliding speed with 20 N load for this composite. With the addition of more Y_2O_3 (vol%), more wear debris were generated due to agglomeration of these reinforcement particles as discussed above. Due to these wear debris when the load is increased during sliding wear of 10 vol% composite samples, surface of the test samples gets more damaged with increasing load. Wear increased in 10 vol% and 15 vol% composites at a sliding speed of 1 m/s at different loads due to more loose particles. The loose particles at the surface may be aluminum alloy, oxides of aluminum and iron or Y_2O_3 particles. The alloy particle are soft but during sliding a fresh surface is exposed to air which oxidizes rapidly leading to the formation of aluminum oxide particles which causes more surface wear. Wear decreases at 2 m/s sliding speed for composites containing 10 vol% and 15 vol% Y_2O_3 when tested at constant load due to formation of a tribolayer. At a sliding speed of 2 m/s, the temperature of the wear surface increases fast and due to wear a fresh surface is exposed. This fresh surface exposed to air at higher temperature oxides rapidly forming aluminum oxide all over the surface which acts as a tribolayer initially. As the wear progresses breaking of the tribolayer due to surface cracking led to wear debris to come out causing the surface to be rougher. At slow sliding speeds the dominant mechanism responsible for wear is adhesive wear. At 1 m/s sliding speed wear rate is not improved even with increase in harder reinforcement content. This is because hardness of the asperities rather than bulk hardness plays a major role during wear at slow speed.

(a) 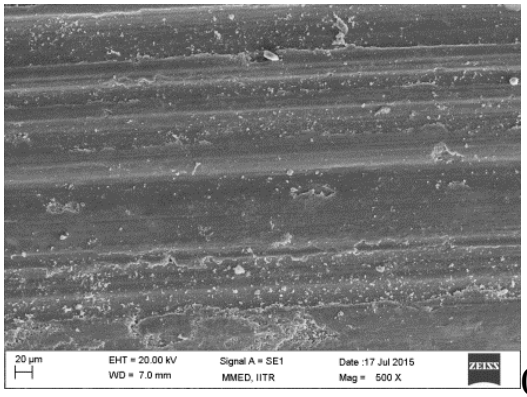

(b) 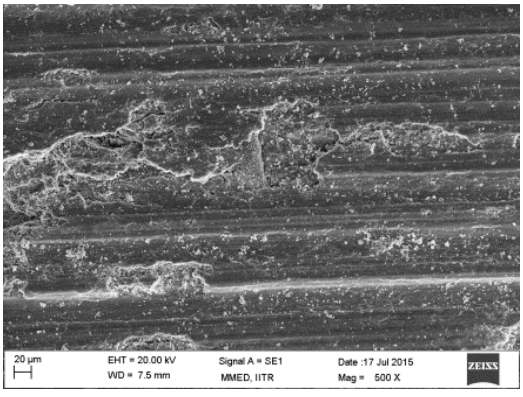

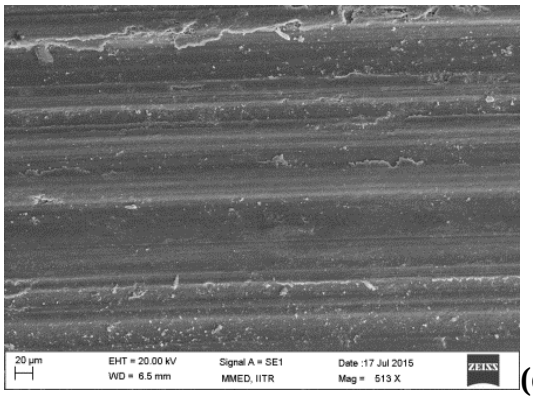
20 µm
EHT = 20.00 kV
WD = 6.5 mm
Signal A = SE1
MMED, IITR
Date :17 Jul 2015
Mag = 513 X
ZEISS

(c)

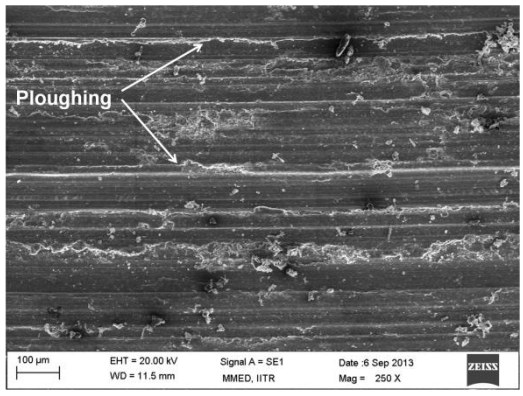
Ploughing
100 µm
EHT = 20.00 kV
WD = 11.5 mm
Signal A = SE1
MMED, IITR
Date :6 Sep 2013
Mag = 250 X
ZEISS

(d)

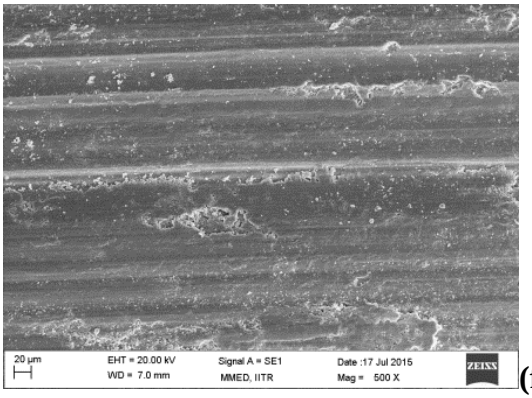
20 µm
EHT = 20.00 kV
WD = 7.0 mm
Signal A = SE1
MMED, IITR
Date :17 Jul 2015
Mag = 500 X
ZEISS

(e)

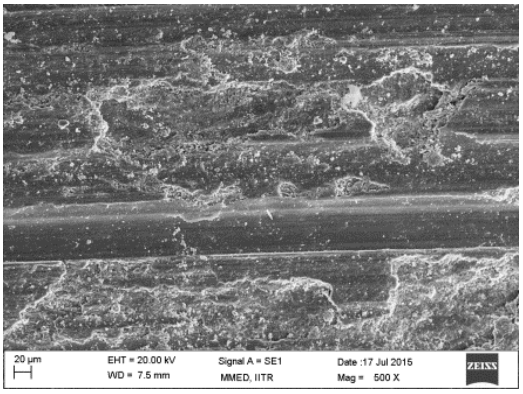
20 µm
EHT = 20.00 kV
WD = 7.5 mm
Signal A = SE1
MMED, IITR
Date :17 Jul 2015
Mag = 500 X
ZEISS

(f)

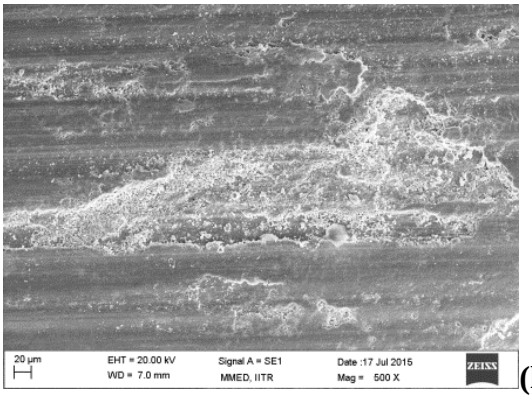
20 µm
EHT = 20.00 kV
WD = 7.0 mm
Signal A = SE1
MMED, IITR
Date :17 Jul 2015
Mag = 500 X
ZEISS

(g)

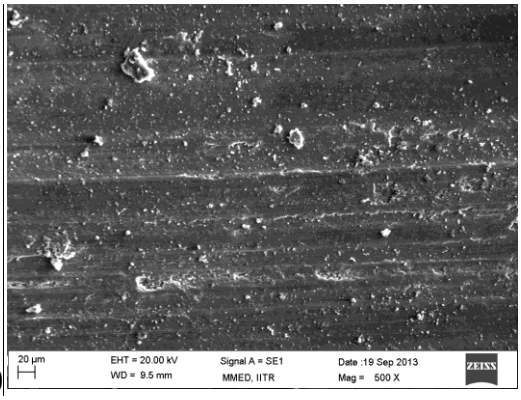
20 µm
EHT = 20.00 kV
WD = 9.5 mm
Signal A = SE1
MMED, IITR
Date :19 Sep 2013
Mag = 500 X
ZEISS

(h)

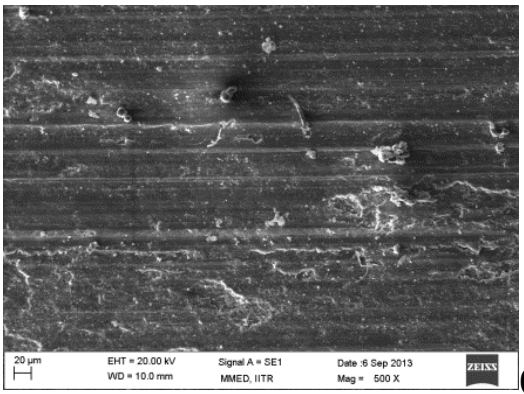
20 µm
EHT = 20.00 kV
WD = 10.0 mm
Signal A = SE1
MMED, IITR
Date :6 Sep 2013
Mag = 500 X
ZEISS

(i)

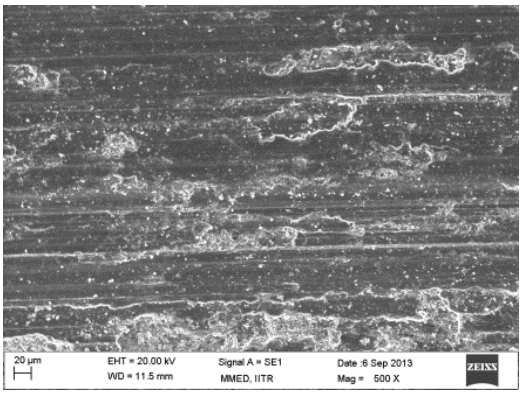
20 µm
EHT = 20.00 kV
WD = 11.5 mm
Signal A = SE1
MMED, IITR
Date :6 Sep 2013
Mag = 500 X
ZEISS

(j)

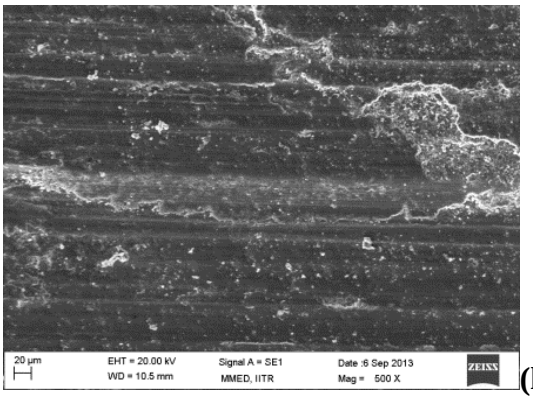
20 µm
EHT = 20.00 kV
WD = 10.5 mm
Signal A = SE1
MMED, IITR
Date :6 Sep 2013
Mag = 500 X
ZEISS

(k)

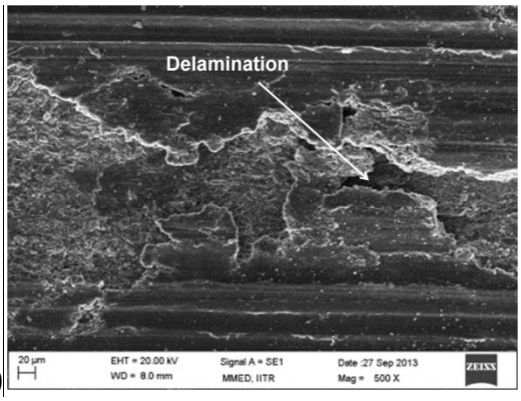
Delamination
20 µm
EHT = 20.00 kV
WD = 8.0 mm
Signal A = SE1
MMED, IITR
Date :27 Sep 2013
Mag = 500 X
ZEISS

(l)

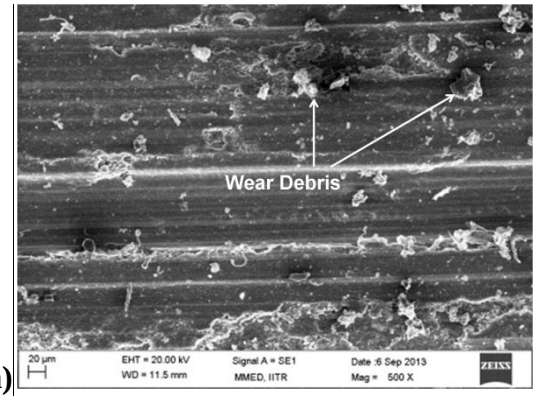
Wear Debris
20 µm
EHT = 20.00 kV
WD = 11.5 mm
Signal A = SE1
MMED, IITR
Date :6 Sep 2013
Mag = 500 X
ZEISS

(m)

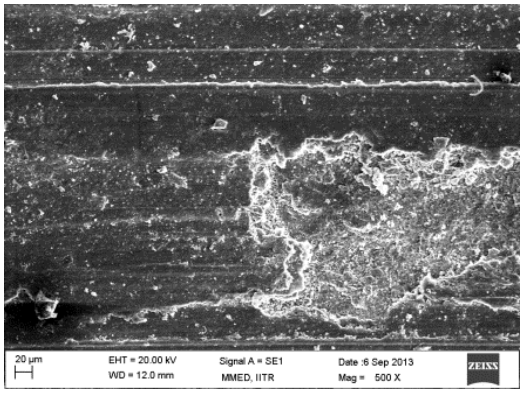
20 µm
EHT = 20.00 kV
WD = 12.0 mm
Signal A = SE1
MMED, IITR
Date :6 Sep 2013
Mag = 500 X
ZEISS

(n)

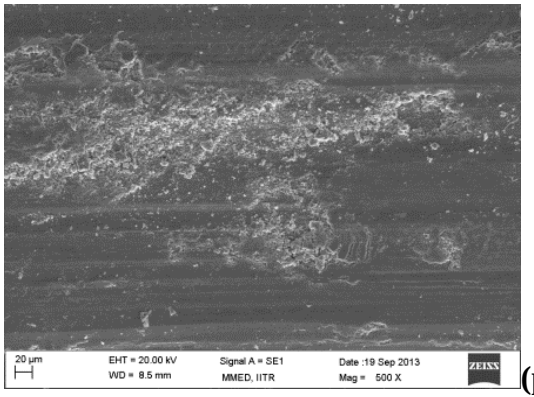
20 µm
EHT = 20.00 kV
WD = 8.5 mm
Signal A = SE1
MMED, IITR
Date :19 Sep 2013
Mag = 500 X
ZEISS

(o)

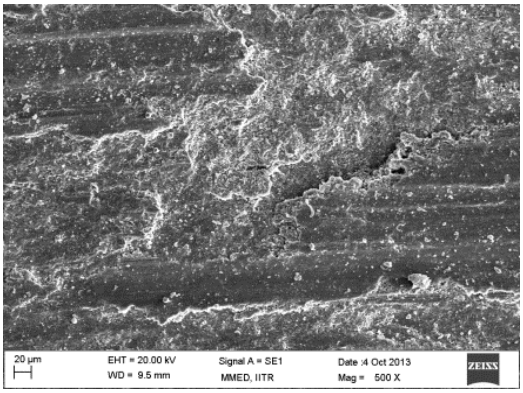
20 µm
EHT = 20.00 kV
WD = 9.5 mm
Signal A = SE1
MMED, IITR
Date :4 Oct 2013
Mag = 500 X
ZEISS

(p)

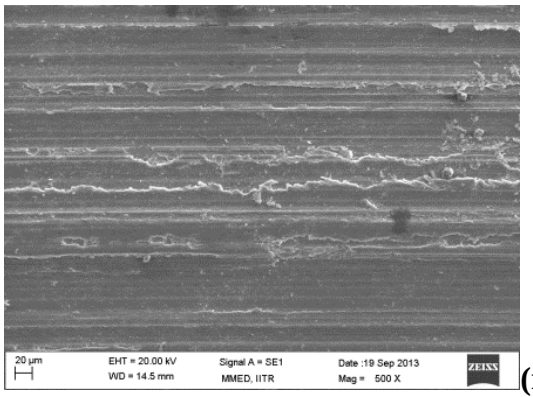
20 µm
EHT = 20.00 kV
WD = 14.5 mm
Signal A = SE1
MMED, IITR
Date :19 Sep 2013
Mag = 500 X
ZEISS

(q)

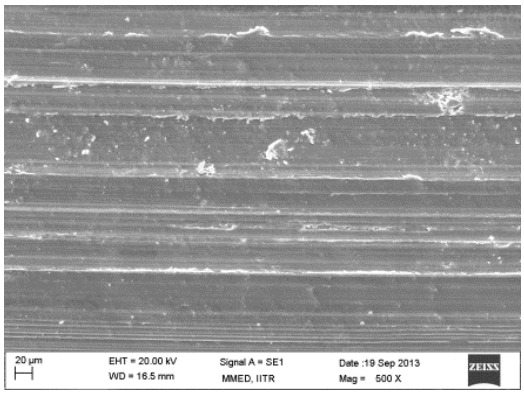
20 µm
EHT = 20.00 kV
WD = 16.5 mm
Signal A = SE1
MMED, IITR
Date :19 Sep 2013
Mag = 500 X
ZEISS

(r)

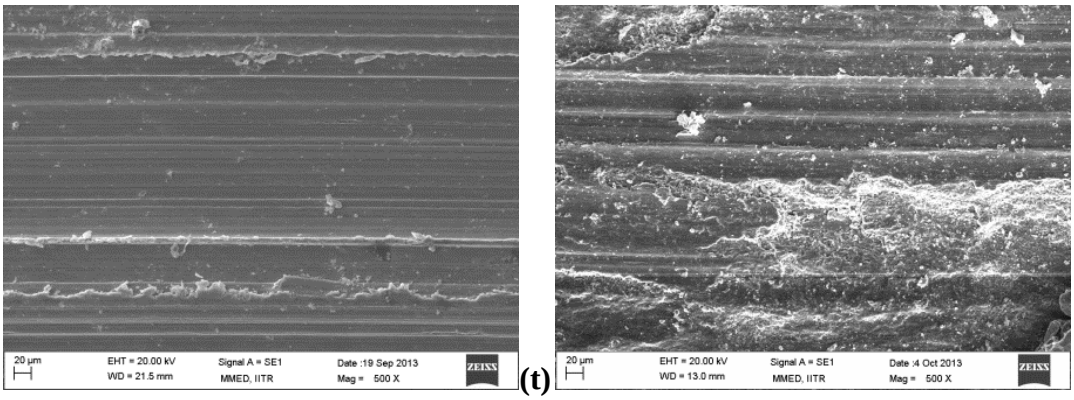

(s) **(t)**

Fig. 5.40: Wear tracks of composites (a) 1M/10N/1ms^{-1}; (b) 1M/20N/1ms^{-1}; (c) 1M/30N/1ms^{-1}; (d) 1M/30N/2ms^{-1}; (e) 3M/10N/1ms^{-1}; (f) 3M/20N/1ms^{-1}; (g) 3M/30N/1ms^{-1}; (h) 3M/30N/2ms^{-1}; (i) 5M/10N/1ms^{-1}; (j) 5M/20N/1ms^{-1}; (k) 5M/30N/1ms^{-1}; (l) 5M /20N/2ms^{-1}; (m) 10M/10N/1ms^{-1}; (n) 10M/20N/1ms^{-1}; (o) 10M/30N/1ms^{-1}; (p) 10M/20N/2ms^{-1}; (q) 15M/10N/1ms^{-1}; (r) 15M/20N/1ms^{-1}; (s) 15M/30N/1ms^{-1} and (t) 15M/20N/2ms^{-1}

5.3.3.3 Wear surface of Nanometric Composites

Wear tracks of nanometric composites after sliding wear at three loads and two sliding speeds are shown in Fig.5.41. It was observed that there is no sharp change in the surface of 0.1 vol% nano composite worn at 10, 20 and 30 N. Wear scratches along with the wear debris at the surface can be seen in Fig. 5.41(a-c). Fig. 5.41(b) shows more worn surface due to a higher sliding speed during wear test. Composite with 0.5 vol% nano Y_2O_3 shows quite less worn surface for all loads at a sliding speed of 1 m/s compared to other nanometric composites. At a load of 10 N less wear grooves are visible though the wear debris are more in number on the surface. The surface has a low roughness at higher loads of 20 N and 30 N for 0.5vol% nano Y_2O_3 as shown in Fig 5.41(b) and 5.41(c) but at a high sliding speed the surface condition is same alike 0.1N composite at 2 m/s. Higher content of hard Y_2O_3 nano reinforcement in composite 1 vol% and 3 vol% has a considerable effect on the plastic deformation of the sample surface. At higher speed of 2 m/s the surface is worn out with delaminated wear but with small patches of delamination as compared to composites having 0.1 vol% and 0.5 vol% nanometric Y_2O_3.

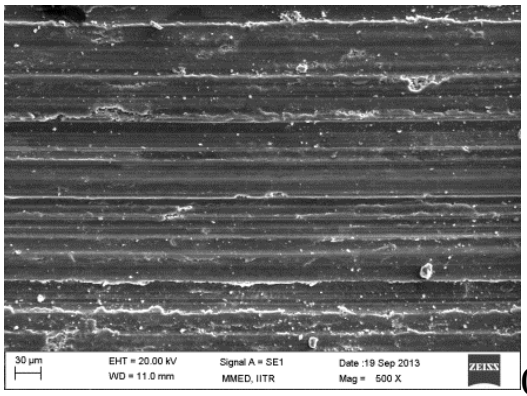
30 µm
EHT = 20.00 kV
WD = 11.0 mm
Signal A = SE1
MMED, IITR
Date :19 Sep 2013
Mag = 500 X
ZEISS

(a)

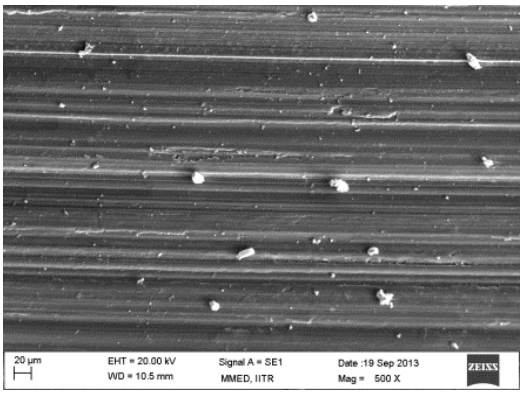
20 µm
EHT = 20.00 kV
WD = 10.5 mm
Signal A = SE1
MMED, IITR
Date :19 Sep 2013
Mag = 500 X
ZEISS

(b)

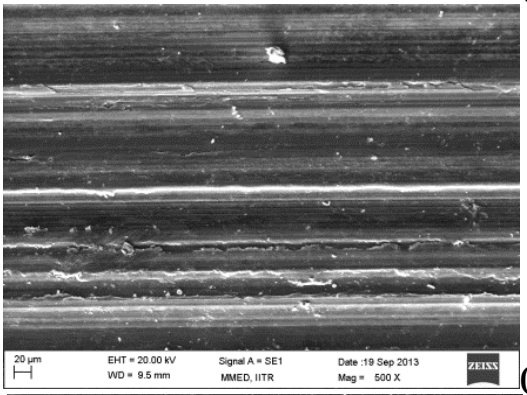
20 µm
EHT = 20.00 kV
WD = 9.5 mm
Signal A = SE1
MMED, IITR
Date :19 Sep 2013
Mag = 500 X
ZEISS

(c)

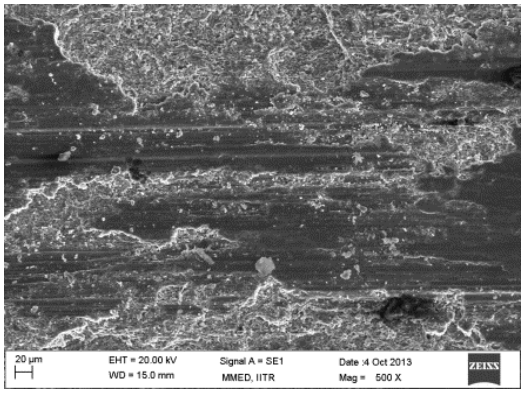
20 µm
EHT = 20.00 kV
WD = 15.0 mm
Signal A = SE1
MMED, IITR
Date :4 Oct 2013
Mag = 500 X
ZEISS

(d)

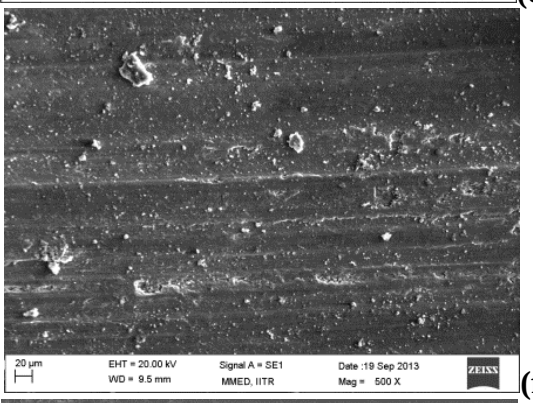
20 µm
EHT = 20.00 kV
WD = 9.5 mm
Signal A = SE1
MMED, IITR
Date :19 Sep 2013
Mag = 500 X
ZEISS

(e)

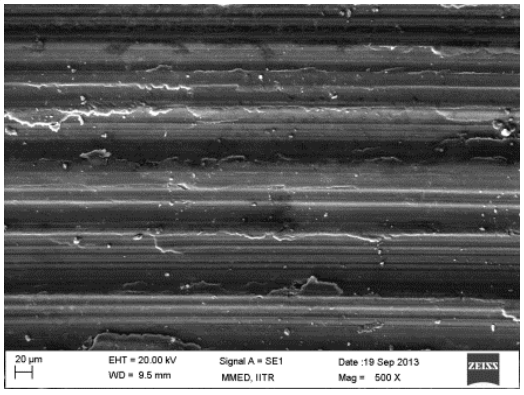
20 µm
EHT = 20.00 kV
WD = 9.5 mm
Signal A = SE1
MMED, IITR
Date :19 Sep 2013
Mag = 500 X
ZEISS

(f)

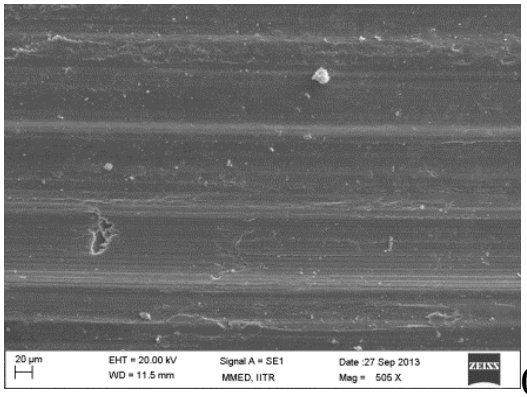
20 µm
EHT = 20.00 kV
WD = 11.5 mm
Signal A = SE1
MMED, IITR
Date :27 Sep 2013
Mag = 505 X
ZEISS

(g)

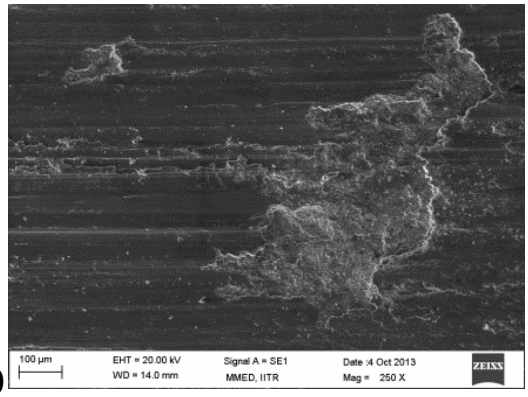
100 µm
EHT = 20.00 kV
WD = 14.0 mm
Signal A = SE1
MMED, IITR
Date :4 Oct 2013
Mag = 250 X
ZEISS

(h)

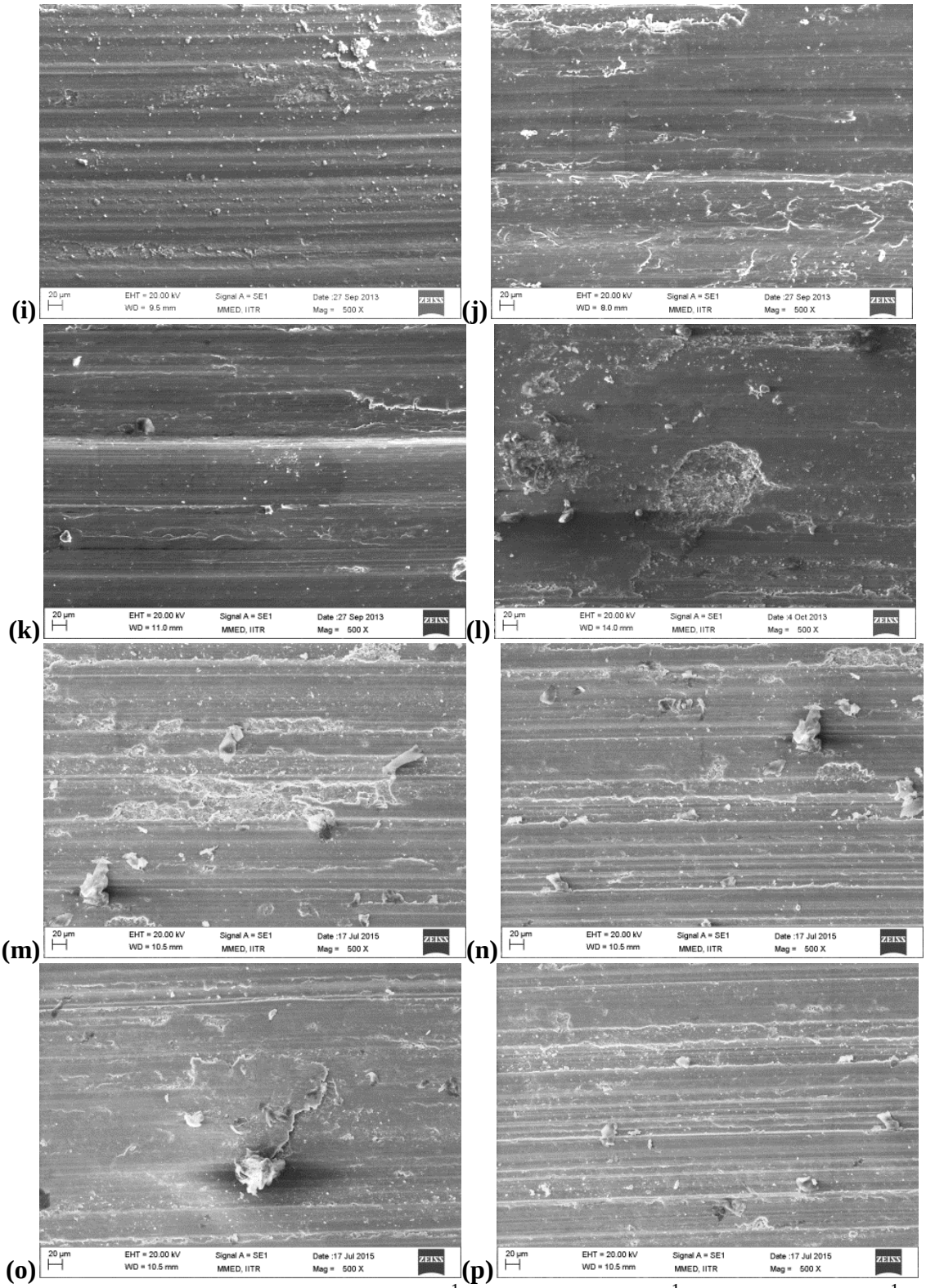

Fig. 5.41: Wear tracks of (a) 0.1N/10N/1ms^{-1}; (b) 0.1N/20N/1ms^{-1}; (c) 0.1N/30N/1ms^{-1}; (d) 0.1N/20N/2ms^{-1}; (e) 0.5N/10N/1ms^{-1}; (f) 0.5N/20N/1ms^{-1}; (g) 0.5N/30N/1ms^{-1}; (h) 0.5N/20N/2ms^{-1}; (i) 1N/10N/1ms^{-1}; (j) 1N/20N/1ms^{-1}; (k) 1N/30N/1ms^{-1}; (l) 1N/20N/2ms^{-1}; (m) 3N/10N/1ms^{-1}; (n) 3N/20N/1ms^{-1}; (o) 3N/30N/1ms^{-1} and (p) 3N/20N/2ms^{-1}

5.3.4 Wear Debris

Wear debris for micrometric and nanometric reinforced composites at a moderate load of 20 N and at a sliding speed of 1 m/s are shown in Fig. (5.42). Suppressed wear debris were observed for nanometric composite having 0.5 vol% Y_2O_3 in Fig. 5.42(a). These were likely due to soft matrix and low amount of hard Y_2O_3 reinforcement in the matrix. Another image of nanometric composite having 3 vol% Y_2O_3 shows small irregular debris (Fig. 5.42(b)). Wear debris of micrometric composites were found in mixed mode of suppressed as well as finer particles. Finer particles were seen increasing in micrometric composites as the Y_2O_3 reinforcement content increased (Fig. 5.42(c-d)).

The wear debris are likely to consist of aluminum oxide particles, reinforcement particles and some iron oxide particles from the disc. These particles are harder than the sample matrix. These harder wear debris create more patches in the sample surface and increases the COF. Further increment of load to 30 N suppresses the wear debris. The wear debris in suppressed form acts as a layer on the surface at a low reinforcement content. At higher loads when the reinforcement content is increased, more reinforcement particles are collected at the wear surface as wear debris. These wear debris get fractured with effectively higher load and acts as a rolling media in between the sample and the counterdisc resulting in decreased COF values.

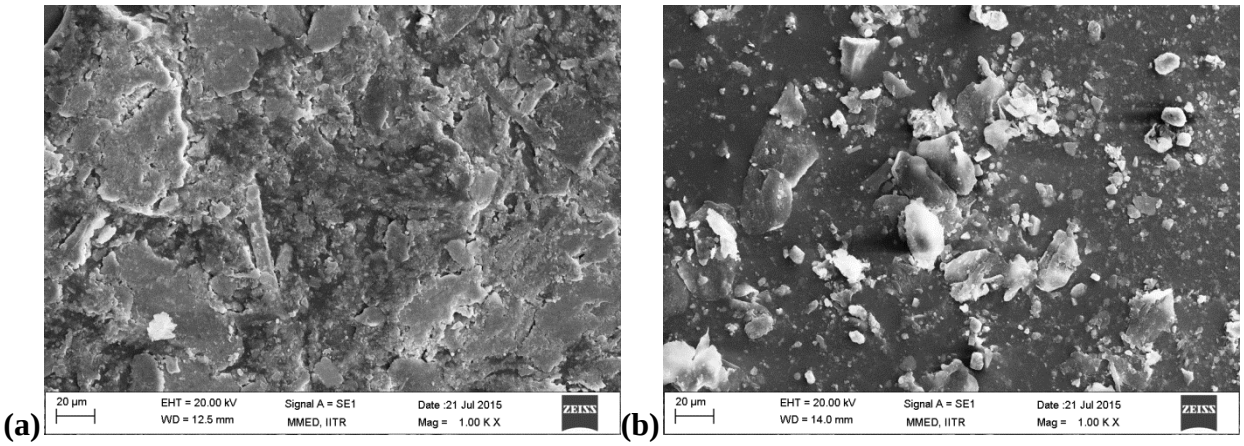

(c) 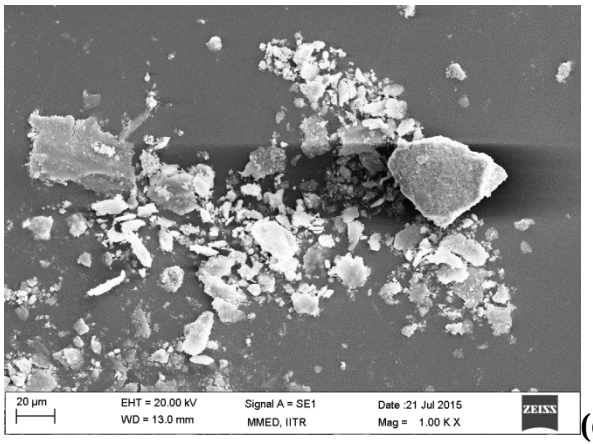

(d) 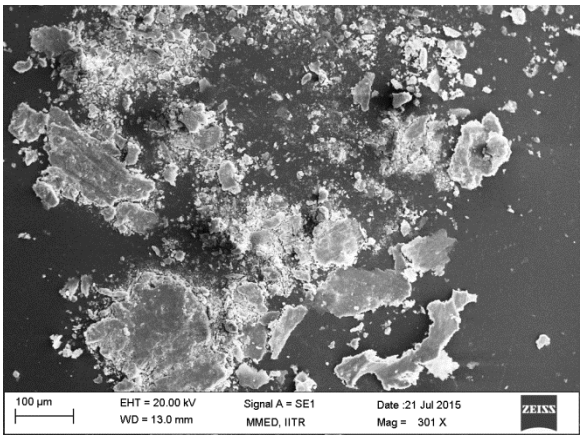

Fig 5.42: Wear debris for (a) 0.5N/20N/1ms^{-1}; (b) 3N/20N/1ms^{-1}; (c) 5M/20N/1ms^{-1} and (d) 15M/20N/1ms^{-1}

5.3.5. Summary

- The basic wear mechanism of pure aluminum alloy and reinforced composites consists of adhesive wear with plastic deformation followed by abrasive wear. Major wear in the samples is due to ploughing, oxidation and delamination.
- The COF initially increased with micrometric size Y_2O_3 addition in the alloy matrix, then decreased with further addition while the COF continuously decreased with the addition of nano Y_2O_3 reinforcement.
- A minimum wear was found for the composition having 5 vol% micrometric Y_2O_3 addition and 0.5 vol% in case of nano Y_2O_3 addition. At a constant volume fraction the overall wear was found to be less for the compositions having nano Y_2O_3 as compared to Y_2O_3 of micron size for all the test conditions.
- The addition of Y_2O_3 is helpful for lowering the wear of aluminum alloy 7075. Wear rate for all the composites decreased with addition of Y_2O_3, optimized at a fixed composition and then again increased with further addition of Y_2O_3.
- A large volume fraction addition of Y_2O_3 reinforcement in nano or micrometer size resulted in agglomeration of these particles. Ploughing out of these agglomerates during wear testing further increases wear of the composites.

5.4 Machinability Studies of Powder Forged Micrometric and Nanometric Y_2O_3 Reinforced AA-7075 Composites

The present sub-section deals with machinability studies of Al-7075 and its composites in solutionized and peak aged conditions (T_6 condition). Machining of the samples was carried out in the form of drilling with the help of radial drilling machine. Drill forces in the form of thrust force and torque, were measured and compared with different volume fractions of Y_2O_3 reinforcement addition. Surface roughness of machined surface was measured with the help of surface profilometer to estimate the extent of final finish. Machined surfaces were further examined with SEM to observe the surface morphology and roughness. To ascertain the ease of machining, chips during machining were collected and examined for size, shape and morphology by SEM. The effect of machining operation on the drill hole surface was investigated by measuring the strain affected zone around the drill hole.

5.4.1 Forces during Machining

Drilling forces measured in the form of thrust forces and torque for solutionized and T_6 conditions are shown in Fig. 5.43 and Fig. 5.44. The two forces are compressive in nature and discussed in following separate sections.

5.4.1.1 Thrust Forces

Thrust force for Al-7075, micrometric and nanometric composites were measured in solutionized (Fig. 5.43(a)) and T_6 conditions (Fig. 5.44(b)). The thrust force for pure alloy in solutionized condition was 149 N. The thrust force with addition of micrometric Y_2O_3 initially decreased with a volume fraction of 1 vol% thereafter it increased at 3 vol% and 5 vol%. Upon further Y_2O_3 addition, the thrust force dropped at 10 vol% followed by a slight increase at 15 vol% Y_2O_3 addition. For micrometric composites, the maximum thrust force was measured as 212 N for 5 vol% Y_2O_3 addition while the minimum thrust force was 63 N at 1 vol% Y_2O_3 addition. With nanometric Y_2O_3 addition, the thrust force increased for a volume fraction of 0.1 vol% and 0.5 vol%, thereafter it decreased for 1 vol% and 3 vol%. In case of nanometric composites maximum thrust force was 230 N at 0.5 vol% Y_2O_3 while the minimum was 134 N at 3 vol% Y_2O_3.

Thrust force in T_6 condition for Al-7075 was measured as 163 N and considerably increased with the addition of Y_2O_3 reinforcement of both micron as well as nano sizes. The thrust forces exhibited a fairly similar trend in T_6 condition as that observed in the solutionized condition except that the values were higher. The thrust force was measured highest as 346 N with 5 vol%

micrometric Y_2O_3 addition amongst micrometric composites and highest as 359 N with the addition of 0.5 vol% amongst nanometric composites. The lowest value of thrust forces was recorded as 238 N for 10 vol % micrometric Y_2O_3 addition and 199 N for 3 vol% nanometric Y_2O_3 additions.

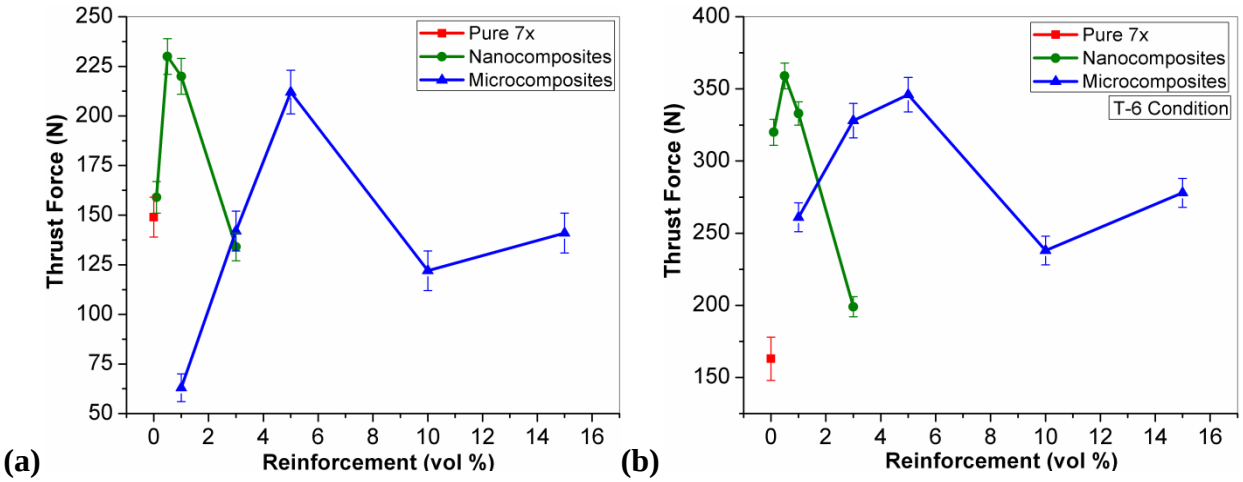

Fig. 5.43: Thrust Forces with different amount of Yttrium Oxide Reinforcement (a) at solutionized condition (b) at T_6 condition

The thrust force represents the force component exerted on the sample by the cutting edges of drill in the direction of feed. This force increases with the resistance to cutting offered by the material. Hardness of the material plays an important role for imparting the resistance to cutting. Except in very ductile materials which may generate a built-up edge, low values of hardness are favorable for improved machinability. Further, lower the hardness lower is the energy required to shear the metal and the easier the chip will break and reduces the shear forces. In both the solutionized as well as T_6 conditions, the thrust forces exhibit a somewhat similar trend as that of hardness as discussed earlier in section 5.2. In solutionized condition, the hardness is mainly due to the reinforcement size and content and to a lesser extent on the Al-7075 matrix. The Al-7075 matrix is a super saturated solid solution of the alloying elements (Cu, Mg, Zn) in aluminum. In this condition the hardness of the material increases with the reinforcement addition and so do the thrust forces, but this takes place till a certain volume fraction after which the thrust forces decreases due to agglomeration of the reinforcements. The hard reinforcement (Y_2O_3) helps in resisting cutting when uniformly distributed in the matrix but with the addition of reinforcement particles beyond a limit, the agglomeration of these particles take place which hinders the metallurgical bonding between the powder particles. This weak bonding further results in an easy

piercing of drill tool and subsequent higher material removal rate (MRR) during drilling operation. The weak interface between the agglomerated particles and matrix also acts as a site for crack propagation during machining.

The thrust forces were considerably higher in the T_6 condition as compared to the solutionized condition due to higher hardness in the T_6 condition. In T_6 condition, the thrust forces increase with increasing hardness till a certain volume fraction of reinforcement after which it decreases as the hardness of the material decreases with further increase in the reinforcement content. As explained earlier in section 5.2 due to the thermal mismatch between the yttria reinforcements and the Al-7075 matrix, dislocations are created which act as nucleation sites for the precipitates. A volume fraction of 0.5% for nano yttria and 5% for micron yttria were sufficient for production of an optimum level of dislocation density which creates sites for precipitation. At lower volume fractions of reinforcements, sufficient dislocations were not generated while at higher fractions due to agglomeration of reinforcement particles enough dislocations are not generated. Thus, the hardness in the peak aged condition was the highest at these compositions of nano and micron yttria. In the T_6 condition, the hard precipitates as well as the reinforcements both resist the cutting forces during machining whereas in the solutionized condition only the reinforcements play a role. The increase in thrust force in T_6 condition as compared to that in the solutionized condition for nanometric composites was 57% while for the micrometric composites was 61% for the highest values in both these composites. The same was around 10% for the pure Al-7075 alloy which indicates that the reinforcements had a profound influence on the precipitation kinetics. In the solutionized as well as T_6 conditions the thrust forces can also be related to the interaction of dislocations (generated during machining) with the reinforcements as well as the precipitates. During machining localized plastic deformation occurs with very high strains and exceptionally high strain rates. This leads to an increase in the average dislocation density which interacts with the reinforcements as well as precipitates. The interaction depends on the size as well as the volume fraction of both the reinforcement as well as the precipitates.

5.4.1.2 Cutting Torque

Cutting torque for Al-7075, micrometric and nanometric composites is shown in Fig. 5.44(a) and Fig. 5.44(b). The cutting torque for Al-7075 in solutionized condition (Fig. 5.44 (a)) was measured as 0.3 N-m. Cutting torque increased with the addition of Y_2O_3 reinforcement upto 5

vol% for micrometric size and upto 0.5 vol% for nanometric size. Adding more amount of Y_2O_3 resulted in lowering the cutting torque for both reinforcement sizes. A maximum cutting torque was measured as 0.34 N-m for 5 vol% micrometric Y_2O_3 and 0.43 N-m with 0.5 vol% nanometric Y_2O_3. A minimum cutting torque was observed as 0.23 N-m for 1 vol% micrometric Y_2O_3 addition and 0.15 N-m for 3 vol% nanometric Y_2O_3.

Cutting torque in T_6 condition for pure alloy and composites is shown in Fig. 5.44(b). Cutting torque for pure alloy in T_6 condition was measured as 0.33 N-m. The cutting torque increased with the addition of Y_2O_3 initially and then decreased with higher amount of Y_2O_3 additions. The cutting torque was measured highest as 0.37 N-m for 5 vol% micrometric Y_2O_3 addition and 0.49 N-m for 0.5 vol% nanometric Y_2O_3 addition. The lowest value of cutting torque was noted as 0.3 N-m with 1 vol % micrometric and 0.31 N-m with 3 vol% nanometric Y_2O_3 additions.

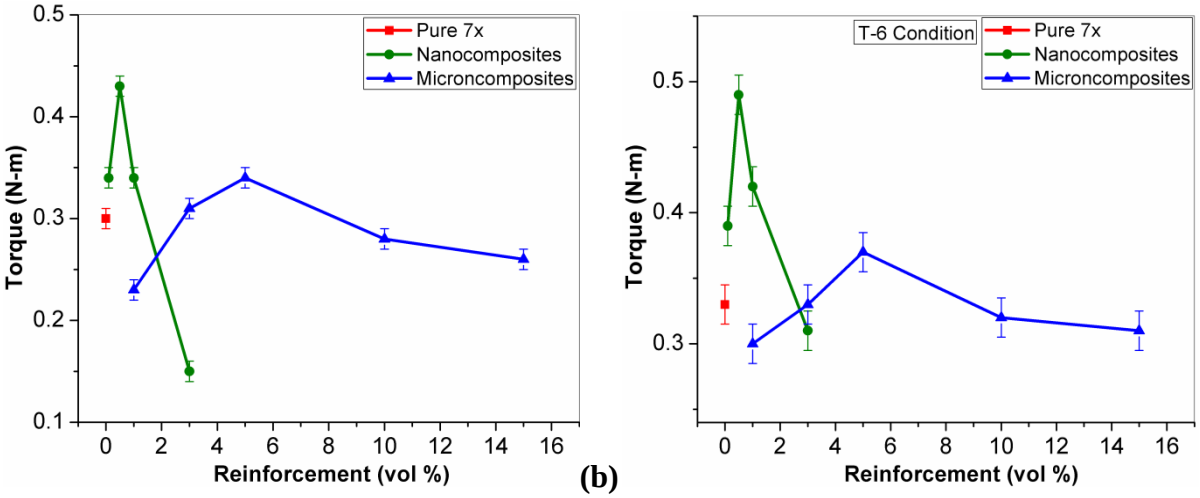

Fig. 5.44: Cutting torque with different amount of Yttrium Oxide reinforcement (a) at solutionized condition (b) at T_6 condition

Cutting torque is generated during interaction of cutting tool edge with the drill hole surface. It is further determined by calculating the horizontal cutting force component which acts perpendicular to the feed direction. The cutting torque depends upon the hardness of the material as well as the bond strength of the matrix. It can be proportionally correlated with the thrust forces; means it increases with increase in thrust force and vice versa as shown in Fig. 5.44 (a) and (b). The cutting torque was higher in the T_6 condition as compared to the solutionized condition. Further, the cutting torque exhibited a similar trend as that of thrust forces as similar factors governed it as explained earlier.

5.4.2 Surface Roughness of Machined Surfaces

Surface roughness values (measured in micrometers) for pure alloy and its composites in solutionized as well as in T_6 condition are shown in Fig.5.45. In the solutionized condition (Fig.5.45 (a)) roughness values ranged from 5.71 µm to 8.36 µm. The roughness for Al-7075 was measured as 5.71 µm in solutionized condition and it increased for the composites with the addition of micrometric and nanometric Y_2O_3. Addition of 5 vol% Y_2O_3 was found effective for improved surface finish with a roughness value of 5.5 µm. The highest roughness value amongst nanometric composites was found as 7.59 µm for 1 vol% Y_2O_3 addition; while that amongst micrometric composites was found as 8.36 µm for 15 vol % Y_2O_3 addition.

The surface roughness values for pure alloy and composites in T_6 condition are shown in Fig. 5.45(b). The roughness values are considerably less for all the composites compared to Al-7075. The roughness value in T_6 condition for Al-7075 was 2.09 µm. Amongst Nanometric composites, the roughness increased with increase in Y_2O_3 upto 1 vol% beyond which it decreased. The lowest value of roughness was measured as 1 µm for 0.1 vol% nanometric Y_2O_3 addition and the highest value was noted as 1.74 µm for 1 vol%. In micrometric composites, surface roughness continuously increased with the addition of Y_2O_3. Amongst micrometric composites, the lowest roughness value as 1.27 µm was measured for 1 vol% and the highest value as 1.85 µm was recorded for 15 vol% Y_2O_3 addition.

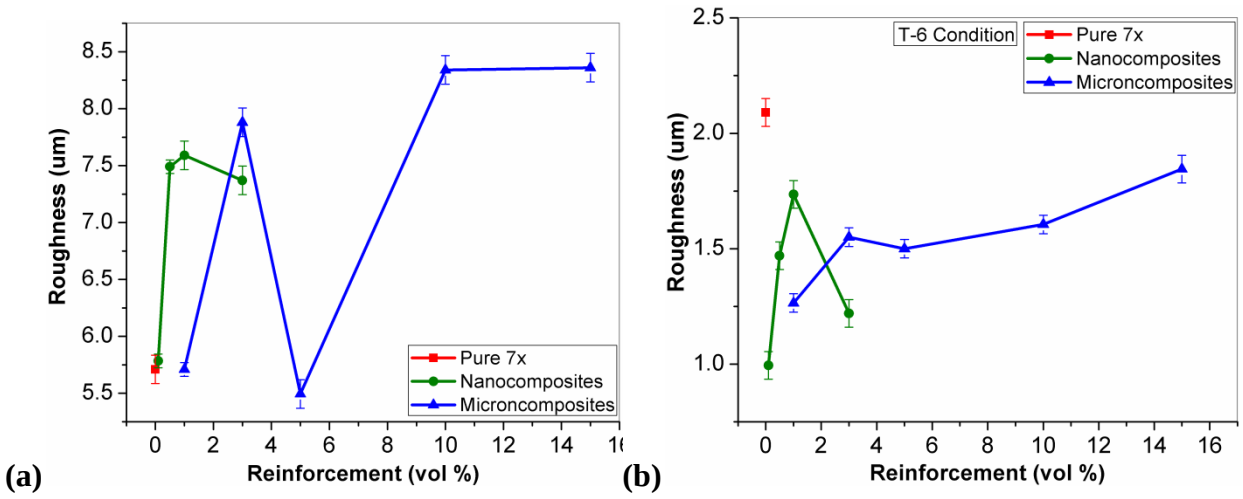

Fig.5.45 Surface Roughness for different amount of Yttrium Oxide Reinforcement (a) in solutionized condition (b) in T_6 condition

Surface roughness is a function of cutting speed, feed rate, sample hardness and surface integrity of the sample material. The surface roughness of Al-7075 was lower than the composites in the solutionized condition while it was higher than the composites in the T_6 condition. Average roughness values of all the samples in T_6 condition were lower than the solutionized condition. In the solutionized condition, the hardness of the material is lower than that in the T_6 condition which results in a poor surface finish. At lower hardness, the surface asperities generated during machining operation are larger due to soft matrix. The asperities elongate during repeated motion of drill due to more plasticity at lower hardness. Thus, these elongated asperities cause more surface roughness in solutionized condition. However the surface asperities were less in T_6 condition and repeated operation of drill finished the surface due to polishing or honing effect.

The surface roughness increased with the addition of Y_2O_3 reinforcement particles of micrometric size. In the micrometric reinforced composites, upon addition of more reinforcement amount the surface integrity looses due to agglomeration of reinforcement particles. The surface roughness of composites having nanometric Y_2O_3 increases with the reinforcement addition upto 1 vol% and decreased thereafter for 3 vol% Y_2O_3 addition. Surface integrity and hardness of the material are two major factors affecting surface roughness. In most of the cases surface roughness increases with decreasing hardness. However in powder metallurgically processed material, the roughness majorly increases with decreasing surface integrity independent of hardness.

5.4.3 Microscopy of Machined Surfaces

The surface roughness was also examined by observing the SEM images of the machined surfaces. Figure 5.46 shows the SEM images of selected compositions in the T_6 condition. Al-7075 has a higher level of roughness due to debris present at the surface during drilling operation. The debris contains aluminum oxide which was initially in the form of surface oxide at the particles and partially formed during machining operation. During machining, the fresh layer of aluminum alloy got revealed after material removal and was exposed to the atmosphere. The fresh aluminum layer reacted with oxygen present in atmosphere and formed aluminum oxide. The formation of surface oxide accelerated when temperature of the sample rose due to machining process. Machined surface of nanometric composite having 0.1 vol% Y_2O_3 shows a better surface integrity but rough surface was observed due to plastic flow of the material (Fig. 5.46.b). Plastic flow due to machining is also prominent in nanometric composite having 0.5 vol% Y_2O_3 however a higher surface finish can be observed. Micrometric composites (Fig. 5.46 (d) and (e)) show a

rough surface with machining debris present at the surface. These debris were caused by Y_2O_3 reinforcement agglomerates which increases with increase in micrometric reinforcement content.

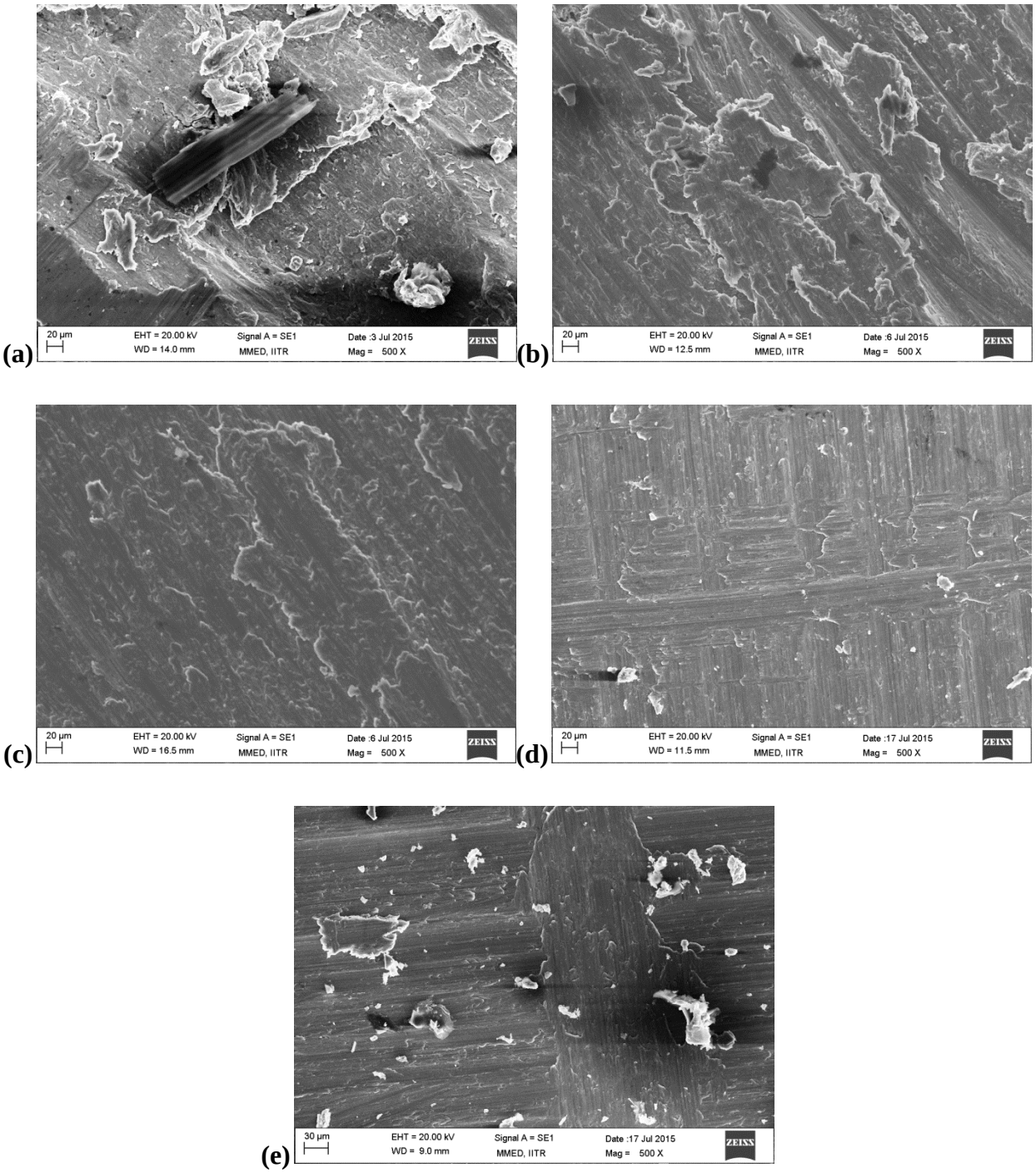

Fig. 5.46 : Drill hole surface at T_6 condition for (a) Pure 7x (b) 0.5 N (c) 3 N (d) 3M (e) 15 M

5.4.4 Characterization of Chips during Machining

Chips collected during machining of Al-7075 and composites are shown in Fig.5.47. A general observation of SEM images of collected chips indicates the formation of discontinuous chips during machining operation. Figure 5.47(a) shows the chip morphology of Al-7075 which has a longer chip formation with saw tooth like edge formation. These types of edges are responsible for breaking of the chip which is an advantage during machining operations as it improves surface finish and reduces tool wear. Machining operation carried out at a moderate feed and slow speed contributed to these discontinuous chips. Addition of Y_2O_3 reinforcement in Al-7075 matrix promotes smaller chips during machining operation. Composite chips having 3 vol% nanometric Y_2O_3 addition and 5 vol% micrometric Y_2O_3 addition are shown in Fig. 5.47(b) and (c) respectively.

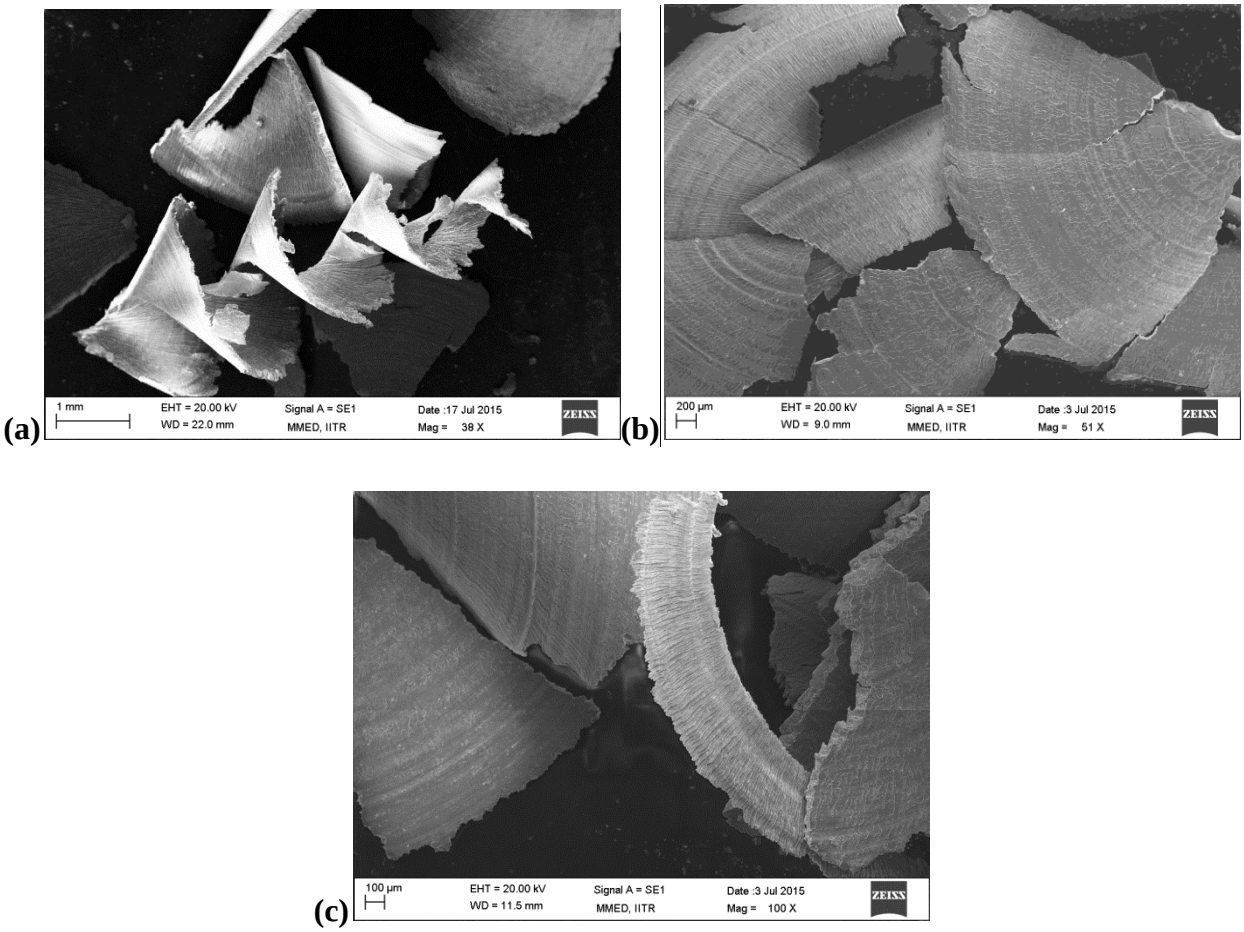

Fig. 5.47: Chips generated during machining (a) Al-7075; (b) 3N and (c) 5 M

Generally size and shape of chip depends upon the work piece material, tool material, tool geometry and working conditions. A soft material is likely to exhibit a continuous chip length during machining due to less brittleness. Al-7075 has a higher hardness compared to pure aluminum and other aluminum alloys. Addition of Y_2O_3 reinforcement to Al-7075 leads to an increase in brittleness of the composites. Saw tooth like edge of the chip acts as a notch at the end and it generates a crack for the chip breakage. Generation of cracks during machining operation for Al-7075, 3 vol% nanometric composite and 5 vol% micrometric composite are shown in Fig. 5.48 (a-c).

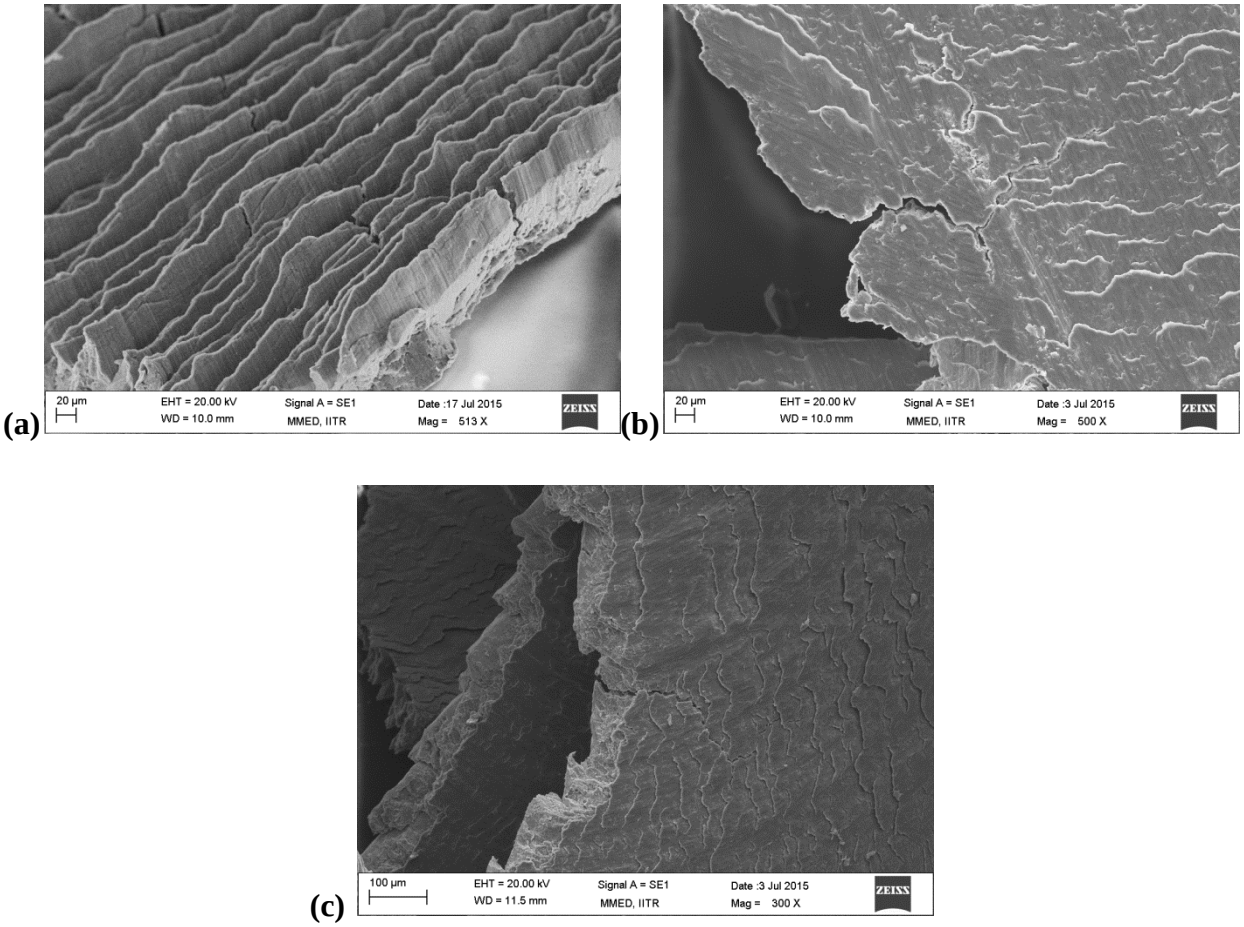

Fig. 5.48: High magnification of selected chip area showing generation of crack (a) Al-7075 (b) 3N and (c) 5 M

During machining operation when the chip length tends to increase, the chip curls and breaks due to propagation of crack at the notch. Other reason of the discontinuous chips of the composite samples can be explained with the help of reinforcement particles pull out. During machining operation, force generated from the drill tries to pull out the yttrium oxide particles

from the surface. These “pull out” region acts as crack initiation points and when the chip curls due to tool advancement, the crack propogates resulting in fracture of the chip. Reinforcement clustering further enhances the pull out regions as shown in Fig. 5.49. A cluster of reinforcement particles was found at the teared surface around the crack which was confirmed as yttrium oxide from the EDS scan. Discontinuous chips are easy to dispose thus the Y_2O_3 reinforcement particles are quite advantageous in terms of machinability due to their ability as chip breakers.

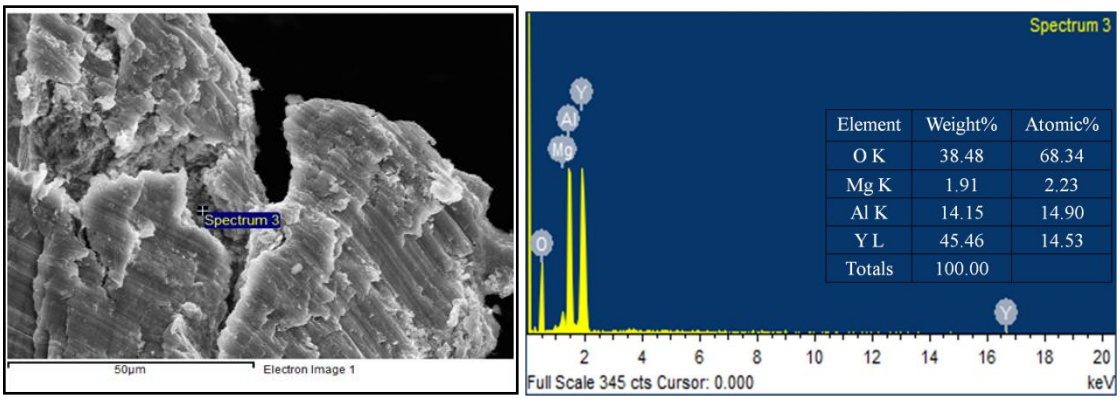

Fig.5.49 EDS analysis of crack tip in 15 M

5.4.5 Strain Affected Zone around Drill Hole

Strain affected zone around the drill hole was measured using SEM images. The SEM images of the zone thicknesses of Al-7075 as well as some selected micrometric and nanometric composite samples in T_6 condition are shown in Fig.5.50. The maximum zone thickness for pure alloy was measured as 65.45 µm which was higher than the composites due to a lower hardness value of pure alloy. The thickness decreased with addition of reinforcements to the matrix as the composite hardness increased. The maximum thickness of affected zone for micrometric composites having 3 vol% and 15 vol % Y_2O_3 reinforcement were 7.1 µm and 12.44 µm respectively. The same for nanometric composites having 0.5 vol% and 3 vol% Y_2O_3 reinforcement were 2.1 µm and 53.46 µm respectively. This corresponded well with the hardness values discussed in section 5.2, i.e. a higher hardness led to smaller strain affected zones while a lower hardness led to larger strain affected zones.

The strain affected zone was affected by the drilling forces and residual stresses in the samples after machining operation. The tool exerts a compressive as well as shear force on the hole surface and the material plastically deforms before removal in the form of chips. The uncut

layer is subjected to a compressive or thrust force from the tool motion during machining operation. This compressive force initiates a shear force and when this shear force exceeds the bearing limit of the material, removal of material occurs in the form of chips. The layer at the surface tries to redistribute the energy received from the tool which was initially in the form of thrust forces. The remaining energy is stored in the material in the form of residual strains and can be observed later in the form of deformed zone. This affected zone thickness depends upon the matrix hardness, reinforcement size / content and number of hardening precipitates present at the time of machining which increases after T_6 heat treatment. In composite samples, the effect of precipitation hardening phenomenon was more prominent then that shown by 7075 alloy. These precipitates hinder the motion of dislocations during deformation process resulting in an increase in dislocation density around the drill holes. In other words it can be said that the area is strain hardened due to mechanical working. This strain hardening effect was larger in the composite samples rather than Al-7075.

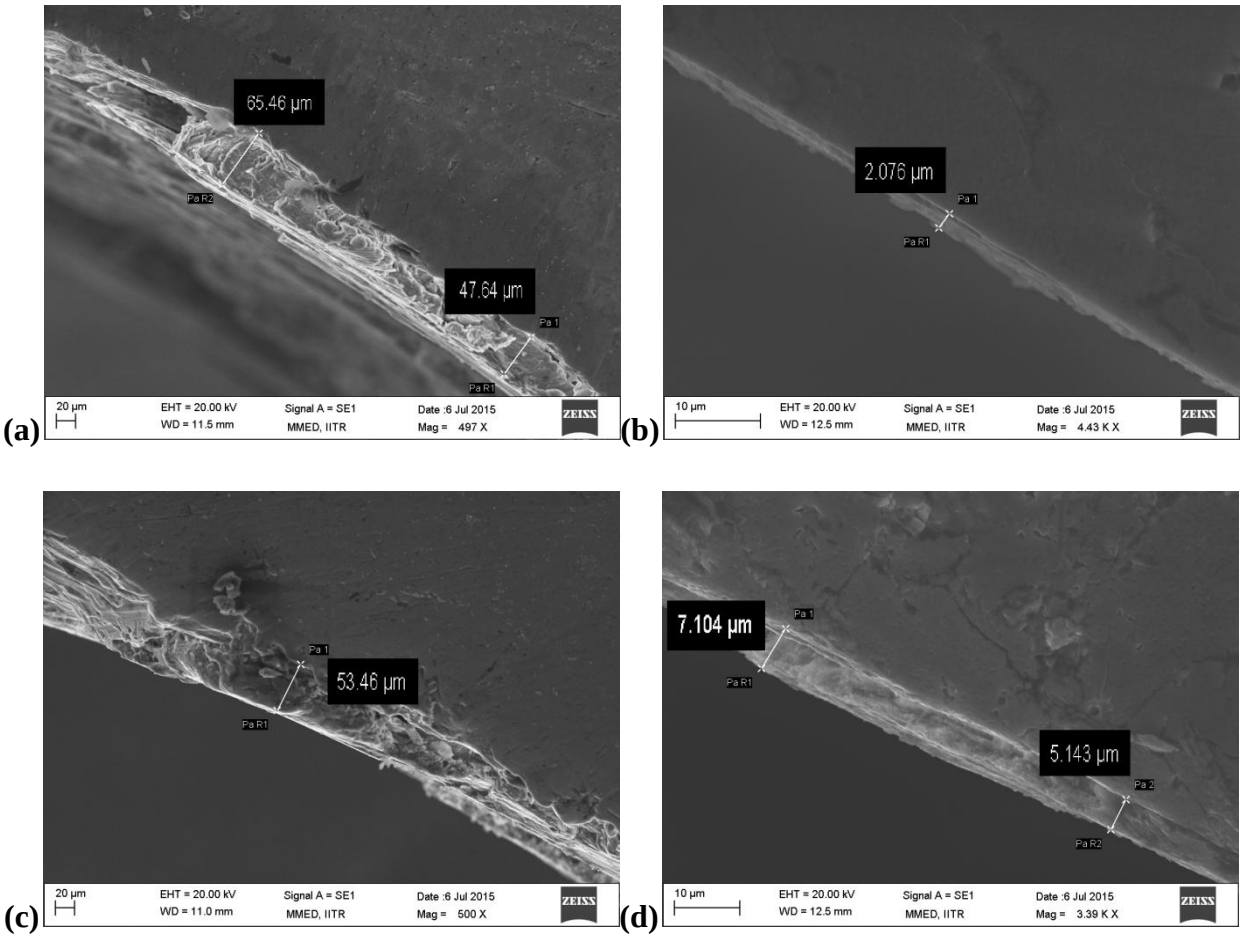

(a) **(b)**

(c) **(d)**

(e) 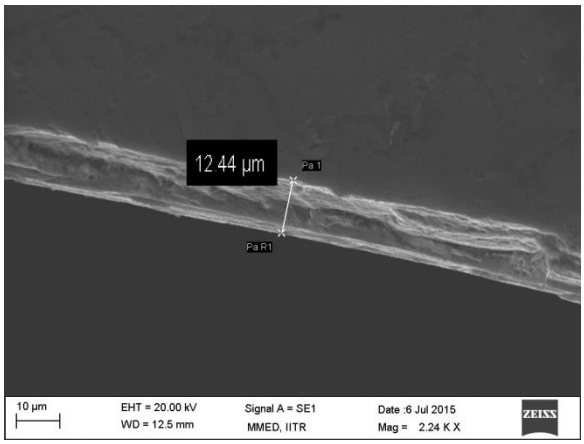

Fig.5.50 Affected zone around drill hole for (a) Pure alloy (b) 0.5N (c) 3N (d) 3M and (e) 15M

5.4.6 Summary

- The thrust forces as well as torque exhibited a similar trend as that of the hardness of the material in both the solutionized as well as in the T_6 condition. Moreover the thrust forces were higher in the T_6 condition as compared to the solutionized condition due to the higher hardness in the peak aged condition.
- As compared to the pure alloy the surface roughness was found to be higher for the composites in the solutionized condition due to more wear of soft surface by the secondary reinforcement particles. On the other hand the surface roughness was lower for the composites as compared to the pure alloy in the T_6 condition due to polishing or honing effect caused by secondary reinforcement particles on a relatively hard surface.
- SEM images of machined surface indicated that during machining the reinforcement particles pulled out from the material and acted as secondary particles on the surface causing more scratches on the surface.
- Relatively smaller chips were generated in T_6 condition during drilling operation as compared to those in the solutionized condition. Further these were smaller in the composites as compared to those in the pure alloy. These small chips are helpful in machining operation due to easy chip disposal and thus increase tool life.
- The thickness of the strain affected zone around the drill hole was smaller in the T_6 condition as compared to that in the solutionized condition due to the higher hardness of the former. This strain affected area also reduced with the addition of reinforcement.

Chapter 6
CONCLUSIONS

6.1 Conclusions

The important contributions of the present work include establishing the sinter-forge route to develop the Al-7075 alloys and its composites with micrometric and nanometric Y_2O_3 as reinforcement, determining the mechanical and tribological properties as well as the machinability of these composites. The important conclusions obtained from these studies have been discussed below.

Hot forging of the sintered Al-7075 preforms led to a relative density in excess of 99.6% whereas the average density of the sintered and green preforms was of the order of 89% and 81% respectively. The deformation of the powder particles after forging was larger in the longitudinal direction as compared to the transverse direction. In the longitudinal direction with increase in temperature and strain initially pore filling by plastic deformation took place, followed by flattening / elongation of the particles and finally shearing off of the oxide layer from the particle surface. In the longitudinal direction, at a temperature of 0.8 T_m and strain of 0.92, the initiation of disruption of oxide layer was observed. The marginally higher hardness in the longitudinal section (48.9 to 59.2 VHN) as compared to the transverse section (47.3 to 55.5 VHN) indicates a low level of anisotropy in these powder forged alloys. In the longitudinal direction almost similar hardness values at 0.92 and 1.14 strain and their insignificant increase with respect to forging temperature indicates that the strain of 0.92 is sufficient for optimum deformation and consolidation of the particles even at lower forging temperatures of $0.6T_m$. The close to full density (99.6%) coupled with disruption of oxide layer leading to a homogeneous structure and low level of anisotropy indicates the benefits of aluminium powder forging.

Aluminum 7075 matrix composites with varying contents of micrometric and nanometric Y_2O_3 reinforcements were successfully processed using the powder forging route. The process employed a temperature of 0.8 T_m and strain of 0.9 to obtain densities in excess of 99.4%. The incorporation of nano yttria in the AA-7075 powders lead to an increase in the relative green density while the same led to a decrease in the relative sintered density. Micrometric Y_2O_3 addition led a decrease in both the green as well as sintered relative densities. Densification parameter was found to be positive for both the composites which justifies occurrence of densification during sintering. The variation between the relative forged densities with micron and

nano yttria reinforcements was marginal and in excess of 99.4% relative density. In the solutionized condition the hardness values were similar to that of the as-forged hardness while in the T_6 condition the hardness values were considerably higher than those in the solutionized and as-forged conditions. The hardness values in T_6 condition peaked at a volume fraction of 0.5% for nano yttria and at a volume fraction of 5% for micron yttria. The incorporation of nano and micron yttria did not cause any change in the peak aging time but the hardness values were significantly affected. Tensile and compressive strengths improved upon addition of Y_2O_3 reinforcement in the alloy matrix but the properties degraded at higher Y_2O_3 contents due to reinforcement agglomeration. Both the tensile strength and compressive strength values were higher with the incorporation of nano yttria as compared to micron yttria in the T_6 condition. The tensile strength values in general for the micrometric composites were lower than those reported in literature while for the nanometric composites they were at par with those reported.

The wear progress started with adhesive wear followed by abrasive wear due to formation of wear debris at later stages. The coefficient of friction (COF) during wear testing initially increased with micrometric Y_2O_3 addition in the alloy matrix, and then decreased with further addition while the COF continuously decreased with the addition of nano Y_2O_3 reinforcement. A minimum wear was found for the composition having 5 vol% micrometric Y_2O_3 addition and 0.5 vol% in case of nanometric Y_2O_3 addition. At a constant volume fraction the overall wear was found to be less for nanometric Y_2O_3 composites as compared to micrometric Y_2O_3 composites for all the test conditions. The addition of Y_2O_3 is helpful for lowering the wear of aluminum alloy 7075. Wear rate for all the composites decreased with addition of Y_2O_3, optimized at a fixed composition and then again increased with further addition of Y_2O_3. A large volume fraction addition of Y_2O_3 reinforcement in nano or micrometer size resulted in agglomeration of these particles. Ploughing out of these agglomerates during wear testing further increased wear of the composites.

Machinability performance was found satisfactory in terms of low drilling forces (thrust force and cutting torque) in solutionized condition as compared to T_6 heat treated condition. The thrust forces as well as cutting torque during machinability studies exhibited a fairly similar trend as that of the hardness of the material in both the solutionized as well as in the T_6 condition. Moreover the thrust forces were higher in the T_6 condition as compared to the solutionized condition due to the higher hardness of the former. As compared to the pure alloy, the surface roughness was found to be higher for the composites in the solutionized condition. On the other

hand the surface roughness was lower for the composites as compared to the pure alloy in the T_6 condition. Chip length of Al-7075 was found larger than micrometric and nanometric composites however it was significantly less and easily disposable. Y_2O_3 reinforcement particles in composite samples were found helpful in initialization of crack in machining chips which resulted in smaller and discontinuous chip formation. Lower machining forces and discontinuous chips during machining were observed in the solutionized condition however a high surface finish was achieved in T_6 condition. The thickness of the strain affected zone around the drill hole was smaller in the T_6 condition as compared to that in the solutionized condition. Further, this zone was larger in Al-7075 as compared to the composites due to lower hardness of the former.

6.2 Suggestions for future work

There is always a need for future work in any area of materials research. Some suggestions for future work are listed below.

1) Present investigation was based on the powder consolidation of the 7075 alloy composites by forging technique. Secondary consolidation of powder metallurgical 7075 alloy and its composites can be optimized using hot rolling and extrusion.
2) Recrystallization behavior was observed during forging at high temperatures and large strain values. The recrystallization during forging of 7075 alloy and its composites can be studied with the help of transmission electron micrography in detail. Effect of recrystallization on the mechanical properties can be observed and discussed with respect to processing parameters.
3) An artificial aging have been performed for the pure 7075 alloy and its composites. There is no change in peak aging time after addition of reinforcement in the alloy. There is a further need to investigate the effect of reinforcement particles on the nucleation of precipitates and dislocation densities. Nucleation of precipitates in under aged condition and their growth upto peak age condition in a composite can be further studied with the help of TEM observation. Aging characteristics of the composites can be studied in details for better understanding of precipitation hardening mechanism.
4) Room temperature mechanical properties for composites were determined and discussed in the present research work. High temperature properties of the composites can be investigated and function of yttrium oxide can be explored during high temperature testing.
5) Tribological behavior of the powder metallurgically processed composites has been presented. There is still a need for explaining this behavior at different sliding speed ranges with respect to various load conditions. The present study was performed at room temperature and the effect of increasing temperature on wear behavior still needs to be understood.
6) The effect of reinforcement content on Al-7075 at a fixed speed and fixed feed was studied in the present work. Machinability studies can be studied with different feed rates and with various drill rpm to better understand the effect of different conditions with varying reinforcement content.

REFERENCES

1. Adachi Hiroki, Osamura Kozo, Ochiai Shojiro, Kusui Jun and Kazuhiko Yokoe, (2001), "Mechanical property of nanoscale precipitate hardening aluminum alloys", Scripta mater, vol. 44,pp.1489–1492.
2. Ahmed A, Neely AJ and Shankar K. (2007a) "Effect of Ceramic Reinforcements on the Mechanical Behavior of 7xxx series Aluminum Matrix Composites", In: 5th Australasian Congress on Applied Mechanics, ACAM 2007, Brisbane, Australia,.pp.10-12.
3. Ahmed A., Neely A.J., Shankar K., Nolan P., Moricca S., and Eddowes T. (2010), "Synthesis, Tensile Testing, and Microstructural Characterization of Nanometric SiC Particulate-Reinforced Al 7075 Matrix Composites", Metallurgical and Materials Transactions A, Vol. 41A, pp. 1582-1592.
4. Ahmed A., Neely, A.J., Shankar K.K., and Chan S.L.I. (2007b), "Tensile behaviour of nano-particulate reinforced Al matrix composites at elevated temperatures", Materials Science Forum, Vols. 561-565, pp. 761-764.
5. Akbulut H., and M. D. F. Y. (1998)," Dry wear and friction properties of t -Al2O3 short fiber reinforced AI-Si (LM 13) alloy metal matrix composites", Wear, Vol. 215, pp.170–179.
6. Alahelisten A., Bergman F., Olsson M.,and Hogmark S. (1993), "On the wear of aluminium and magnesium metal matrix composites", Wear, Vol. 165, pp.221–226.
7. Alpas T., and Zhang J. (1994), "Effect of microstructure (particulate size and volume fraction) and counterface material on the sliding wear resistance of particulate-reinforced aluminium matrix composites", Metallurgical and Materials Transactions A, Vol.25(5), pp.969–983.
8. Archard J.F. (1953), "Contact and rubbing of flat surface", J Appl Phys, Vol. 24, pp.981-988.

9. Arnott D.R., Hinton B.R.W., and Ryan N.E. (1987), "Mater. Performance" Vol. 26 (8), pp. 42.

10. ASM Handbook Vol. 21: Composites, ASM International (2001), Materials Park, OH USA.

11. ASM Handbook, Vol 7: "Powder Metal Technologies and Applications", ASM International (1998), Materials Park, OH USA.

12. ASM Handbook, Vol. 18: Friction, Lubrication, and Wear Technology, ASM International (1992), Materials Park, OH USA.

13. ASM Handbook, Vol.4: Heat Treating, ASM International. (1991), Materials Park, OH, USA.

14. ASM Specialty Handbook, Davis J.R., (1993) Aluminum and Aluminum Alloys.

15. Atkinson H. V. and Davies S. (2000), "Fundamental Aspects of Hot Isostatic Processing: An Overview" Invited review", Metall. and Mater. Trans, A, Vol. 31, pp.2981-3000.

16. Badini C., Vecchia G., La, Fino P., and Valente T. (2001), "Forging of 2124/SiC p composite: preliminary studies of the effects on microstructure and strength",Journal of Materials Processing Technology, Vol. 116, pp.289–297.

17. Baker T., Gorton A., and Song Y. (1996), "Powder processing of AA 6061 aluminium metal matrix composites using hot forging as means of consolidation", Powder Metallurgy, Vol.39(3), pp.223–229.

18. Balasundar M. Sudhakara Rao, and Raghu T. (2009), "Equal channel angular pressing die to extrude a variety of materials", Materials and Design, Vol. 30 pp. 1050–1059.

19. Balout B., Songmene V., and Masounave J. (2002), "Usinabilité des alliages de magnésium et d'aluminium Partie I: Forces de coupe. proc. of the international symposium on enabling technologies for light metal and composite materials and their endproducts", 41th conf. of metallurgists of CIM, Vancouver, BC, Canada , pp. 223-242.

20. Banerjee S., Robi P. S. and Srinivasan A. (2010), Calorimetric Study of Precipitation Kinetics of Al–Cu–Mg and Al–Cu–Mg–0.06 wt.% Sn Alloys, Met. Mater. Int., Vol. 16, No. 4, pp. 523-531.

21. Baradeswaran A. Elaya Perumal (2013), "Influence of B4C on the tribological and mechanical propertiesof Al 7075–B4C composites, Composites: Part B", Vol. 54 pp. 146–152.

22. Baradeswaran A., and Elaya Perumal (2014), "Wear and mechanical characteristics of Al 7075/graphite composites", Composites: Part B Vol. 56, pp.472-476.

23. Billard S., Fondere J.P., Bacroix B. and Dirras G.F. (2006), "Macroscopic and microscopic aspects of the deformation and fracture mechanisms of ultrafine-grained aluminum processed by hot isostatic pressing", Acta Materialia, Vol. 54, pp.411–421.

24. Bishop D. P., Cahoon J. R., Chaturvedi M. C., Kipouros G. J., and Caley W. F. (2000)," On enhancing the mechanical properties of aluminium P/M alloys", Materials Science and Engineering: A, Vol.290(1-2), pp.16–24.

25. Bishop D. P., Caley W. F., Kipouros G. J., Hexemer R. L., and Donaldson I. W. (2011), "Powder metallurgy processing of 2xxx and 7xxx series aluminium alloys", Canadian Metallurgical Quarterly, Vol. 50(3), pp. 246–252.

26. Bora Anil, Singha P.P., Robi P.S. &, Srinivasan A. (2004), "Powder metallurgy processing of ruthenium aluminum alloys", Journal of Materials Processing Technology, Vol.153–154 pp.952–957.

27. Bouaeshi W.B., Li D.Y. (2007) "Effects of Y_2O_3 addition on microstructure, mechanical properties, electrochemical behavior, and resistance to corrosive wear of aluminum", Tribology International, vol.40, (2), pp.188-199.

28. Cai B., Adams B.L., and Nelson T.W. (2007), "Relation between precipitate-free zone width and grain boundary type in 7075-T7 Al alloy", Acta Materialia, vol. 55, pp. 1543–1553.

29. Cepeda-Jimenez C.M., Pozuelo M., Ruano O.A., and Carreno F. (2009), "Influence of the thermal treatment on the microstructure and hardness evolution of 7075 aluminium

layers in a hot-rolled multilayer laminate composite", Journal of Alloys and Compounds, Vol.478, pp.154–162.

30. Ceschini L., Minak G., Morri A. & Tarterini F. (2009), "Forging of the AA6061/23 vol.%Al2O3p composite: Effects on microstructureand tensile properties", Materials Science and Engineering A, Vol. 513–514, pp. 176–184.

31. Chawla N., Andres C., Jones J.W., and Allison J.E. (1998), "Effect of SiC Volume Fraction and Particle Size on the Fatigue Resistance of a 2080 Al/SiCp Composite", Metallurgical And Materials Transactions A, Vol. 29, pp. 2843-2854.

32. Chawla N., Williams J. and Saha R. (2002)," Mechanical behavior and microstructure characterization of sinter-forged SiC particle reinforced aluminium matrix composites", Journal of Light Metals, Vol.2(4), pp. 215–227.

33. Dashwood R., and Schaffer G. (2002), "Powder forging of a sintered Al–3.8Cu–1Mg–0.8Si–0.1Sn alloy", Materials Science and Engineering: A, Vol.323(1-2), pp.206–212.

34. Delgado M. L., Ruiz-Navas E. M., Gordo E., and Torralba, J. M., (2005), "Enhancement of liquid phase sintering through Al–Si additions to Al–Cu systems", Journal of Materials Processing Technology, Vol. (162-163), pp. 280–285.

35. Demir H., and Süleyman Gündüz (2009), "The effects of aging on machinability of 6061 aluminium alloy", Materials and Design, (30), pp 1480–1483.

36. Deng K.K., Wu K., Wu Y.W., Nie K.B., & Zheng M.Y. (2010) "Effect of submicron size SiC particulates on microstructures and mechanical properties of AZ91 magnesium matrix composites", J Alloy Compd, Vol.7, pp.504-542.

37. Derakhshandeh R. H., Jenabali A., Jahromi, (2011), "An investigation on the capability of equal channel angular pressing for consolidation of aluminum and aluminum composite powder", Materials and Design, Vol. 32 pp.3377–3388.

38. Dey G. K., Prakash Deep, Savalia R.T., Mandal R.K. and Banerjee S. (1994), "Formation of Quasicrystalline Phase in Rapidly Solidified $A1_{23}CuFe_{4}$", Scripta Metallurgica et Materialia, Vol. 30(8), pp. 1073-1078,.

39. Dieter, George Ellwood, (1961), Mechanical metallurgy, New York: McGraw-Hill.

40. Doel T.J.A. and Bowen P. 1996, “Tensile properties of particulate-reinforced metal matrix composites”, Composites Part A, vol. 27, pp. 655-665.

41. Du Z.W., Sun Z.M., Shao B.L., Zhou T.T., and Chen C.Q. (2006), “Quantitative evaluation of precipitates in an Al–Zn–Mg–Cu alloy after isothermal aging”, Materials Characterization, vol. 56,pp.121–128.

42. Evangelista E., Di Russo E., McQueen H.J.& Merchant H.D.et al., eds Warrendale, P.A., and Mengucci P. (1988), ‘‘Homogenization and Annealing of Al and Cu Alloys”, Met. Soc. AIME, pp.209–226.

43. F. Thummler & R. Oberacker, (1993), “Introduction to Powder Metallurgy”, Institute of Materials, London, pp. 122.

44. Figueiredo R.B., Celtin P.R. & Langdon T.G. (2007), “The processing of difficult-to-work alloys by ECAP with an emphasis on magnesium alloys”, Acta Mater, Vol. 55, pp.4769–79.

45. Flores-Campos R., Mendoza-Ruiz D.C., Amézaga-Madrid P., Estrada-Guel I., Miki-Yoshida M., Herrera-Ramírez J.M., and Martínez-Sancheza R. (2010), “Microstructural and mechanical characterization in 7075 aluminum alloy reinforced by silver nanoparticles dispersion”, Journal of Alloys and Compounds, vol. 495 pp.394–398.

46. Ganesan G., Raghukandan K., Karthikeyan R. & Pai B.C. (2004), “Development of processing maps for 6061 Al/15% SiCp composite material”, Materials Science and Engineering A, Vol. 369, pp.230–235.

47. German R. (1997), “Supersolidus liquid-phase sintering of prealloyed powders”, Metallurgical and Materials Transactions A, pp.1553–1567.

48. German R. M. (1984), “Powder Metallurgy Science, Metal Powder Industries Federation, NJ”, pp. 114.

49. Giribaskar S., Gouthama, & Prasad R. (2008), "TEM Studies on the Effect of Nature of Precipitates in Al-Li Alloy on Microstructural Evolution during Severe Plastic Deformation", Materials Science Forum, Vol. 584-586, pp 411-416.

50. Giribaskar S., Gouthama, & Prasad R., (2012), "Dynamic Recrystallization in Al-Li Based Alloy during Equal Channel Angular Extrusion", Materials Science Forum, Vol. 715-716, pp. 286-291.

51. Greasley A., and Shi H. (1993), "Microstructural development during hot working of powdered aluminium alloy", Powder Metallurgy, Vol. 36(4), pp.288–292.

52. Griffiths T., Davies R., and Bassett M. (1976), "Compatibility equations for the powder-forging process", Powder Metallurgy, Vol. (4), pp.216–220.

53. Hai Su, Wenli Gao, Zhaohui Feng, and Zheng Lu, (2012), "Processing, microstructure and tensile properties of nano-sized Al_2O_3 particle reinforced aluminum matrix composites", Materials and Design, vol. 36 pp.590–596.

54. Hansen N., and Bay B. (1972), "The effect of particle content, particle distribution and cold deformation on the recrystallization of low oxide Al-Al_2O_3 products", Journal of Materials Science, Vol.(7), pp.1351–1362.

55. Hassana S.F., Tun K.S. & Gupta M. (2011), "Effect of sintering techniques on the microstructure and tensile properties of nano-yttria particulates reinforced magnesium nanocomposites", Journal of Alloys and Compounds, Vol. 509, pp. 4341–4347.

56. Hendrickson, Machmeier P. M., & Smith D. W. (2000), "Impact forging of sintered steel preforms", Powder Metallurgy, Vol.43(4), pp.327–344.

57. Hinton B.R.W., Arnott D.R.,and Ryan N.E. (1984), "Inhibition of aluminum alloy corrosion by cerous cations", Met. Forum, vol. 7, pp. 211-217.

58. Hosseini N., Karimzadeh F., Abbasi M.H., and Enayati M.H. (2010), "Tribological properties of Al6061–Al_2O_3 nanocomposite prepared by milling and hot pressing", Materials and Design, Vol. 31, pp. 4777–4785.

59. Hunt Jr., and W. H. (2000), "Aluminium metal matrix composites today", Materials Science Forum, Vol. 331-337, pp.71–84.

60. Hunt W. J. (2000), "New directions in aluminium: Based P/M materials for automotive applications", Society of Automotive Engineers, vol.1(3), pp.1–8.

61. Hutchings I. (1994), “Tribological properties of metal matrix composites”, Materials Science and Technology, pp. 513–517.

62. Ichikawa J., and Morita K. (2010), “Manufacturing method of sinter forged aluminium parts with high strength”, US Patent, Vol. 7, pp.651,659.

63. Iwai Y., Yoneda H., and Honda T. (1995), “Sliding wear behavior of SiC whisker-reinforced aluminium composite” Wear, Vol. (181-183), pp.594–602.

64. Iwata Y., Mae S., Urai Y., and Tsunoda T. (1989), “Aluminium alloy having an excellent forgiability”, US Patent , Vol. 4, pp.889,557.

65. John J., Burke and Volker Weiss, (2012), “Advances in Deformation Processing”, Sagamore Army Materials Research Conference Proceedings, Springer Science & Business Media,

66. Jones W. D. (1960), Fundamental Principles of Powder Metallurgy, London, Edward Arnold.

67. Joshi T. C., Prakash U. & Dabhade V. V. (2015), “Microstructural development during hot forging of Al 7075 powder”, Journal of Alloys and Compounds, Vol. 639, pp. 123–130.

68. Kambakas K., & Tsakiropoulos P., (2006), “Sedimentation casting of wear resistant metal matrix composites”, Materials Science and Engineering A, Vol. 435–436, pp.187–192.

69. Karanjai M., Kumar Manoj B.V., Sundaresan R., Basu B.,T.R. Rama Mohan, & Kashyap B.P. (2008), “Fretting wear study on Ti–Ca–P biocomposite in dry and simulated body fluid”, Materials Science and Engineering A, Vol. 475, pp. 299–307.

70. Karanjai Malobika, Ranganathan Sundaresan, Tallapragada Raja Rama Mohan, & Kashyap Bhagwati Prasad, (2008), “Evaluation of growth of calcium phosphate ceramics on sintered Ti–Ca–P composites”, Materials Science and Engineering C, Vol. 28, pp.1401–1407.

71. Kato K. (2000), “Wear in relation to friction - a review”, Wear, Vol. 241(2), pp.151–157.

72. Kato K. (2002), “Classification of wear mechanisms/models”, Proceedings of the Institution of Mechanical Engineers, Part J”, Journal of Engineering Tribology, Vol. 216(6), pp. 349–355.

73. Khalid Rafi, Janaki Ram G.D., Phanikumar G.& Prasad Rao K.(2010), “Microstructure and tensile properties of friction welded aluminum alloy AA-7075-T_6” Materials and Design, Vol. 31, pp.2375–2380.

74. Kipouros G., Caley W., and Bishop D. (december 2006), “On the advantages of using powder metallurgy in new light metal alloy design”, Metallurgical and Materials Transactions A, Vol. (37 A), pp.3429–3436.

75. Kondoh K., Kimura A., and Watanabe R. (2001), “Effect of Mg on sintering phenomenon of aluminium alloy powder particle”, Powder Metallurgy, Vol. 44(2), pp.161–164.

76. Kouam J., Masounave J. & Songmene V. (2010), “Pre-holes Effect on Cutting Forces and Particle Emission During Dry Drilling”, 49th Annual Conference of Metallurgists of CIM, 4-6 Oct., Vancouver, BC, Canada, pp. 253-263.

77. Kutz Myer, Handbook of material selection (Wiley), 1994.

78. LaDelpha A.D.P., Neubing H., & D.P. Bishop, (2009) “Metallurgical assessment of an emerging Al–Zn–Mg–Cu P/M alloy”, Materials Science and Engineering A, Vol.520, pp. 105–113.

79. Lesch C., Lvarez P.A., Bleck W., & Gil Sevillano J. (2007), “Rapid Transformation Annealing: a Novel Method for Grain Refinement of Cold-Rolled Low-Carbon Steels”, Metallurgical and Materials Trans. A, Vol. 38A, pp. 1882-90.

80. Lin Y.C., QiangJiang -Yu, Xiao-MinChen, Dong-XuWen, and Hua-MinZhou, (2013), “Effect of creep aging on precipitates of 7075 aluminum alloy”, Materials Science & Engineering A, vol.588pp.347–356

81. Liu Z. Y., Sercombe T. B., and Schaffer G. B. (2007), “The effect of particle shape on the sintering of aluminium” Metallurgical and Materials Transactions A, Vol.38(6), pp.1351–1357.

82. Lumley R. N., & Schaffer, G. B. (1998), "The effect of additive particle size on the mechanical properties of sintered aluminium-copper alloys", Scripta Materialia, Vol. 39(8), pp.1089–1094.

83. Lumley R. N., Sercombe T. B., and Schaffer G. M. (1999), "Surface oxide and the role of magnesium during the sintering of aluminium", Metallurgical and Materials Transactions A, Vol. 30(2), pp.457–463.

84. Lumley R. N.,& Schaffer G. B. (1996), "The effect of solubility and particle size on liquid phase sintering", Scripta Materialia, Vol. 35(5), pp.589–595.

85. Lumley R.N., Sercombe T.B. and Schaffer G.B. (1999), "Surface Oxide and the Role of Magnesium during the Sintering of Aluminum", Metallurgical and Materials Transactions A, Vol. 30a, pp.457.

86. Ma Z.Y., Li Y.L., LiangL Y., Zheng F., BP J., and Tjong S.C., (1996), "Nanometric Si3N 4 particulate-reinforced aluminum composite", Materials Science and Engineering A, vol.219, pp.229-231.

87. Ma Z.Y., Tjong S.C., and Wang, Z.G., (1999), "Cyclic and static creep behavior of Al-Cu alloy composite reinforced with in-situ Al_2O_3 and TiB_2 particulates", Volume 264(1) pp. 177-187.

88. MacAskill I. A., Hexemer R. L., Donaldson I. W., & Bishop D. P. (2010), "Effects of magnesium, tin and nitrogen on the sintering response of aluminium powder", Journal of Materials Processing Technology, Vol. 210(15), pp. 2252–2260.

89. Majzoobi G.H., Azadikhah K.,& Nemati J. (2009) ,"The effects of deep rolling and shot peening on fretting fatigue resistance of Aluminum-7075-T6", Materials Science and Engineering A, Vol. 516, pp. 235–247.

90. Mansfeld F., Lin S., Kim K., & Shih H. (1987), "Pitting and surface modification of SIC/Al", Corrosion Sci., Vol. 27 (9), pp. 997.

91. Marlaud T. A., Bley F., Lefebvre W., and Baroux B., (2010) "Evolution of precipitate microstructures during the retrogression and re-ageing heat treatment of an Al–Zn–Mg–Cu alloy", Acta Materialia, vol. 58, pp.4814–4826.

92. Martín J., & Castro F. (2003), “Liquid phase sintering of P/M aluminium alloys: effect of processing conditions”, Journal of Materials Processing Technology, Vol. 143, pp. 814–821.

93. Mazahery A., Abdizadeh H., & Baharvandi H.R. (2009), “Development of high-performance A356/nano-Al_2O_3 composites” Mater Sci Eng A, Vol. 518, pp. 61–4.

94. Miyajima T., and Iwai Y. (2003), “Effects of reinforcements on sliding wear behavior of aluminium matrix composites”, Wear, Vol. 255(1-6), pp. 606–616.

95. Mohammadi S. M., Simchi A. & Gierl C. (2010), “Phase formation and microstructural evolution during sintering of Al–Zn–Mg–Cu alloys”, Powder Metallurgy, Vol. 53 (1), pp. 62-71.

96. Mohan B., Venugopal S., Rajadurai A., & Mannan S.L.,(2008), “Optimization of the Machinability of the Al-SiC Metal Matrix Composite Using the Dynamic Material Model”, Metallurgical and Materials Transactions A, Vol. 39a, pp.2008—2931.

97. Mondal C., Mukhopadhyay A.K., Raghu T., & Varma V.K. (2007), “Tensile properties of peak aged 7055 aluminum alloy extrusions”, Materials Science and Engineering A, Vol. 454–455 pp.673–678.

98. Mosecker L., Göttmann A., Saeed-Akbari A., Bleck W., Bambach M. & Hirt G. (2013), “Deformation mechanisms of Ti6Al4V sheet material during the incremental sheet forming with laser heating”, Key Engineering Materials, Vol. 549, pp.372-380.

99. Murray J. L. (1988),"The Al—Mg (Aluminum--Magnesium) system,"ASM International, Phase Diagrams of Binary Magnesium Alloys,pp.17-34.

100. Murray J. L. (1983), “The Al−Zn (Aluminum-Zinc) system”, Bulletin of Alloy Phase Diagrams, Volume 4(1), pp 55-73.

101. Murray J.L., (1985), “The aluminium-copper system”, Int. Met. Rev., Vol. 30(1), pp.211-234.

102. Nair V., Tien J. K., & Bates R. C. (1985), “SiC-reinforced aluminium metal matrix composites”, International Metals,Reviews, Vol. 30 (6), pp 275-290.

103. Nam H.W., Jung S.W., Lee J. S., Han K. S. (1998), "Creep Behavior and Rupture Life of Short Fiber Reinforced Metal Matrix Composites", Key Engineering Materials, Vols. 145-149, pp. 711-720.

104. NING Ai-lin, LIU Zhi-yi, PENG Bei-shan, and ZENG Su-min, (2007), "Redistribution and re-precipitation of solute atom during retrogression and reaging of Al-Zn-Mg-Cu alloys", Trans. Nonferrous Met. SOC. China, vol. 17, pp.1005-1011.

105. Odani Y. (1994), "Powder forged Al alloy to challenge ferrous metals", Metal Powder Report, pp. 36–41.

106. Padmavathi C., Upadhyaya A., and Agrawal D. (2011), "Effect of microwave and conventional heating on sintering behavior and properties of Al–Mg–Si–Cu alloy" Materials Chemistry and Physics, 130(1-2), 449–457.

107. Padmavathi, C., and Upadhyaya, A. (2011). Sintering Behaviour and Mechanical Properties of Al–Cu–Mg–Si–Sn Aluminium Alloy", Transactions of the Indian Institute of Metals, Vol. 64(4-5), pp. 345–357.

108. Pal S., Mitra R. and Bhanuprasad V. V. (2008), "Aging behavior of Al-Cu-Mg alloy-SiC composites", Materials Science and Engineering A, Vol. 480, pp. 496–505.

109. Pandey A.B., Majumdar B.S. & Miracle D.B. (2000), "Deformation and fracture of a particle-reinforced aluminium alloy composite: Part I. Experiments", Metallurgical and Materials Transactions A, vol. 31, pp. 921-936.

110. Pant M., & Bleck W. (2005),"Continuous impact wear resistance of duplex surface-modified hot work tool steel H10", Wear, Vol. 259, pp. 377–382.

111. Park J. et al., (2001), "An experimental study on the optimization of powder forging process parameters for an aluminium-alloy piston", Journal of Materials Processing Technology, Vol. (113), pp.486–492.

112. Peng Yu, & Schaffer G.B., (2009), "Microstructural evolution during pressureless infiltration of aluminium alloy parts fabricated by selective laser sintering", Acta Materialia, Vol. 57, pp. 163–170.

113. Pickens J. R. (1981), "Review Aluminium powder metallurgy technology for high-strength applications", Journal of Materials Science, Vol. (16), pp.1437–1457.

114. Pieczonka T., Schubert T., Baunack S., & Kieback B. (2008), "Dimensional behaviour of aluminium sintered in different atmospheres", Materials Science and Engineering: A, Vol. 478(1-2), pp. 251–256.

115. Prakash Deep, Sharma B. P., Rama Mohan T. R., & Gopalan P. (2000), "Flux Additions in Barium Titanate: Overview and Prospects", Journal of Solid State Chemistry, Vol.155, pp. 86-95.

116. Raghu T., Sivakesavam O. & Saha G.G. (1994)," Friction characteristics of magnesium alloy ZM-21", J. Mater. Process. Techno l, Vol.42 pp. 349-360.

117. Razaghian, Yu A., D. & Chandra T. (1998), "Fracture behaviour of a SiC-particle-reinforced aluminium alloy at high temperature", Composites Science and Technology, vol.58, pp. 293- 298.

118. Rehimian M., Ehsani N., Perveen N., & Hamid R. B. (2009) ,"The Effect of particle size, sintering temperature and sintering time on the properties of Al-Al_2O_3 composites made by powder metallurgy", Journal of Materials Processing Technology, vol. 209(14), pp.5387-5393

119. Robi P.S., Pai B. C., Satyanarayana K. G., Pillai S. G. K., and P. Prabhaker Rao (1991), The Role of Surface Treatments and Magnesium Additions on the Dispersoid/Matrix Interface in Cast AI-Si-Mg-15 wt.% SiCp Composites, Materials Characterization 27:11--18.

120. Rokni M. R., Widener C. A., & Champagne V.R. (2014), "Microstructural evolution of 6061 aluminum gas-atomized powder and high-pressure cold-sprayed deposition", Journal of Thermal Spray Technology, Vol. 23(3), pp.514–524.

121. Sahin Y. (1998), "Wear behaviour of planar-random fibre-reinforced metal matrix composites", Wear, Vol. (223), pp.173–183.

122. Sahin Y., and Murphy S. (1998), "The effect of sliding speed and microstructure on the dry wear properties of metal-matrix composites" Wear, Vol. (214), pp.98–106.

123. Sands R. L. & Shakespeare C.R. (1966), "Powder Metallurgy, William Clowes and Sons, London", pp. 67-70.

124. Sankar R.& Paramanand Singh (1998), "Synthesis of 7075 Al/SiC particulate composite powders by mechanical alloying", Materials Letters, Vol. 36 , pp. 201–205.

125. Sannino P., & Rack H. J. (1995). “Dry sliding wear of discontinuously reinforced aluminium composites: review and discussion” Wear, Vol. 189(1-2), pp.1–19.

126. Sawant Pooja, Varma S., Gonal M.R., Wani B.N., Prakash Deep, & Bharadwaj S.R. (2014), “Effect of Ni Concentration on Phase Stability”, Microstructure and Electrical Properties of $BaCe0.8Y0.2O_3$-Ni Cermet SOFC Anodeand its application in proton conducting ITSOFC”, Electrochimica Acta , Vol.120, pp.80–85.

127. Sawtell R., Hunt Jr W., and Rodjom T. (1996), “Method of producing structural metal matrix composite products from a blend of powders”, US Patent, Vol. 5, pp. 561,829.

128. Schaffer G. (2004), “Powder processed aluminium alloys”, Materials Forum, Vol. 28, pp.65–74.

129. Schaffer G., and Hall B. (2002),”The influence of the atmosphere on the sintering of aluminium”, Metallurgical and Materials Transactions A, Vol.33, pp.3279–3284.

130. Schaffer G., and Huo S. (1999), “On development of sintered 7xxx series aluminium alloys”, Powder Metallurgy, Vol.(42) 3, pp.219–226.

131. Schaffer G., Hall B., Bonner S., Huo S., and Sercombe T. (2005), “The effect of the atmosphere and the role of pore filling on the sintering of aluminium”, Acta Materialia, Vol. (54), pp.131–138.

132. Schaffer G., Sercombe T., & Lumley R. (2001), “ Liquid phase sintering of aluminium alloys”, Materials Chemistry and Physics, Vol. 67, pp.85–91.

133. Schatt W., & Wieters K. P. (1997), “Powder Metallurgy: Processing and Materials”, EPMA Publications, Vol. 132, pp. 121-124.

134. Seon F.M. (1989), “Rare earths for materials corrosion protection”, J. Less Common Met. Vol. 148, pp.73-78.

135. Sercombe T. (2003), “On the sintering of uncompacted, pre-alloyed Al powder alloys”, Materials Science and Engineering: A, Vol.341(1-2), pp.163–168.

136. Sercombe T., & Schaffer G. (1999), “On the use of trace additions of Sn to enhance sintered 2xxx series Al powder alloys”, Materials Science and Engineering A, Vol. 268(1-2), pp 32–39.

137. Shahmohammadi M., Simchi A., Danninger H., & Arvand, A. (2007), "An investigation on the sintering behavior of high strength Al-Zn-Mg-Cu alloy prepared from elemental powders", Materials Science Forum, Vol. 534-536, pp. 489–492.

138. Shang J.K. & Ritchie R.O. (1989), "On the particulate dependence of fatigue-crack propagation thresholds in SiC-particulate-reinforced aluminium-alloy composites: Role of crack closure and crack trapping", Acta Metallurgica, vol. 37, pp. 2267-2278.

139. Shao G., & Tsakiropoulos P. (2000), "On the structural evolution of Fe-A1 laminates obtained by physical vapour deposition", Philosophical Magazine, Vol. 80, pp. 693-710.

140. Sharma M. M., Amateaub M. F. & Eden T. J., (2006), " Aging response of Al-Zn-Mg-Cu spray formed alloys and their metal matrix composites", Materials Science and Engineering A, Vol. 424, pp. 87–96.

141. Shaw, M.C. (2005). Metal Cutting Principles, 2nd edition, Oxford, New York, chap 9, pp. 183.

142. Shercliff H. R., and Ashby M. F. (1994), "Design with metal matrix composites" Materials Science and Technology, Vol. 10, pp.443–451.

143. Sidney Avner H., (1997) "Introduction to Physical Metallurgy", Tata McGraw-Hill Education, ISBN 0074630067, 9780074630068.

144. Siegert K., &Ringhand D. (1994), "Flashless and precision forging of connecting rods from P/M aluminium alloys", Journal of Materials Processing Technology, Vol.46, pp.157–167.

145. Singh J., & Alpas A. T. (1995), "Elevated temperature wear of Al6061", Scripta Metallurgica et Materiala, Vol. 32(7), pp.1099–1105.

146. Singh J., and Alpas A. T. (1996), "High-Temperature Wear and Deformation Processes in Metal Matrix Composites", Metallurgical and Materials Transactions A, Vol. (27), pp.3135–3148.

147. Slipenyuk A., Kuprin V., Milman Yu., Goncharuk V., and Eckert J., (2006), "Properties of P/M processed particle reinforced metal matrix composites specified by reinforcement concentration and matrix-to-reinforcement particle size ratio", Acta Materialia, vol.54 pp.157–166.

148. Smith G.T., (1998), “Getting the measure of PM machinability, Metal Powder Report”, Vol. 53, (5), pp. 31–35.

149. Songmene V., Khettabi R., Zaghbani I., Kouam J., & Djebara A. (2011), “Machining and Machinability of Aluminum Alloys, Aluminium Alloys, Theory and Applications, Prof. Tibor Kvackaj (Ed.)”, ISBN: 978-953-307- 244-9, pp. 377-400.

150. Stolyarova V.V., Lapovok R., Brodovac I.G.,& Thomson P.F. (2003) “Ultrafine-grained Al– 5 wt.% Fe alloy processed by ECAP with backpressure”, Mater Sci Eng A, Vol. 357, pp.159–67.

151. Suh N. P. (1977), “An overview of the delamination theory of wear”, Wear, vol. (44), pp.1–16.

152. Suh N. P., (1973) “The delamination theory of wear”, Wear, Vol. 25, pp.111-124.

153. Surappa M. (2003), “Aluminium matrix composites: challenges and opportunities”, Sadhana, pp. 319–334.

154. Tang F., Liao C.-P., Ahn B., Nutt S. R., & Schoenung J. M. (2007), ”Thermal stability in nanostructured Al-5083/SiC composites fabricated by cryomilling”, Powder Metallurgy, Vol. 50(4), pp.307–312.

155. Thummler F., & Oberacker R. (1993), “Introduction to Powder Metallurgy”, Institute of Materials, London, pp. 7.

156. Tofigh A.A. & Ebrahimi M., (2013), “Effect of nano-size Al2O3 reinforcement on the mechanical behavior of synthesis 7075 aluminum alloy composites by mechanical alloying.Mobasherpour”, Materials Chemistry and Physics, Vol. 138, pp.535-541.

157. Trent E.M. (1989), “Metal cutting. 3rd ed. London: Butterworths Press.

158. Tsakiropoulos P., & Shao G. (2004), “Phase selection in non-equilibrium processed TM–Al intermetallic alloys”, Materials Science and Engineering A, Vol. 375–377, pp.201–206.

159. Tun K.S., & Gupta M. (2007) “Improving mechanical properties of magnesium using nano-yttria reinforcement and microwave assisted powder metallurgy method”, Composites Science and Technology, Vol. 67, pp. 2657–2664.

160. Unal A. (1990). “Production of rapidly solidified aluminium alloy powders by gas atomisation and their applications”, Powder Metallurgy, Vol. 1, pp.33.

161. Unal R. and Kainer K. U. (1998), “Production of high strength AI-Mg-Sc alloys by PM”, Powder Metallurgy, Vol. 41(2), 119-122.

162. Upadhyaya G. S. (1997), “Powder Metallurgy Technology”, Cambridge International Science Publishing, pp. 96–117.

163. Varma Vijay K, Kamat S.V., Mahajan Y.R., & Kutumbarao V.V. (2001), “Effect of reinforcement size on low strain yielding behaviour in Al-Cu-Mg/SiCp composites”, Materials Science and Engineering A, Vol. 318, pp. 57–64.

164. Vedani M., Errico F. D. & Gariboldi E. (2006), “Mechanical and fracture behavior of aluminum-based discontinuously reinforced composites at hot working temperatures”, Composites Science and Technology, Vol. 66, pp. 343–349.

165. Veeresh Kumar G.B., Rao C.S.P., & Selvaraj N. (2011), “Mechanical and dry sliding wear behaviour of Al7075 alloy-reinforced with SiC particles”, Journal of Composite Materials, Vol. 0(0), pp.1–9.

166. Venugopal P., Venugopal S., and Seetharaman V. (1990), “Influence of strain rate and temperature on the friction factor of commercialy pure titanium” Journal of Materials Processing Technology, Vol. (22), pp.91–97.

167. Vogt R.G., Zhang Z., Topping T.D., Lavernia E.J., & Schoenung J.M. (2009) “Cryomilled aluminum alloy and boron carbide nano-composite plate”, Journal of Materials Processing Technology, Vol. 209, pp. 5046–5053

168. Wang A., & Rack H. J. (1991a), “Abrasive wear of silicon carbide particulate and whisker reinforced 7091 aluminium matrix composites” Wear, Vol. 146, pp. 337–348.

169. Wang A., & Rack H. J. (1991b),”Dry sliding wear in 2124 Al-Sicw /1 7-4 PH stainless steel syatems” Wear, Vol.147, pp.355–374.

170. Williams, J., Piotrowski, G., Saha, R., and Chawla, N. (2002). Effect of overaging and particle size on tensile deformation and fracture of particle-reinforced aluminium matrix composites. Metallurgical and Materials Transactions A, 3861–3869.

171. Xie J.Q., Bayoumi, A.E. & Zbib, H.M. (1996), "Study on shear banding in chip formation of orthogonal machining", Int. J. Machine Tools & Manufacture, Vol. 36,(7), pp. 835- 847.

172. Yang Y., Lan J.,& Li X.C. (2004), "Study on bulk aluminum matrix nano-composite fabricated by ultrasonic dispersion of nano-sized SiC particles in molten aluminum alloy", Mater Sci Eng A, Vol. 380, pp.373–378.

173. Yarra R., Venkatachalam P., Kumar R.S., Ravisankar B., Jayasankar K. & Mukherjee P.S. (2010), "Densification of Al-Y2O3 composite powder by equal channel angular pressing", Transactions of The Indian Institute of Metals, Vol. 63(5), pp.813 – 817.

174. Yilmaz O., & Buytoz S. (2001), "Abrasive wear of Al2O3-reinforced aluminium-based MMCs", J Compos Sci Technol, Vol. 61, pp.2381-2392.

175. Yu J.H., Kim T.H., Lee J.S. (1997), "Particle growth during liquid phase sintering of nanocomposite W-Cu powder", Nanostructured Materials, Vol. 9, 1–8), pp.229–232.

176. Yu, S., He, Z., & Chen K. (1996), "Dry sliding friction and wear behaviour of short fibre reinforced zinc-based alloy composites" Wear, Vol. 198(1-2), pp.108–114.

177. Zhang Tiancheng, Li D.Y. (2001) "Improvement in the resistance of aluminum with yttria particles to sliding wear in air and in a corrosive medium" Wear, Vol. 251, pp. 1250–1256.

178. Zhao Naiqin, Nash Philip, & Yang Xianjin (2005) , "The effect of mechanical alloying on SiC distribution and the properties of 6061 aluminum composite", Journal of Materials Processing Technology, Vol. 170, pp.586–592.